DEVELOPMENT OF NOVEL NANOMATERIALS FOR HIGH-PERFORMANCE AND LOW-COST FUEL CELL APPLICATIONS

(Spine title: Nanomaterials for Fuel Cells)

(Thesis format: Integrated-Article)

by

Shuhui Sun

Graduate Program in Mechanical and Materials Engineering

A thesis submitted in partial fulfillment
of the requirements for the degree of
Doctor of Philosophy

The School of Graduate and Postdoctoral Studies
The University of Western Ontario
London, Ontario, Canada

THE UNIVERSITY OF WESTERN ONTARIO
THE SCHOOL OF GRADUATE AND POSTDOCTORAL STUDIES

CERTIFICATION OF EXAMINATION

Supervisor   Examiners

_____   _____
Dr. Xueliang (Andy) Sun   Dr. Zhongwei Chen

                                                       _____
Supervisory Committee   Dr. Zhifeng Ding

_____   _____
Dr. Robert Klassen   Dr. Robert Klassen

_____   _____
Dr. Jun Yang   Dr. Liying Jiang

The thesis by

Shuhui <u>Sun</u>

entitled:

Development of Novel Nanomaterials for High-Performance and Low-Cost Fuel Cell Applications

is accepted in partial fulfillment of the
requirements for the degree of
Doctor of Philosophy

Date: December 8, 2011   Dr. Mark Workentin
                                                       Chair of the Thesis Examination Board

ii

ABSTRACT

Proton exchange membrane fuel cells (PEMFCs) are promising energy converting technologies to generate electricity by mainly using hydrogen as a fuel, producing water as the only exhaust. However, short life-time and high cost of Pt catalyst are the main obstacles for the commercialization of PEMFCs. In the conventional carbon black supported platinum nanoparticle (NP) commercial catalyst, carbon supports are prone to oxidation and corrosion over time that results in Pt NPs migration, coalescence, even detaching from the catalyst support. In addition, Ostwald ripening of the Pt NPs could also occur due to their high surface energy and zero dimensional structural features. All these contribute to the degradation of fuel cell performance. This research aims at fabricating various advanced nanomaterials, including (1) Pt-based highly efficient nanocatalysts and (2) alternative nanostructured durable catalyst supports, to address the above-mentioned challenges in PEMFCs.

It is well known that the catalytic activity and durability of Pt catalysts are highly dependent on their size and shape. In contrast to commercially-used Pt spherical nanoparticles, one-dimensional (1D) structures of Pt, such as nanowires (NWs), exhibit additional advantages associated with their anisotropy and unique structure.

We first reported a new approach to address both activity and durability challenges of PEM fuel cells by using 1D Pt nanowires (PtNWs) as electrocatalyst. Pt NWs were synthesized via a very simple environmentally-friendly aqueous solution route at room temperature, without the need of heating, surfactants or complicated experimental apparatus. This novel PtNW nanostructure showed much improved activity and durability than the state-of-the-art commercial Pt/C catalyst which is made of Pt nanoparticles. Further, Pt NWs were grown on Sn@CNT nanocable support to form a novel 3D fuel-cell electrode (PtNW/Sn@CNT). This approach allows us to combine the advantages of both PtNW catalyst and Sn@CNT 3D nanocable support for fuel cell applications. The PtNW/Sn@CNT 3D electrodes

showed greatly enhanced electrocatalytic activities for ORR, MOR and improved CO tolerance than commercial Pt/C nanoparticle catalyst.

To save more platinum, ultrathin Pt NWs with even smaller diameters of 2.5 nm (vs. 4 nm reported in our previous work) have been successfully synthesized when using N-doped CNTs as support. Direct evidence for the formation of ultrathin Pt NWs was provided by systematically investigating their growth process under TEM. Nitrogen doping in CNTs played a key role in the formation of ultrathin Pt nanowires.

In terms of low durability of PEM fuel cell catalysts, the corrosion of current commonly-used carbon black support materials have been identified to be the major contributor to the catalyst failure. One of the major challenges lies in the development of inexpensive, efficient, and highly durable alternative catalyst supports that possess high corrosion resistance, high conductivity and high surface area. In this work, a series of promising alternative nanostructured catalyst supports, including 0D Nb-doped TiO_2 hollow nanospheres, 1D $TiSi_x$-NCNT nanostructures, and 2D graphene nanosheets, have been synthesized by various methods and used as catalyst supports. Pt nanoparticles were then deposited on these novel supports, showing enhanced catalytic activities and durabilities. Most interestingly, a new technique, atomic layer deposition (ALD), was used to uniformly deposit Pt nanoparticles, subnanometer clusters and single atoms on graphene nanosheets. Downsizing Pt nanoparticles to clusters or even single atoms could significantly increase their catalytic activity and is therefore highly desirable to maximize the efficiency.

In summary, the discoveries in this thesis contribute to applying various novel nanostructured materials to design highly active and stable electrocatalyst and durable catalyst support to develop high performance and low cost PEM fuel cells.

CO-AUTHORSHIP

1.

Title: A Highly Active and Durable Platinum Nanocatalyst for Proton Exchange Membrane Fuel Cells: Multiarmed Starlike Nanowire Single Crystal

Authors: **<u>Shuhui Sun,</u>** Gaixia Zhang, Dongsheng Geng, Yougui Chen, Ruying Li, Mei Cai, and Xueliang Sun

All the experimental and theoretical work was carried out by Shuhui Sun under the guidance of Dr. Xueliang Sun. The initial draft and the followed modifications of this manuscript were conducted by Shuhui Sun under the supervision of Dr. Xueliang Sun. The other coauthors contributed to the formation of the final version with discussion and related characterization. The final version of this manuscript has been published in *Angewandte Chemie International Edition*, 2011, 50, 422-426.

2.

Title: Direct Growth of Single-Crystal Pt Nanowires on Sn@CNT Nanocable: 3D Electrodes for Highly Active Electrocatalysts

Authors: **<u>Shuhui Sun,</u>** Gaixia Zhang, Dongsheng Geng, Yougui Chen, Ruying Li, Mei Cai, and Xueliang Sun

All the experimental and theoretical work was carried out by Shuhui Sun under the guidance of Dr. Xueliang Sun. The initial draft and the followed modifications of this manuscript were conducted by Shuhui Sun under the supervision of Dr. Xueliang Sun. The other coauthors contributed to the formation of the final version with discussion and related characterization. The final version of this manuscript has been published in *Chemistry–A European Journal*, 2010, 16, 825-839.

3.

Title: Ultrathin single crystal Pt nanowires grown on N-doped carbon nanotubes

Authors: <u>Shuhui Sun,</u> Gaixia Zhang, Yu Zhong, Hao Liu, Ruying Li, Xiaorong Zhou and Xueliang Sun

All the experimental and theoretical work was carried out by Shuhui Sun under the guidance of Dr. Xueliang Sun. The initial draft and the followed modifications of this manuscript were conducted by Shuhui Sun under the supervision of Dr. Xueliang Sun. The other coauthors contributed to the formation of the final version with discussion and related characterization. The final version of this manuscript has been published in *Chemical Communications*, 2009, 7048-7050.

4.

Title: Highly Stable and Active Pt/Nb-TiO$_2$ Carbon-free Electrocatalyst for Proton Exchange Membrane Fuel cells

Authors: <u>Shuhui Sun,</u> Gaixia Zhang, Xueliang Sun, Mei Cai, and Martin Ruthkosky

All the experimental and theoretical work was carried out by Shuhui Sun under the guidance of Dr. Mei Cai and Dr. Xueliang Sun. The initial draft and the followed modifications of this manuscript were conducted by Shuhui Sun under the supervision of Dr. Mei Cai and Dr. Xueliang Sun. The other coauthors contributed to the formation of the final version with discussion and related characterization. The final version of this manuscript was submitted for publishing.

5.

Title: Pt/TiSi$_x$-NCNT Janus Nanostructures for Highly Stable and CO-Tolerant PEM Fuel Cell Electrocatalyst

Authors: **Shuhui Sun,** Mohammad Norouzi Banis, Gaixia Zhang, Mei Cai, Yong Zhang, Ruying Li, and Xueliang Sun

All the experimental and theoretical work was carried out by Shuhui Sun under the guidance of Dr. Xueliang Sun. The initial draft and the followed modifications of this manuscript were conducted by Shuhui Sun under the supervision of Dr. Xueliang Sun. The other coauthors contributed to the formation of the final version with discussion and related characterization. The final version of this manuscript is to be submitted for publishing.

6.

Title: Enhanced Electrocatalytic Activity of Platinum Subnanoclusters on Graphene Prepared by Atomic Layer Deposition

Authors: **Shuhui Sun,** Xiangbo Meng, Gaixia Zhang, Dongsheng Geng, Ruying Li, Xueliang Sun, Nicolas Gauquelin, Gianluigi Botton, Siyu Ye, and Shanna Knights

All the experimental and theoretical work was carried out by Shuhui Sun under the guidance of Dr. Xueliang Sun. The initial draft and the followed modifications of this manuscript were conducted by Shuhui Sun under the supervision of Dr. Xueliang Sun. The other coauthors contributed to the formation of the final version with discussion and related characterization. The final version of this manuscript is to be submitted for publishing.

7.

Title: Controlled Synthesis of Pt on Graphene Nanosheets by ALD and their Electrochemical Properties

Authors: **Shuhui Sun,** Gaixia Zhang, Xiangbo Meng, Ruying Li, Xueliang Sun, Nicolas Gauquelin, Gianluigi Botton, Jigang Zhou, Ning Chen, Songlan Yang, Tsun-Kong Sham, Siyu Ye, Shanna Knights

All the experimental and theoretical work was carried out by Shuhui Sun under the guidance of Dr. Xueliang Sun. The initial draft and the followed modifications of this manuscript were conducted by Shuhui Sun under the supervision of Dr. Xueliang Sun. The other coauthors contributed to the formation of the final version with discussion and related characterization. The final version of this manuscript is to be submitted for publishing.

DEDICATION

This thesis is dedicated to my beloved wife, Gaixia. It is your support and belief that has given me the courage to pursue my dreams. You are a soul mate whom I shall evermore love and cherish. Also, to my beloved children, Amy and Kevin, I thank you both for all your contributions to our family with so much happiness and pride. It has been a blessing watching the two of you grow, and you have my unwavering support for whatever path you follow.

I love you all, forevermore!

ACKNOWLEDGMENTS

This Ph.D. thesis work was carried out in Dr. Sun's Nanomaterials and Clean Energy Lab at the University of Western Ontario (UWO), Canada. After all those years, I've got quite a list of people who contributed in some way to this thesis, for which I would like to express thanks.

First and foremost, I would like to express my profound gratitude to my supervisor, Dr. Xueliang Sun, the Canada Research Chair in Nanomaterials for Clean Energy, a professor in the Department of Mechanical & Materials Engineering at UWO, for providing me with the opportunity to work under his guidance. I am very indebted to him for his patience, encouragement, insightful advice, and strong support in various ways. Without his extensive and comprehensive help, this thesis could not have been possible. His profound knowledge, rigorous attitude and enthusiasm in research also benefit me for life long. He is a role model for me as an excellent scientist.

I am very grateful to Mrs. Ruying (Kathy) Li, Dr. Sun's wife and a research engineer in the group. She arranged everything perfect in our lab and made our lab a wonderful workplace. Besides teaching me a lot of skills on characterizing nanomaterials and experiments, Mrs. Li gave her kindness and generosity to my routine life as well. She was always ready to give me a hand whenever I was encountered with any problem. My wife and I are really appreciated Andy and Kathy's always kind help and strong support. They might never know how important they are for us and we are indebted to them more than they know.

I am also very grateful to my former supervisors, Dr. Jean-Pol Dodelet (Canada industrial chair in electrocatalysis, INRS-EMT) and Dr. Edward Sacher (Ecole Polytechnique), for their always kind guidance, helpful suggestions and much help to my work and life, even after I left their groups.

I would like to sincerely thank my advisory committee members Dr. Jun Yang and Dr. Robert Klassen, two professors in MME at UWO for their valuable advices to my

TABLE OF CONTENTS

LIST OF TABELS

LIST OF FIGURES

………………………….…………..**Chapter 7**…………….…………….……….

………………….……….………..**Chapter 9**………….…..……….…..……..

LIST OF APPENDICES

LIST OF ABBREVIATIONS

0D: zero dimentional

1D: one dimentional

2D: two deimentional

3D: three dimentional

A

ALD: atomic layer deposition

ADT: accelerated durability test

B

BF: bright-field

C

CA: chronoamperometry

CB: carbon black

CLS: canadian light source

CNFs: carbon nanofilbers

CNTs: carbon nanotubes

CO: carbon monoxide

CP: carbon paper

CV: cyclic voltammetry

CVD: chemical vapor deposition

D

DF: dark-field

DMFC: direct methanol fuel cell

E

ECs: electrical cars

ECSA: electrochemical surface area

EDS: energy dispersive X-ray spectroscopy

EDX: energy dispersive X-ray spectroscopy

EELS: electron energy loss spectroscopy

EXAFS: extended X-ray absorption fine structure

EVs: electrical vehicles

F

FCC: face-centered cubic

FCs: fuel cells

FESEM: field emission scanning electron microscope

FFT: fast Fourier transforms

FWHM: full width at half maximum

G

GC: glassy carbon

GM: general motors

GNS: graphene nanosheets

H

HAADF: high angle annular dark field

HRTEM: high resolution transmission electron microscopy

HXMA: hard X-ray micro-analysis

I

ICP-OES: inductively coupled plasma-optical emission spectroscopy

M

MCFC: molten carbonate fuel cell

MEA: membrane electrode assembly

MOR: methonal oxidation reaction

MWCNTs: multiwalled caron nanotubes

N

N-CNTs: nitrogen-doped carbon nanotubes

NPs: nanoparticles

NWs: nanowires

O

ORR: oxygen reaction reduction

P

PAFC: phosphoric acid fuel cell

PECVD: plasma enhanced CVD

PEMFCs: proton exchange membrane fuel cells

R

RDE: rotating disk electrode

RHE: reversible hydrogen electrode

RRDE: rotating ring-disk electrode

S

SAED: selected area electron diffraction

SCE: saturated calomel electrode

SEM: scanning electron microscopy

SMSI: strong metal support interaction

SOFC: solid oxide fuel cell

SWCNTs: single-walled carbon nanotubes

SR: synchronton-radiation

STEM: scanning transmission electron microscopy

T

TEM: transmission electron microscope

X

XAS: X-ray absorption spectroscopy

XANES: X-ray absorption near edge structure

XPS: X-ray photoelectron spectrometer

XRD: X-ray diffraction

Chapter 1. Introduction

1.1 Introductions to fuel cells

1.1.1 Fundamentals of fuel cells

Due to the rising energy demands, depletion of fossil fuel reserves, and environmental pollution problems, a growing demand for exploring clean and sustainable energy sources, as a replacement for combustion-based energy sources, has sparked significant interest. As a promising candidate for environmentally benign electric power generation technology, fuel cells (FCs) have drawn a great deal of attention because of their high efficiency, high energy density, and low or zero emissions. Accordingly, fuel cells have wide applications covering portable electronics, transportation, stationary and back-up power [1-3].

Fuel cells are electrochemical devices which can, with the help of catalysts, convert the chemical energy of the fuel directly into electrical energy without the combustion process [4]. Electrochemical reactions take place at the two separated electrodes, the electrochemical oxidation of the fuel at the anode and the electrochemical reduction of the oxidant at the cathode. The electrons pass through the external circuit to provide electricity. Generically, most fuel cells consume hydrogen (or hydrogen-rich fuels) and oxygen (or air) to produce electricity, following a simply chemical process:

$$2H_2 + O_2 \rightarrow 2H_2O + E \tag{1.1}$$
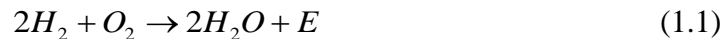
Since the only byproduct of the reaction is water, fuel cells are very clean and environmental-friendly.

Another selling point of fuel cells is their high efficiency [5]. Under favourable circumstances, this efficiency can be up to 60 %, which is 2-3 times that of combustion engines using fossil fuels (normally in the range of 20-30 %). This is because fuel cells convert chemical energy directly to electrical energy, and this

process does not involve conversion of heat or mechanical energy, as shown in Figure 1.1. Therefore, fuel cells are not constrained by Carnot limit and their efficiencies can exceed the Carnot limit even when operating at relatively low temperatures, e.g., 80 ℃. On the contrary, the traditional energy conversion process involves three steps: first, converting chemical energy to heat energy through a combustion engine; second, converting heat energy to mechanical energy through a heat engine; third, generating electricity through a generator. There is a certain energy loss in every step; especially the second step which is confined by the Carnot cycle. Thus, fuel cells have much higher efficiency.
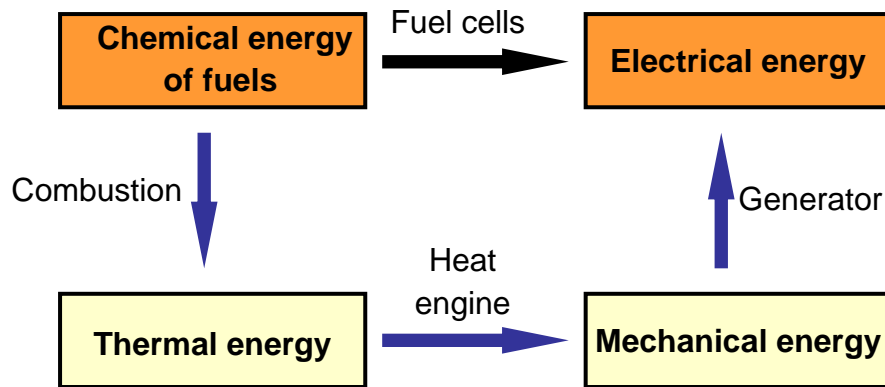
Figure 1.1. A graphical illustration of energy conversion differences between fuel cells and the traditional methods.

Further, compared to the limited capacity of batteries, fuel cells can continuously produce electricity as long as the fuels are supplied. Thus, the capability of continuous generating electricity makes fuel cells are particular suitable for automobile applications. Finally, fuel cells can provide powers range from volts to megavolts, thus fuel cells have broad potential applications ranging from portable electronics to transportation and stationary.

Traditionally, according to the types of electrolyte employed, fuel cells can be classified into five categories: (i) Alkaline Fuel Cells (AFCs), (ii) Phosphoric Acid Fuel Cells (PAFCs), (iii) Molten Carbonate Fuel Cells (MCFCs), (iv) Solid Oxide Fuel Cells (SOFCs), and (v) Proton Exchange Membrane Fuel Cells (PEMFCs). The recently developed Direct Methanol Fuel Cells (DMFCs) can be classified as PEMFCs since they also use proton exchange membranes (PEM) as the electrolyte. Generally, almost all fuel cells (with the exception of DMFCs) consume hydrogen and oxygen to produce electrical current, as mentioned above; however, different fuel cell types have their strengths and weaknesses and, as a result, they have their application areas.

Table 1.1. Comparison of different types of fuel cells.

Fuel cell type	Mobile Ion	Operating Temperature	Fuel	Electrical Efficiency	Start-Up	Applications
Alkaline (AFC)	OH^-	$90 - 100\ ^0C$	H_2	60%	Fast	• Military • Space
Phosphoric Acid (PAFC)	H^+	$150 - 200\ ^0C$	H_2	>40%	Moderate	• Distributed generation
Molten Carbonate (MCFC)	CO_3^{2-}	$600 - 700\ ^0C$	H_2	45 -47%	Slow	• Electric utility • Large distributed generation
Solid Oxide (SOFC)	O^{2-}	$600 - 1000\ ^0C$	H_2/CO	35 - 43%	Slow	• Auxiliary power • Electric utility • Large distributed generation
Polymer Electrolyte Membrane (PEMFC)	H^+	$50 - 100\ ^0C$	H_2	53 - 58% (transportation) 25 – 35 % (stationary)	Fast	• Backup power • Portable power • Small distributed generation • Transportation • Specialty vehicles

From the fuel cell types listed in Table 1, molten carbonate fuel cells and solid oxide fuel cells are classified as high temperature fuel cells, the rest are low temperature fuel cells, even if the operating temperatures of phosphoric acid and alkaline fuel cells exceed 200 °C.

Alkaline fuel cells are very efficient and cheapest to manufacture, but the electrolyte is sensitive to carbon dioxide and therefore oxidant air has to be scrubbed before use, or pure oxygen used, which makes operating AFCs expensive. The primary fuel is hydrogen, but also the use of low alcohols and sodium borohydride has been studied. AFCs are used in applications that require high performance regardless of price, e.g. space and military applications.

Phosphoric acid fuel cell was the first commercial fuel cell type. Owing to the higher operating temperature that is close to 200 °C in PAFCs, Pt catalyst is less sensitive to CO in the fuel, but still requires noble metal catalysts to enhance oxygen reduction reaction at the cathode, and corrosion tolerant materials because of the highly corrosive electrolyte. PAFCs have been used mostly for stationary electricity and heat production, but the interest has decreased since the potential for reducing cost is considered limited.

The focus of molten carbonate fuel cell has been on larger stationary or marine power plants, where slow start-up time and large footprint are not an issue. Thanks to the relatively high operating temperature, electrode reactions do not require noble metal catalysts. In addition to many common fossil and renewable fuels that can be reformed internally, MCFCs can use also CO as a fuel. However, high operating temperature and corrosive electrolyte require expensive materials for cell components for mechanical stability and sufficient life time. Furthermore, carbonate forming reaction at the cathode needs a source of carbon dioxide, which is usually provided by recycling from anode exhaust gas.

Solid oxide fuel cells utilize a ceramic oxygen ion conductive electrolyte and operate at high temperature. Therefore, there is no need for noble metal catalysts and carbon

monoxide can be used as a fuel. High operating temperature also allows using various hydrocarbons as fuels and using waste heat for cogeneration or in steam turbines. However, high operating temperature also has some drawbacks. For example, the thermal expansion has to be controlled carefully and the corrosion of metal components is a challenge. SOFCs are best suited for stationary and distributed power generation, either in heat and power cogeneration or hybrid systems with gas turbines.

The proton exchange membrane fuel cells (PEMFCs) are also known as polymer electrolyte membrane fuel cells. A PEMFC contains an electrolyte that is a layer of solid polymer that allows protons to be transmitted from one face to the other. PEMFCs require hydrogen and oxygen as inputs, and these gases must be humidified. PEMFCs operate at a temperature range of 50-100 ℃ that is much lower than other types of fuel cells. The PEMFC can be contaminated by CO, reducing the performance and damaging catalytic materials within the cell.

Among the multitude of fuel cell technologies available, PEMFCs have become increasingly important because they operate at relatively low temperatures and have short start-up and transient-response times compared to other types of fuel cells that operate at higher temperatures (200 ℃ to 800 ℃) [6]. During PEMFC operations, oxygen gas is fed in cathode and electrochemically reduced while fuel (including hydrogen, methanol, formic acid and ethanol) with low standard redox potential are electrochemically oxidized at anode. Accordingly, based on the type of fuels used, PEMFCs can be further categorized into direct hydrogen fuel cell (DHFC), direct methanol fuel cell (DMFC), direct formic acid fuel cell (DFAFC) and so on [7].

1.1.2 Proton exchange membrane fuel cells (PEMFCs)

PEM fuel cells were first invented in the early 1960s by General Electric (GE). Initially, sulfonated polystyrene membranes were used for electrolytes, but soon they were replaced by Nafion ionomer, which is proved to be superior in performance and durability and is still the most popular electrolyte membrane in use today. Since

Ballard Power systems Inc. pioneered PEMFCs research in late 1980s, PEMFCs have drawn a world-wide interest. In addition, demonstrations are also emerging all over the world. For example, most of the major automobile manufacturers have demonstrated a prototype fuel cell automotive. British Columbia's Hydrogen Highway successfully served the 2010 Winter Olympic Games in Vancouver, British Columbia, Canada.
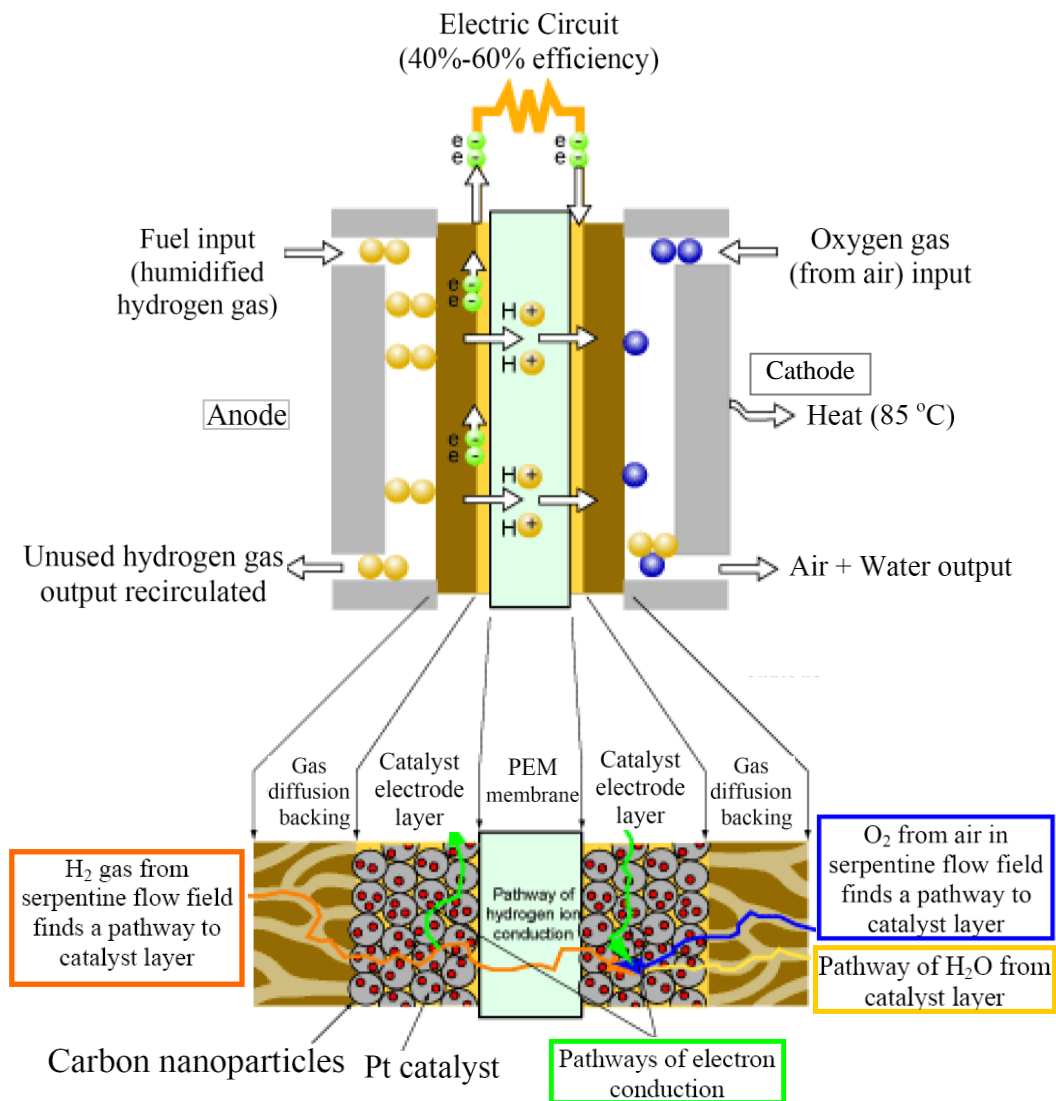
Figure 1.2. Schematic of the working principle for fuel cells [8].

The schematic of a PEMFC is shown in Figure 1.2. It consists of anode, cathode, electrolyte membrane and the external circuit. The main part is the membrane electrode assembly (MEA), which composes a polymer electrolyte membrane (usually Nafion®) sandwiched between the anode and cathode. Beside the MEA, graphite gas flow fields and metal current collect plates are supporting parts. The polymer electrolyte membrane separates the gas at either side and conduct only protons. The electrochemical reactions take place at the catalysts at the two electrodes.

The half cell reaction at the anode side is:

$$2H_2 \rightarrow 4\ H^+ + 4\ e^- \qquad\qquad E^0_a = 0 \text{ V vs. SHE} \qquad\qquad (1.2)$$
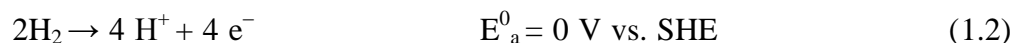
(SHE=standard hydrogen electrode)

The half cell reaction at the cathode side is:

$$O_2 + 4\ H^+ + 4\ e^- \rightarrow 2H_2O \qquad E^0_c = 1.229 \text{ V vs. SHE} \qquad\qquad (1.3)$$
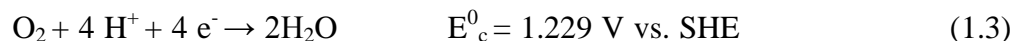
The overall reaction is:

$$O_2 + 2H_2 \rightarrow 2H_2O \qquad\qquad E^0 = 1.229 \text{ V} \qquad\qquad (1.4)$$

At the anode, H_2 is fed in and split into protons and electrons with the help of catalysts. The protons go through the membrane to the cathode side, while the electrons travel in an external circuit, supplying electricity. At the cathode, O_2 reacts with the protons and electrons to form water, leading to zero emissions. Therefore, PEMFCs are clean energy technologies [6].

1.2 Challenges of PEMFCs

The high cost and insufficient durability of PEM fuel cell technology are two of the major challenges hindering its commercialization. Among the components in a PEM fuel cell, platinum (Pt)-based electrocatalysts and their associated catalyst layers contribute over 50% of the total price [9,10]. Unfortunately, Pt is currently the most

efficient electrocatalyst (which is very hard to replace) in practical PEM fuel cells due to its outstanding catalytic and electrical properties and superior resistant characteristics to corrosion. As the demand for Pt grows, the price of Pt has increased by more than three times from $600 per oz in 2001 to $1800 per oz in 2011 over the last decade [11]. It is predicted that the demand for Pt will grow by another 10% in the next fiscal year [12]. Given the climbing price of Pt, we must find ways to reduce the Pt loading (particularly in the cathode catalyst layer) without compromising fuel cell performance in order to meet the cost requirements for fuel cell commercialization. In other words, the design of novel Pt catalyst requires not only reducing the amount of Pt used, but also enhancing its catalytic activity and durability [10, 13].

At present, the most widely used cathode catalyst consists of platinum nanoparticles (2–5 nm) supported on carbon black supports. The major problem associated with the supported Pt nanoparticle catalyst is the degradation of catalytic performance. In practical fuel cells, carbon supports are known to undergo electrochemical corrosion that results in Pt nanoparticles migration, coalescence, even detaching from the catalyst support. In addition, Ostwald ripening of the Pt nanoparticles could also occur due to their high surface energy and zero dimensional structural features [14]. All these contribute to the degradation of fuel cell performance.

1.3. The solutions with nanomaterials

The advent of nanomaterials and nanotechnology has shed light on almost every field of science and technology, particularly in the development of renewable energies, including PEM fuel cells. Nano materials are structures with at least one dimension in the range of 1–100 nm. They can be classified into three categories according to their dimensions: zero-dimensional (0D) (nanoparticles, quantum dots and fullerene), one-dimensional (1D) (nanotubes, nanowires and nanobelts) and two-dimensional (2D) (nanofilms, nanowalls and graphene) nanomaterials [15]. One of the reasons for the considerable interest in nanomaterials is that such materials frequently display

unusual physical (structural, electronic, magnetic and optical) and chemical (catalytic) properties that vary from their bulk counterparts [16,17].

1.3.1. Novel nanostructures of Pt catalyst

Fuel cell applications require the use of Pt in a finely divided state. Great effort has been made to control the size of Pt nanoparticles in order to increase their catalytic activities. Interestingly, it has been established that the catalytic activity and durability of platinum nanostructures depends highly on their morphology (size, shape and dimensionality), and therefore the design and synthesis of platinum nanostructures with well controlled shapes and sizes is crucial for their applications, especially in the field of catalysis. Great effort has been made to increase the ratio of surface area to volume by reducing the size of Pt nanoparticles. Studies have also shown that by altering the surface structure of a bulk single crystal one can manipulate the catalytic properties of a Pt catalyst [18,19]. For example, platinum nanocubes are found four times more active than polyhedral (truncated cubic) Pt NPs for oxygen reduction reaction (ORR), indicating a dominant effect of NP shapes on the ORR in PEMFC reaction conditions [20]. It has also been established that a rough surface containing terraced, stepped, and kinked sites is generally more active than a flat, low-index surface [21]. The reaction kinetics of platinum surface can also be tuned by changing the dimensionality. Very recently, one-dimensional (1D) Pt nanowires have been reported to exhibit much enhanced activity and durability, for ORR, than commercial Pt/C catalyst which is made of Pt nanoparticles [22-25]. 1D nanomaterials with their inherent large specific surface areas and continuous transport path for charge carriers are useful for energy conversion applications, which are mostly associated with surface reaction and carrier transport. When the diameter of a material is reduced below a critical value, the additional advantage of 1D nanomaterials may appear which further enhances their activities. By taking into account both size and surface structure, one can tailor the catalytic activity and durability of a Pt catalyst at the nanoscale by controlling the morphology of Pt nanocrystals during their chemical syntheses. All these advances in shape-controlled

synthesis of Pt nanocrystals provide an opportunity to engineer their catalytic properties for fuel cell applications. However, it remains to be fully explored and understood how the sizes, shapes, surface structures, and capping agents affect the electrocatalytic properties of Pt nanostructures. Once these relationships have been established, it will become possible to design the next-generation highly active and durable electrocatalysts for fuel cell applications. In this thesis, I focused on the syntheses of Pt nanocrystals with well-defined and controllable shapes and their use as electrocatalysts in PEM fuel cell applications.

1.3.2. Nanostructured catalyst supports

With the current state of technology, the state-of-the-art and the most practical electrocatalysts for PEM fuel cells are still carbon black (Vulcan XC-72R) supported Pt catalysts [14]. Although these carbon black supports are outstanding in some aspects in terms of their large surface area, high electrical conductivity, and pore structures, the corrosion caused by electrochemical oxidation in a PEM fuel cell operating environment has been identified to be the major drawback in terms of catalyst durability and reliability. Oxidation of the carbon support to produce CO_2 can occur, resulting in the separation of Pt particles from the carbon support and loss of performance. These separated Pt particles would become electronically isolated, leading to a low Pt utilization as well as degraded fuel cell performance. Therefore, it is necessary to explore more stable alternative catalyst supports to replace the traditional carbon black based supporting materials. The alternative catalyst support should have several important properties including excellent electronic conductivity, high corrosion resistivity, uniform particle size distribution, high surface area, strong cohesive force to catalyst particles, easy formation of uniform dispersion of catalyst particles on their surface, etc. With this respect, considerable work has been done in the past decades. The materials developed include nitride, carbide, conducting polymers, carbon nanotubes, metal oxides, and metal silicide, as well as the newly discovery graphene. Based on various nanomaterials synthesized in our lab, the

authors purposely selected some promising materials as catalyst supports, such as metal oxide, metal silicide, N-doped carbon nanotubes, and graphene.

Metal oxides have been studied by different research groups as alternative catalyst support materials, such as sub-stoichiometric titanium oxide [26,27], indium tin oxide [28], niobium-doped titanium oxide [29], tungsten oxide [30,31], and tin oxide [32]. Among these, titanium oxides are promising as catalyst supports due to their stability in fuel cell operation atmosphere, low cost, commercial availability, stability in water, and strong metal support interaction (SMSI) [33-34]. The use of Nb doping has been found to significantly improve the electrical conductivity of TiO_2, which allows its use in electrocatalytic reactions [29, 35-37].

Recently, transitional metal silicides, such as $TiSi_x$, have attracted tremendous interest as the potential catalyst supports, for replacing carbon, in PEMFCs due to their excellent thermal stability, corrosion resistance, and very high electrical conductivity [38-40]. Previous studies have indicated that using transition-metal silicides as electrocatalyst supports showed higher durability under fuel cell conditions [41], as well as higher electrocatalytic activity for methanol oxidation [42].

The recent emergence of graphene has opened a new avenue for utilizing 2-dimensional carbon material as a support in PEM fuel cells [43, 44]. One hopes to employ such 2-D sheets as conductive mats to both anchor electrocatalysts and modulate the electrochemical reactions in a controlled fashion [45-49]. The combination of the high surface area (theoretical value of 2630 m^2/g), high conductivity, unique graphitized basal plane structure and potential low manufacturing cost makes graphene a promising candidate for catalyst support in PEMFCs [50]. It is expected that graphene may offer a new carbon-metal nanocomposite as the catalyst material for next generation catalysts [46].

1.4 Thesis objectives

PEM fuel cells are innovative clean energy technologies with high efficiency, which have great potential to solve both energy shortage and environmental pollution problems. However, the high cost and low durability of PEM fuel cells are two of the major challenges hindering their commercialization. Nanomaterials and nanotechnology hold one of the key solutions to solve the above-mentioned challenges.

In this content, the authors devoted to develop various advanced nanomaterials for high efficiency catalysts to address the challenges in PEMFCs. The efforts were mainly focused on the synthesis of highly active and stable electrocatalysts with novel nanostructures, such as Pt nanowires, ultrathin Pt nanowires, Pt nanostar, Pt nanoparticles, sub-nanometer Pt clusters and individual Pt atoms, via various novel methods. Different novel nanostructured supports were used in the production of the aforementioned Pt nanostructures. i.e., and 0D Nb-doped TiO_2 hollow nanospheres, 1D N-doped carbon nanotubes, Sn@CNT nanocables, $TiSi_x$-NCNT nanostructures, and 2D graphene nanosheets have been synthesized by various methods and used as catalyst supports. The as-synthesized nanocomposite catalysts were expected to show much enhanced performance than the state of the art commercial Pt/C catalysts. Specific goals are as follows:

Part I: To design highly active and durable electrocatalysts

(1) To develop a variety of methods for the controlled-synthesis of various Pt novel nanostructures. The experimental parameters, such as the reaction system (solvent, surfactant and reducer), reaction temperature, pH value, concentration, etc., have significant effect on the morphology of the products. Through adjusting the above mentioned parameters, to select the facile, efficient and environmental friendly synthetic route.

(2) To compare the electrochemical properties of various Pt nanostructures and to explore the underlying mechanism for their enhanced fuel cell performance, so as to select the good catalyst for fuel cells. It is well known that the catalytic

activity and durability of Pt catalysts are highly dependent on their size and shape, for which determine the exposure facets of a catalyst. By adjusting the shape and size of Pt nanostructure, we can purposely design highly efficient fuel cell catalyst.

(3)   To study the growth processes of novel Pt nanostructures in order to explore their underlying growth mechanism. This information will provide insightful guidance to design better catalyst.

(4)   To design 3D electrode with open structure based on the selected good catalyst and 3D support. The interconnected opening structure promotes a higher gas permeability and enhanced mass transport. This approach will allow us to combine the advantages of the good catalyst and the good catalyst support for fuel cell applications.

(5)   To adjust, more precisely, the diameter of Pt nanowires in order to find the optimized the size-surface-performance relationship.

Part II: To employ various alternative nanostructured catalyst supports.

(1)   To design 0D nanostructured supports for catalyst deposition. Through creating hollow and porous structures, the 0D supports could have much more surface for metal catalyst deposition. Certain metal oxides have better corrosion resistance than carbon, and their electrical conductivity could be improved through doping certain elements.

(2)   To design 1D nanostructured supports for catalyst deposition. 1D shape exhibit additional advantages associated with their anisotropy and unique structure. Metal silicides are promising candidates for catalyst support due to their excellent corrosion resistance and electrical conductivity.

(3)   To design 2D nanostructured supports for catalyst deposition. The combination of the ultra-high surface area, high conductivity, unique graphitized basal plane

structure and potential low manufacturing cost makes graphene a promising candidate for catalyst support in fuel cells.

(4)   On the same graphene support, to combine a new promising technique, atomic layer deposition (ALD), to investigate the morphological evolution of the deposited metals with increased deposition cycles. A distinguishing advantage of ALD is its precise deposition at the atomic level. Through simply controlling the number of ALD cycles, precise control on the morphologies and sizes of deposited materials can be purposely realized.

1.5 Thesis organization

This thesis consists of ten chapters (two introductory chapters, seven articles and one final chapter) and fulfills the requirements on "Integrated-Article" form as outlined in the *Thesis Regulation Guide* by the School of Graduate and Postdoctoral Studies (SGPS) of the University of Western Ontario. Specifically, it includes the following arrangement.

Chapter 1 gives an introduction to fuel cells, especially proton exchange membrane fuel cells (PEMFCs), as well as the challenges of the catalyst electrodes and the solutions offered by nanomaterials and nanotechnology. Besides these, the research objectives, and the thesis organization of this study are also clearly stated.

Chapter 2 presents several experimental analytical techniques, which were used to study and characterize the samples.

The principal results of this thesis are presented in the chapters 3-9, and their interrelationships are shown in Figure 1.3.
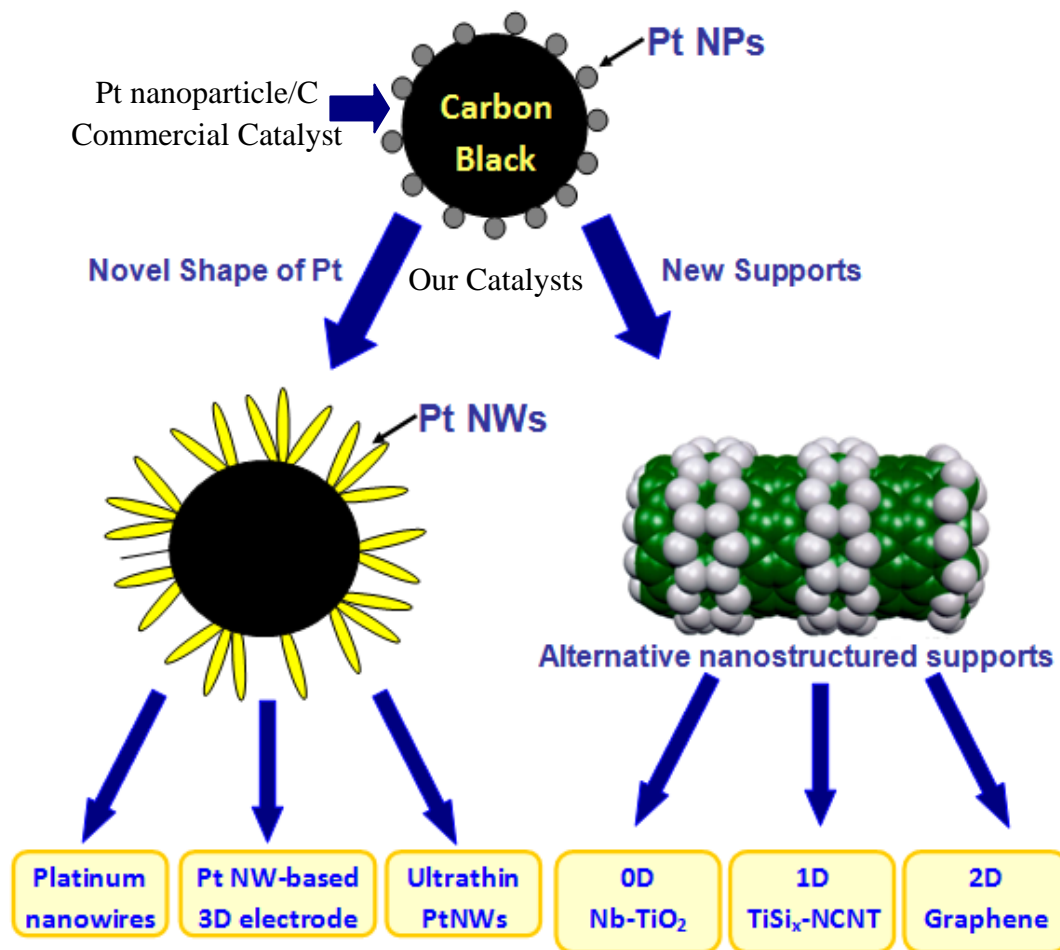
Figure 1.3. The interrelationships of the principal results of the thesis.

At present, the most widely used cathode catalyst consists of platinum nanoparticles (2–5 nm) supported on carbon black supports. The major problem associated with the supported Pt nanoparticle catalyst is the degradation of catalytic performance. In operational fuel cells, carbon supports are known to undergo electrochemical corrosion that resulted in Pt nanoparticle migration, coalescence, even detaching from the catalyst system. In addition, Ostwald ripening of the Pt nanoparticles could also

occur due to their high surface energy and zero dimensional structural features. All these contribute to the degradation of fuel cell performance. One of the strategies for improving the activity and durability of Pt-based catalysts is using 1D Pt nanostructured catalysts owing to their inherent structural characteristics, i.e., high stability, preferential exposure of highly active crystal facets, and easy electron transport. In this thesis, three types of 1D Pt nanostructures are presented in chapter 3 (Pt nanowires), chapter 4 (Pt nanowire-based 3D electrode) and chapter 5 (ultrathin Pt nanowires). Another strategy is to exploit alternative catalyst supports, which have higher corrosion resistance, high surface area and high conductivity, to replace carbon black support. In my work in this thesis, three types of novel nanostructured supports were reported in four chapters, specifically, chapter 6 (0D Nb-doped TiO_2 hollow nanospheres), chapter 7 (1D $TiSi_x$-NCNT nanostructures), chapter 8 and chapter 9 (2D graphene nanosheets).

Chapter 3 (A Highly Active and Durable Pt Nanocatalyst for PEM Fuel Cells: Multiarmed Starlike Nanowire Single Crystal) reports a facile environmentally-friendly aqueous solution method to synthesize carbon-supported Pt nanowire (PtNW/C) electrocatalyst at room temperature, without the need of heating, surfactants or complicated experimental apparatus. This novel PtNW nanostructure showed much improved activity and durability than the state-of-the-art commercial Pt/C catalyst which is made of Pt nanoparticles. 1D Pt nanostructure provides a new approach to enhance both activity and durability of the catalyst in PEM fuel cells.

Chapter 4 (Direct Growth of Single-Crystal Pt Nanowires on Sn@CNT Nanocable: 3D Electrodes for Highly Active Electrocatalysts) describes a novel strategy to further improve the Pt utilization, i.e., to grow Pt nanowires on Sn@CNT nanocable supports, forming a novel 3D fuel-cell electrode (PtNW/Sn@CNT) with open structure. This novel structure combines the advantages of both a PtNW catalyst and a Sn@CNT 3D nanocable support for fuel cell applications. In this study, the electrocatalytic performance, such as oxygen reduction reaction (ORR), methanol oxidation reaction (MOR) and CO tolerance, between our catalyst and commercial

Pt/C catalyst were compared and the reasons for the enhanced performance of our catalyst were discussed as well.

Chapter 5 (Ultrathin single crystal Pt nanowires grown on N-doped carbon nanotubes) makes an attempt to fabricate ultrathin Pt nanowires with diameters of only 2.5 nm. The growth process of ultrathin Pt nanowires on N-CNT support was systematically investigated, providing a direct evidence for the formation mechanism of Pt nanowires. Combined with various characterization techniques, we found that nitrogen doping played a key role in the formation of ultrathin Pt nanowires.

Chapter 6 (Highly Stable and Active Pt/Nb-TiO$_2$ Carbon-free Electrocatalyst for Proton Exchange Membrane Fuel Cells) demonstrates an alternative catalyst support, 0D mesoporous Nb-doped TiO$_2$ hollow spheres, used for Pt nanoparticles (NPs) deposition. The use of Nb-TiO$_2$ hollow spheres as substrate provides a new type of cost-effective support with high corrosion resistance for fuel cells. The growth density of Pt NPs on Nb-TiO$_2$ support could be controlled by manipulating the mass ratios between Pt precursor and Nb-TiO$_2$ support. The electrocatalytic activity and stability of PtNP/Nb-TiO$_2$ catalyst were compared with commercial Pt/C catalyst.

Chapter 7 (Pt/TiSi$_x$-NCNT Janus Nanostructures for Highly Stable and CO-Tolerant PEM Fuel Cell Electrocatalyst) explores another new type of alternative support, TiSi$_x$-NCNT 1D structure, for Pt deposition, forming Pt/TiSi$_x$-NCNT Janus nanostructure. This novel Janus nanostructure were prepared by sputtering TiSi$_x$ only on one side of NCNT, followed by wet-chemical deposition of Pt nanoparticles on the other side. Electrochemical properties, such as durability and CO-tolerance, of Pt/TiSi$_x$-NCNT Janus nanostructures were compared with Pt/NCNT and commercial Pt/C catalysts. Pt/TiSi$_x$-NCNT Janus nanostructure is a new type of promising electrocatalyst for PEMFC applications.

Chapter 8 (Atomic Layer Deposition of Subnanometer Pt Clusters on Graphene as Highly Active and CO-tolerant Electrocatalyst for Methanol Oxidation) studies a wonder material, 2D graphene nanosheets, used as promising catalyst support. A new

technique, atomic layer deposition (ALD), was used to uniformly deposit ultrafine platinum (Pt) nanoparticles on graphene nanosheets. ALD deposits materials in an atomic layer-by-layer fashion, allowing one to precisely control the morphology of the deposited metal. Graphene nanosheets give rise to an extraordinary modification to the properties of Pt nanocatalysts. The electrochemical properties of ALD Pt/graphene were investigated and compared with commercial Pt/C catalyst.

Chapter 9 (Controlled synthesis of Pt on graphene nanosheets by ALD and their electrochemical properties) continually studies the combination of 2D graphene nanosheets support and ALD of Pt. The morphology, size, density and loading of Pt on graphene can be precise controlled by simply adjusting the number of ALD cycles. The electrochemical properties of ALD Pt/graphene with different ALD cycles were systematically investigated and compared. X-ray Absorption Spectroscopy measurements were conducted to study the interaction between Pt and supports.

Chapter 10 summarizes the results and contributions of the thesis work. In addition, the author gives some personal opinions and suggestions for future work.

References

[1] A. M. Herring, Zawodzinski, Jr. T. A. S. J. Hamrock, Fuel Cell Chemistry and Operation; ACS Symposium Series; American Chemical Society: Washington, DC, 2010.

[2] G. Hoogers, Fuel Cell Technology Handbook; CRC Press: Boca Raton, London, New York, Washington, DC, 2003.

[3] M. A. Cropper, S. Geiger, D. M. Jollie, Fuel cells: a survey of current developments. *J. Power Sources* **2004**, *131*, 57–61.

[4] Website of hydrogen, fuel cells & infrastructure technologies program: http://www1.eere.energy.gov/hydrogenandfuelcells/fuelcells/fc_types.html.

[5] V. M. Vishnyakov, Proton exchange membrane fuel cells. *Vacuum* **2006**, *80*, 1053–1065.

[6] J. Larmine, A. Dicks, Fuel cell systems explained, John Wiley & Sons Ltd., West Sussex, England 2003.

[7] R. Borup, J. Meyers, B. Pivovar, Y. S. Kim, R. Mukundan, N. Garland, D. Myers, M. Wilson, F. Garzon, D. Wood, P. Zelenay, K. More, K. Stroh, T. Zawodzinski, J. Boncella, J. E. McGrath, M. Inaba, K. Miyatake, M. Hori, K. Ota, Z. Ogumi, S. Miyata, A. Nishikata, Z. Siroma, Y. Uchimoto, K. Yasuda, K. Kimijima, N. Iwashita, Scientific aspects of polymer electrolyte fuel cell durability and degradation. *Chem. Rev.* **2007**, *107*, 3904–3951.

[8] Z. M. Peng, H. Yang, Designer platinum nanoparticles: Shape, composition in alloys, nanostructure and electrocatalytic property. *Nano Today* **2009**, *4*, 143–164.

[9] R. Bashyam, P. Zelenay, A class of non-precious metal composite catalysts for fuel cells. *Nature*, **2006**, *443*, 63–66.

[10] Y. Bing, H. Liu, L. Zhang, D. Ghosh, J. Zhang, Nanostructured Pt-alloy electrocatalysts for PEM fuel cell oxygen reduction reaction. *Chem. Soc. Rev.*, **2010**, *39*, 2184–2202.

[11] http://www.platinum.matthey.com/cgi-bin/dynamic.pl?year=2001&month=January&template=historical.

[12] B. C. Gates, G. W. Huber, C. L. Marshall, P. N. Ross, J. Sirola, Y. Wang, Catalysts for emerging energy applications. *MRS Bull.* **2008**, *33*, 429–435.

[13] V. Stamenković, T. J. Schmidt, P. N. Ross, N. M. Marković, Surface composition effects in electrocatalysis: kinetics of oxygen reduction on well-defined Pt_3Ni and Pt_3Co alloy surfaces. *J. Phys. Chem. B* **2002**, *106*, 11970–11979.

[14] M. Mathias, R. Makharia, H. Gasteiger, J. Conley, T. Fuller, C. Gittleman, S. Kocha, D. Miller, C. Mittesteadt, T. Xie, S. Yan, P. Yu, Interface **2005**, *14*, 24–35.

[15] G. Cao, Nanostructures & nanomaterials synthesis, properties & applications, Imperial College Press, 2004.

[16] C. M. Lieber, Nanoscale Science and Technology: Building a Big Future from Small Things, *MRS Bull.*, **2003**, *28*, 486–491.

[17] M. C. Daniel, D. Astruc, Gold nanoparticles: assembly, supramolecular chemistry, quantum-size-related properties, and applications toward biology, catalysis, and nanotechnology. *Chem. Rev.*, **2004**, *104*, 293–346.

[18] G. A. Somorjai. Chemistry in Two Dimensions: Surfaces (Cornell University Press, Ithaca, NY) 1981.

[19] J. Chen, B. Lim, E. P. Lee, Y. Xia, Shape-controlled synthesis of platinum nanocrystals for catalytic and electrocatalytic applications. *Nano Today* **2009**, *4*,

81–95.

[20] C. Wang, H. Daimon, T. Onodera, T. Koda, S. Sun, A general approach to the size- and shape-controlled synthesis of platinum nanoparticles and their catalytic reduction of oxygen. *Angew. Chem. Int. Ed.* **2008**, *47*, 3588–3591.

[21] G. C. Bond, Small particles of the platinum metals. *Platinum metals Rev.* **1975**, *19*, 126–134.

[22] S. Sun, F. Jaouen, J. Dodelet, Controlled growth of Pt nanowires on carbon nanospheres and their enhanced performance as electrocatalysts in PEM fuel cells. *Adv. Mater.,* **2008**, *20*, 3900–3904.

[23] S. H. Sun, G. X. Zhang, D. S. Geng, Y. G. Chen, R. Y. Li, M. Cai, X. Sun, A highly durable platinum nanocatalyst for proton exchange membrane fuel cells: multiarmed starlike nanowire single crystal. *Angew. Chem. Int. Ed.* **2011**, *50*, 422–426.

[24] Z. W. Chen, M. Waje, W. Z. Li, Y. S. Yan, Supportless Pt and PtPd nanotubes as electrocatalysts for oxygen-reduction reactions. *Angew. Chem. Int. Ed.*, **2007**, *46*, 4060–4063.

[25] S. M. Alia, G. Zhang, D. Kisailus, D. S. Li, S. Gu, K. Jensen, Y. S. Yan, Porous platinum nanotubes for oxygen reduction and methanol oxidation reactions. *Adv. Funct. Mater.,* **2010**, *20*, 3742–3746.

[26] T. Ioroi, H. Senoh, S. Yamazaki, Z. Siroma, N. Fujiwara, K. Yasuda, Stability of corrosion-resistant magné̀ di-phase Ti_4O_7-supported PEMFC catalysts at high potentials. *J. Electrochem. Soc.* **2008**, *155*, B321–326.

[27] T. Ioroi, N. Fujiwara, S. Yamazaki, K. Yasuda, Sub-stoichiometric titanium oxide-supported platinum electrocatalyst for polymer electrolyte fuel cells. *Electrochem. Commun.* **2005**, *7*, 183–188.

[28] H. Chhina, S. Campbell, O. Kesler An oxidation-resistant indium tin oxide catalyst support for proton exchange membrane fuel cells. *J. Power Sources* **2006**, *161*, 893–900.

[29] G. Chen, S. R. Bare, T. E. Mallouk, Development of supported bifunctional electrocatalysts for unitized regenerative fuel cells. *J. Electrochem. Soc.* **2002**, *149*, A1092–A1099.

[30] H. Chhina, S. Campbell, O. Kesler, Ex situ evaluation of tungsten oxide as a catalyst support for PEMFCs. *J. Electrochem. Soc.* **2007**, 154, B533–B539.

[31] M. S. Saha, M. N. Banis, Y. Zhang, R. Li, M. Cai, X. Sun, Tungsten oxide nanowires grown on carbon paper as Pt electrocatalyst support for high performance PEM fuel cells. *J. Powder Sources* **2009**, *192*, 330–335.

[32] M. S. Saha, R. Li, M. Cai, X. Sun, High electrocatalytic activities of platinum nanoparticles on SnO_2 nanowire-based electrodes. *Electrochem. Solid-State Lett.* **2007**, *10*, B130–B133.

[33] S. Tauster, S. Fung, R. Garten, Strong metal-support interactions. Group 8 noble metals supported on titanium dioxide. *J. Am. Chem. Soc.* **1978**, *100*, 170–175.

[34] F. Leroux, P. Dewar, M. Intissar, G. Ourard, L. Nazar, Study of the formation of mesoporous titania via a template approach and of subsequent Li insertion. *J. Mater. Chem.* **2002**, *12*, 3245–3253.

[35] M. Koninck, P. Manseau, B. Marsan, Preparation and characterization of Nb-doped TiO_2 nanoparticles used as a conductive support for bifunctional $CuCo_2O_4$ electrocatalyst. *J. Electroanal. Chem.* **2007**, *611*, 67–79.

[36] K. Park, K. Seol, Nb-TiO_2 supported Pt cathode catalyst for polymer electrolyte membrane fuel cells. *Electrochem. Commun.* **2007**, *9*, 2256–2260.

[37] M. Cai, Y. Lu, Z. Wu, L. Feng, M. Ruthkosky, J. Johnson, F. Wagner Making electrocatalyst supports for fuel cells. US patent, 2010, Application number: 12/716360.

[38] A. L. Schmitt, J. M. Higgins, J. R. Szczech, S. Jin, Synthesis and Applications of Metal Silicide Nanowires. *J. Mater. Chem.* **2010**, *20*, 223–235.

[39] S. Zhou, X. H. Liu, Y. J. Lin, D. W. Wang, Spontaneous growth of highly conductive two-dimensional TiSi2 nanonets. *Angew. Chem. Int. Ed.* **2008**, *47*, 7681–7684.

[40] S. Zhou, X. H. Liu, D. W. Wang, Si/TiSi2 Heteronanostructures as High-Capacity Anode Material for Li Ion Batteries. *Nano. Lett*. **2010**, *10*, 860–863.

[41] B. Merzougui, I. C. Halalay, J. T. Johnson, G. C. Garabedian, M. P. Balogh, S. Swathirajan, U.S. Patent Pub. No. US 2008/0118818 A1.

[42] T. Ukawa, H. Daimon, Japanese Patent Pub. No. P2005-310418A.

[43] A. K. Geim, K. S. Novoselov. The rise of graphene. *Nat. Mater.* **2007**, *6*, 183–191.

[44] B. Seger, P. V. Kamat Electrocatalytically Active Graphene-Platinum Nanocomposites. Role of 2-D Carbon Support in PEM Fuel Cells. **2009**, *113,* 7990–7995.

[45] R. Kou, Y. Shao, D. Wang, M. H. Engelhard, Ja H. Kwak, J. Wang,V. V. Viswanathan, C. Wang, Y. Lin, Y. Wang, I. A. Aksay, J. Liu. Enhanced activity and stability of Pt catalysts on functionalized graphene sheets for electrocatalytic oxygen reduction. *Electrochem. Commun.* **2009**, 11, 954–957.

[46] E. Yoo, T. Okata, T. Akita, M. Kohyama, J. Nakamura, I. Honma. Enhanced Electrocatalytic Activity of Pt Subnanoclusters on Graphene Nanosheet Surface. *Nano. Lett.* **2009**, *9*, 2255–2259.

[47] P. Ferreira-Aparicio, M. A. Folgado, L. Daza, High surface area graphite as alternative support for proton exchange membrane fuel cell catalysts. *Journal of Power Sources*, **2009**, 192, 57–62.

[48] Y. Shao, S. Zhang, C. Wang, Z. Nie, J. Liu, Y. Wang, Y. Lin, Highly durable graphene nanoplatelets supported Pt nanocatalysts for oxygen reduction. *Journal of Power Sources.* **2010**, 195, 4600–4605.

[49] Y. Li, L. Tang, J. Li Preparation and electrochemical performance for methanol oxidation of Pt/graphene nanocomposites. *Electrochem. Commun.* **2009**, *11*, 846–849.

[50] L. Tang, Y. Wang, Y. Li, H. Feng, J. Lu, J. Li. Preparation, Structure, and Electrochemical Properties of Reduced Graphene Sheet Films. *Adv. Funct. Mater.* **2009**, *19*, 1–8.

Chapter 2. Experimental and Characterization Techniques

2.1 Experimental

2.1.1. Synthesis of Pt nanowires and nanoparticles via solution method

The synthesis of Pt nanowires and nanoparticles were conducted in aqueous solution, by the chemical reduction of Pt precursor with formic acid at room temperature and 80 ^{o}C, respectively, under ambient atmosphere [1-3]. All aqueous solutions were prepared with ultrapure water from a Barnstead Nanopure water system. Specifically, for the synthesis of Pt nanowires, in a typical procedure, 0.032 g hexachloroplatinic acid ($H_2PtCl_6.6 H_2O$, 99.95 %, Aldrich) and 1 mL formic acid (HCOOH, 98 %, Aldrich) were dissolved in 20 mL H_2O and stored at room temperature for 72 h. The solution turned from golden-orange to grey and then to dark brown. While for the synthesis of Pt nanoparticles, similar procedure was used, but the reaction was conducted at 80 ℃ for about 15 min [4,5]. We have tried various experimental parameters, such as different solvents, different surfactants and reducers, different reaction temperatures, different pH values, different concentrations, etc. The current conditions used in this thesis are the optimized parameters.

2.1.2. Synthesis of Sn@CNT nanocable and N-doped CNT via chemical vapor deposition (CVD) method

The synthesis of Sn@CNT nanocable structures was carried out by a CVD method [6], as shown in Figure 2.1. In a typical process, pure Sn powders (2 g, −325 mesh, 99.8 %) were placed in an alumina boat located at the center of a quartz tube in a horizontal tube furnace. A small piece of commercially available carbon paper (ETEK, 0.17 mm thick, 81 % porosity) was placed aside of the metal powder, acting as the substrate. The reaction chamber was first heated to 850 °C rapidly (in about 15 min) from room temperature under an atmosphere of flowing Ar and 2 % ethylene (200 sccm), and then kept at 850 °C for 2 h. After the furnace was cooled down to

room temperature, a gray dark thin film was observed on the surface of the carbon paper substrate.
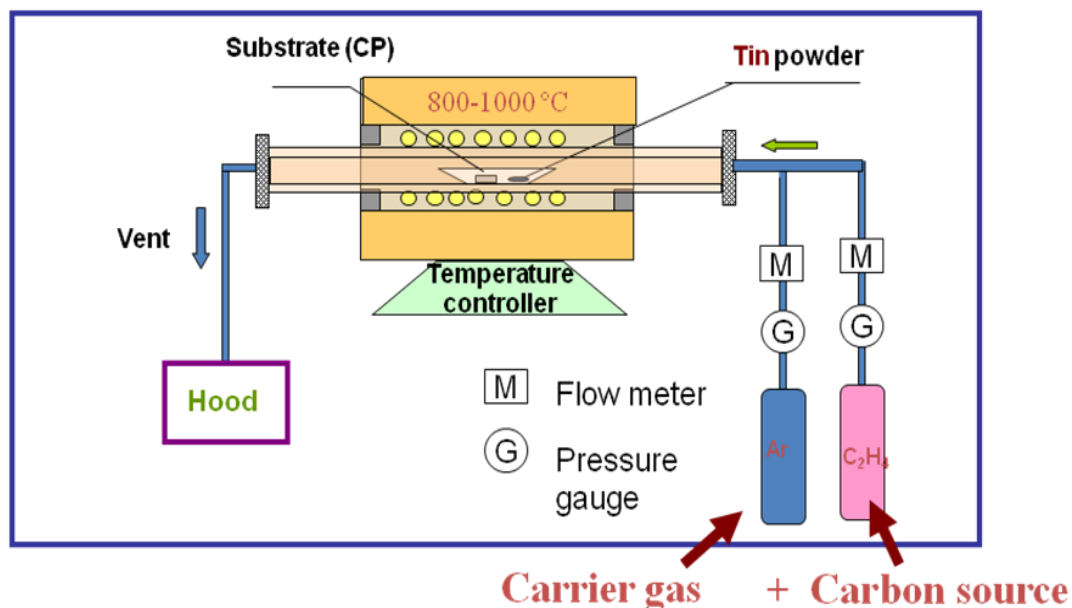
Figure 2.1. Schematic of CVD synthesis of Sn@CNT nanocables.

The synthesis of N-doped carbon nanotubes (N-CNTs) was carried out via CVD method too, as shown in Figure 2.2 [7]. Typically, pure melamine power (2 g) was placed in an alumina boat that was inserted at the entrance of a quartz tube in a horizontal tube furnace, while the substrate (carbon paper sputtered with 5 nm Fe film on the surface) was loaded in the centre of the quartz tube. The distance between the source and substrate was around 12 cm. The system was heated to 800 ^{o}C rapidly under an Ar flow of 320 sccm and kept at this temperature for 30 minutes, and then cool down to room temperature. A dark thin film was observed on the surface of the carbon paper substrate.
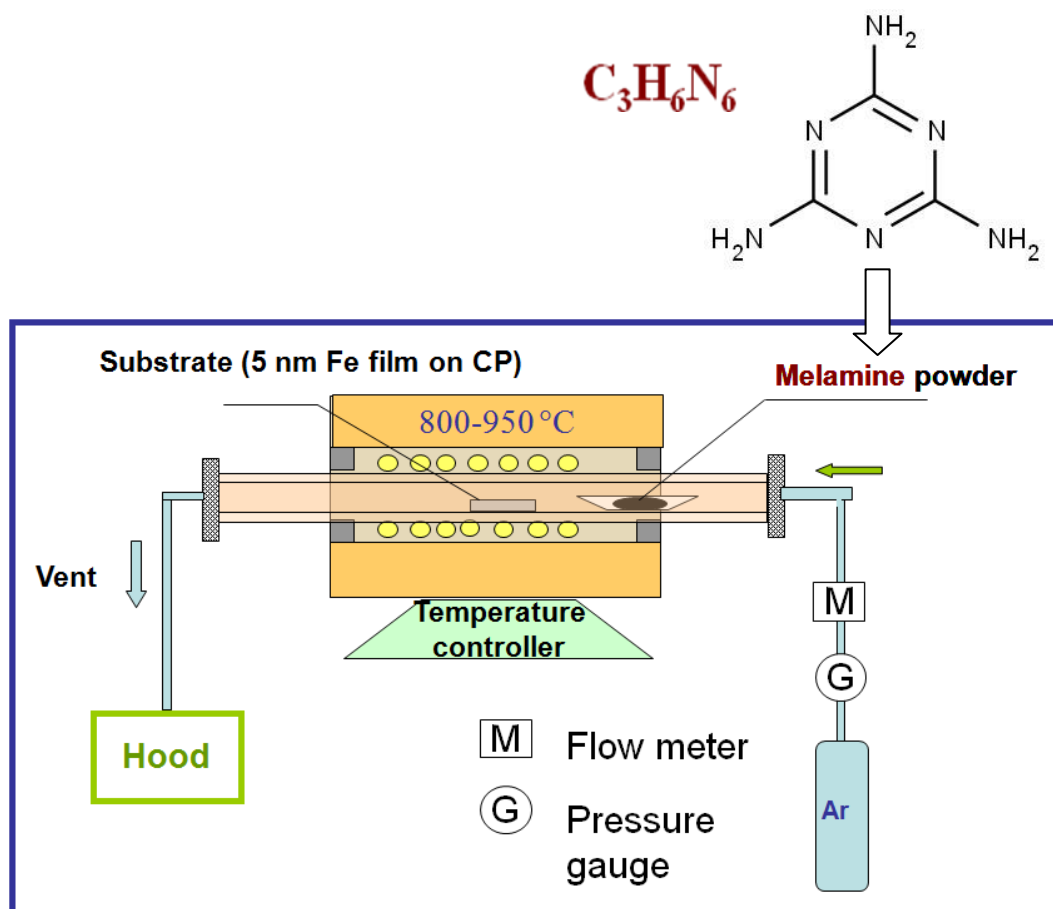
Figure 2.2. Schematic of CVD synthesis of N-CNTs.

2.1.3. Synthesis of Nb-TiO$_2$ hollow spheres via sol-gel method

The mesostructured Nb-TiO$_2$ support was prepared according to the method described in reference 8. Briefly, 0.015 g of hexadecyltrimethylammoniumbromide (HATB), 14.7 mL of aqueous latex suspension (Duke Scientific,10% by wt), and 105 mL of ethanol were added in a PTFE beaker, and then the solution was stirred vigorously for 30 min while HNO$_3$ was added to adjust the pH to 3. A second solution was prepared by adding the precursors, 6.9 mL of Titanium isopropoxide (TTIP) and 0.5 mL

niobium (V) ethoxide to 100 mL of ethanol. The second solution was added to the stirred latex-surfactant mixture using a peristaltic pump at a rate of 1 mL/min. The resulting suspension was processed using a Buchi B-290 spray drier to produce a fine white powder, consisting of the Nb–TiO$_2$ and latex template, which was followed by heat treatment at 500 ◦C for 2 h under argon in order to remove the latex template. To obtain rutile phase [9], the as-synthesized Nb–TiO$_2$ powder were heated at 1050 ◦C under hydrogen.

2.1.4. Synthesis of TiSi$_x$-NCNT via CVD and sputter deposition

TiSi$_x$-NCNT nanostructures were synthesized by a two-step approach through the combination of chemical vapour deposition (CVD) process and magnetron sputtering. In this process, nitrogen doped carbon nanotubes (NCNTs) were first synthesized on carbon paper which was pre-sputtered with an aluminum buffer layer (30 nm) and an iron catalyst layer (1 nm), via a CVD process at 800 ^{o}C. In this method, melamine was use as source for both carbon and nitrogen [10]. Then the carbon paper grown with N-CNTs was placed in a modified plasma enhanced CVD (PECVD)/sputtering system, 10 cm far from the sputtering target. Before the sputtering process, the chamber pressure was lowered to 1.9×10^{-5} torr to purge the oxygen from the system. Pure Argon was introduced into the system to adjust the pressure to 1.5×10^{-3} torr. During the sputtering process, a flow of 15 sccm Ar was maintained. A 100 nm layer of TiSi$_x$ is deposited on the NCNTs from a TiSi$_2$ (2-inch) target using a RF magnetron (150W, 10 min).

2.1.5. Synthesis of graphene via chemical method

Graphene nanosheets were synthesized via a modified Hummers method [11,12] which involves graphite oxidation, thermal exfoliation, and chemical reduction. In detail, natural graphite powder (1 g, 99.99%, Sigma-Aldrich) was first stirred in concentrated sulphuric acid (H$_2$SO$_4$, 23 mL) with a following addition of sodium nitrate (NaNO$_3$, 0.5 g) at room temperature. The stirring lasted for 16 h, and then the mixture was cooled down to 0 ◦C. Potassium permanganate (K$_2$MnO$_4$, 3 g) was then

added into the solution. After 2 h, the solution formed green slurry at around 35 ℃, which was stirred for another 3 h. Then, H$_2$O (46 mL) was slowly added at around 98 ℃. The suspension was kept at this temperature for 30 min before it was further diluted with another addition of water and hydrogen peroxide (H$_2$O$_2$, 140 mL). The suspension was subsequently filtered and washed until reaching a neutral pH, and dried in a vacuum oven at 60 ℃ to obtain graphite oxide (GO). To obtain graphene, the as-synthesized GO was heated at around 1050 ℃ in Ar atmosphere for 30 s in a tube furnace.

2.1.6. Synthesis of Pt nanoparticles and single atoms via atomic layer deposition (ALD)

Figure 2.3. Schematic diagram of an ALD process [13].

Atomic Layer Deposition (ALD) is a technique that allows the growth of discrete tiny nanoparticles and/or continuous thin films, atomic layer by layer, based on the

sequential use of a gas phase chemical process. The majority of ALD reactions use two chemicals, typically called precursors. These precursors react with a surface one-at-a-time in a sequential manner. By exposing the precursors to the growth surface repeatedly, tiny nanoparticles or thin films are formed. A schematic illustration of the sequential, self-limiting surface reactions during ALD is displayed in Figure 2.3 [13]. Generally, four steps are identified in each cycle: 1) pulse precursor 1 (reactant) into the reactor; 2) purge with inert gas (nitrogen or argon) to remove excess reactant molecules; 3) pulse precursor 2 (counter-reactant) to make a reaction with the molecules of precursor 1 on the substrate; 4) purge to remove products/excess counter-reactant. Repeat steps 1-4 as many times as desired, thereby to obtain a high quality film with excellent conformality and precise thickness.
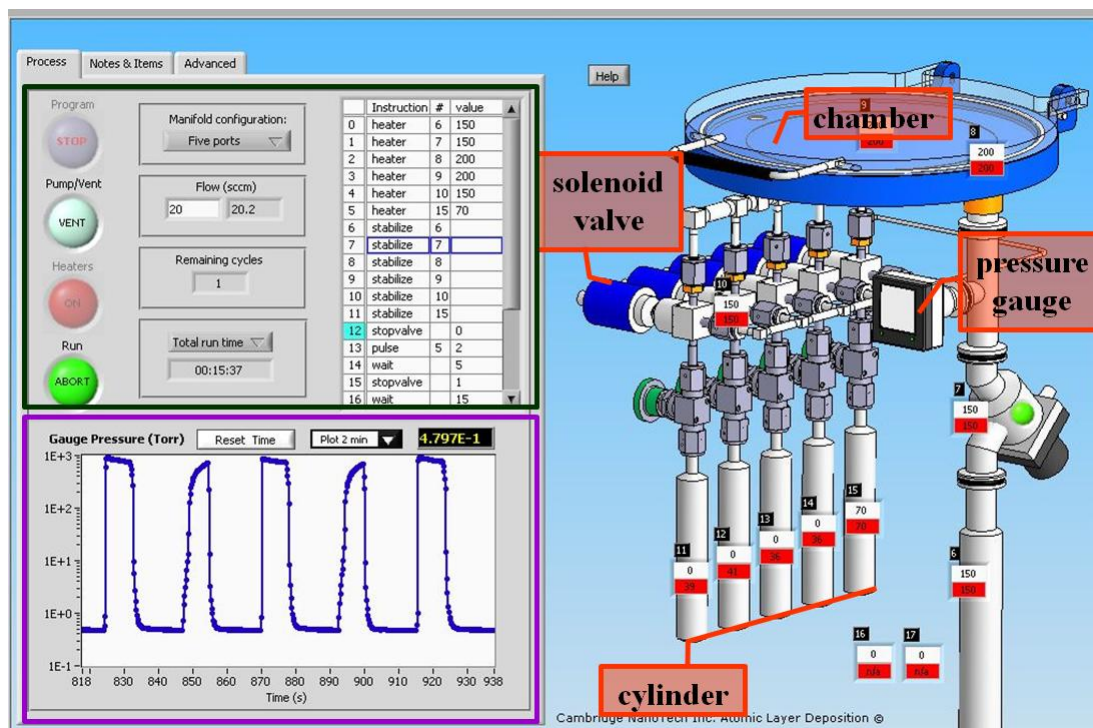
Figure 2.4. A screen snapshot on the LabVIEW program of the ALD system.

During ALD processes, the deposition behaviors are controlled by a LabVIEW program installed in the computer. ALD parameters such as temperatures, pressures, and precursor supplies can be set and operated via the program. Figure 2.4 shows a screen snapshot on the LabVIEW program. The right part shows the ALD system. The left upper part displays the inputted parameters; the lower part shows the changing curve of pressure.
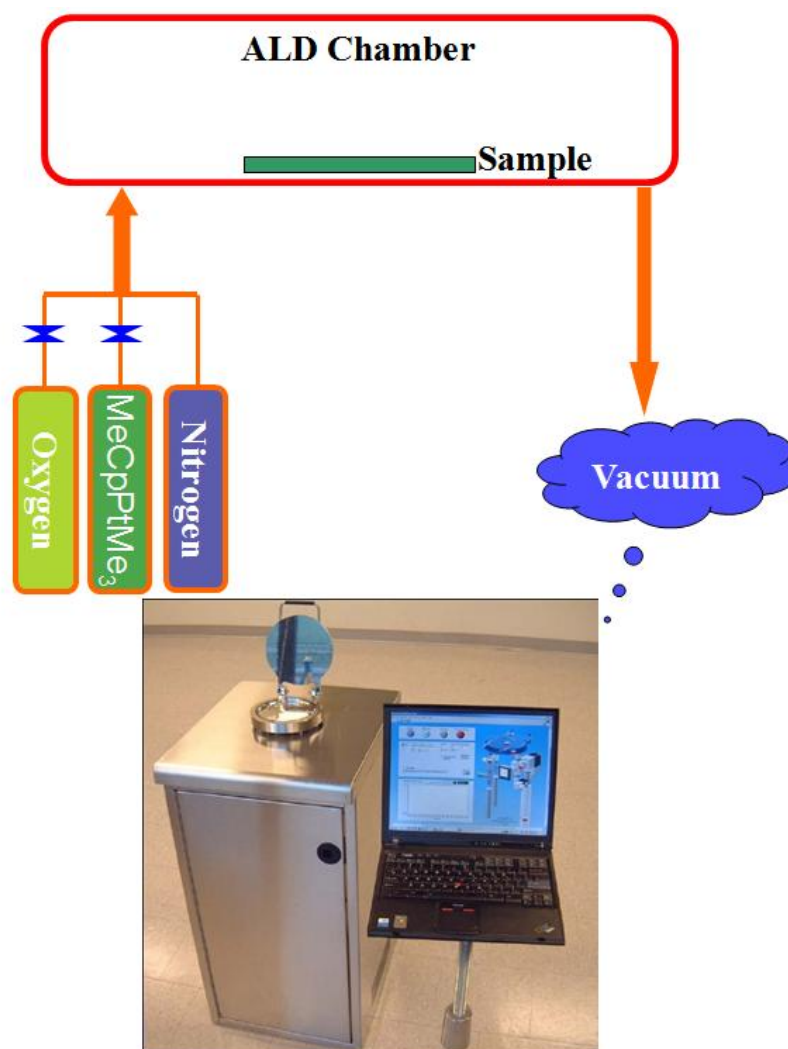
Figure 2.5. Experimental setup for ALD.

Platinum was deposited on graphene supports by ALD (Savannah 100, Cambridge Nanotechnology Inc., USA) using the (methylcyclopentadienyl)-trimethylplatinum (MeCpPtMe$_3$, Aldrich, purity 98 %) and oxygen (99.999 %) as precursors, and nitrogen (99.9995 %) as purge gas. The schematic illustration of the apparatus used for ALD is shown in Figure 2.5. It consists of a wall reactor with an outlet leading to a vacuum pump which can also prevent air from getting into the system. The inlet is connected to a system of valves which can control the delivery of purge gas and precursors. To increase the heat transfer from the stage to the graphene, hot wall conditions were replicated by placing graphene powder inside a machined stainless steel container with a perforated Al lid. The container for graphene was then placed inside the reactor directly on the heated stage. The wall and stage temperatures of the reactor were kept at 150 ^{o}C and 250 ^{o}C, respectively. The container for MeCpPtMe$_3$ was kept at 65 ^{o}C, providing a steady state flux of MeCpPtMe$_3$ to the reactor [14]. In each ALD cycle, 1 s of MeCpPtMe$_3$ pulse and 5 s of O$_2$ pulse were separated by 20 s of N$_2$ purge.

2.2   Characterization techniques

2.2.1. Physical characterization (SEM, TEM, EDX, XPS, XRD)

To fully understand physical and chemical properties of the samples, a variety of analytical techniques have been used in this thesis.

The scanning electron microscope (SEM) is capable of producing high-resolution images of a sample surface, which is one of the most widely employed instruments for directly studying solid surface structures. The as-prepared samples were examined by SEM (Hitachi S-4800) operated at 5kV. The instrument is shown in Figure 2.6.
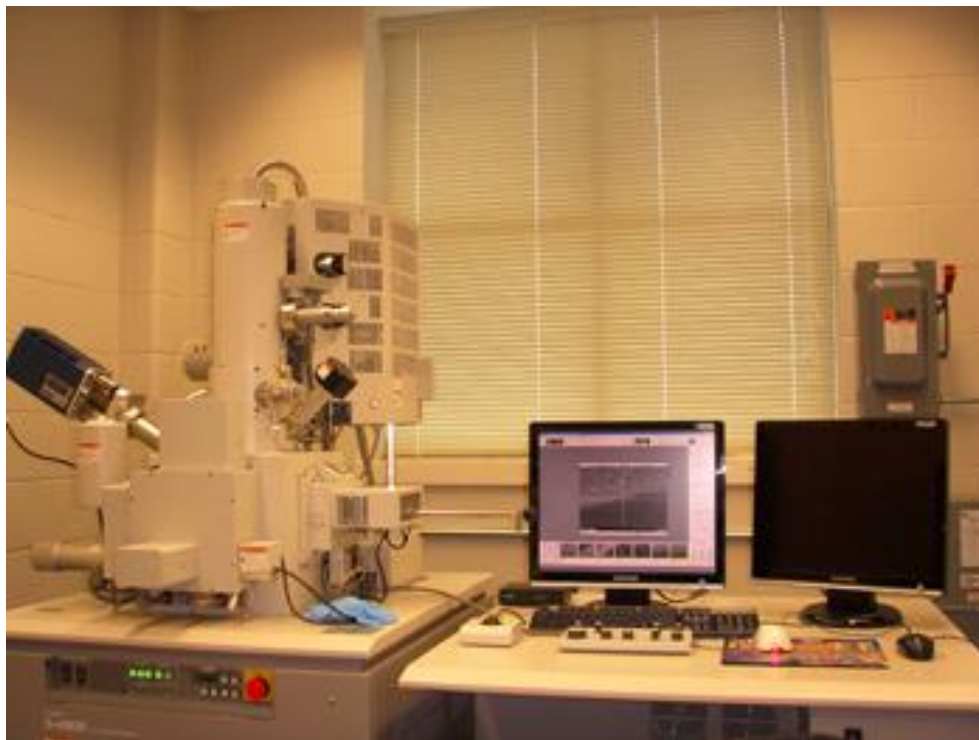
Figure 2.6. A photo of our SEM (Hitachi S-4800).

Transmission electron microscopy (TEM) is another widely used imaging technique to obtain structural information. In comparison to SEM, the resolution of the TEM is about an order of magnitude higher. As its name implies, the TEM specimens shall be prepared thin enough to transmit electrons. The regular TEM images were obtained via Philips CM10, as shown in Figure 2.7; while the high resolution TEM images were obtained via JEOL JEM-2100, operated at 200 kV. Subangstrom-resolution aberration-corrected scanning transmission electron microscopy (STEM, FEI Titan 80-300 Cubed TEM) was used to characterize the dispersion and configuration of Pt clusters and single atoms on graphene. The instrument is fitted with a Super-Twin lens in order to achieve sub-angstrom resolution both for phase contrast imaging and

STEM. Individual heavy atoms in practical catalysts can be discerned with atomic resolution in high angle annular dark field (HAADF) images.

Figure 2.7. A photo of our TEM (Philips CM10).

Energy dispersive X-ray spectroscopy (EDX) is an analytical technique used for the elemental analysis of characterization of a sample. Generally, EDX is in conjunction with either SEM or TEM. It relies on the investigation of a sample through interactions between electromagnetic radiation and matter, analyzing X-rays emitted from the sample during bombardment by an electron beam to characterize the elemental composition of the analyzed volume [15].
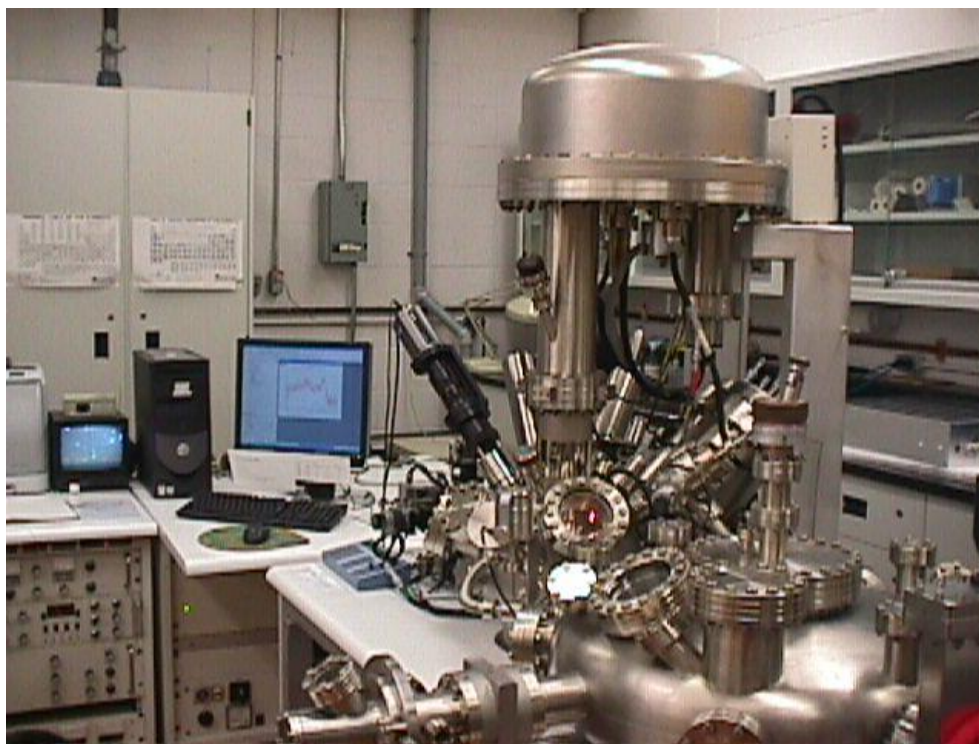
Figure 2.8. A photo of VG ESCALAB 220iXL XPS [19].

X-ray photoelectron spectroscopy (XPS), also known as ESCA (Electron Spectroscopy for Chemical Analysis), is an extremely surface-sensitive, non-destructive analytical technique, which is widely used to determine the elemental composition and chemical states of the surface and near surface regions of various materials [16-18]. The XPS analysis was carried out in a VG ESCALAB 220iXL, as shown in Figure 2.8, using monochromated Al Ka source (1486.6 eV), at a base pressure of 2×10^{-9} mbar. High resolution spectra were obtained at a perpendicular take-off angle, using a pass energy of 20 eV and steps of 0.05 eV. All the binding energies were calibrated by referring to the C1s line at 284.8 eV from adventitious carbon. After Shirley background removal, the component peaks were separated using the public domain XPSPeak program version 4.1.

Figure 2.9. A photo of Bruker D8 Advance XRD [20].

X-ray diffraction (XRD) is a versatile, non-destructive technique that reveals detailed information about the chemical composition and crystallographic structure of natural and manufactured materials. For our sample characterizations, the XRD patterns were recorded on a Bruker D8 Advance diffractometer (Figure 2.9) equipped with a Cu Ka radiation source.

2.2.2. Electrochemical characterization

The electrochemical characterizations of the catalysts were conducted in a standard three-compartment electrochemical cell using a glassy carbon (GC) rotating disk electrode (RDE) setup on an Autolab potentiostat/galvanostat (Model, PGSTAT-30, Ecochemie, Brinkman Instruments) with rotation control (MSR, Pine Instruments) (as shown in Figure 3.0). A Pt wire was used as the counter electrode and a Ag/AgCl (3 M NaCl) or saturated calomel electrode (SCE) was used as the reference electrode. For convenience, all potentials in this thesis are referenced to the reversible hydrogen electrode (RHE). The working electrode involved in this thesis is either a Pt/Sn@CNT/carbon paper, a Pt/TiSi$_x$-NCNT/carbon paper composite electrode or thin film electrode made from catalyst powders. The thin film electrode was prepared as follows. Typically, the catalyst dispersions (either Pt/CB, Pt/Nb-doped TiO$_2$ or Pt/graphene) were prepared by mixing 5 mg of catalyst in 5 mL aqueous solution containing 1 mL of isopropyl alcohol and 30 μL of 5 wt% Nanfion solution (4:1:0.0017 v/v/v) followed by 12 min ultrasonication. GC disk electrodes (5 mm diameter, 0.196 cm^2, Pine Research Instrument) served as the substrate for the catalyst and were polished to a mirror finish. An aliquot of catalyst suspension was pipetted onto the glassy carbon electrode. The catalyst films were dried under flow N$_2$ at room temperature.

2.2.2.1 Cyclic voltammetry (CV)

Each working electrode loaded with catalyst was first cycled between 0 and 1.2 V for 50 times in an Ar-purged H$_2$SO$_4$ solution (0.5 M) at room temperature, to produce a clean electrode surface. The scan rate used was 50 mV s^{-1}. Then the cyclic voltammetry (CV) measurements were conducted by cycling the potential between 0 and 1.2 V, with sweep rate of 50 mV s^{-1}. For each sample, at least three tests were run under the same condition, and all the data were very repeatable. The electrochemical surface areas (ECSA) were calculated by measuring the charge associated with the H$_{ads}$ (Q_H) between 0 and 0.4 V and assuming Q_{ref}=0.21 mC cm^{-2},
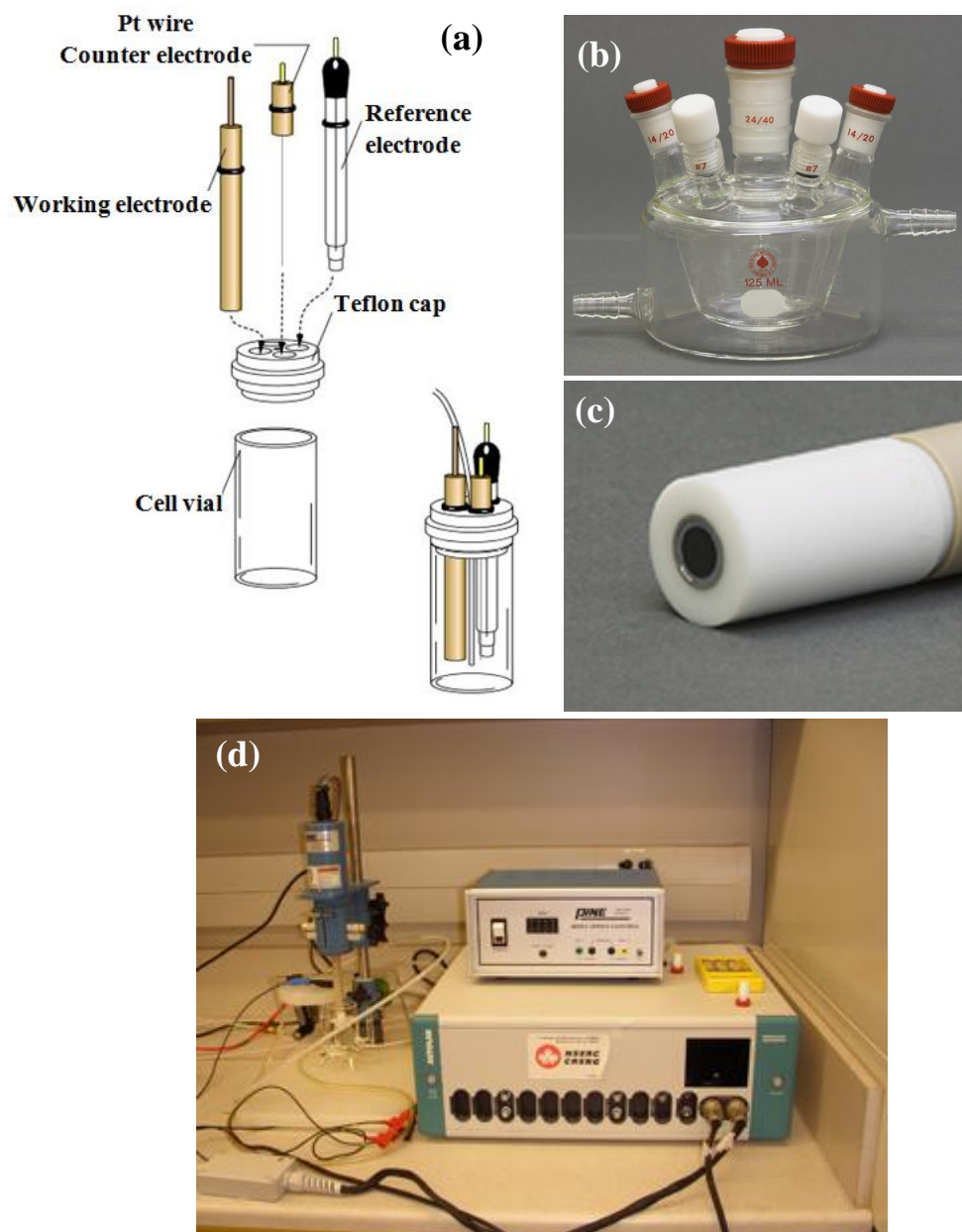
Figure 2.10. (a) diagram illustration of standard three-electrode cell; (b) Water-jacketed EuroCell; (c) RRED working electrode; (d) Autolab potentiostat/galvanostat (Model, PGSTAT-30, Ecochemie, Brinkman Instruments) with rotation control (MSR, Pine Instruments).

corresponding to a surface density of 1.3×10^{15} Pt atoms per cm^2, which is generally accepted for polycrystalline Pt electrodes. The ECSA of Pt was calculated based on the relation ECSA=$Q_H/(Q_{ref} m)$ where Q_H is the charge for H adsorption (mC cm^{-2}), m is the Pt loading (mg cm^{-2}) in the electrode, and Q_{ref} is the charge required for the monolayer adsorption of hydrogen on a Pt surface (0.21 mC cm^{-2}) [21]. The adsorption of hydroxy species was calculated based on the OH$_{ad}$ peak in the CV curves at the potential larger than 0.6 V. Dividing the hydroxy adsorption area by the overall active surface area resulted in the surface coverage of OH$_{ad}$ species (Θ_{OHad}).

2.2.2.2 Oxygen reduction reaction (ORR)

The catalytic activity for the oxygen reduction reaction (ORR) was evaluated by using the rotating ring-disk electrode (RRDE, Pine Instruments). O$_2$ was bubbled through the solution for 20 min to achieve saturation. With gentle O$_2$ bubbling, RRDE tests were conducted at 10 mV/s with a rotation speed of 1600 rpm (revolution per minute). Current densities were normalized in reference to the geometric area of the GC RDE (0.196 cm^2).

2.2.2.3 Methanol oxidation reaction (MOR) and CO stripping

The catalytic activity toward the methanol oxidation reaction was investigated in an air-free aqueous solution containing 1 M MeOH and 0.5 M H$_2$SO$_4$. During the methanol oxidation reaction carbon monoxide (CO) is formed, which strongly adsorbs onto the platinum catalyst, reducing the Pt active surface area and thus the degradation of fuel cell performance. Therefore, CO tolerance is an important parameter to evaluate the performance of a catalyst. For CO stripping voltammetry, pure CO (99.5%) was purged into the solution at a position close to the working electrode for 30 min to achieve saturation, with the electrode polarized at 0.05 V versus RHE in a fume hood. A monolayer of CO absorbed on the Pt surface was obtained by purging with N$_2$ for 30 min with the working electrode polarized at 0.05 V. Voltammetry was then applied to strip the CO. To test the CO adsorption rate,

30%CO/N_2 gas was purged into the solution at a position close to the working electrode for different time durations vary from 1 s to 20 min, with the electrode polarized at 0.05 V vs RHE in a fume hood. The excess CO was purged with Ar for 30 min under potential control followed by CO stripping at a scan rate of 50 mVs^{-1}.

2.2.2.4 Accelerated durability test (ADT)

The accelerated durability test [22] was conducted with a thin film electrode. The electrode was cycled between 0.6 and 1.2 V for 4,000 cycles in an O_2-saturated H_2SO_4 solution (0.5 M) at room temperature, with scan rate of 50 mV s^{-1}. Meanwhile, full-scale voltammograms between 0.05 and 1.2 V in N_2 saturated 0.5 M H_2SO_4 were recorded to track the degradation of the Pt catalysts. The scan rate was kept at 50 mV/s constantly.

References

[1]   S. H. Sun, D. Q. Yang, D. Villers, G. X. Zhang, E. Sacher, J. P. Dodelet, Template-free, Surfactant-free Room Temperature Synthesis of Self-Assembled 3D Pt Nanoflowers from Single-Crystal Nanowires. *Adv. Mater.* **2008**, *20*, 571–574.

[2]   S. H. Sun, D. Q. Yang, G. X. Zhang, E. Sacher, J. P. Dodelet, Synthesis and Characterization of Carbon Nanotube–Platinum Nanowire Heterostructures. *Chem. Mater.* **2007**, *19*, 6376–6378.

[3]   S. H. Sun, F. Jaouen, J. P. Dodelet, Controlled Growth of Pt Nanowires on Carbon Nanospheres and Their Enhanced Performance as Electrocatalysts in PEM Fuel Cells. *Adv. Mater.* **2008**, *20*, 3900–3904.

[4]   D. Q. Yang, S. H. Sun, H. Meng, J. P. Dodelet, E. Sacher, Formation of porous platinum nanoparticle froth for electrochemical applications, produced without templates, surfactants, or stabilizers. *Chem. Mater.* **2008**, *20*, 4677–4681.

[5]   D. Q. Yang, S. H. Sun, J. P. Dodelet, E. Sacher, A facile route for the self-organized high-density decoration of Pt nanoparticles on carbon nanotubes. *J. Phys. Chem. C* **2008**, *112*, 11717–11721.

[6]   R. Li, X. Sun, Y. Zhou, M. Cai, X. Sun**.** Aligned Heterostructures of Single-Crystalline Tin Nanowires Encapsulated in Amorphous Carbon Nanotubes. *J. Phys. Chem. C* **2007**, *111*, 9130–9135.

[7]   S. Trasobares, O. Stephan, C. Colliex, W. K. Hsu, H. W. Kroto and D. R. M. Walton, Compartmentalised CN_x nanotubes; Chemistry, morphology and growth. *J. Chem. Phys.*, 2002, **116**, 8966–8972.

[8]   M. Cai, Y. Lu, Z. Wu, L. Feng, M. Ruthkosky, J. Johnson, F. Wagner, Making electrocatalyst supports for fuel cells. US patent, 2010, Application number: 12/716360.

[9]   E. Traversa, M. L. Divona, S. Licoccia, M. Sacerdoti, M. C. Carotta, L. Crema, G. Martinelli. Sol-gel processed TiO_2-based nano-sized powders for use in thick-film gas sensors for atmospheric pollutant monitoring. *J. Sol–Gel Sci. Technol.* **2001**, *22*, 167–179.

[10]   Y. Zhong, M. Jaidann, Y. Zhang, G. Zhang, H. Liu, R. Li, X. Sun, H. Abou-Rachid, L. Lussier, Synthesis of High Nitrogen-Doping of Carbon Nanotubes and Modeling the Stabilization of Filled DAATO@CNTs (10, 10) for Nanoenergetic Materials. *J. Phys. Chem. Soli.* **2010**, *71*, 134–139.

[11]   W. S. Hummers, R. E. Offeman, Preparation of graphite oxide. *J. Am. Chem. Soc.* **1958**, *80*, 1339–1339.

[12]   D. Geng, S. Yang, Y. Zhang, J. Yang, J. Liu, R. Li, T. K. Sham, X. Sun, S. Ye, S. Knights. Nitrogen Doping Effects on the Structure of Graphene. *Applied Surface Science*, **2011**, *257*, 9193–9198.

[13]   M. Knez. K. Nielsch. L. Niinistö, Synthesis and surface engineering of complex nanostructures by atomic layer deposition, *Adv. Mater.* **2007**, *19*, 3425–3438.

[14]   C. Liu, C. C. Wang, C. C. Kei, Y. C. Hsueh, T. P. Perng, Atomic Layer Deposition of Platinum Nanoparticles on Carbon Nanotubes for Application in Proton-Exchange Membrane Fuel Cells. *Small* **2009**, *5*, 1535–1538.

[15]   J. C. Russ, Fundmentals of energy dispersive x-ray analysis, Butterworths, London-Toronto, 1984.

[16]   R. M. Wang, C. L. Chu, T. Hu, Y. S. Dong, C. Guo, X. B. Sheng, P. H. Lin, C. Y. Chung, P. K. Chu, Surface XPS characterization of NiTi shape memory

alloy after advanced oxidation processes in UV/H$_2$O$_2$ photocatalytic system. *Appl. Surf. Sci.* **2007**, *253*, 8507–8512.

[17] Z. Q. Jiang, W. H. Zhang, L. Jin, X. Yang, F. Q. Xu, J. F. Zhu, W. X. Huang, Direct XPS evidence for charge transfer from a reduced rutile TiO$_2$ (110) surface to Au clusters. *J. Phys. Chem. C* **2007**, *111*, 12434–39.

[18] J. H. Zhou, Z. J. Sui, J. Zhu, P. Li, D. Chen, Y. C. Dai, W. K. Yuan, Characterization of surface oxygen complexes on carbon nanofibers by TPD, XPS and FT-IR. *Carbon* **2007**, 45, 785–796.

[19] http://lmn.emt.inrs.ca/FR/FichesLMN/Fiche_20.htm.

[20] http://www.bruker-axs.com/d8_advance.html.

[21] T. J. Schmidt, H. A. Gasteiger, G. D. Stab, P. M. Urban, D. M. Kolb, R. J. Behm, Characterization of high-surface-area electrocatalysts using a rotating disk electrode configuration. *J. Electrochem. Soc.* **1998**, *145*, 2354–2358.

[22] J. Zhang, K. Sasaki, R. R. Adzic, Stabilization of platinum oxygen-reduction electrocatalysts using gold clusters, *Science*, **2007**, *315*, 220–222.

Chapter 3. A Highly Durable Platinum Nanocatalyst for Proton Exchange Membrane Fuel Cells: Multiarmed Starlike Nanowire Single Crystal

Shuhui Sun[1], Gaixia Zhang[1], Dongsheng Geng[1], Yougui Chen[1], Ruying Li[1], Mei Cai[2], and Xueliang Sun[1,]*

[1]*Department of Mechanical and Materials Engineering, The University of Western Ontario, London, Ontario, N6A 5B9 (Canada)*
[2]*General Motors Research and Development Center, Warren, MI 48090-9055 (USA)*
E-mail: xsun@eng.uwo.ca

PEM fuel cells produce electricity through the electrochemical oxidation of hydrogen (or other small molecules) at the anode and the reduction of oxygen at the cathode, and both reactions need to be conducted on catalyst surfaces. At present, Pt is currently the most efficient electrocatalyst (which is very hard to replace) in practical PEM fuel cells due to its outstanding catalytic and electrical properties and superior resistant characteristics to corrosion. However, since Pt is very expensive and rare, people must find ways to reduce the Pt loading without compromising fuel cell performance in order to meet the cost requirements for fuel cell commercialization. In other words, the design of novel Pt catalyst requires not only reducing the amount of Pt used, but also enhancing its catalytic activity and durability.

It is well accepted that the catalytic activity and durability of Pt catalysts are not only dependent on their size but also their shape. In contrast to the commercially-used Pt

spherical nanoparticles, one-dimensional (1D) structures of Pt, such as nanowires (NWs), exhibit additional advantages associated with their anisotropy and unique structure. Pt NWs have been demonstrated exhibiting enhanced activity and durability, for oxygen reduction reaction (ORR) and methanol oxidation reaction (MOR), than Pt nanoparticle based commercial Pt/C catalyst.

In this chapter, the authors report a novel approach to address both activity and durability challenges of PEM fuel cells by using star-like single-crystal platinum nanostructures, each with several nanowire arms with diameters of ~4 nm, on carbon black (star-like PtNW/C) as electrocatalyst. Pt NWs were synthesized via an environmentally-friendly aqueous solution route at room temperature, without the need of heating, surfactants or complicated experimental apparatus. This novel nanostructure showed much improved activity and durability than the state-of-the-art commercial Pt/C catalyst that is made of Pt nanoparticles. Moreover, the durability can be further improved (5.2 and 3.1 times better than that of E-TEK Pt/C and carbon-supported PtNW catalysts, respectively) by using supportless Pt nanowires as the electrocatalyst.

Due to their unique 1D morphology, the star-like Pt nanowire electrocatalyst can provide various advantages including: First, the interconnected network consists of multiarmed star shape and tens nanometers length of 1D NWs which makes the Pt less vulnerable to dissolution, Ostwald ripening, and aggregation during fuel cell operation compare to Pt nanoparticles; second, this network structure reduces the embedded sites of electrocatalyst in the microspores of carbon black supports which commonly happens to nanoparticles; third, the mass transfer within the electrode can be effectively facilitated by networking the anisotropic morphology.

3.1 Introduction

Despite significant recent advances, the long-term durability of Pt catalyst at the cathode is still being recognized as one of the key challenges that must be addressed before the commercialization of proton exchange membrane fuel cells (PEMFCs) [1,2]. The loss of Pt electrochemical surface area (ECSA) over time, because of corrosion of the carbon support and Pt dissolution/aggregation/Oswald ripening, is considered one of the major contributors to the degradation of fuel cell performance [3]. Up to now, highly dispersed Pt nanoparticles (NPs, 2–5 nm) on carbon supports are still being widely used as the state-of-the-art commercial catalysts, and most reported studies are focused on nanoparticles of Pt [4]. However, Pt with nanosized particle morphologies has high surface energies, thereby inducing severe Oswald ripening and/or grain growth during fuel cell operation.

One-dimensional (1D) nanostructures of Pt, such as nanowires (NWs) and nanotubes (NTs), have been demonstrated to overcome the drawbacks of NPs in fuel cells, owning to their unique 1D morphologies [5-11]. Yan et al. [11] reported that unsupported Pt nanotubes exhibit much enhanced catalytic activity and durability as fuel cell cathode catalyst. Sun et al. [9] and Zhou et al. [10] reported the improved oxygen reduction reaction (ORR) activities of Pt NWs at the cathode under fuel cell operating conditions. However, up to now, the durability of Pt NW-based electrocatalysts has never been reported in the literature.

Here we describe a new approach to address, for the first time, both the activity and durability issues by using carbon-supported multiarmed starlike Pt nanowires (starlike PtNW/C) as electrocatalysts. Interestingly, the durability can be further improved by eliminating the carbon support, that is, using unsupported Pt nanowires as the cathode catalyst. As a result of their unique 1D morphology, the starlike Pt nanowire electrocatalyst can provide various advantages. First, the interconnected network consists of multiarmed, star-shaped 1D NWs with arm lengths of tens of nanometers which makes the Pt less vulnerable to dissolution, Ostwald ripening, and

aggregation during fuel cell operation compared to Pt nanoparticles [11]. Second, this network structure reduces the number of embedded electrocatalyst sites in the micropores of the carbon supports relative to those in nanogrannular Pt. Third, the mass transfer within the electrode can be effectively facilitated by networking the anisotropic morphology [12].

3.2 Experimental

3.2.1 Synthesis of platinum nanowires

Platinum nanowires were synthesized by the chemical reduction of Pt precursor with formic acid [13]. All the experiments were conducted in aqueous solution, at room temperature and under ambient atmosphere. In a typical synthesis, 0.032 g hexachloroplatinic acid (H_2PtCl_6 6 H_2O, 99.95 %, Aldrich) and 1 mL formic acid (HCOOH, 98 %, Aldrich) were dissolved in 20 mL H_2O and stored at room temperature for 72 h. The solution turned from golden-orange to grey and then to dark brown. All aqueous solutions were prepared with ultrapure water from a Barnstead Nanopure water system. For the growth of 40 wt % Pt on carbon, a suspension of 7.5 mg carbon black (Vulcan XC72R) in 21 mL reaction solution (14.67 mg H_2PtCl_6 6 H_2O and 1 mL HCOOH in 20 mL of water) was sonicated for 30 min. After this initial dispersion, the solution is stored at room temperature for 72 h. The product was collected by centrifugation and washed several times with water, and then dried in an oven at 60 °C for further use in characterization and electrochemical measurements.

3.2.2 Physical characterizations

Scanning electron microscopy (SEM) images were taken on a Hitachi S-4800 microscope, operating at 5 kV. Transmission electron microscopy (TEM) observations were performed with a Philips CM10 microscope at an accelerating voltage of 100 kV. High-resolution TEM (HRTEM) images were obtained with a

JEOL 2010F microscope, operating at 200 kV. The Pt loading were confirmed by inductively coupled plasma-optical emission spectroscopy (ICP-OES).

3.2.3 Electrochemical characterizations

Electrochemical properties of the catalysts were measured on an Autolab potentiostat/galvanostat (Model, PGSTAT-30, Ecochemie, Brinkman Instruments) with rotation control (MSR, Pine Instruments) using a three-electrode system that consists of a glassy carbon (GC) rotating disk electrode (RDE), a Pt wire counter electrode, and a Ag/AgCl (3 M NaCl) reference electrode which was separated from the working electrode compartment by a closed electrolyte bridge. For convenience, all potentials in this study are referenced to the reversible hydrogen electrode (RHE). The working electrode was prepared with a procedure similar to the one reported previously [20]. Typically, the catalyst dispersions were prepared by mixing 5 mg of catalyst in 5 mL aqueous solution containing 1 mL of isopropyl alcohol and 30 μL of 5 wt % Nanfion solution (4:1:0.0017 v/v) followed by 12 min ultrasonication. GC disk electrodes (5 mm diameter, 0.196 cm^2, Pine Research Instrument) served as the substrate for the support and were polished to a mirror finish. An aliquot of catalyst suspension was pipetted onto the carbon substrate, leading to a Pt loading of about 6 μg$_{Pt}$ for all catalysts. The catalyst films were dried under flow N$_2$ at room temperature.

The working electrode was first cycled between 0 and 1.2 V for 50 times in an Ar-purged H$_2$SO$_4$ solution (0.5 M) at room temperature, to produce a clean electrode surface. The scan rate used was 50 mV s^{-1}. Then the cyclic voltammetry (CV) measurements were conducted by cycling the potential between 0 and 1.2 V, with sweep rate of 50 mV s^{-1}. The electrochemical surface areas (ECSA) were calculated by measuring the charge associated with the H$_{ads}$ (Q_H) between 0 and 0.4 V and assuming Q_{ref}=0.21 mC cm^{-2}, corresponding to a surface density of 1.3×10^{15} Pt atoms per cm^2, which is generally accepted for polycrystalline Pt electrodes. The ECSA of Pt was calculated based on the relation ECSA=$Q_H/(Q_{ref} m)$ where Q_H is the charge for H adsorption (mC cm^{-2}), m is the Pt loading (mg cm^{-2}) in the electrode, and Q_{ref} is the

charge required for the monolayer adsorption of hydrogen on a Pt surface (0.21 mC cm^{-2}) [17a]. The adsorption of hydroxy species was calculated based on the OH$_{ad}$ peak in the CV curves at the potential larger than 0.6 V. Dividing the hydroxy adsorption area by the overall active surface area resulted in the surface coverage of OH$_{ad}$ species (Θ_{OHad}) [3c]. The oxygen reduction reaction (ORR) experiments were performed in oxygen-saturated H$_2$SO$_4$ solution (0.5 M) at room temperature. The RDE rotating rate was 1600 rpm and sweep rate was 10 mV s^{-1}. Current densities were normalized in reference to the geometric area of the GC RDE (0.196 cm^2). The CV measurements for accelerated durability test (ADT) were conducted by potential cycling between 0.6 and 1.2 V (vs. RHE) for 4000 cycles in O$_2$-saturated H$_2$SO$_4$ solution (0.5 M) at room temperature, with scan rate of 50 mV s^{-1}. Meanwhile, full-scale voltammogram between 0.0 and 1.2 V in N$_2$-saturated H$_2$SO$_4$ solution (0.5 M) were recorded periodically to track the degradation of Pt catalysts.

3.3. Results and Discussion

Carbon-supported multiarmed starlike platinum nanowires were synthesized by the chemical reduction of a Pt precursor with formic acid in aqueous solution at room temperature and under ambient atmosphere [13]. No surfactant, which is usually harmful for catalytic activities, was used in the experiments.

Figure 3.1 A and B show the representative scanning electron microscopy (SEM) and transmission electron microscopy (TEM) images, respectively, of carbon-supported Pt nanowires at 40 wt% loading of Pt. It can be seen that the as-synthesized Pt is nanostar-shaped, being composed of several short arms of Pt nanowires. The number of arms of each nanostar is found to vary ranging from several to over ten. Occasionally, single-armed nanowires standing on the carbon surface can also be observed. Diameter and length of the arms of starlike Pt nanowires are about 4 nm and 15 nm, respectively. More interestingly, from the connected atomic arrangement shown in the high-resolution TEM (HRTEM) images (see Figure SI-3.1 in the
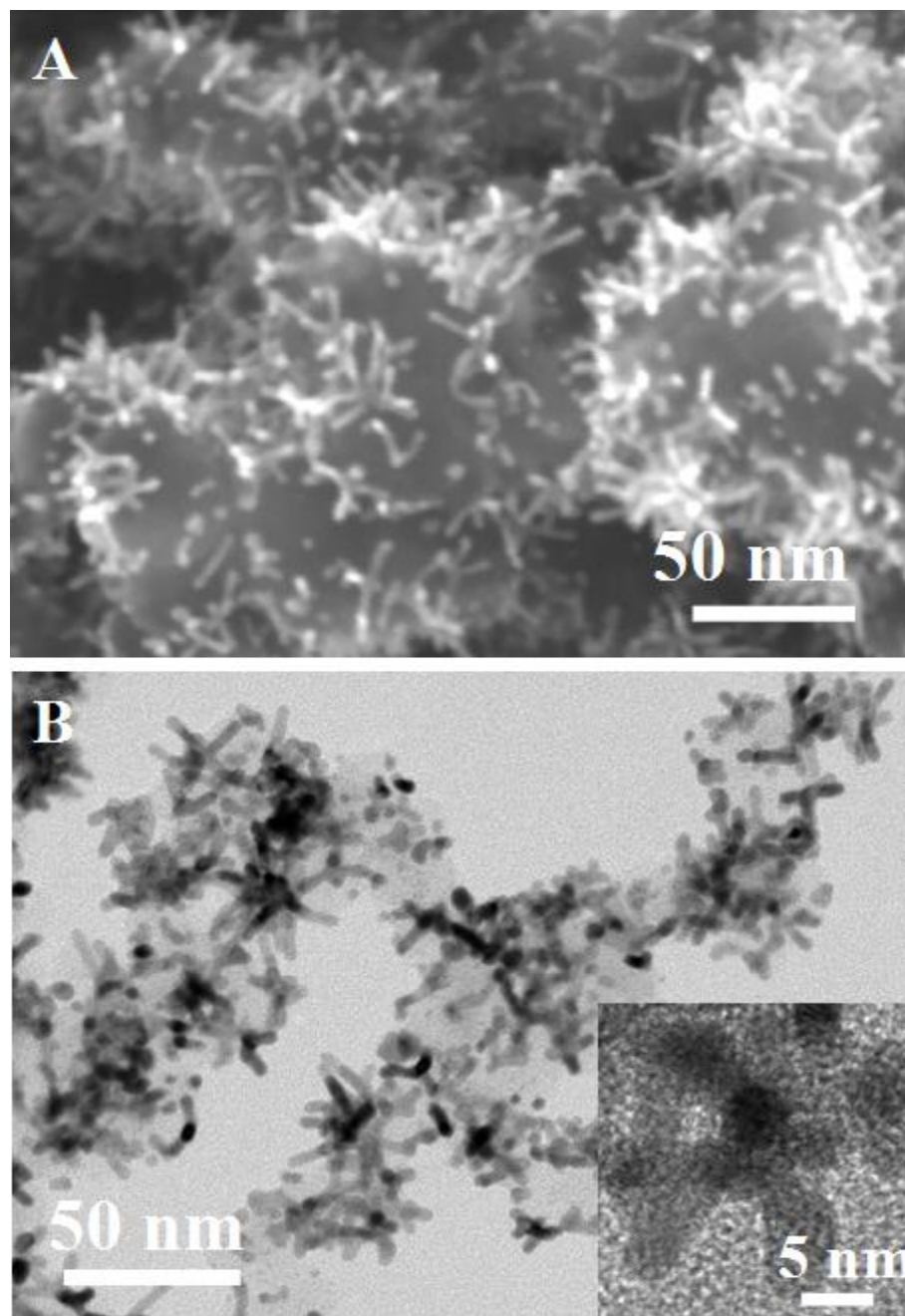
Figure 3.1. A) SEM and B) TEM image of carbon-supported multiarmed starlike Pt nanowire catalyst.

Supporting Information and the inset in Figure 3.1 B), the nanostar is found to be a single crystal. The fast Fourier transform (FFT; see inset in Figure SI-3.1) of the original HRTEM image shows a dotted pattern, further proving that the nanostar is a single crystal. This indicates that the formation mechanism of the nanostar involves seeded growth rather than an aggregation of seeded particles or an assembly process of the nanowires [14]. The X-ray diffraction (XRD) pattern (Figure SI-3.2) confirms that the carbon-supported Pt nanowires are crystallized in a face-centered-cubic (fcc) structure similar to bulk Pt [15], which is consistent with the HRTEM investigations.

We believe that the growth of the multiarmed starlike PtNWs on carbon black supports follows a similar process to that for Pt NWs on other supports [13b]. Typically, Pt nuclei are first formed in solution through the reduction of H_2PtCl_6 by HCOOH, and they deposit on the surface of carbon spheres. The freshly formed nuclei act as the sites for further nucleation through the continual absorption and reduction of Pt(IV) ions leading to the formation of particle seeds. For fcc structures, the sequence of surface energies is $\gamma_{\{111\}} < \gamma_{\{100\}} < \gamma_{\{110\}}$, which implies the single-crystal seeds are expected to exist finally as truncated octahedrons enclosed by a mix of {111} and {100} facets in order to maximize the expression of {111} facets and minimize the total surface energy [16]. As the reaction is conducted at room temperature, the reduction rate is very low; therefore, according to the lowest-energy principle, the anisotropic growths along the closed-packed <111> directions are enhanced [13a]. Finally, multiarmed starlike PtNWs are formed based on the truncated octahedron seeds which have several {111} facets. The exact formation mechanism is still under investigation. However, we believe that the key is to reduce the reduction rate of Pt ions, which favors the growth of {111} planes and therefore leads to the formation of 1D nanowires.
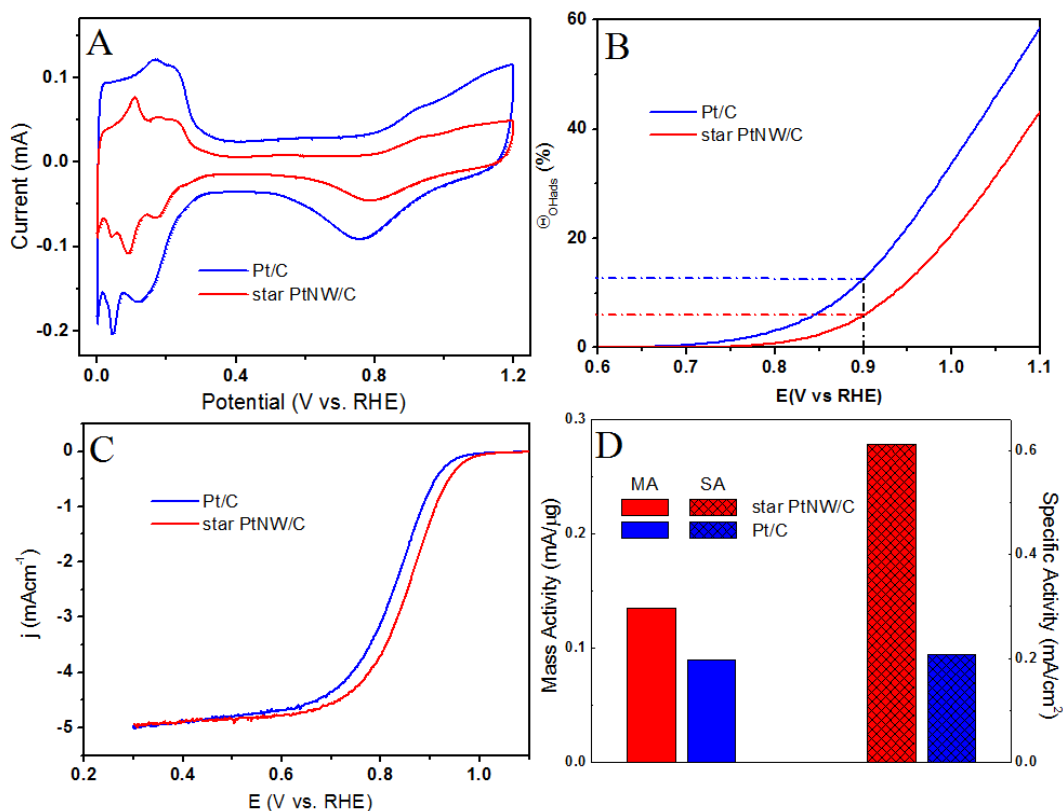
Figure 3.2. A) CV curves and B) hydroxy surface coverage (Θ_{OH}) for Pt/C (E-TEK, blue curve) and starlike PtNW/C (40 wt % Pt; red curve) catalysts. C) Polarization curves for ORR of Pt/C (E-TEK; blue curve) and starlike PtNW/C catalysts (red curve) in O_2-saturated 0.5 M H_2SO_4 solution at room temperature (1600 rpm, sweep rate 10 mV s^{-1}). D) Mass activity and specific activity at 0.9 V (vs. RHE) for the two catalysts.

We benchmarked the electrochemical properties of starlike PtNW/C against a commercial catalyst made of Pt nanoparticles on carbon support (E-TEK, 30 wt % Pt). Figure 3.2 A shows the cyclic voltammetry (CV) curves of these two catalysts recorded at room temperature in an Ar-purged H_2SO_4 solution (0.5 M) with a sweep rate of 50 mV s^{-1}. Both CV curves exhibit strong peaks associated with hydrogen adsorption/desorption and Pt oxide formation/reduction. Well-defined multiple

hydrogen adsorption and desorption peaks on different Pt low-index surfaces became more definable for the carbon-supported Pt nanowire catalyst. The electrochemical surface areas (ECSA) were calculated by measuring the charge associated with the H_{ads} (Q_H) between 0 and 0.4 V and assuming Q_{ref}=0.21 mC cm^{-2} for the adsorption of a hydrogen monolayer [17], corresponding to a surface density of 1.3×10^{15} Pt atoms per cm^2, which is generally accepted for polycrystalline Pt electrodes. The specific ECSA of the starlike PtNW/C was 22.1 m^2 g^{-1} Pt, which is about half (51 %) of that of commercial E-TEK Pt/C catalyst (43.3 m^2 g^{-1} Pt). Interestingly, the dimensional change of Pt nanostructures from particle (0D) to wire (1D) also greatly altered the ability to adsorb hydroxy species (OH$_{ad}$, E>0.6 V) (Figure 3.2 B). Both the onset and peak potentials for the starlike PtNW/C show positive shifts compared with E-TEK carbon-supported Pt nanoparticles on the backward sweep, indicating the fast hydroxy desorption from the Pt nanowires surface [3c].

Figure 3.2 C shows typical ORR polarization curves of starlike PtNW/C and Pt/C (E-TEK) catalysts obtained at room temperature in oxygen-saturated 0.5 M H$_2$SO$_4$ by using a glassy carbon rotating disk electrode (RDE) at 1600 rpm. The half-wave potentials for the starlike PtNW/C and Pt/C catalysts were 0.848 and 0.813 V, respectively, indicating that the catalytic activity of carbon-supported starlike PtNWs was higher than that of the commercial Pt/C catalyst made of Pt nanoparticles. Mass activity and specific activity are good indicators of the quality of an electrocatalyst. As shown in Figure 3.2 D, starlike PtNW/C exhibited a mass activity of 0.135 mA μg^{-1} Pt at 0.9 V (vs. RHE), which is 1.5-times greater than that of the Pt/C (E-TEK) catalyst (0.09 mA μg^{-1} Pt). Interestingly, this improvement occurred in spite of about a 50 % lower Pt active surface area for starlike PtNW/C catalyst. Taking into account both effects, a specific ORR activity for the starlike Pt NW/C of 0.611 mA cm^{-2} Pt was obtained at 0.9 V, which was nearly three times that for E-TEK Pt/C catalyst (0.207 mA cm^{-2} Pt). This improvement agrees well with those reported for Pt NWs obtained under full cell operating conditions [9].
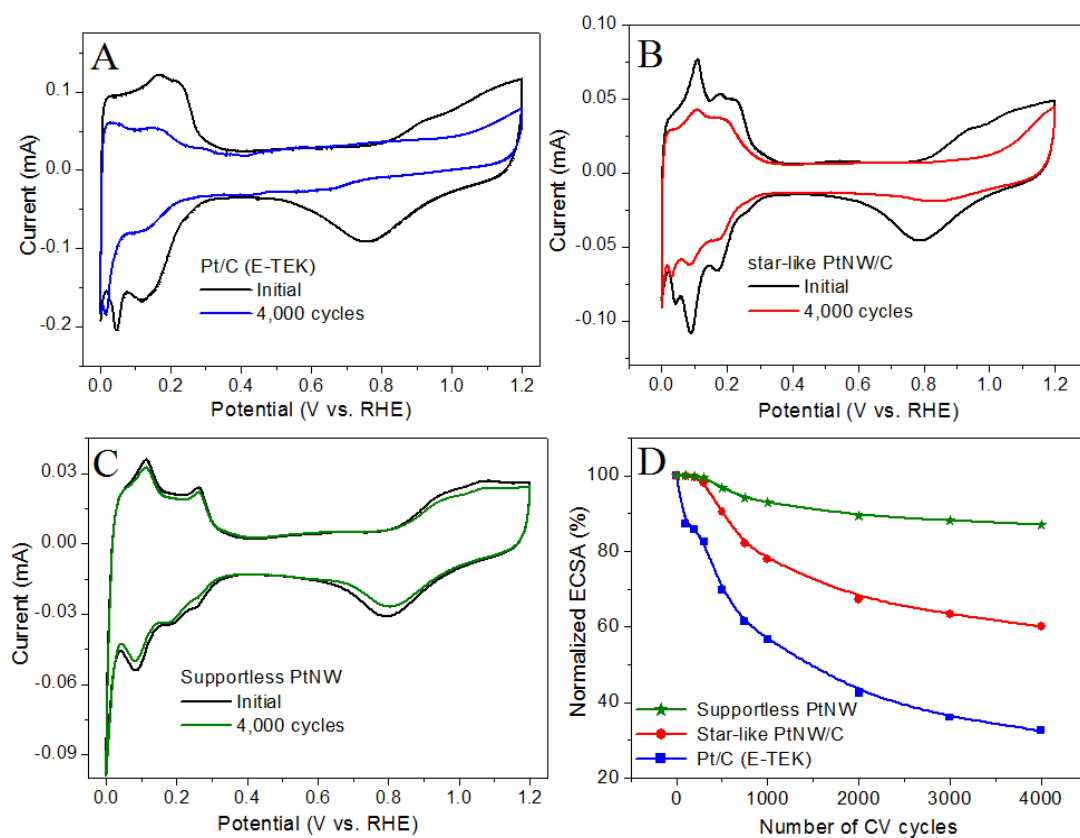
Figure 3.3. CV curves for A) Pt/C (E-TEK), B) starlike PtNW/C, and C) unsupported PtNW catalysts before (black curves) and after 4000 cycles (blue, red, and green curves). D) Loss of electrochemical surface area (ECSA) of Pt/C (E-TEK; blue), starlike PtNW/C (red), and unsupported PtNW catalysts (green) as a function of cycling numbers in O_2-purged 0.5 M H_2SO_4 solution at room temperature (0.6–1.2 V vs RHE, sweep rate 50 mV s^{-1}).

The improved activity for the starlike nanowires compared with nanoparticles of Pt could be due to several factors, including 1) the changes in morphology (1D vs. 0D) because the 1D shape could facilitate the reaction kinetics and improve the O_2 diffusion to Pt surface; 2) fewer surface defects borne by the nanowires which have a closer resemblance to the surface of large single Pt crystals that exhibit even higher ORR specific activities; and 3) the preferential exposure of certain crystal facets of Pt nanowires since the different low-index surfaces have markedly different activities [9,11,18]. In addition, the adsorbed OH_{ad} species on the Pt surface could block the active surface for O_2 adsorption and thus have a negative impact on the ORR. Pt NWs bear comparatively smooth atomic surfaces, which have a small number of low coordination atoms, thus they are more active than surfaces with a high concentration of such sites because of the reduced interaction with OH species. Therefore, the low OH_{ad} coverage on the surface of carbon-supported starlike Pt NW catalyst helps to improve the ORR kinetics, resulting in enhanced activities [19].

The accelerated durability tests (ADT) of the catalysts were conducted by potential cycling between 0.6 and 1.2 V vs. RHE in O_2-purged H_2SO_4 solution (0.5 M) at room temperature, with scan rate of 50 mV s^{-1}. After 4000 cycles, the starlike PtNW/C catalyst had lost 40 % of the Pt initial ECSA (Figure 3.3 B and D) and showed a degradation of 20 mV in the half-wave potential (Figure SI-3.3B), while the degradation of E-TEK Pt/C catalyst was quite severe, with 67.5 % loss of the initial Pt ECSA (Figure 3.3 A and D) and a large decrease of 88 mV in the half-wave potential (Figure SI-3.3A). Interestingly, the durability of Pt nanowire catalyst could be further improved by removing the corrosion effect of the carbon support. The ADT tests (Figure 3.3 C and D) showed that the Pt ECSA of the unsupported Pt NWs decreased about 13 % after 4000 cycles, which was 5.2- and 3.1-times better than that of E-TEK Pt/C and carbon-supported PtNW catalysts, respectively. In addition, it showed a quite small negative shift of 9 mV in the half-wave potential (Figure SI-3.3C).
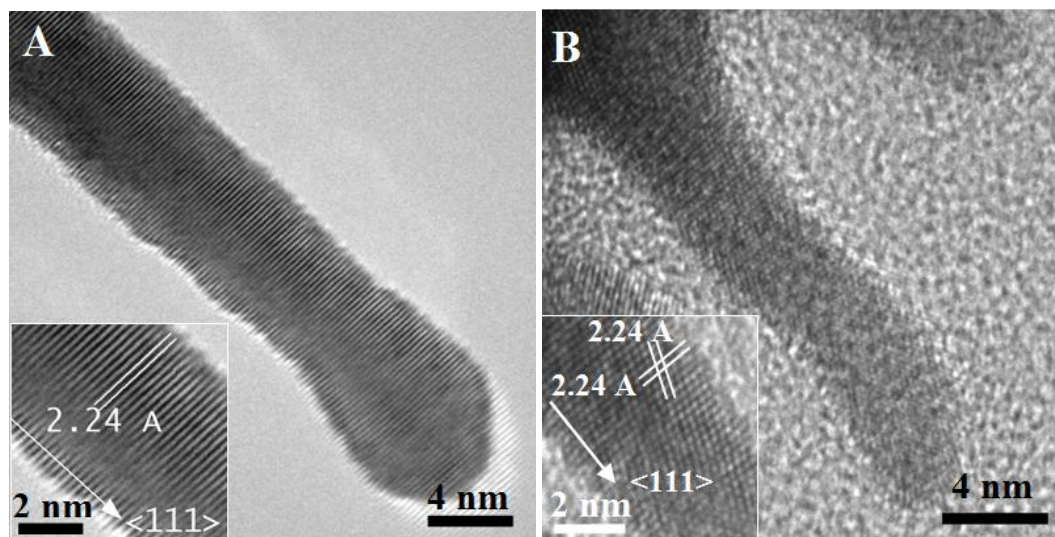
Figure 3.4. TEM images of unsupported Pt NW A) before, and B) after accelerated CV test. Insets of (A) and (B) show the corresponding HRTEM images, respectively.

The morphology changes of the E-TEK Pt/C, carbon-supported starlike Pt NWs, and unsupported Pt NWs were investigated by TEM before and after ADT cycling (Figure 3.4 and Figure SI-3.4). The Pt nanoparticle size in the E-TEK Pt/C commercial catalyst increased from 2–5 nm to 5–25 nm (by a factor of up to 5). In addition, the density of Pt particles on carbon became much less, confirming that the major cause for the Pt ECSA loss of Pt/C catalyst was by Pt nanoparticle ripening, the aggregation and falling off of Pt because of corrosion of the carbon support. By contrast, there were no obvious morphological changes for the carbon-supported Pt NW catalyst after ADT cycling. Their star shape and 1D morphology remained the same, with slight aggregation, which might be a result of the corrosion of the carbon support. Meanwhile, the unsupported Pt NWs maintained their 1D morphology and the <111> growth direction after 4000 cycles of ADT test. The diameters of Pt NWs decreased slightly and their surfaces (especially the edges) became rough
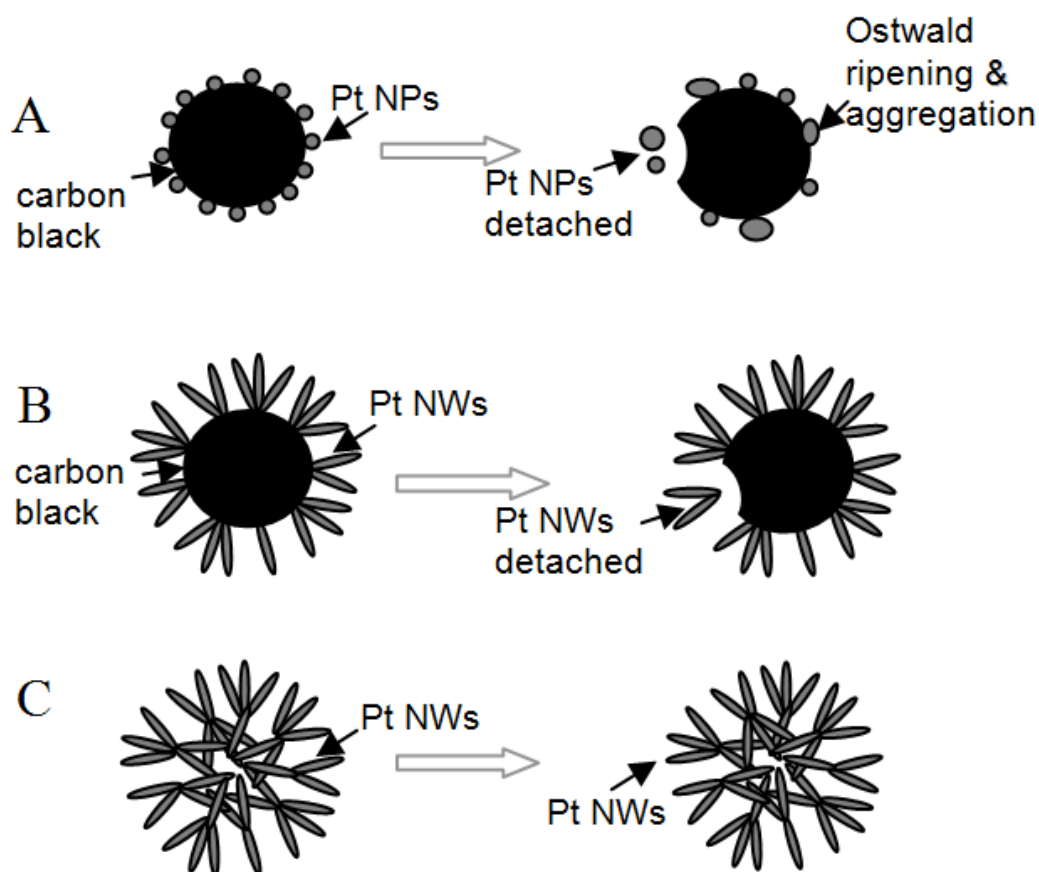
Figure 3.5. Schematic of morphology changes that occur in Pt during accelerated electrochemical cycling. A) Pt NPs/C (E-TEK), B) Pt NWs/C, and C) unsupported PtNWs.

because of the possible mild dissolution of Pt. This might be the main reason for the small drop in Pt ECSA of unsupported PtNWs. As shown in the schematic illustration of morphology changes that occurred in Pt during accelerated electrochemical cycling (Figure 3.5), the Ostwald ripening and aggregation of Pt, as well as corrosion of the carbon support in the case of the absence of carbon, can be significantly mitigated by introducing 1D and the starlike network Pt morphology [11].

3.4 Conclusions

In summary, we have demonstrated a promising electrocatalyst based on starlike Pt nanowires with both good catalytic activity and durability. The novel starlike Pt nanowire structure may also be used in other industrial applications.

Acknowledgements

References

[1]   R. Borup, J. Meyers, B. Pivovar, Y.S. Kim, R. Mukundan, N. Garland, D. Myers, M. Wilson, F. Garzon, D. Wood, P. Zelenay, K. More, K. Stroh, T. Zawodzinski, J. Boncella, J.E. McGrath, M. Inaba, K. Miyatake, M. Hori, K. Ota, Z. Ogumi, S. Miyata, A. Nishikata, Z. Siroma, Y. Uchimoto, K. Yasuda, K. Kimijima, N. Iwashita, Scientific aspects of polymer electrolyte fuel cell durability and degradation. *Chem. Rev.* **2007**, *107*, 3904–3951.

[2]   Z. M. Peng, H. Yang, Designer platinum nanoparticles: Shape, composition in alloys, nanostructure and electrocatalytic property. *Nano Today* **2009**, *4*, 143–164.

[3]   a) Y. Y. Shao, G. P. Yin, Y. Z. Gao, Understanding and approaches for the durability issues of Pt-based catalysts for PEM fuel cell. *J. Power Sources* **2007**, *171*, 558–566; b) P. J. Ferreira, G. J. O La, Y. Shao-Horn, D. Morgan, R. Makharia, S. Kocha, H. A. Gasteiger Instability of Pt/C electrocatalysts in proton exchange membrane fuel cells: A mechanistic investigation. *J. Electrochem. Soc.* **2005**, *152*, A2256–A2271; c) Z. M. Peng, H. Yang, Synthesis and Oxygen Reduction Electrocatalytic Property of Pt-on-Pd Bimetallic Heteronanostructures. *J. Am. Chem. Soc.* **2009**, *131*, 7542–7543.

[4]   J. Q. Tian, S. P. Jiang, Z. Liu, L. Li, Polyelectrolyte-stabilized Pt nanoparticles as new electrocatalysts for low temperature fuel cells. *Electrochem. Commun.* **2007**, *9*, 1613–1618.

[5]   E. Formo, E. Lee, D. Campbell, Y. N. Xia, Functionalization of electrospun TiO2 nanofibers with Pt nanoparticles and nanowires for catalytic applications. *Nano Lett.* **2008**, *8*, 668–672.

[6]   Y. S. Kim, S. H. Nam, H. S. Shim, H. J. Ahn, M. Anand, W. B. Kim, Electrospun bimetallic nanowires of PtRh and PtRu with compositional

variation for methanol electrooxidation. *Electrochem. Commun.* **2008**, *10*, 1016–1019.

[7]   H. J. Kim, Y. S. Kim, M. H. Seo, S. M. Choi, W. B. Kim, Pt and PtRh nanowire electrocatalysts for cyclohexane-fueled polymer electrolyte membrane fuel cell . *Electrochem. Commun.* **2009**, *11*, 446–449.

[8]   E. P. Lee, Z. M. Peng, D. M. Cate, H. Yang, C. T. Campbell, Y. N Xia, Growing Pt nanowires as a densely packed array on metal gauze. *J. Am. Chem. Soc.* **2007**, *129*, 10634–10635.

[9]   S. H. Sun, F. Jaouen, J. P. Dodelet, Controlled Growth of Pt Nanowires on Carbon Nanospheres and Their Enhanced Performance as Electrocatalysts in PEM Fuel Cells. *Adv. Mater.* **2008**, *20*, 3900–3904.

[10] H. J. Zhou, W. P. Zhou, R. R. Adzic, S. S. Wong, Enhanced Electrocatalytic Performance of One-Dimensional Metal Nanowires and Arrays Generated via an Ambient, Surfactantless Synthesis. *J. Phys. Chem. C* **2009**, *113*, 5460–5466.

[11] Z. W. Chen, M. Waje, W. Z. Li, Y. S. Yan, Supportless Pt and PtPd Nanotubes as Electrocatalysts for Oxygen-Reduction Reactions. *Angew. Chem. Int. Ed.* **2007**, *46*, 4060–4063.

[12] Y. S. Kim, H. J. Kim, W. B. Kim, Composited hybrid electrocatalysts of Pt-based nanoparticle and nanowires for low temperature polymer electrolyte fuel cells. *Electrochem. Commun.* **2009**, *11*, 1026–1029.

[13] a) S. H. Sun, D. Q. Yang, D. Villers, G. X. Zhang, E. Sacher, J. P. Dodelet, Template- And surfactant-free room temperature synthesis of self-assembled 3D Pt nanoflowers from single-crystal nanowires. *Adv. Mater.* **2008**, *20*, 571–574; b) S. H. Sun, D. Q. Yang, G. X. Zhang, E. Sacher, J. P. Dodelet, Synthesis and characterization of platinum nanowire-carbon nanotube heterostructures. *Chem. Mater.* **2007**, *19*, 6376–6378.

[14] M. A. Mahmoud, C. E. Tabor, M. A. El-Sayed, Y. Ding, Z. L. Wang, A New Catalytically Active Colloidal Platinum Nanocatalyst: The Multiarmed Nanostar Single Crystal. *J. Am. Chem. Soc.* **2008**, *130*, 4590–4591.

[15] J. Y. Chen, T. Herricks, M. Geissler, Y. N. Xia, Single-crystal nanowires of platinum can be synthesized by controlling the reaction rate of a polyol process. *J. Am. Chem. Soc.* **2004**, *126*, 10854–10855.

[16] Y. N. Xia, Y. J. Xiong, B. Lim, S. E. Skrabalak, Shape-Controlled Synthesis of Metal Nanocrystals: Simple Chemistry Meets Complex Physics? *Angew. Chem. Int. Ed*. **2009**, *48*, 60–103.

[17] a) T. J. Schmidt, H. A. Gasteiger, G. D. Stab, P. M. Urban, D. M. Kolb, R. J. Behm, Characterization of High-Surface-Area Electrocatalysts Using a Rotating Disk Electrode Configuration. *J. Electrochem. Soc.* **1998**, *145*, 2354–2358; b) B. Lim, M. J. Jiang, P. H. C. Camargo, E. C. Cho, J. Tao, X. M. Lu, Y. M. Zhu, Y. N. Xia, Pd-Pt Bimetallic Nanodendrites with High Activity for Oxygen Reduction. *Science*, **2009**, *324*, 1302–1305.

[18] V. R. Stamenkovic, B. Fowler, B. S. Mun, G. Wang, P. N. Ross, CA. Lucas, N. M. Markovic, Improved Oxygen Reduction Activity on $Pt_3Ni(111)$ via Increased Surface Site Availability. *Science* **2007**, *315*, 493–497.

[19] a) J. L. Zhang, Y. Mo, M. B. Vukmirovic, R. Klie, K. Sakaki, R. R. Adzic, Platinum Monolayer Electrocatalysts for O_2 Reduction: Pt Monolayer on Pd(111) and on Carbon-Supported Pd Nanoparticles. *J. Phys. Chem. B* **2004**, *108*, 10955–10964; b) J. L. Zhang, M. B. Vukmirovic, Y. Xu, M. Mavrikakis, R. R. Adzic, Controlling the catalytic of platinum-monolayer electrocatalysts for oxygen reduction with different substrates. *Angew. Chem. Int. Ed.* **2005**, *44*, 2132–2135.

[20] M. S. Saha, R. Li, M. Cai, X. Sun, High Electrocatalytic Activities of Platinum Nanoparticles on SnO_2 Nanowire-based Electrodes. *Electrochem. Solid-State Lett.*, **2007**, *10*, B130–B133.

Supporting Information
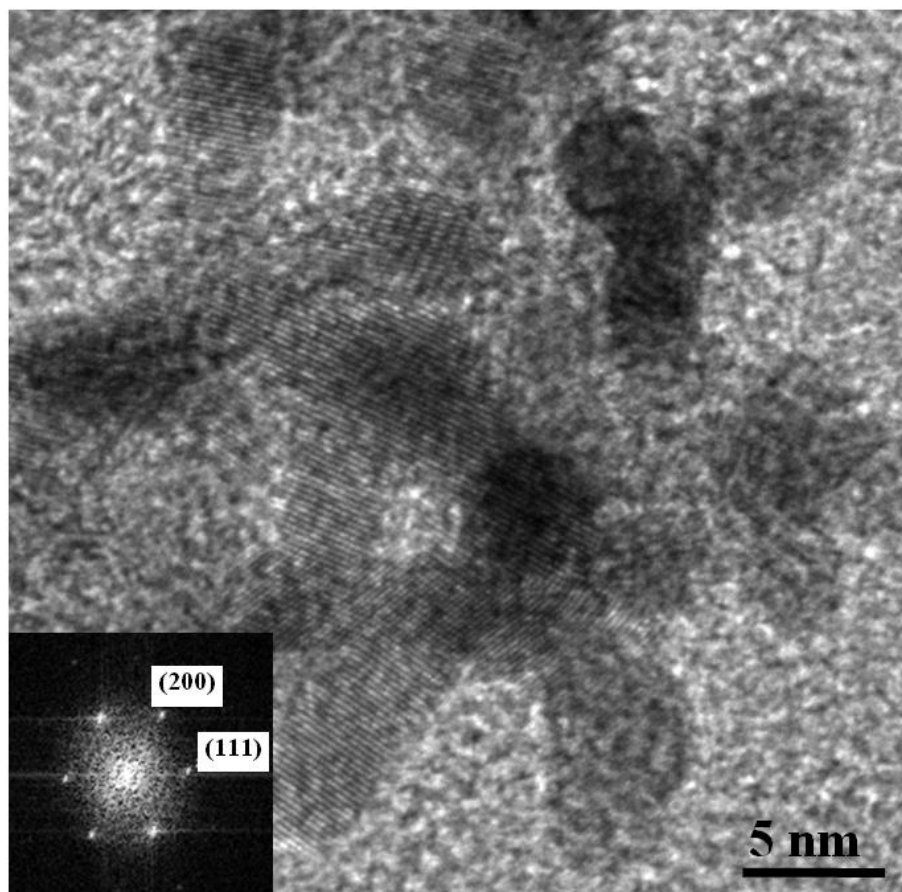
Figure SI-3.1. HRTEM image of a multiarmed single-crystal nanostar. The inset shows the fast Fourier Transform (FFT) diffraction pattern of the nanostar, indicating that the nanowire is single crystalline.
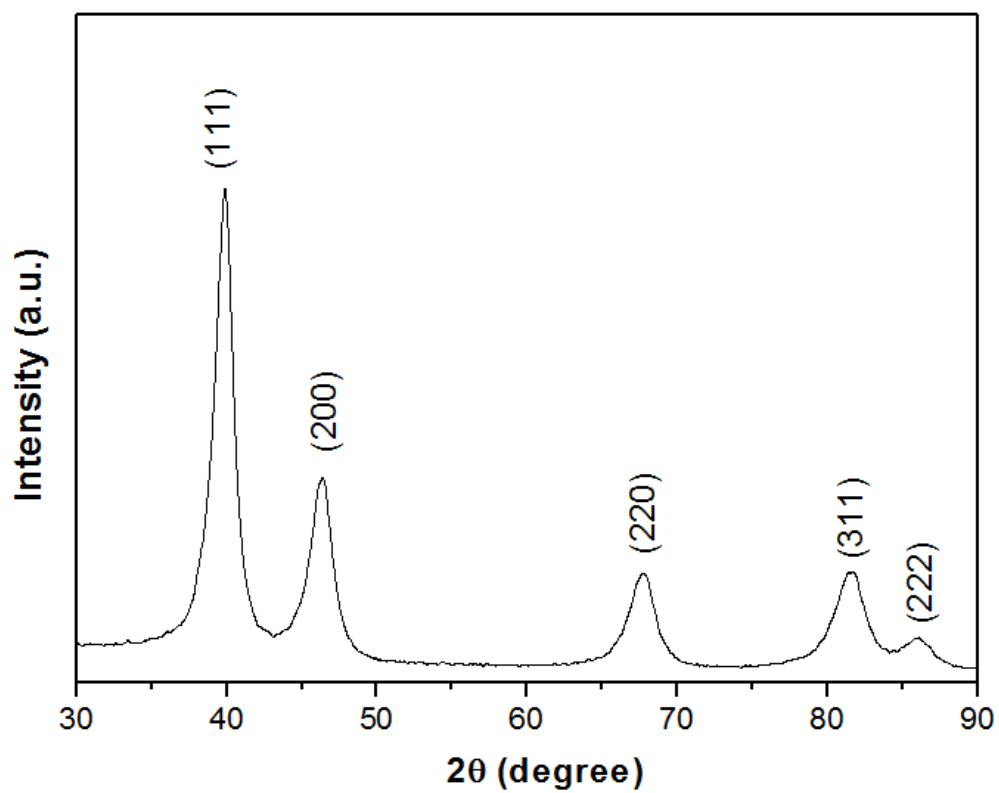
Figure SI-3.2. A typical X-ray diffraction pattern of carbon-supported star-like Pt nanowires, showing characteristic crystalline faces of Pt.
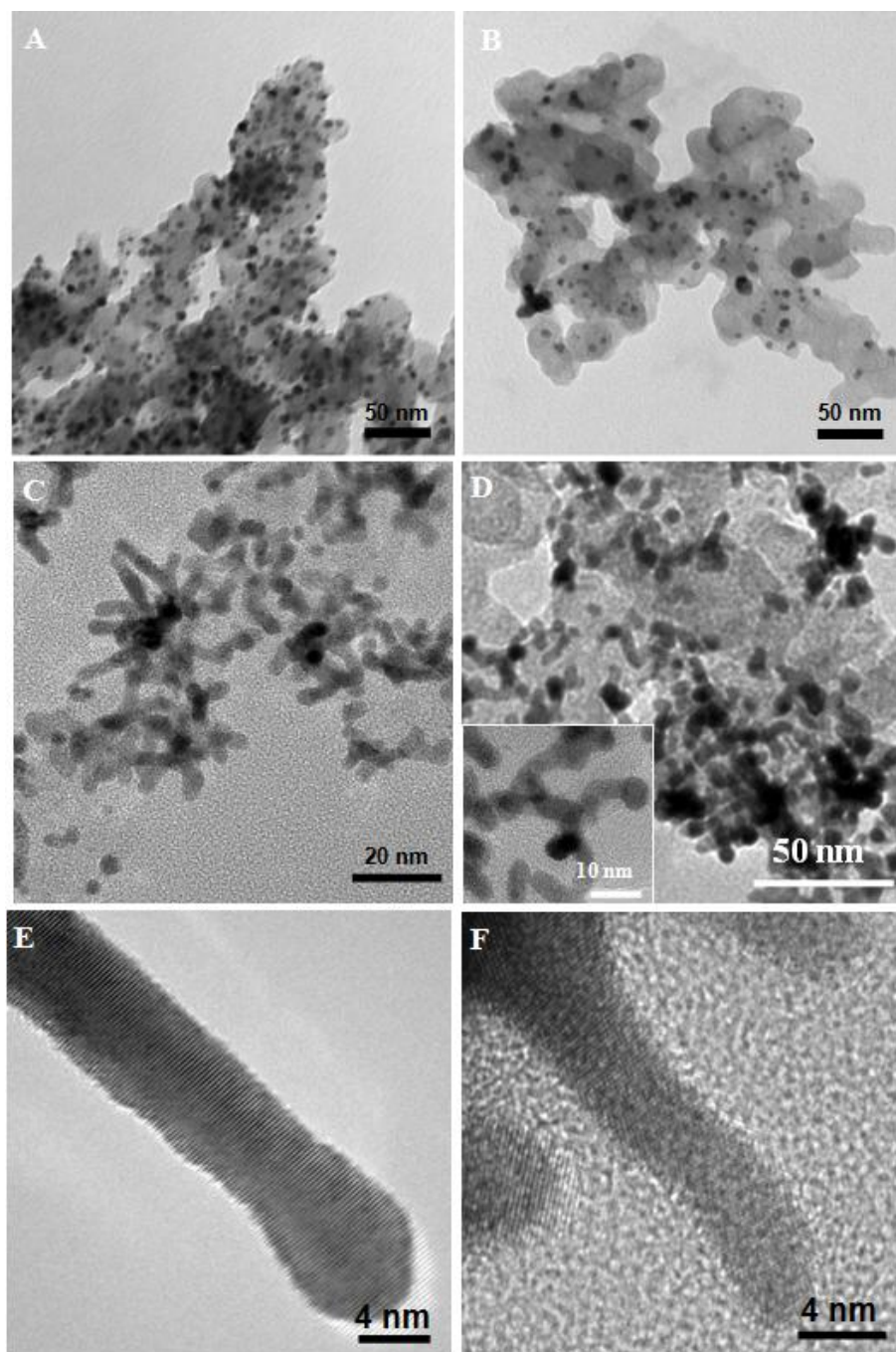
Figure SI-3.3. TEM images of Pt/C (E-TEK) (A) before, and (B) after accelerated CV test; 40wt% PtNW/C (C) before, and (D) after accelerated CV test; supportless Pt NW (E) before, and (F) after accelerated CV test.

Chapter 4. Direct Growth of Single Crystal Pt Nanowires on Sn@CNT Nanocable: 3D Supports for Highly Active Electrocatalysts

Shuhui Sun[1], Gaixia Zhang[1], Dongsheng Geng[1], Yougui Chen[1], Mohammad Norouzi Banis[1], Ruying Li[1], Mei Cai[2], and Xueliang Sun[1],*

[1] *Department of Mechanical and Materials Engineering, The University of Western Ontario, London, Ontario, N6A 5B9 (Canada)*
[2] *General Motors Research and Development Center, Warren, MI 48090-9055 (USA)*
E-mail: xsun@eng.uwo.ca

To improve the Pt utilization and enhance their catalytic activity, Pt catalysts are often deposited onto a variety of carbon supports, including carbon black (CB), carbon nanofibers (CNFs), and carbon nanotubes (CNTs). Among these supporting materials, CNTs are considered to be a more attractive candidate owing to their outstanding mechanical characteristics such as high tensile strength coupled with high surface area, high electric conductivity, and thermal conductivity. Moreover, CNTs supported Pt nanoparticles have been reported showing enhanced ORR and MOR activities as well as better CO tolerance. Recently, our group along with other research groups have reported that by supporting Pt onto CNTs directly grown on the carbon fibers of a fuel cell carbon paper backing, much improved Pt utilization had been achieved through the 3D open structure. The unique advantage of this approach is that all the deposited Pt particles are in electrical contact with the external electrical circuit.

Following the same concept, our research efforts have been expanded to the synthesis and utilization of metal oxide nanowires (e.g. SnO_2 and $W_{18}O_{49}$) and carbon-coated metal/metal oxide nanowires (Sn@CNT, $W_{18}O_{49}$@CNT) as electrocatalyst supports for fuel cells. The advantages of such nanowire-based electrodes include 3D electrode structure which enables higher gas permeability, improved metal-support interactions, and enhanced mass transport.

Previously, we reported a new type of highly active and stable Pt nanowire catalyst. In this chapter, 1D Pt nanowires (a good catalyst) were directly grown on, 1D Sn@CNT nanocables (a good support), forming a novel 3D fuel cell electrode (PtNW–Sn@CNT). This approach allows us to combine the advantages of both PtNW catalyst and Sn@CNT/carbon paper support for fuel cell applications. The PtNW–Sn@CNT 3D electrodes showed higher electrocatalytic activities on oxygen reduction, methanol oxidation and improved CO tolerance than commercial ETEK Pt/C catalyst made of Pt nanoparticles.

4.1 Introduction

Platinum is the key electrocatalyst in polymer electrolyte membrane (PEM) fuel cells [1-3], where it catalyzes oxygen reduction reaction (ORR) at the cathode and fuel (including hydrogen and methanol) oxidation reaction at the anode [4,5]. Interestingly, it has been established that the catalytic reactivity of Pt nanostructures depends highly on their morphology (including dimensionality and shape), and therefore the design and synthesis of well-controlled shapes and sizes of Pt nanostructures is crucial for their applications, especially in the field of electrocatalysis for fuel cells [6,7].

To date, considerable efforts have been devoted to the synthesis of Pt nanostructures; however, most of these studies focused on spherical nanoparticles or nanoparticles with an undetermined shape [8-10]. Very recently, one dimensional (1D) Pt structures, such as nanowires, have drawn much attention owing to their unique anisotropic structure and surface properties, as well as excellent electrocatalytic activities [11-14]. Platinum nanowires have been synthesized by templating against the channels of hard or soft templates, however, polycrystalline nanowires were normally obtained [15]. The first attempt to generate single-crystal Pt nanowires was accomplished by Xia and coworkers through a polyol process, combined with the introduction of a trace amount of iron species; poly(vinyl pyrrolidone) was used as a surfactant, and the reaction was carried out at $110\,°C$ [11]. It still remains a grand challenge to synthesize single-crystalline Pt nanowires through surfactant-free routes under mild conditions.

To improve the Pt utilization and enhance their catalytic activity, Pt catalysts are often dispersed onto a variety of carbon supports, including carbon black (CB) [16], carbon nanofibers (CNFs) [17], and carbon nanotubes (CNTs) [18]. Among these supporting materials, CNTs are considered to be one of the most attractive candidates, owing to their outstanding mechanical characteristics, such as high tensile strength coupled with high surface area, high electric conductivity, and thermal conductivity [19-20]. Indeed, CNTs supported Pt nanoparticles showed enhanced ORR and

methanol oxidation (MOR) activities in fuel cells [21-24]. Moreover, the addition of tin (Sn) or its oxide to Pt/CNT catalysts can further enhance their performance according to the bi-functional mechanism [25-27]. Despite the progress made in the past, the production of Pt catalyst with great catalytic performance and utilization efficiency is still costly and far from being trivial.

In this study, through a facile surfactant-free aqueous solution method, we synthesized ultrathin single-crystal Pt nanowires, at room temperature, on a Sn@CNT nanocable support directly grown on carbon paper fuel cell backing to form a novel 3D fuel-cell electrode (PtNW–Sn@CNT). Such a Sn@CNT 3D nanocable support holds many advantages, including enhancing effect of tin, higher gas permeability, improved metal-support interactions, and enhanced mass transport. This approach allows us to combine the advantages of both a PtNW catalyst and a Sn@CNT 3D nanocable support for fuel cell applications. The PtNW–Sn@CNT 3D electrodes showed greatly enhanced electrocatalytic activities for oxygen reduction, methanol oxidation and improved CO tolerance than commercial ETEK Pt/C catalyst made of Pt nanoparticles.

4.2 Experimental

4.2.1 Sn@CNT nanocables synthesis

The synthesis of Sn@CNT nanocable structures was carried out by a thermal evaporation method [28]. In a typical process, pure Sn powders (2 g, −325 mesh, 99.8 %) were placed in an alumina boat located at the center of a quartz tube in a horizontal tube furnace. A small piece of commercially available carbon paper (ETEK, 0.17 mm thick, 81 % porosity) was placed aside of the metal powder, acting as the substrate. The reaction chamber was first heated to 850 °C rapidly (in about 15 min) from room temperature under an atmosphere of flowing Ar and 2 % ethylene (200 sccm), and then kept at 850 °C for 2 h. After the furnace was cooled down to room temperature, a gray dark thin film was observed on the surface of the carbon paper substrate.

4.2.2 Growth of Pt nanowires on Sn@CNT/carbon paper and characterization

The growth of Pt nanowires on Sn@CNT support was conducted by the chemical reduction of Pt precursor with formic acid [12]. In a typical procedure, 0.032 g hexachloroplatinic acid ($H_2PtCl_6 \cdot 6 H_2O$, Aldrich) and 1 mL formic acid (HCOOH, Aldrich) were added simultaneously into 20 mL H_2O at room temperature to form a golden orange solution. The Sn@CNT/carbon paper was immersed into the solution, acting as the growth substrates, and then the reaction proceeded at room temperature without stirring for up to 3 days until the solution color gradually changed to colorless. After the completion of the reaction, PtNW−Sn@CNT/carbon paper was washed with deionized water and dried at 80 °C over night in a vacuum oven. The Pt loading was determined to be 0.4136 mg cm^{-2} by using inductively coupled plasma-optical emission spectroscopy (ICP-OES) (the total amount of Pt divided by the geometric surface area of the composite electrode). The morphology of the prepared catalyst were characterized by using SEM (Hitachi S-5200) and TEM (JEOL 2100F).

4.2.3 Electrochemical measurements

The electrochemical properties of the PtNW−Sn@CNT/carbon paper composites were evaluated by using cyclic voltammetry (CV) in a standard three-electrode cell at room temperature. A Pt wire was used as the counter electrode and a saturated calomel electrode (SCE) was used as the reference. CV measurements were carried out by using an Autolab potentiostat/galvanostat (Model, PGSTAT-30, Ecochemie, Brinkman Instruments), using 0.5 M H_2SO_4 solution purged with N_2 at a sweep rate of 50 mV s.$^{-1}$ The electrochemical surface areas (ECSA) of Pt were calculated from the hydrogen adsorption peak of the CV. For methanol oxidation reaction, the CVs were measured in an air-free aqueous solution containing 1 M MeOH and 0.5 M H_2SO_4. For CO stripping voltammetry, pure CO (99.5 %) was purged into the solution at a position close to the working electrode for 1 h, with the electrode polarized at 0.05 V versus RHE in a fume hood. The electrode was then purged with pure Ar for 1 h under potential control followed by voltammetric stripping.

For comparison, a conventional electrode made with commercial 30 wt % Pt/C catalyst from ETEK (USA), was also evaluated. The electrode was prepared with a procedure similar to the one reported previously [37]. Typically, 10 mg catalyst was sonically mixed with 1 mL H_2O/isopropanol (1/1 in volume ratio) to make a suspension. GC disk electrodes (5 mm diameter, Pine Research Instrument) that serve as the support were polished to a mirror finish before using. 20 μL of catalyst suspension was pipetted onto the GC disk substrate, leading to a Pt loading of 0.3058 mg cm^{-2}, which is similar to that for PtNW–Sn@CNT composite electrode. The catalyst films were dried under flow N_2 at room temperature. Finally, a 10 μL Nafion (0.05 wt %) solution was pipetted onto the catalyst film, and then dried. The currents were normalized on the basis of Pt loading.

4.3. Results and Discussion

The approach and schematic illustration for the synthesis of Pt nanowires on Sn@CNT nanocable supports is demonstrated in Figure 4.1. The actual synthetic procedure is very facile, and only two chemicals (H_2PtCl_6 and HCOOH) were used throughout the whole synthesis process, which did not require a stabilizing agent. Further, the reaction was conducted at room temperature in environmentally friendly aqueous solution.

Typical scanning electron microscopy (SEM) and transmission electron microscopy (TEM) images of the pristine Sn@CNT nanostructures grown on a commercially-available carbon paper fuel cell backing are shown in Figure 4.2. The carbon paper substrate is made of many graphite fibers with a diameter between 5 and 10 μm. As shown in Figure 4.2a and inset, after the growth of Sn@CNT, the surface of carbon fibers was completely covered with dense rod-like structures, approximately 5–10 μm in length and 150–200 nm in diameter. The TEM image of a coaxially integrated nanocable structure that consists of a Sn core and CNT shell with void space between the two is shown in Figure 4.2b. The carbon shell is about 60 nm thick and the diameter of the Sn core is about 70 nm. Energy dispersive X-ray spectroscopy (EDS)
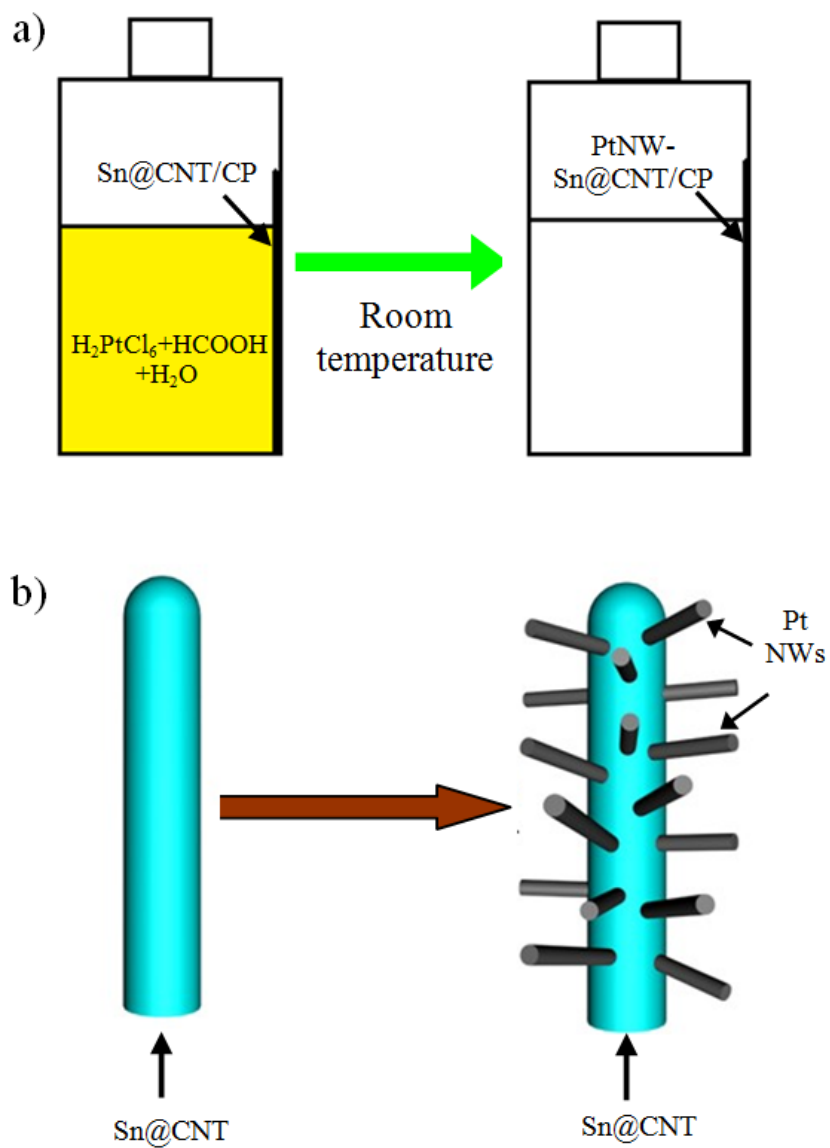
Figure 4.1. a) Schematic representation of the approach in the synthesis of PtNW–Sn@CNT nanocomposites. b) Schematic image depicting the growth of PtNWs on Sn@CNT nanocable support.
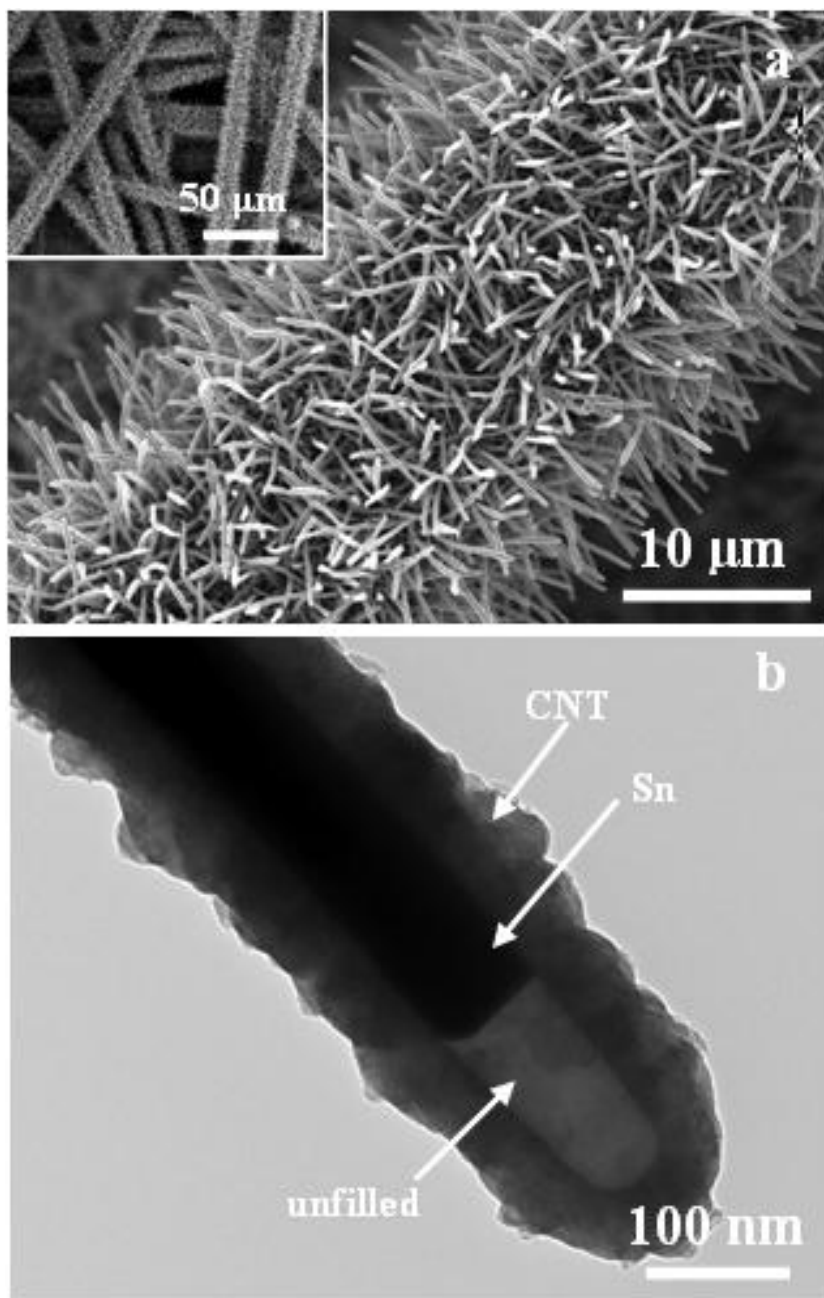
Figure 4.2. a) SEM and b) TEM images of pristine Sn@CNT nanocables, before the growth of Pt NWs.

and selected area electron diffraction (SAED) of the core-shell structure confirmed the presence of metallic Sn and amorphous carbon [28]. The less graphitic form of carbon could promote H^+ diffusion into the Sn core through the "gaps" in the carbon shell [29].
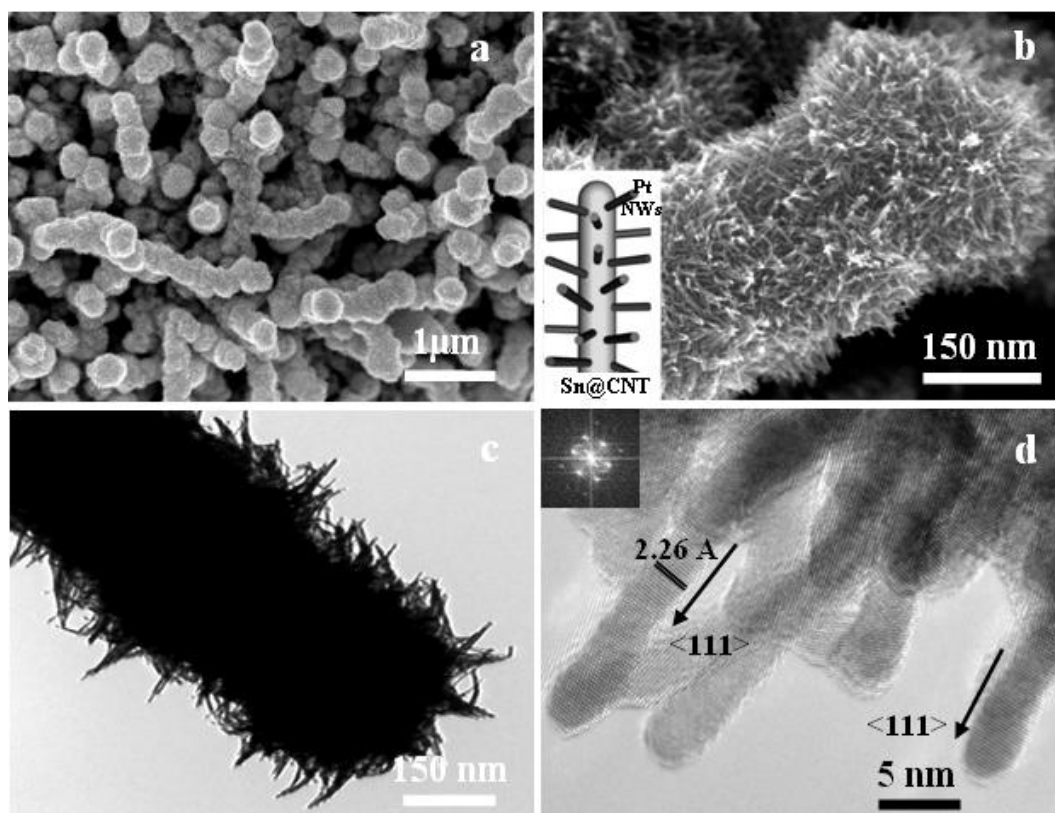
Figure 4.3. a) SEM, b) HRSEM, and c) TEM images of PtNW–Sn@CNT heterostructures, d) HRTEM image of Pt NWs grown on Sn@CNT nanocables.

Typical SEM images of the PtNWs grown on Sn@CNT nanocables, at two magnifications, are shown in Figure 4.3a and b, respectively. They reveal that, after the complete surface coverage with hundred-nanometer long PtNWs, the Sn@CNT nanocables still maintain their "free-standing" 3D structures. The TEM image (Figure 4.3c, and Figure SI-4.1) further confirms the SEM investigation, showing that PtNWs grow uniformly over Sn@CNT surface with lengths of up to hundred nanometers. High-resolution (HR) TEM examination (Figure 4.3d) shows that the Pt nanowires are ≈4 nm in diameter and they grow along the <111> direction. The crystallographic alignment of nanowires reveals that the entire nanowire is one single crystal with a lattice spacing between the {111} planes of 0.226 nm, which is in agreement with the value of bulk Pt crystal [12]. The fast Fourier transform (FFT) of the atomic-lattice fringing, apparent in the inset of Figure 4.3d, further confirms the single crystallinity of Pt nanowires.

The chemical state of PtNWs growth on Sn@CNT nanocable supports were determined by X-ray photoelectron spectroscopy (XPS). High resolution Pt 4f spectrum was deconvoluted into asymmetric doublet (Figure 4.4a) peaks centered at 71.4 and 74.7 eV, which can be attributed to Pt^0 $4f_{7/2}$, and Pt^0 $4f_{5/2}$, respectively. These are in good agreement with those of pure bulk platinum [30]. In addition, no obvious shoulders at higher binding energies, representing Pt^{2+} and Pt^{4+}, were found. Based on these analyses, we believe that the Pt NWs grown on Sn@CNT nanocable supports are pure metallic Pt. The X-ray diffraction (XRD) pattern, shown in Figure 4.4b, reveals that the Pt nanowires grown on Sn@CNT nanocable 3D supports were crystallized in a face-centered-cubic (fcc) structure similar to bulk Pt, which is consistent with the HRTEM investigations.
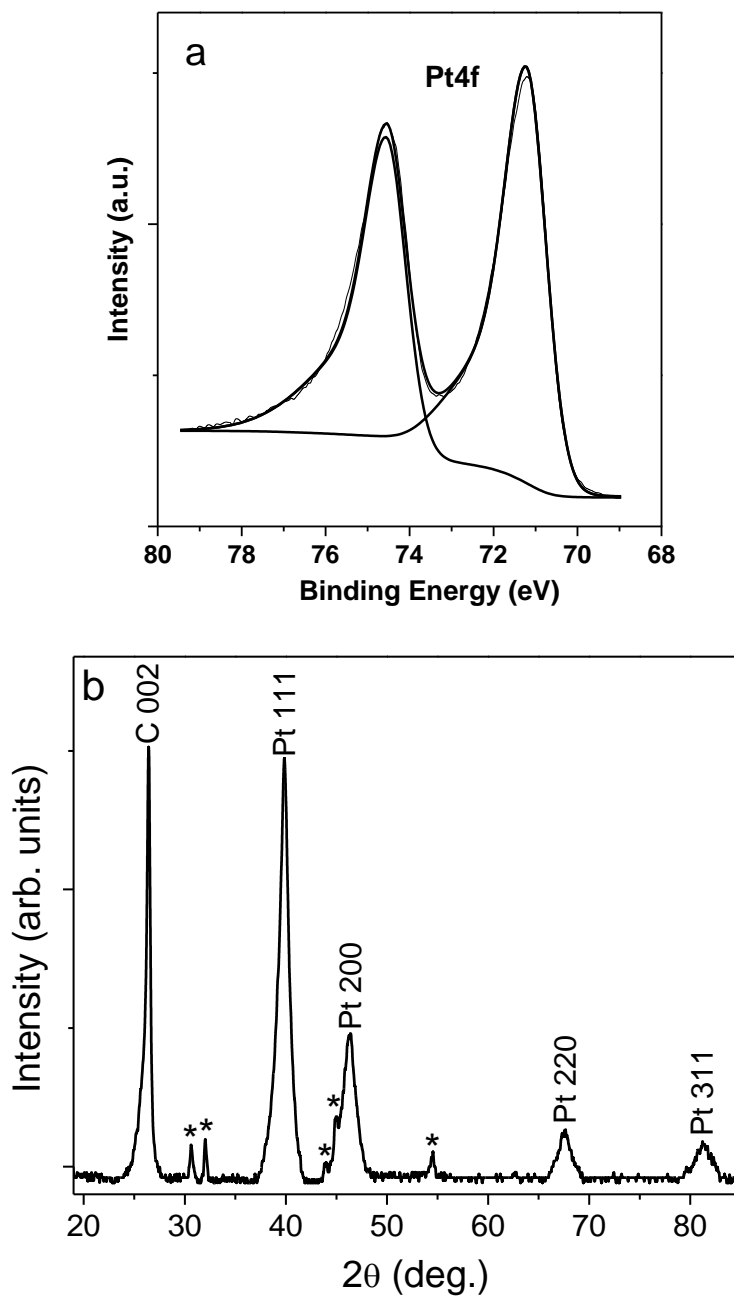
Figure 4.4. a) Pt4f XPS spectrum separation, and b) XRD patterns of Pt NWs grown on Sn@CNT nanocables. The * in b) represents the XRD patterns originated from Sn.

We believe that the growth of PtNWs on Sn@CNT supports follows the similar process to that for Pt NWs on MWCNTs [12b]. Typically, Pt nuclei are first formed in solution through the reduction of H_2PtCl_6 by HCOOH, and they deposit on the surface of Sn@CNT nanocables. The freshly formed nuclei act as the sites for further nucleation, through the continually absorption of Pt^{4+} ions, leading to the formation of clustered particles. As the reaction is conducted at room temperature, the reduction rate is very slow, and the anisotropic growth is favored because, for fcc structures, the order of surface energies is (111)<(100)<(110) [12a]. Therefore, according to the lowest energy principle, the growth rate along the closed-packed <111> direction is enhanced. We believe that the key to synthesize the Pt nanowires is to reduce the rate of Pt ion reduction, favoring the growth of {111} planes, and therefore leading to the formation of 1D nanowires.

We evaluated the electrochemical properties of the PtNW–Sn@CNT composite and, for comparison, pristine Sn@CNT nanocable structures and 30 wt % Pt/C (ETEK) catalysts, using cyclic voltammetry (CV). The CVs recorded between −0.25 and 0.95 V vs SCE in a deaerated 0.5 M H_2SO_4 solution are shown in Figure 4.5. Before Pt deposition, only background currents representing characteristic of carbon electrodes, are observed (solid line a). After the growth of Pt nanowires, clear and characteristic Pt surface electrochemistry is observed (solid line b), with hydrogen adsorption and desorption between 0.05 and −0.25 V, and Pt oxidation in the range of 0.55 to 0.95 V with reduction peak at 0.59 V. Multiple peaks for hydrogen adsorption and desorption, rather than a single broad peak, were observed, indicating that the reaction involved multiple exposed Pt crystallographic planes. The electrochemically active surface areas (ECSA) of the samples were calculated based on the hydrogen adsorption wave capacity (Q_H) according to the following [Eqn. (1)][24]:

$$A_{EL} = Q_H/(210 \ \mu C \ cm^{-2} \times Pt \ loading) \tag{4.1}$$

The obtained value of A_{EL} for the PtNW–Sn@CNT is 17.2 $m^2 \, g^{-1}$(Pt), which is 50 % of that for the ETEK Pt/C catalyst [34.5 $m^2 \, g^{-1}$(Pt)] made of Pt nanoparticles on

carbon black (CB). This can be attributed to the intrinsic 1D morphology of nanowires compared to that of nanoparticles [14].
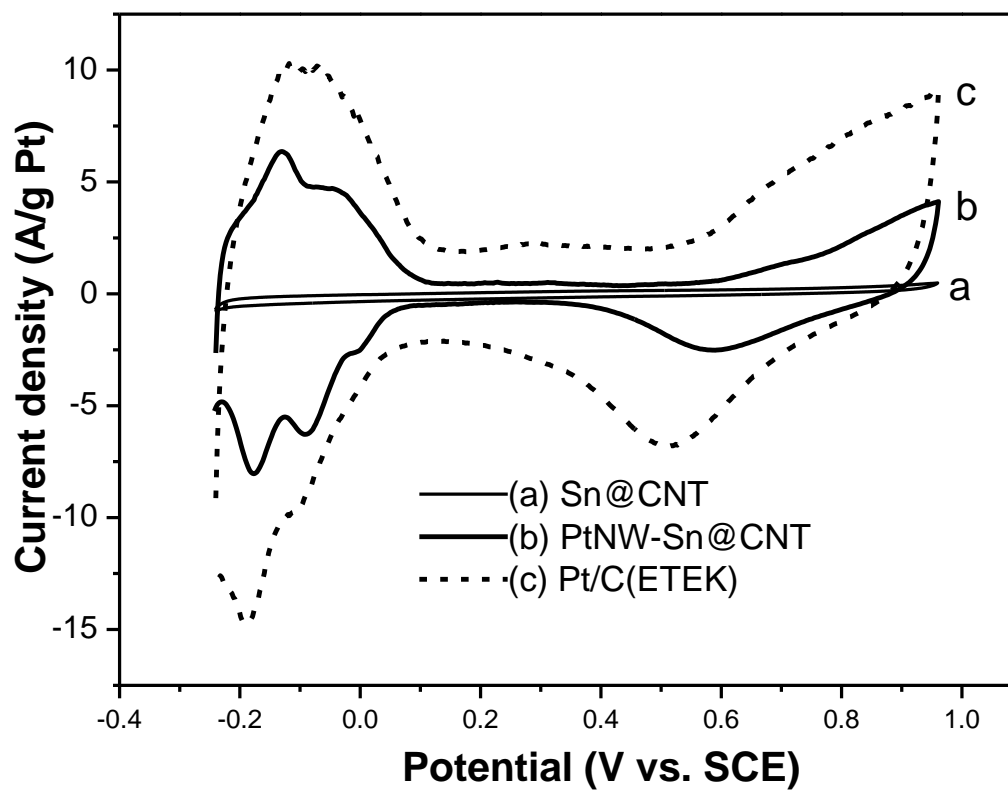
Figure 4.5. Cyclic voltammograms of a) pristine Sn@CNT; b) PtNW–Sn@CNT; and c) 30 wt %Pt/C commercial catalysts (ETEK). Measured at a scan rate of 50 mV s,$^{-1}$ in degassed 0.5 M H_2SO_4.
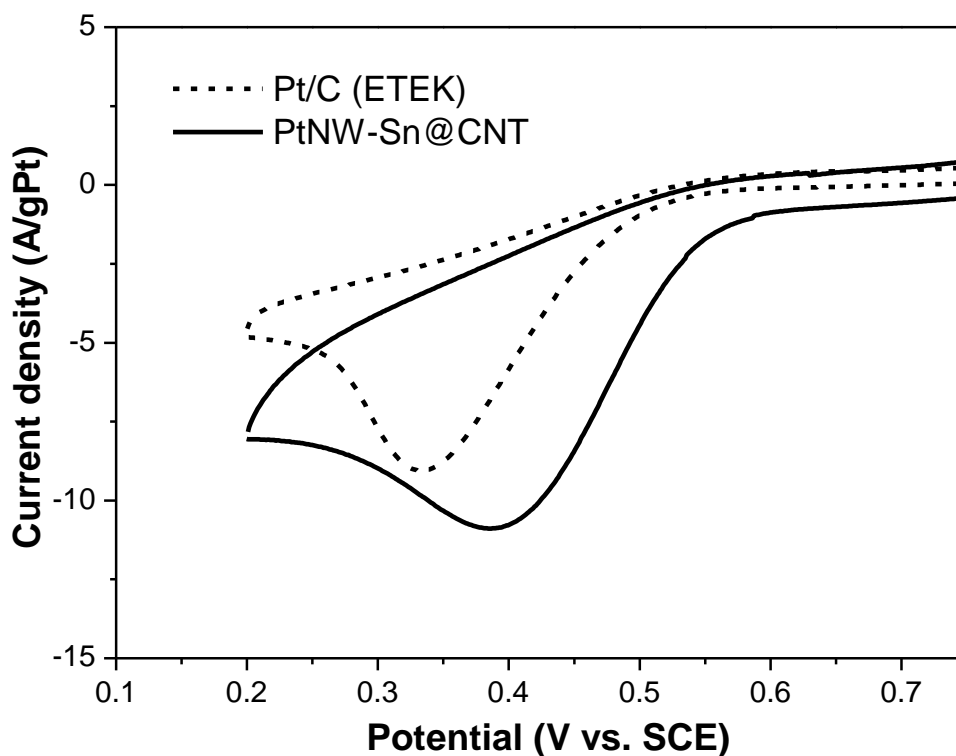
Figure 4.6. CVs for oxygen reduction reaction in O-saturated $0.5\,M$ H_2SO_4 at PtNW–Sn@CNT (—) and commercial Pt/C electrode (ETEK) (- - - -). Potential scan rate 50 mV s.$^{-1}$

The ORR activities of PtNW–Sn@CNT composite electrode and commercial Pt/C catalyst (ETEK) are shown in Figure 4.6. Both CVs were obtained in an O_2-saturated aqueous electrolyte solution containing $0.5\,M$ H_2SO_4. It can be seen that a 60 mV positive shift of the onset potential for oxygen reduction at the PtNW–Sn@CNT composite was observed as compared to commercial Pt/C electrode. The oxygen reduction peak current, normalized on the basis of Pt loading, is 10.9 A g^{-1}(Pt) for the PtNW–Sn@CNT composite, which is 1.2 times that for the ETEK Pt/C catalyst [9.0 A g^{-1}(Pt)]. Interestingly, this improvement occurred in spite of a 50 % lower Pt active

surface area for the Pt nanowire catalyst. Taking into account both effects, a specific ORR activity for PtNW–Sn@CNT of 0.63 A m^{-2}(Pt) was obtained, which is 2.4 times better than for the ETEK Pt/C catalyst [0.26 A m^{-2}(Pt)]. The higher specific activity of the PtNW–Sn@CNT as compared to Pt nanoparticles on CB (ETEK) might be owed to the preferential exposure of certain crystal facets of the Pt NWs [14-31], and/or the unique 3D structure of Sn@CNT-based electrode, which facilitates the O$_2$ diffusion to Pt surface. These results indicate a significant improvement of electrocatalytic activity for ORR in PtNW–Sn@CNT composite.
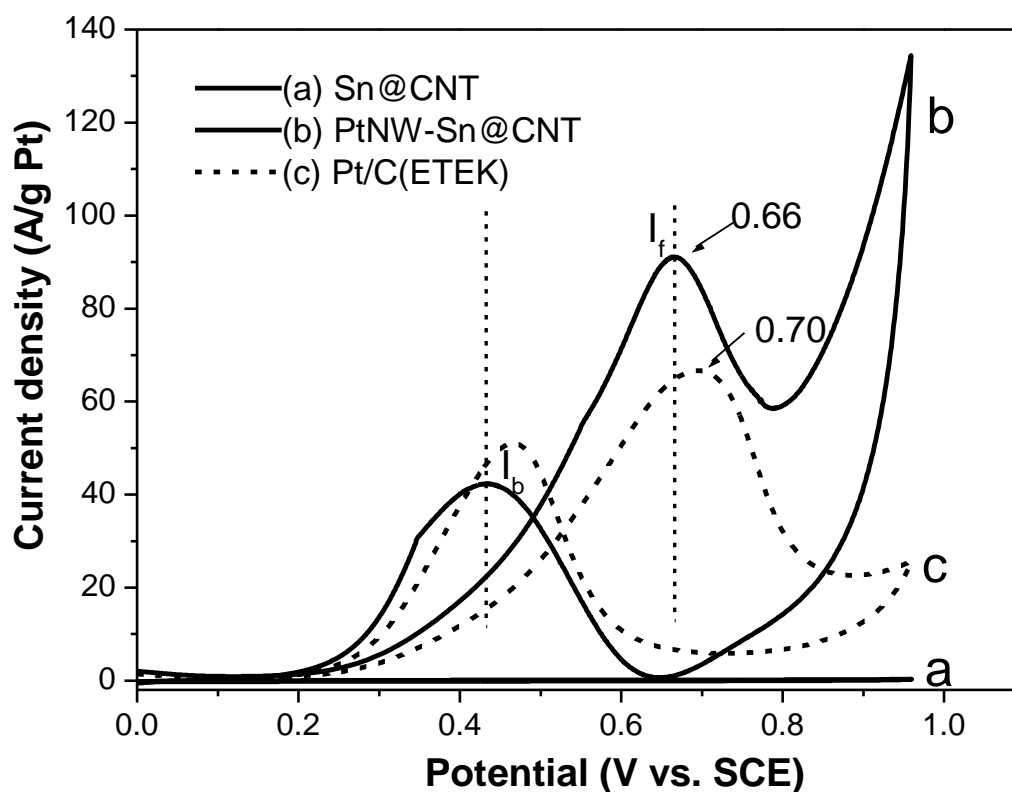
Figure 4.7. Cyclic voltammograms for methanol oxidation (1 M methanol in 0.5 M H$_2$SO$_4$). Trace a) before growth of PtNWs; trace b) after growth of PtNWs on Sn@CNT; trace c) ETEK commercial catalyst of Pt nanoparticles on carbon black.

The electrocatalytic activity of the PtNW–Sn@CNT composite for methanol oxidation, which is the heart of direct methanol fuel cell (DMFC) application in the anodic half-cell reaction, was also demonstrated by using a well-used electrochemical reaction in a solution containing 1 M MeOH and 0.5 M H_2SO_4. For comparison, the pristine Sn@CNT and the commercial ETEK Pt/C catalyst (30 wt % Pt) were also tested under the same experimental conditions. From the voltammograms shown in Figure 4.7, no obvious oxidation peaks could be observed from the CV curve of the pristine Sn@CNT electrode, indicating the support itself is catalytically inactive for methanol oxidation (curve a). Two typical oxidation peaks appear for the CV curves of the PtNW–Sn@CNT (curve b) and Pt/C catalysts (curve c), which arise from the oxidations of methanol and their intermediates [32]. Obviously, the peak potential for methanol oxidation in the forward scan on PtNW–Sn@CNT composite (0.66 V vs. SCE) is much lower than that (0.70 V vs. SCE) for Pt/C catalyst. This indicates that the PtNWs supported on Sn@CNT nanocables are able to significantly reduce the overpotential in methanol oxidation. The methanol oxidation peak current, normalized on the basis of Pt loading, for PtNW–Sn@CNT is about 91.0 A g^{-1}(Pt), which is 1.35 times higher than for the ETEK Pt/C catalyst [66.9 A g^{-1}(Pt)]. In terms of the activity per unit active surface area, $\approx$2.8 times higher specific activity for PtNW–Sn@CNT composite [5.3 A m^{-2}(Pt)] than that for the ETEK Pt/C [1.9 A m^{-2}(Pt)] were obtained. Goodenough et al. suggested the anodic peak in the reverse scan might be attributed to the removal of the incomplete oxidized carbonaceous species, such as CO, $HCOO^-$ and HCO^-, accumulated on catalyst surface during the forward scan. Consequently, the ratio of current densities for these two anodic peaks, I_f/I_b, can be used to infer the CO tolerance of the catalyst [33]. The low I_f/I_b value usually indicates poor oxidation of methanol to CO_2 during the forward anodic scan and excessive accumulation of residual carbon species on catalyst surface. On the other hand, a higher I_f/I_b ratio is indicative of improved CO tolerance. In our study, the observation of a much higher I_f/I_b value on PtNW–Sn@CNT composite (2.2 vs. 1.3 on ETEK Pt/C) suggests that methanol molecules can be more effectively oxidized on PtNW–Sn@CNT during the forward scan, generating relatively less
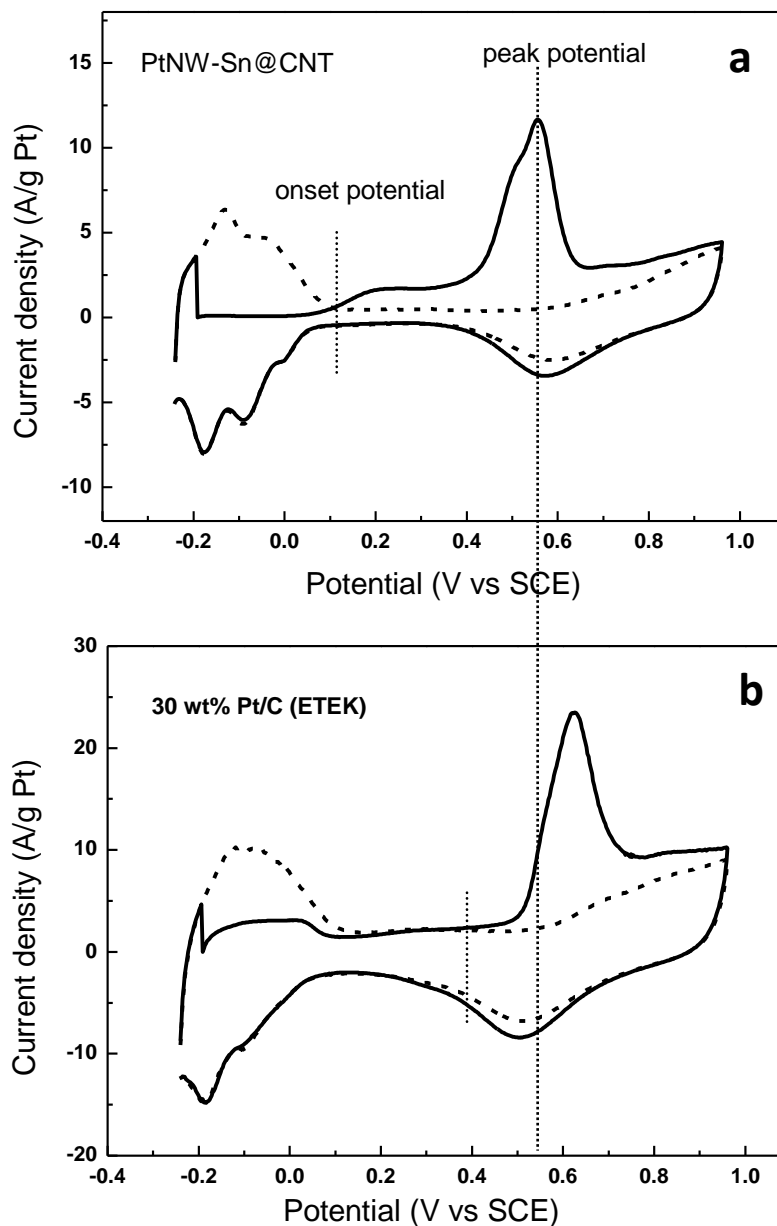
Figure 4.8. CVs of a) PtNW–Sn@CNT/carbon paper 3D electrode and b) a commercial Pt/C electrode in the presence of CO in 0.5 M H_2SO_4 aqueous solution at room temperature. Potential scan rate: 50 mV s.[−1] For both catalysts, a sharp peak appears during the first scan (solid line) and disappears in the subsequent scan (dash line).

poisoning species as compared to commercial Pt/C catalyst, indicating the better CO tolerance. To further explore the observed enhancement of CO tolerance, we carried out a CO electrostripping experiment. From Figure 4.8, we can see, for both catalysts, that a sharp peak appears during the first scan (solid line) and disappears in the subsequent scan (dash line), indicating that the adsorbed CO is completely oxidized during the first forward scan. When comparing the onset potential and the peak potential for CO electro-oxidation, significant differences between the two catalysts can be observed. The onset potential of CO oxidation on PtNW–Sn@CNT composite is at 0.11 V (vs. SCE), which is about 290 mV lower than that on commercial Pt/C catalyst (0.4 V vs. SCE). Further, the oxidative CO-stripping peak potential centers at 0.62 V for the commercial Pt/C catalyst, whereas on PtNW–Sn@CNT, it is located at 0.55 V. The significant negative shifts for the onset and peak potentials of 290 mV and 70 mV, respectively, indicate that the adsorbed CO can be more easily removed from PtNW–Sn@CNT catalyst than from ETEK commercial Pt/C catalyst. All these results indicate that PtNW–Sn@CNT is much more tolerant to CO poisoning.

As to the origin of the enhanced electrocatalytic performance on PtNW–Sn@CNT catalysts, several explanations can be suggested. In previous studies of Pt-based nanoparticle catalysts, the activity and CO tolerance enhancements were also observed on PtSn or $PtSnO_2$ nanostructures, which was attributed to the fact that tin (Sn) or its oxide could supply an oxygen containing (e.g. -OH groups) surface to remove strongly absorbed species like CO, according to a so-called bi-functional mechanism [33-35]. Therefore, the improved catalytic activity and CO tolerance observed in our study may originate partially from the unique core-shell nanocable supports containing a Sn core. In addition, the "free-standing" nanocable supports and Pt nanowires provide excellent electron conductivity, which might facilitate the reaction kinetics on the electrode surfaces, and improve the O_2 and methanol diffusion rate. Furthermore, the preferential exposure of certain crystal facets along with the less surface defects bearing characteristics of Pt nanowires promotes their catalytic activities [14]. More importantly, the unique 1D anisotropic morphology of

Pt nanostructures can improve mass transport and catalyst utilization for the electrocatalytic reactions. Recently, Sun et al [14] found that Pt nanowires on carbon black showed much enhanced specific catalytic activity for oxygen reduction than those of the state-of-the-art Pt nanoparticle catalyst. Meanwhile, Chen et al [31] and Bi et al [36] reported that 1D Pt nanostructures exhibited improved both activity and stability for oxygen reduction and methanol oxidation, respectively. Based on these arguments, it is expected that by growing 1D Pt nanostructures on various metal oxide nanowire supports and forming 3D network structures, the full advantage of several combining factors can be taken. These factors include the enhanced performance of Pt nanowire catalyst, excellent properties of catalyst support, and enhanced mass transport. This approach may open new and exciting possibilities for further improving the performance of PEMFC and DMFC.

4.4 Conclusions

In summary, a facile aqueous solution procedure has been successfully developed to grow single-crystal Pt nanowires on Sn@CNT heterostructured nanocables at room temperature, forming a 3D nanocomposite electrode. The PtNW–Sn@CNT composite shows, for ORR, 1.2 times higher mass activity and 2.4-fold better specific activity, and for MOR, 1.35 times higher mass activity and 2.8-fold better specific activity, than those of the commercial catalyst made of Pt nanoparticles on carbon black. This novel structure has the potential to possess high Pt utilization, high activity, and high durability for fuel cell applications. Further optimization of the dimensional control, the preparation and evaluation of membrane electrode assemblies based on PtNW–Sn@CNT catalysts are underway. This unique approach can be extended to grow Pt nanowires on other 1D nanostructures, such as CNT, SnO_2, WO_3, TiO_2 etc., for wider applications.

Acknowledgements

References

[1] E. Antolini, Formation of carbon-supported PtM alloys for low temperature fuel cells: a review. *Mater. Chem. Phys.* **2003**, *78*, 563–573.

[2] D. R. Rolison, Catalytic Nanoarchitectures: The Importance of Nothing and the Unimportance of Periodicity. *Science* **2003**, *299*, 1698–1701.

[3] H. A. Gasteiger, S. S. Kocha, B. Sompalli, F. T. Wagner, Activity Benchmarks and Requirements for Pt, Pt-Alloys, and Non-Pt Oxygen Reduction Catalysts for PEMFCs. *Appl. Catal. B* **2005**, *56*, 9–35.

[4] N. P. Brandon, S. Skinner, B. C. H. Steele, Recent advances in materials for fuel cells. *Annu. Rev. Mater. Res.* **2003**, *33*, 183–213.

[5] R. K. Rao, D. C. Trivedi, Chemical and electrochemical depositions of platinum group metals and their applications. *Coord. Chem. Rev.* **2005**, *249*, 613–631.

[6] J. Chen, T. Herricks, Y. Xia, Polyol Synthesis of Platinum Nanostructures: Control of Morphology through Manipulation of Reduction Kinetics. *Angew. Chem. Int. Ed.* **2005**, *44*, 2589–2592.

[7] H. Lee, S. E. Habas, S. Kweskin, D. Butcher, G. A. Somorjai, P. Yang, Morphology control of catalytically active Pt nanocrystals. *Angew. Chem. Int. Ed.* **2006**, *45*, 7824–7828.

[8] F. Mirkhalaf, J. Paprotny, D. J. Schiffrin, Synthesis of Metal Nanoparticles Stabilized by Metal−Carbon Bonds. *J. Am. Chem. Soc.* **2006**, *128*, 7400–7401.

[9] T. S. Ahmadi, Z. Wang, T. C. Greem, A. Heglein, M. A. El-Sayed, Shape-Controlled Synthesis of Colloidal Platinum Nanoparticles. *Science* **1996**, *272*, 1924–1925.

[10] H. Bönnemann, K. S. Nagabhushana, Advantageous fuel cell catalysts from colloidal nanometals. *J. New. Mat. Electrochem. Systems.* **2004**, *7*, 93–108.

[11] J. Chen, T. Herricks, M. Geissler, Y. Xia, Single-Crystal Nanowires of Platinum Can Be Synthesized by Controlling the Reaction Rate of a Polyol Process. *J. Am. Chem. Soc.* **2004**, *126*, 10854–10855.

[12] a) S. Sun, D. Yang, D. Villers, G. Zhang, E. Sacher, J. P. Dodelet, Template- and Surfactant-free Room Temperature Synthesis of Self-Assembled 3D Pt Nanoflowers from Single-Crystal Nanowires. *Adv. Mater.* **2008**, *20*, 571–574. b) S. Sun, D. Yang, G. Zhang, E. Sacher, J. P. Dodelet, Synthesis and Characterization of Platinum Nanowire–Carbon Nanotube Heterostructures. *Chem. Mater.* **2007**, *19*, 6376–6378.

[13] E. P. Lee, Z. Peng, W. Chen, S. Chen, H. Yang, Y. Xia, Electrocatalytic Properties of Pt Nanowires Supported on Pt and W Gauzes. *ACS Nano*, **2008**, *2*, 2167–2173.

[14] S. Sun, F. Jaouen, J. P. Dodelet, Controlled Growth of Pt Nanowires on Carbon Nanospheres and Their Enhanced Performance as Electrocatalysts in PEM Fuel Cells. *Adv. Mater*. **2008**, *20*, 3900–3904.

[15] J. Chen, B. J. Wiley, Y. Xia, One-Dimensional Nanostructures of Metals: Large-Scale Synthesis and Some Potential Applications. *Langmuir* **2007**, *23*, 4120–4129.

[16] Z. Zhou, S. Wang, W. Zhou, G. Wang, L. Jiang, W. Li, S. Song, J. Liu, G. Sun, Q. Xin, Novel synthesis of highly active Pt/C cathode electrocatalyst for direct methanol fuel cell. *Chem. Commun.* **2003**, *3*, 394–395.

[17] J. Zheng, M. Wang, X. Zhang, Y. Wu, P. Li, X. Zhou, W. Yuan, Platinum/carbon nanofiber nanocomposite synthesized by electrophoretic

deposition as electrocatalyst for oxygen reduction. *J. Power Sources* **2008**, *175*, 211–216.

[18] S. Guo, S. Dong, E. Wang, Gold/Platinum Hybrid Nanoparticles Supported on Multiwalled Carbon Nanotube/Silica Coaxial Nanocables: Preparation and Application as Electrocatalysts for Oxygen Reduction. *J. Phys. Chem. C* **2008**, *112*, 2389–2393.

[19] T. W. Ebbesen, H. J. Lezec, H. Hiura, J. W. Bennett, H. F. Ghaemi, T. Thio, Electrical conductivity of individual carbon nanotubes. *Nature* **1996**, *382*, 54–56.

[20] R. H. Baughman, A. A. Zakhidov, W. A. Heer, Carbon Nanotubes--the Route Toward Applications. *Science* **2002**, *297*, 787–792.

[21] Y. Lin, X. Cui, C. Yen, C. M. Wai, Platinum/Carbon Nanotube Nanocomposite Synthesized in Supercritical Fluid as Electrocatalysts for Low-Temperature Fuel Cells. *J. Phys. Chem. B* **2005**, *109*, 14410–14415.

[22] Y. Xing, Synthesis and Electrochemical Characterization of Uniformly-Dispersed High Loading Pt Nanoparticles on Sonochemically-Treated Carbon Nanotubes. *J. Phys. Chem. B* **2004**, *108*, 19255–19259.

[23] M. S. Saha, R. Li, X. Sun, High loading and monodispersed Pt nanoparticles on multiwalled carbon nanotubes for high performance proton exchange membrane fuel cells. *J. Power Sources* **2008**, *177*, 314–322.

[24] D. Villers, S. Sun, A. M. Serventi, J. P. Dodelet, Characterization of Pt Nanoparticles Deposited onto Carbon Nanotubes Grown on Carbon Paper and Evaluation of This Electrode for the Reduction of Oxygen. *J. Phys. Chem. B* **2006**, *110,* 25916–25925.

[25] X. Zhao, W. Li, L. Jiang, W. Zhou, Q. Xin, B. Yi, G. Sun, Multi-wall carbon nanotube supported Pt–Sn nanoparticles as an anode catalyst for the direct ethanol fuel cell. *Carbon*, **2004**, **42,** 3263–3265.

[26] C. Du, M. Chen, X. Cao, G. Yin, P. Shi, A novel CNT@SnO$_2$ core–sheath nanocomposite as a stabilizing support for catalysts of proton exchange membrane fuel cells. *Electrochem. Commun.*, **2009**, *11,* 496–498.

[27] M. S. Saha, R. Li, M. Cai, X. Sun. Nanowire-based three-dimensional hierarchical core/shell heterostructured electrodes for high performance proton exchange membrane fuel cells. *J. Powder Sources* **2008**, *185*, 1079–1085.

[28] R. Li, X. Sun, Y. Zhou, M. Cai, X. Sun**.** Aligned Heterostructures of Single-Crystalline Tin Nanowires Encapsulated in Amorphous Carbon Nanotubes. *J. Phys. Chem. C* **2007**, *111*, 9130–9135.

[29] Y. Wang, J. Y. Lee, Electrochemical Switching and Size Selection in Cucurbit[8]uril-Mediated Dendrimer Self-Assembly. *Angew. Chem. Int. Ed.* **2006**, *45*, 7042–7046.

[30] P. Marcus, C. Hinnen, XPS study of the early stages of deposition of Ni, Cu and Pt on HOPG. *Surf. Sci.* **1997**, *392*, 134–142.

[31] Z. W. Chen, M. Waje, W. Li, Y. Yan, Supportless Pt and PtPd Nanotubes as Electrocatalysts for Oxygen-Reduction Reactions. *Angew. Chem. Int. Ed.* **2007**, *46,* 4060–4063.

[32] G. Che, B. B. Lakshmi, E. R. Fisher, R. Martin, Carbon nanotubule membranes for electrochemical energy storage and production. *Nature* **1998**, *393*, 346–349.

[33] R. Manohara, J. B. Goodenough, Methanol oxidation in acid on ordered NiTi. *J. Mater. Chem.* **1992**, *2*, 875–887.

[34] F. Colmati, E. Antolini, E. R. Gonzalez, Effect of temperature on the mechanism of ethanol oxidation on carbon supported Pt, PtRu and Pt_3Sn electrocatalysts. *J. Power Sources* **2006**, *157*, 98–103.

[35] P. Bommersbach, M. Mohamedi, D. Guay, Electro-oxidation of Ethanol at Sputter-Deposited Platinum–Tin Catalysts. *J. Electrochem. Soc.* **2007**, *154*, B876–B882.

[36] Y. Bi, G. Lu, Control growth of uniform platinum nanotubes and their catalytic properties for methanol electrooxidation. *Electrochem.Commun.* **2009**, *11*, 45–49.

[37] M. S. Saha, R. Li, M. Cai, X. Sun, High Electrocatalytic Activity of Platinum Nanoparticles on SnO_2 Nanowire-Based Electrodes. *Electrochem. Solid-State Lett.*, **2007**, *10*, B130–B133.

Supporting Information
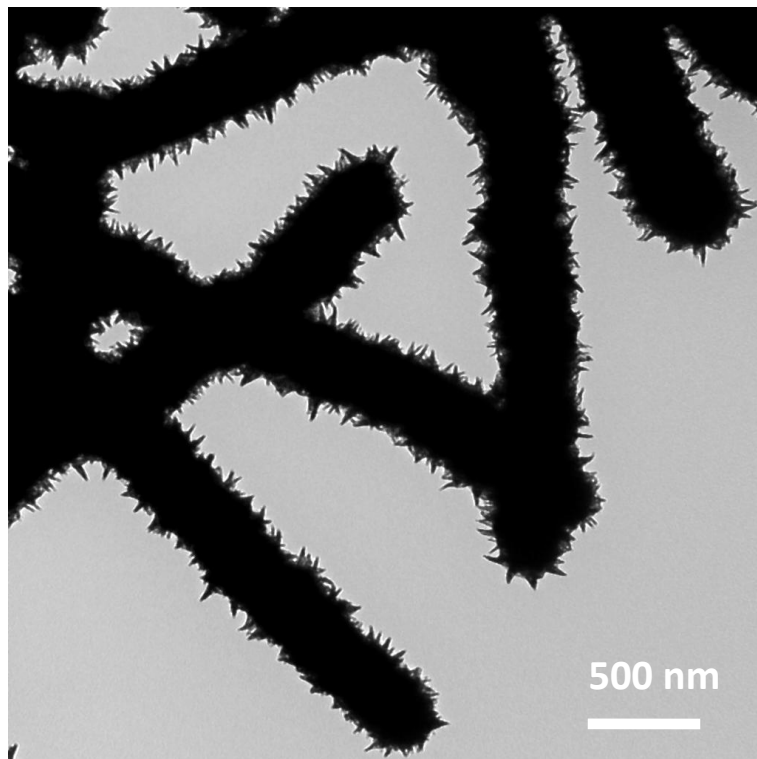
Figure SI-4.1. TEM image of PtNW–Sn@CNT heterostructures.

Chapter 5. Ultrathin single crystal Pt nanowires grown on N-doped carbon nanotubes

Shuhui Sun[1], Gaixia Zhang[1], Yu Zhong[1], Hao Liu[1], Ruying Li[1], Xiaorong Zhou[2], and Xueliang Sun[1,*]

[1]Department of Mechanical and Materials Engineering, The University of Western Ontario, London, Ontario, N6A 5B9 (Canada)
[2]School of Materials, University of Manchester, Manchester, UK, M60 1QD
E-mail: xsun@eng.uwo.ca

In chapters 3 and 4, we have demonstrated that 1D Pt nanowires are a new type of promising catalyst with much enhanced performance for ORR, MOR and CO tolerance than commercial PtNP/C catalyst. It is well accepted that the surface area increases with the diameter decrease of individual wire, which in turn, has immediate effect on surface-related applications. That means, in terms of the same amount Pt, thinner nanowires can provide more surface area, and accordingly potential higher activity. Therefore, ultra-thin Pt nanowires with smaller diameters are highly desirable to further improve their fuel cell performance. From our previous work, we can see that when using carbon black, carbon nanotubes, Sn@CNT nanocable, etc., as supports, the diameters of Pt nanowires were always kept at 4 nm. In this chapter, the authors present a very interesting work. i.e., when N-CNTs were used as the support for Pt nanowire growth, the diameters of Pt nanowires decreased to 2.5 nm in average. Time-dependent growth process of ultrathin Pt nanowires on N-CNT support was systematically investigated by collecting products at different reaction time and investigated under TEM. By combining the TEM results with XPS and EELS

mapping techniques, it is believed that the widely distributed defects, associated with N incorporation, on CNTs surface, confine the Pt atoms and play a key role in the formation of the tiny nuclei that further lead to the anisotropic growth of ultrathin nanowires. This synthetic strategy and the underlying mechanism could provide new insight into the synthesis of other metal, e.g., Au, Pd and Ag, nanowires with dimensions similar to those reported here.

5.1 Introduction

Among various one-dimensional (1D) noble metal nanostructures, platinum nanowires (Pt NWs) are of particular importance and are expected to play a critical role in electronics, catalysis, fuel cells and the automotive industries, as this metal has outstanding catalytic and electrical properties and superior resistance to corrosion [1,2]. To date, various methods have been developed for the synthesis of Pt NWs. However, wet-chemical methods often lead to the formation of relatively large diameter (>10 nm) or polycrystalline wires whereas the commonly used template approach has problems associated with the removal of the template [3]. It is well accepted that the surface area increases with the diameter decrease of individual wire, which in turn, has immediate effect on surface-related applications [4]. There is very limited success in producing ultrafine Pt NWs, especially on the scale below 5 nm [5]. Very recently, a flurry of papers has appeared in the literature regarding the synthesis of Au ultrathin (<3 nm) NWs [6]. However, the synthesis of ultrathin NWs of single crystal Pt with such small diameters is still challenging.

Recently, nitrogen-doped carbon nanotubes (N-CNTs) have attracted much attention due to their unique properties and wide applications [7]. Specifically, they have been widely used as diverse matrices to fabricate various nanocomposites such as Pt/N-CNTs, which possess great potential in fuel cells, electronic devices, and chemical sensors [8].

Here we report a straightforward solution method for the synthesis of single crystalline ultrathin Pt NWs, with uniform diameters of ~2.5 nm and lengths up to 100 nm, on N-CNTs. In addition, direct evidence for the formation of ultrathin Pt NWs was provided by systematically investigating their growth process, and the key role of nitrogen was revealed. The synthetic procedure is very facile, and only two chemicals (H_2PtCl_6 and HCOOH) were used throughout the whole synthetic process, without using any stabilizing agent. Further, the reaction was conducted at room temperature in environmentally friendly aqueous solution.

5.2 Experimental

5.2.1 Synthesis of N-doped carbon nanotubes

The synthesis of N-doped carbon nanotubes (N-CNTs) was carried out via CVD method. Typically, pure melamine power (2 g) was placed in an alumina boat inserted at the entrance of a quartz tube in a horizontal tube furnace, while the substrate (carbon paper sputtered with 5 nm Fe film on the surface) was loaded in the centre of the quartz tube. The distance between the source and substrate was around 12 cm. The system was heated to 800 ^{o}C rapidly under an Ar flow of 320 sccm and kept at this temperature for 30 minutes, and then cool down to room temperature.

5.2.2 Synthesis of platinum nanowires on N-CNTs

In a typical synthesis, 0.032 g hexachloroplatinic acid (H_2PtCl_6 $6H_2O$, Aldrich) and 1 mL formic acid (HCOOH, Aldrich) were added simultaneously to 20 mL H_2O to form a golden orange solution. The N-CNTs (nitrogen content of 10.4 at.%) grown on carbon paper, synthesized by a CVD method [9], were immersed in the above solution, acting as the growth substrates. Then the reaction proceeded at room temperature without stirring for up to 3 days until the solution color gradually changed to colorless. The final product can be easily collected by handling the carbon paper support and washing with deionized water.

5.2.3 Characterizations

The morphologies and microstructures of the as-prepared samples were examined by scanning electron microscope (SEM, Hitachi S-4800) operated at 5kV, and transmission electron microscopy (TEM, JEOL JEM-2100) operated at 200 kV. X-ray photoelectron spectroscopic (XPS) analysis was carried out in a VG ESCALAB 220iXL, using monochromated Al Ka source (1486.6 eV), at a base pressure of 2×10^{-9} mbar. High resolution spectra were obtained at a perpendicular take-off angle, using a pass energy of 20 eV and steps of 0.05 eV. All the binding energies were calibrated

by referring to the C1s line at 284.8 eV from adventitious carbon. After Shirley background removal, the component peaks were separated using the public domain XPSPeak program version 4.1.

5.3. Results and Discussion
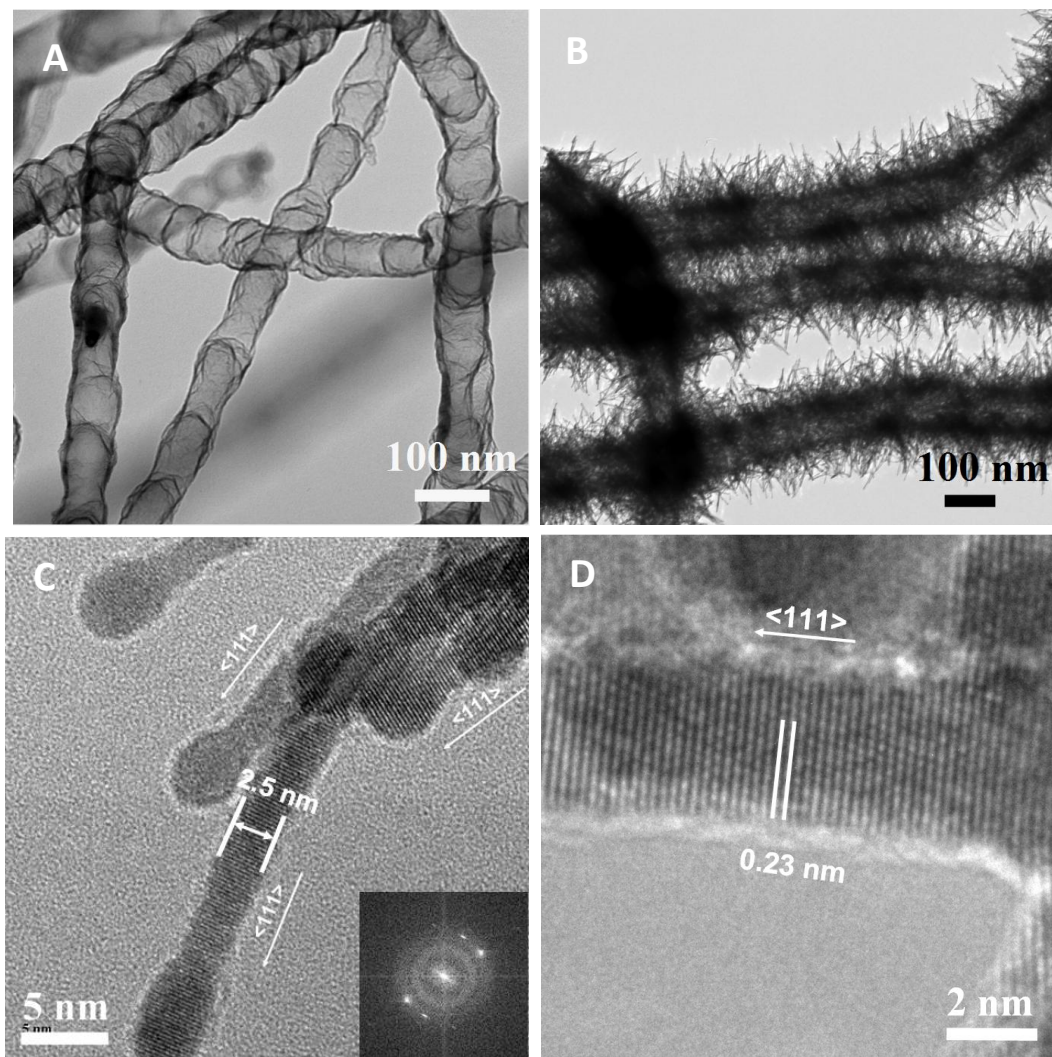
Figure 5.1. TEM images of N-CNTs before (A) and after (B) the growth of Pt NWs; TEM (C) and HRTEM (D) images of ultrathin Pt NWs.

Figure 5.1 shows the representative transmission electron microscopy (TEM) images of N-CNTs before and after growth of the Pt NWs. It can be seen that the pristine N-CNTs have diameters ranging from 40 to 60 nm (Figure 5.1A, and Figure SI-5.1), and the bamboo-like structure can be attributed to the integration of N into the graphitic structure [7]. Figure 5.1B shows that numerous Pt NWs, with lengths up to 100 nm, grow uniformly on N-CNTs, forming a hybrid structure of Pt NWs/N-CNTs. The higher magnification image (Figure 5.1C) indicates that the diameter of the Pt NWs is less than 3 nm. The aspect ratio of Pt NWs easily approaches 50. A survey of several tens of Pt NWs under TEM investigation reveals that the diameters of these NWs are in the range of 2 to 3 nm, with an average of 2.5 nm. Besides the ultrathin nature, these Pt NWs are also single crystalline. Selected area electron diffraction (SAED) pattern recorded from a few NWs confirms their high crystallinity (inset in Figure 5.1C). The high-resolution TEM (HRTEM) image (Figure 5.1D) shows that the Pt NWs grow along <111> direction, and the interplanar distance between the {111} planes is 0.23 nm which matches that for bulk Pt crystals. To the best of our knowledge, this is the first time that single crystal Pt NWs with such thin diameters were synthesized with such a facile method. Interestingly, our previous work shows that under similar synthetic conditions but without using N-incorporated supports, Pt NWs that grew either freely in solution or on CNT and carbon black supports, always have relative larger diameters of 4 nm [2b,5b,c] (also see Figure SI5.2–SI5.4). These reveal that N-doping into CNTs is crucial to the formation of ultrathin Pt NWs with diameter less than 3 nm.

In order to investigate the possible reasons for the formation of ultrathin Pt NWs on N-CNTs, X-ray photoelectron spectroscopy (XPS) was employed to study the chemical composition and status of the product. The asymmetric C1s high-resolution spectrum (Figure 5.2A, centered at ~285 eV) is deconvoluted into five peaks, which can be assigned, respectively, to the C–C bonds in graphite (PC1), alternate defect carbon structures associated with C–N and C–O bonds overlapping (286–289 eV, PC2–4), and PC1 $\pi^* \leftarrow \pi$ shake-up satellite (PC5). Comparing the carbon spectra
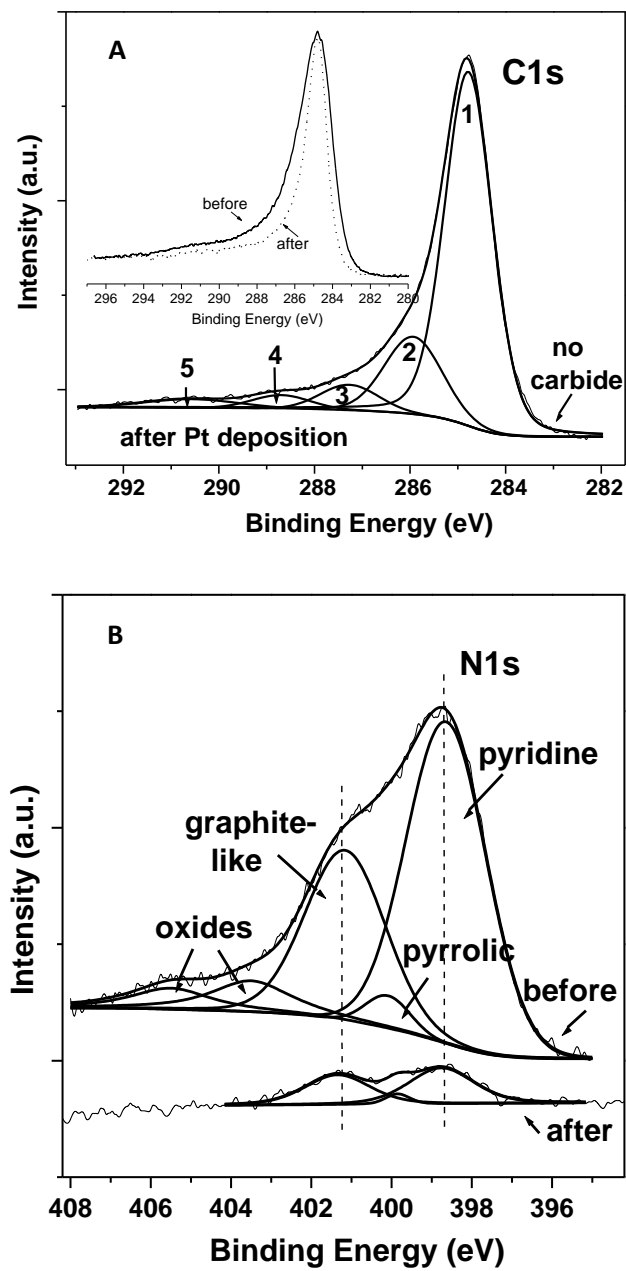
Figure 5.2. Typical XPS spectra of N-CNTs before and after Pt deposition. (A) C1s, and (B) N1s.

before and after Pt growth (inset of Figure 5.2A), the latter one shows a narrower band with significant decrease of PC2–4 peaks corresponding to the localized (defect) carbon atoms [11], which can be attributed to the block effect of Pt NWs to the X-ray. This indicates that Pt NWs are more easy to deposit on the defects of the N-CNTs than on the perfect graphite structures. The deconvolution of the Pt4f spectrum (Figure SI5.5) indicates pure metallic Pt, without obvious carbide and nitride formation. Figure 5.2B shows the N1s spectra of the N-CNTs before and after Pt deposition. The pristine N1s spectrum was deconvoluted into 5 peaks [10]. It is believed that the main peak (398.7 eV) corresponding to the pyridine-like N within the predominantly graphitic framework is responsible for both the wall roughness and interlinked morphologies observed in the N-doped structure [11]. After Pt deposition, in addition to the significant decrease of the whole N1s signal and the almost complete disappearance of two peaks corresponding to the oxide N atoms (403–405 eV), the area ratio of pyridine-like (398.7 eV) to graphite-like (401.0 eV) N decreased from 1.81 to 1.21, further implying that Pt NWs grow preferentially on the defect sites that more associated with pyridine N, of the N-CNTs.

The distribution of nitrogen and carbon in the N-CNTs was studied by elemental mapping using electron energy loss spectroscopy (EELS) (Figure 5.3). The brighter regions represent a higher concentration of the element. Figure 5.3C shows that while the N atoms seem to be present throughout of the N-CNTs, they are more prevalent on the wall ruffles and the interlinked parts (nodes) of N-CNTs which may be assigned mainly to the pyridine-like N [11]. This is consistent with our XPS results since much higher concentration pyridine-like than other types N was detected in pristine N-CNTs. According to our XPS results, these defects induced by N incorporation would provide preferred anchoring sites for Pt deposition.

To reveal the underlying growth mechanism of ultrathin Pt NWs on N-CNTs, products were collected as a function of growth time, and their morphologies were evaluated by TEM and HRTEM. The HRTEM image of a pristine N-CNT (Figure 5.4A) shows that the intersects are usually consist of 4–6 graphitic layers. Between
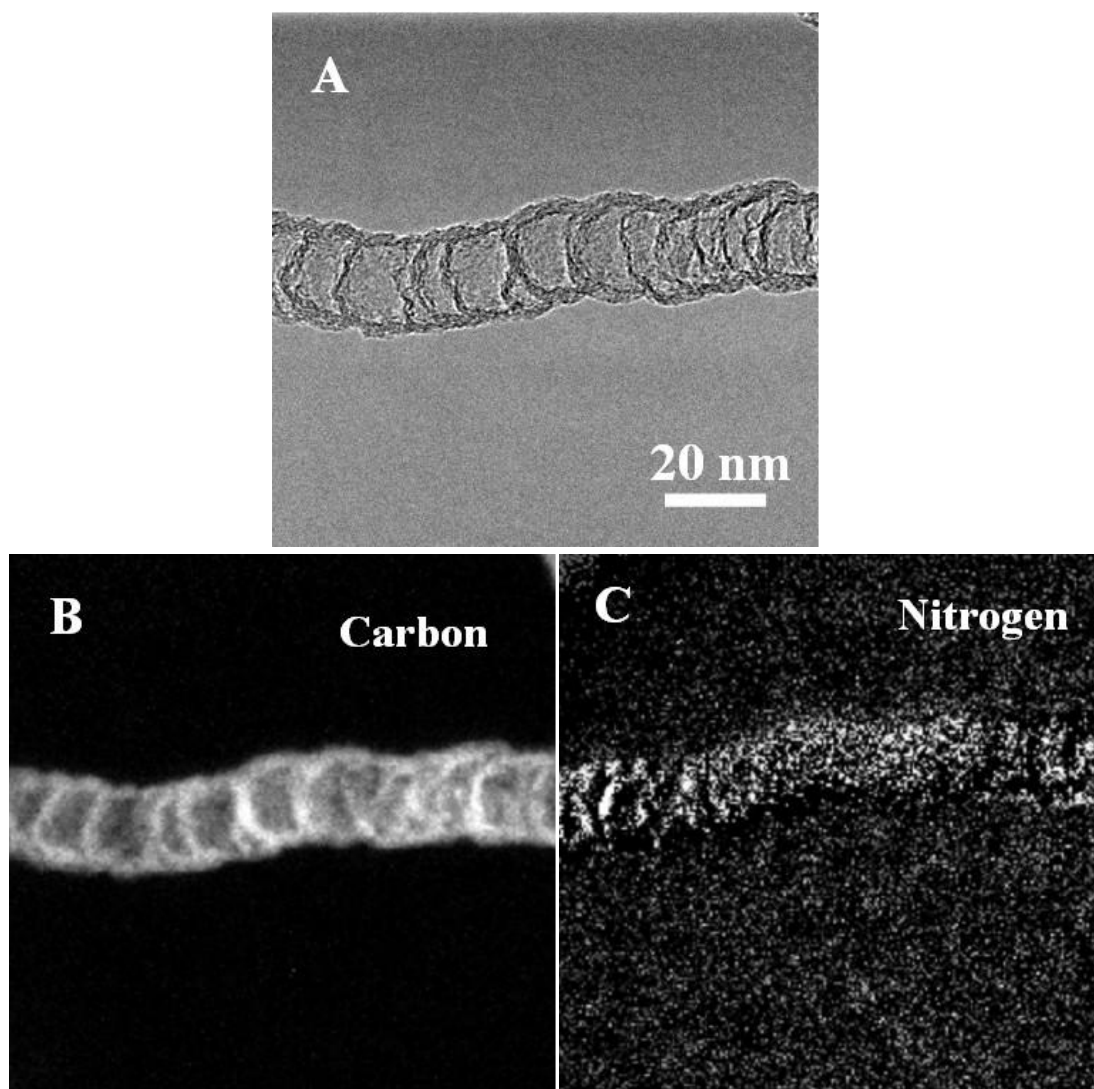
Figure 5.3. EELS mapping of a pristine N-doped CNT: (A) bright field image; (B) carbon map; (C) nitrogen map.
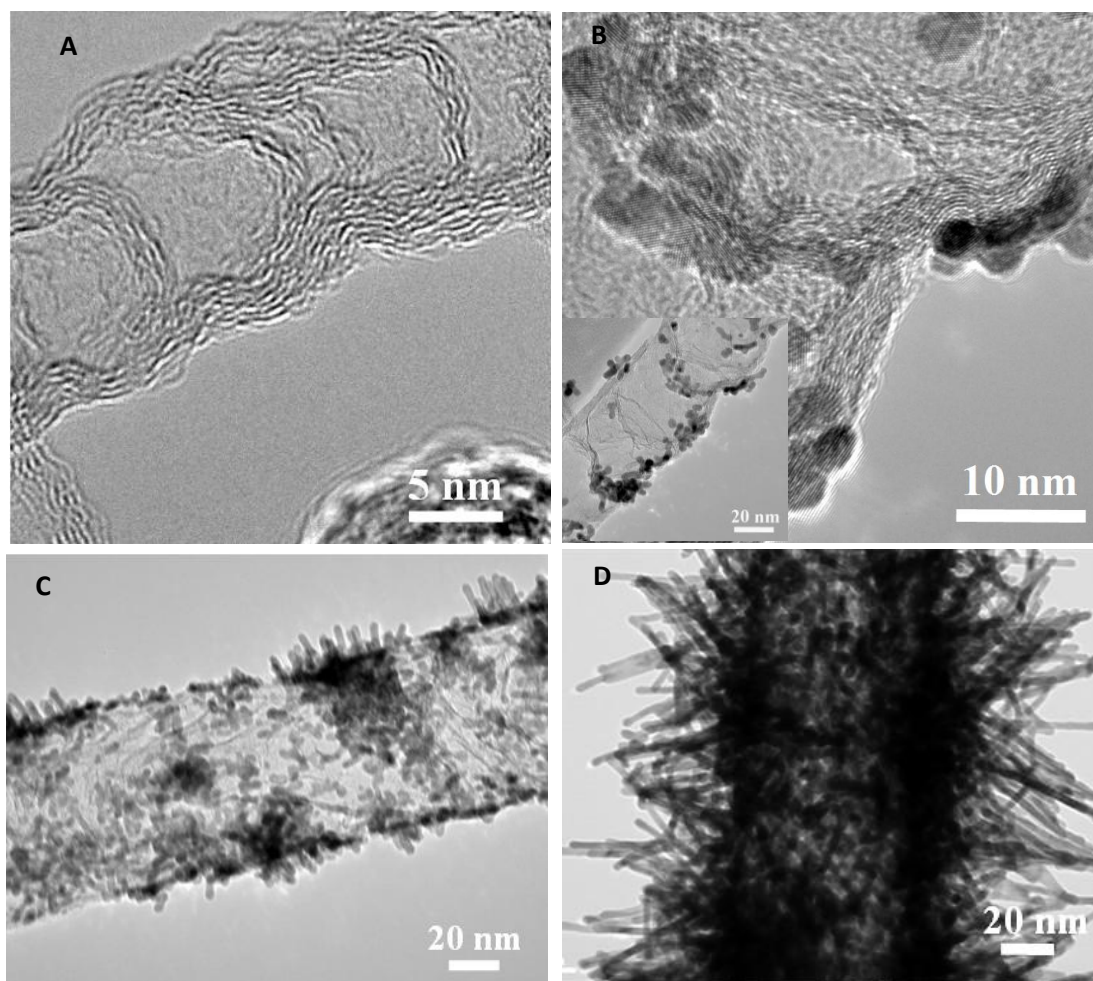
Figure 5.4. TEM images show the growth process of ultrathin Pt NWs on N-CNTs. (A) pristine N-CNT; (B) initial (nuclei), (C) intermediate and (D) final growth stages.

these intersects, there are many irregular web-like structures (2–3 atomic layers) across the surface. Careful inspection reveals the existence of many broken graphitic layers (defects) along the entire surface of the nanotube, suggesting that N incorporation into CNTs promotes not only the bamboo-structured morphology but also strongly affects the tube defect structure. At the initial growth stage (Figure 5.4B and inset), Pt nuclei readily attach to the sites with higher density defects along the N-CNTs, since nitrogen can enhance the Pt adsorption on the CNT surface due to its large electron affinity [12]. Interestingly, the size of the Pt nanoparticles (nuclei) ranges from 2 to 3 nm with an average of 2.5 nm, which is smaller than those on carbon nanotubes and nanospheres. We believed that the broken graphitic layers, which are more associated with the pyridinic N, confine the Pt atoms and provide the main initial nucleation sites for the formation of Pt nanoparticles with small diameters. This may be the key for the formation of ultrathin Pt NWs on N-CNTs. As the growth time increased, a large amount of nanoparticles progressively cover the whole surface of the N-CNTs. These small Pt nuclei act as the seeds to direct the anisotropic growth of Pt NWs, in that the growth rate along the closed-packed <111> direction is enhanced at very slow reduction rate [15], forming Pt NW/N-CNT hybrid novel structures (Figure 5.4C and D).

5.4 Conclusions

Ultrathin (2–3 nm in diameter) Pt NWs have been synthesized on N-CNTs by a very facile aqueous solution method at room temperature. It is believed that the widely distributed defects, associated with N incorporation, on the N-CNTs surface, confine the Pt atoms and play a key role in the formation of the tiny nuclei that further leads to the anisotropic growth of ultrathin nanowires. This synthetic strategy and the underlying mechanism could give new insight into the synthesis of other metal nanowires with dimensions similar to those reported here. Isolated ultrathin nanowires could be obtained if the N-CNT supports were deliberately removed. These ultrathin nanowires and their composites with N-CNTs hold potential for catalysis, fuel cells and electrochemical sensors.

Acknowledgements

References

[1] H. A. Gasteiger, S. S. Kocha, B. Sompalli and F. T. Wagner, Activity benchmarks and requirements for Pt, Pt-alloy, and non-Pt oxygen reduction catalysts for PEMFCs. *Appl. Catal. B: Environ.*, 2005, **56**, 9–35.

[2] (*a*) W. Lu, B. Mi, M. C. W. Chan, Z. Hui, C. Che, N. Zhu and S. T. Lee, Light-Emitting Tridentate Cyclometalated Platinum(II) Complexes Containing σ-Alkynyl Auxiliaries: Tuning of Photo- and Electrophosphorescence. *J. Am. Chem. Soc.*, 2004, **126**, 4958–4971; (*b*) S. Sun, F. Jaouen and J. P. Dodelet, Controlled Growth of Pt Nanowires on Carbon Nanospheres and Their Enhanced Performance as Electrocatalysts in PEM Fuel Cells. *Adv. Mater.*, 2008, **20**, 3900–3904.

[3] Y. Xia, P. Yang, Y. Sun, Y. Wu, B. Mayers, B. Gates, Y. Yin, F. Kim and H. Yan, One-Dimensional Nanostructures: Synthesis, Characterization, and Applications. *Adv. Mater.*, 2003, **15**, 353–389.

[4] L. Cademartiri and G. A. Ozin, Ultrathin Nanowires—A Materials Chemistry Perspective. *Adv. Mater.*, 2009, **21**, 1013–1020.

[5] (*a*) J. Chen, T. Herricks, M. Geissler and Y. Xia, Single-Crystal Nanowires of Platinum Can Be Synthesized by Controlling the Reaction Rate of a Polyol Process. *J. Am. Chem. Soc.*, 2004, **126**, 10854–10855; (*b*) S. Sun, D. Yang, D. Villers, G. Zhang, E. Sacher and J. P. Dodelet, Template- and Surfactant-free Room Temperature Synthesis of Self-Assembled 3D Pt Nanoflowers from Single-Crystal Nanowires. *Adv. Mater.*, 2008, **20**, 571–574; (*c*) S. Sun, D. Yang, G. Zhang, E. Sacher and J. P. Dodelet. Synthesis and Characterization of Carbon Nanotube–Platinum Nanowire Heterostructures. *Chem. Mater.*, 2007, **19**, 6376–6378.

[6]   (*a*) C. Wang, Y. Hu, C. M. Lieber and S. Sun, Ultrathin Au Nanowires and Their Transport Properties. *J. Am. Chem. Soc.*, 2008, **130**, 8902–8903; (*b*) Z. Huo, C. Tsung, W. Huang, X. Zhang and P. Yang, Sub-Two Nanometer Single Crystal Au Nanowires. *Nano Lett.*, 2008, **8**, 2041–2044; (*c*) X. Lu, M. Yavuz, H. Tuan, B. A. Korgel and Y. Xia, Ultrathin Gold Nanowires Can Be Obtained by Reducing Polymeric Strands of Oleylamine−AuCl Complexes Formed via Aurophilic Interaction. *J. Am. Chem. Soc.*, 2008, **130**, 8900–8901; (*d*) N. Pazos-Perez, D. Baranoy, S. Irsen, M. Hilgendorff, L. M. Marzan and M. Giersig, Synthesis of Flexible, Ultrathin Gold Nanowires in Organic Media. *Langumir*, 2008, **24**, 9855–9860; (*e*) Z. Li, J. Tao, X. Lu, Y. Zhu and Y. Xia, Facile Synthesis of Ultrathin Au Nanorods by Aging the AuCl(oleylamine) Complex with Amorphous Fe Nanoparticles in Chloroform. *Nano Lett.*, 2008, **8**, 3052–3055; (*f*) H. Feng, Y. Yang, Y. You, G. Li, J. Guo, T.Yu, Z. Shen, T. Wu and B. Xing, Simple and rapid synthesis of ultrathin gold nanowires, their self-assembly and application in surface-enhanced Raman scattering. *Chem. Commun.*, 2009, **15**, 1984–1986.

[7]   K. Gong, F. Du, Z. Xia, M. Durstock and L. Dai, Nitrogen-Doped Carbon Nanotube Arrays with High Electrocatalytic Activity for Oxygen Reduction. *Science*, 2009, **323**, 760–764.

[8]   M. Saha, R. Li, X. Sun and S.Ye, 3-D composite electrodes for high performance PEM fuel cells composed of Pt supported on nitrogen-doped carbon nanotubes grown on carbon paper. *Electrochem. Commun.*, 2009, **11**, 438–441.

[9]   S. Trasobares, O. Stephan, C. Colliex, W. K. Hsu, H. W. Kroto and D. R. M. Walton, Compartmentalized CN_x nanotubes: Chemistry, morphology, and growth. *J. Chem. Phys.*, 2002, **116**, 8966–8972.

[10]   (*a*) S. V. Dommele, A. Romero-izquirdo, R. Brydson, K. P. De Jong and J. H. Bitter, Tuning nitrogen functionalities in catalytically grown nitrogen-

containing carbon nanotubes. *Carbon*, 2008, **46**, 138–148; (*b*) H. C. Choi, S. Y. Bae, W. S. Jang, J. Park, H. Song, H. J. Shin, H. Jung and J. P. Ahn, Release of N_2 from the Carbon Nanotubes via High-Temperature Annealing. *J. Phys. Chem. B*, 2005, **109**, 1683–1688.

[11] J. Liu, S. Webster and D. L. Carroll, Temperature and Flow Rate of NH_3 Effects on Nitrogen Content and Doping Environments of Carbon Nanotubes Grown by Injection CVD Method. *J. Phys. Chem. B*, 2005, **109**, 15769–15774.

[12] Y. Li, T. Hung and C. Chen, A first-principles study of nitrogen- and boron-assisted platinum adsorption on carbon nanotubes. *Carbon*, 2009, **47,** 850–855.

Supporting Information
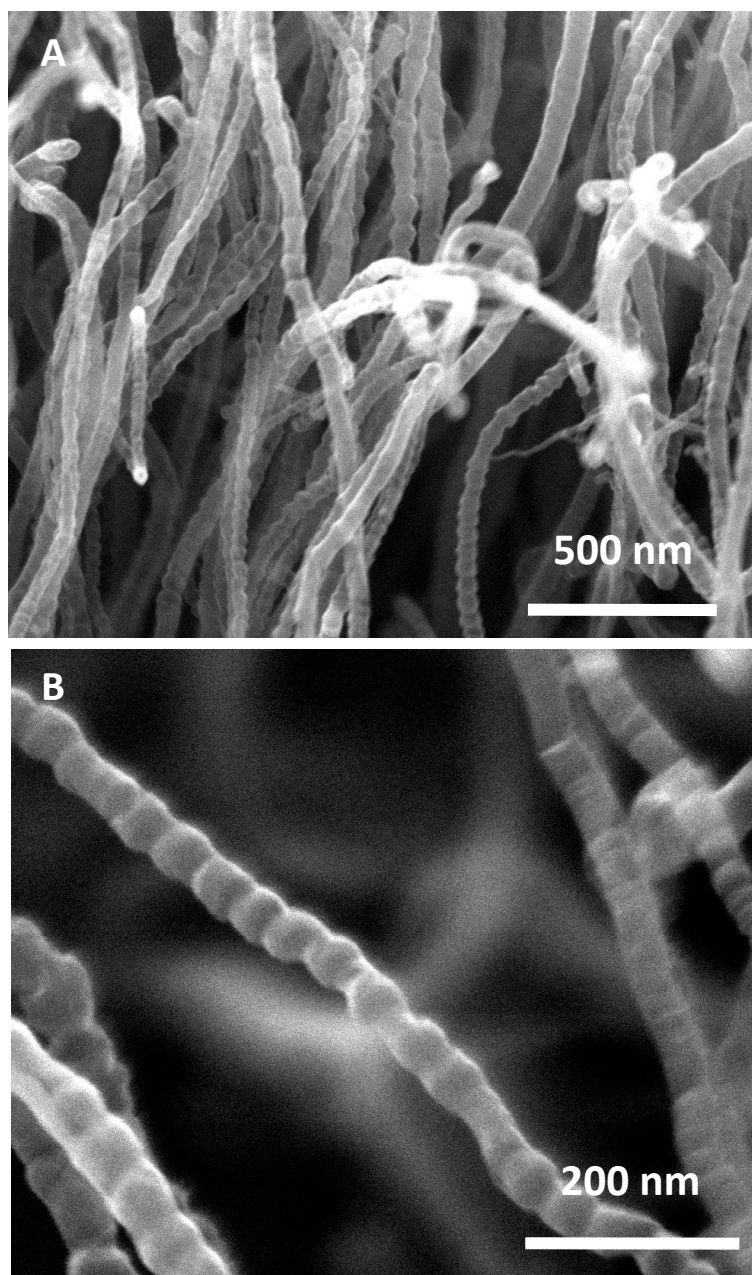
Figure SI-5.1. SEM images of pristine N-CNTs at two different magnifications. The typical bamboo-like structure can be attributed to the integration of N into the graphitic structure.
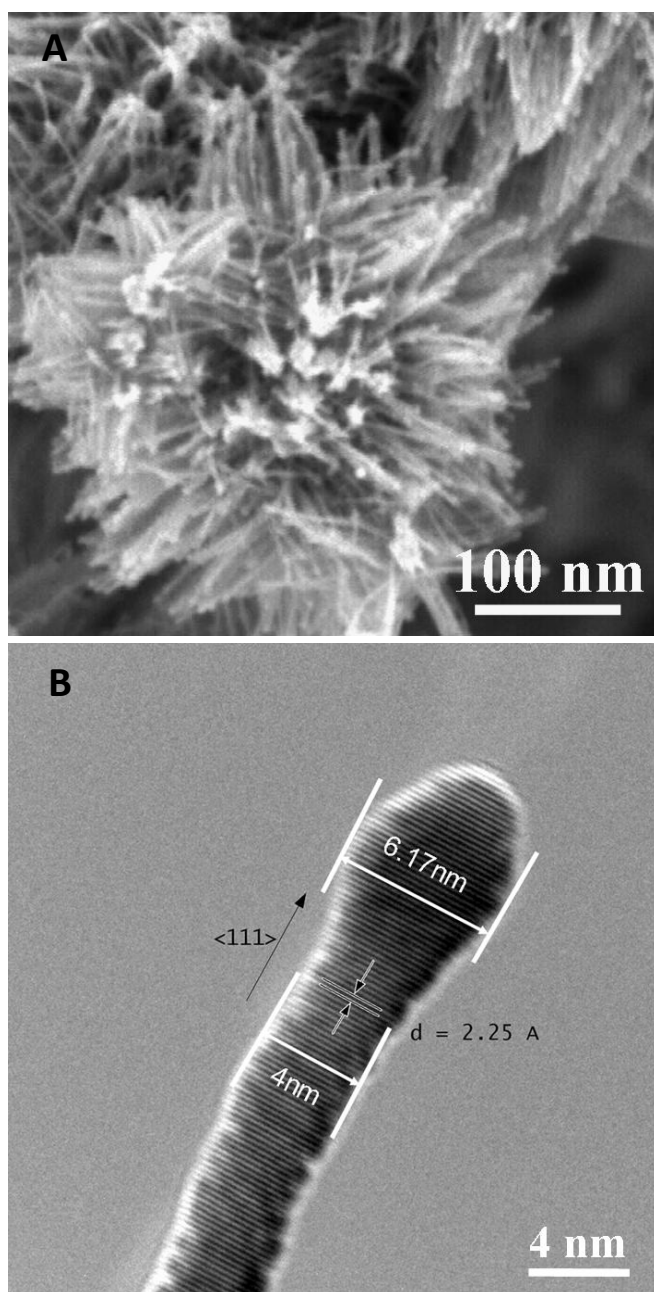
Figure SI-5.2. SEM and TEM images of unsupported Pt nanowires which grew freely in the solution. The average diameter of Pt nanowires is 4 nm.
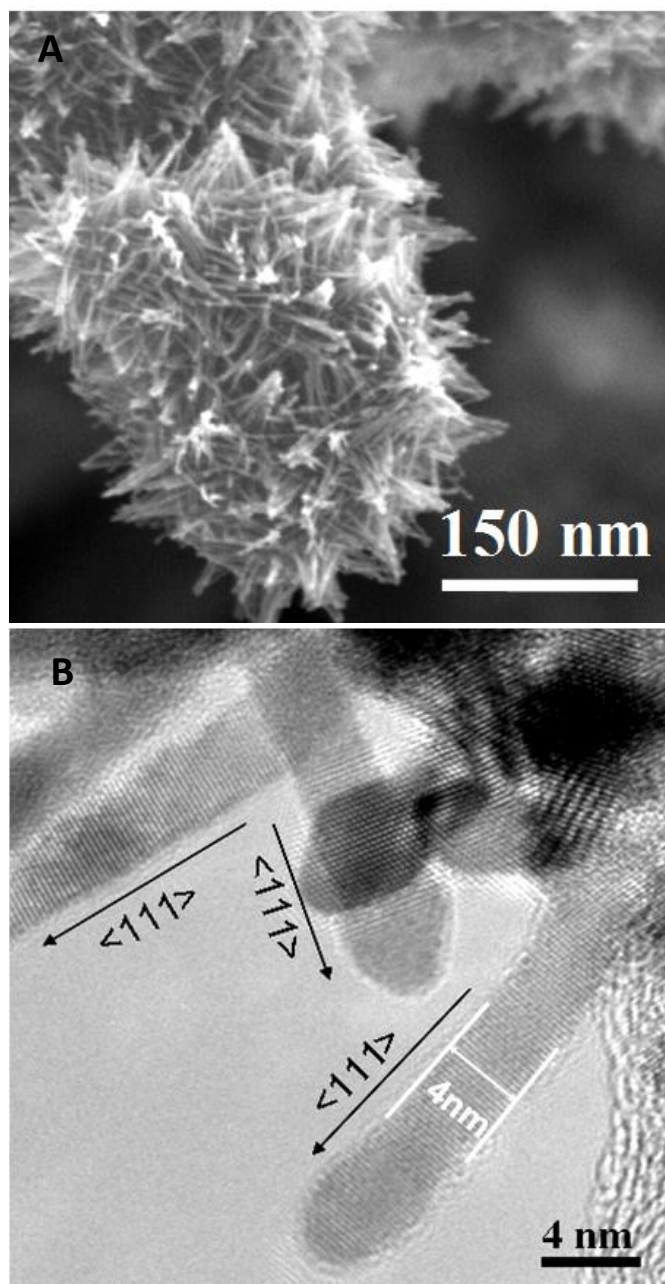
Figure SI-5.3. SEM and TEM images of Pt nanowires grown on carbon black spheres. The average diameter of Pt nanowires is 4 nm.
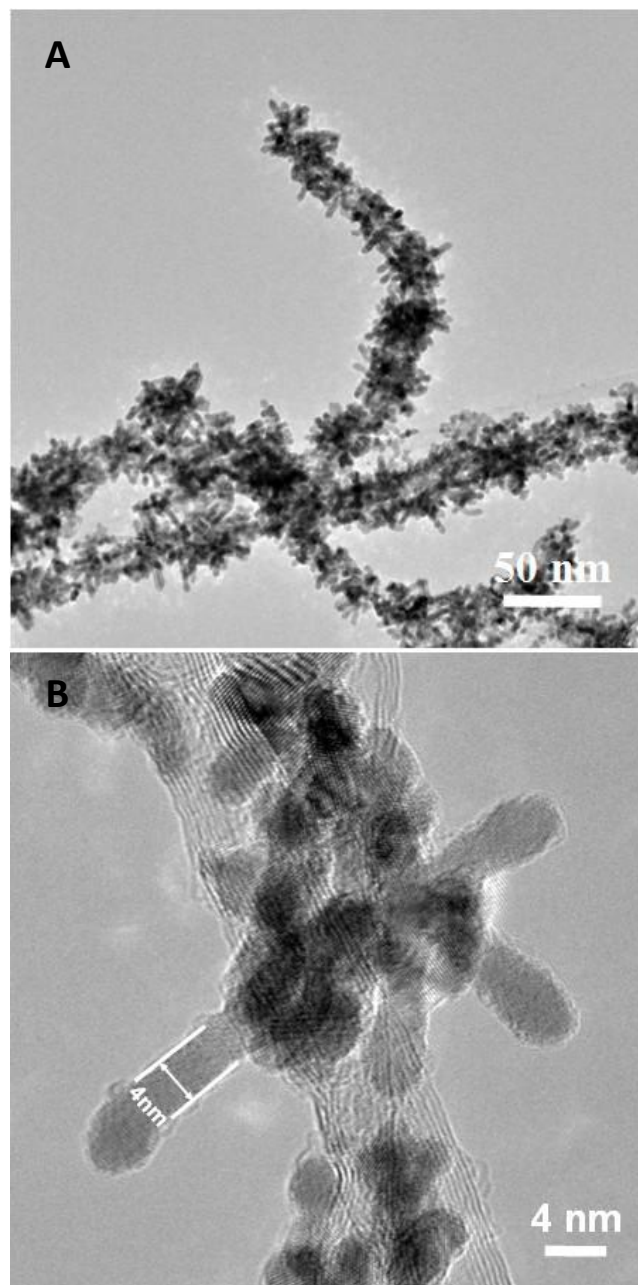
Figure SI-5.4. TEM images of Pt nanowires grown on carbon nanotubes. The average diameter of Pt nanowires is 4 nm.
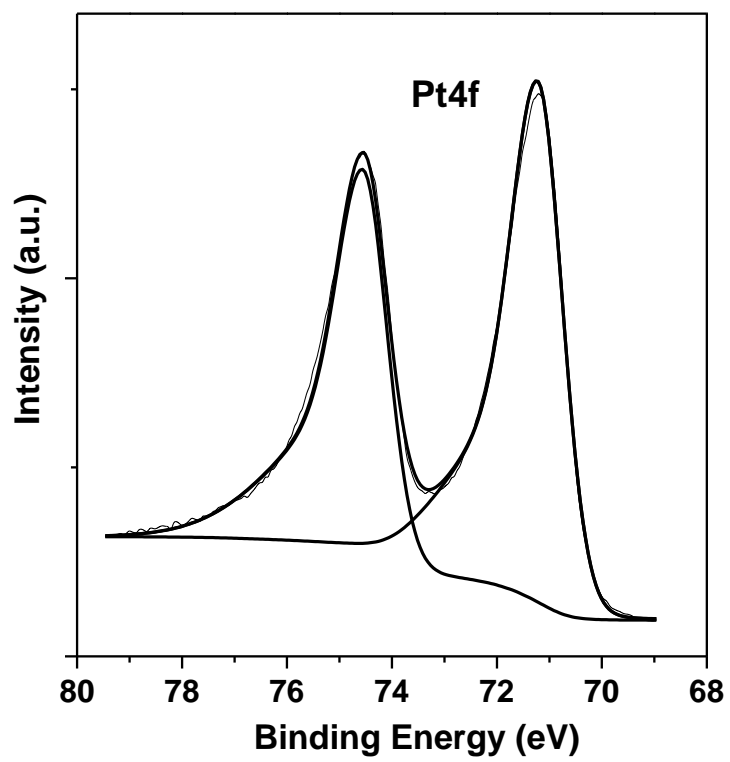
Figure SI-5.5. An typical XPS peak separation of Pt4f.

Chapter 6. Highly Stable and Active Pt/Nb-TiO$_2$ Carbon-free Electrocatalyst for Proton Exchange Membrane Fuel Cells

Shuhui Sun[1], Gaixia Zhang[1], Xueliang Sun[1,*], Mei Cai[2,*], and Martin Ruthkosky[2]

[1]*Department of Mechanical and Materials Engineering, The University of Western Ontario, London, Ontario, N6A 5B9 (Canada)*
[2]*General Motors Research and Development Center, Warren, MI 48090-9055 (USA)*
E-mails: mei.cai@gm.com (M. Cai) and xsun@eng.uwo.ca (X. Sun)

On the other hand, in terms of the low durability of PEM fuel cell catalysts, the corrosion of carbon support materials has been identified to be the major contributor to the catalyst failure. Unfortunately, the current commonly-used carbon black supports in PEMFCs are not sufficiently durable for commercial deployment. One of the major challenges and solutions lies in the development of inexpensive, efficient, and highly durable alternative catalyst supports that possess high corrosion resistance, high conductivity and high surface area.

Metal oxides have been studied by different research groups as alternative catalyst supporting materials, such as sub-stoichiometric titanium oxide (TiO$_x$), indium tin oxide (ITO), niobium-doped titanium oxide (Nb-TiO$_2$), tungsten oxide (WO$_x$), and tin oxide (SnO$_2$). Among such materials, titanium oxides are promising alternative catalyst supports due to their stability in fuel cell operation atmosphere, low cost, commercial availability, stability in water, and strong metal support interaction (SMSI). The use of Nb doping has been found to significantly improve the electrical conductivity of TiO$_2$, and Nb-TiO$_2$ supported Pt catalysts showed very good performance in PEM fuel cells.

In this chapter, the authors demonstrate a new type of carbon-free Pt/Nb-TiO$_2$ electrocatalyst. Mesoporous Nb-TiO$_2$ hollow spheres were synthesized through the sol-gel method by using polystyrene (PS) spheres as templates. Pt nanoparticles (NPs) were then deposited onto mesoporous Nb-TiO$_2$ hollow spheres via a wet-chemical route in aqueous solution at 80 ^{o}C. The Pt loadings on Nb-TiO$_2$ supports could be easily modulated from 10 to 40 %, with similar Pt particle size, by simply adjusting the ratios between precursor and support. Electrochemical studies show that Pt/Nb-TiO$_2$ composites exhibit up to 1.6 times higher activity and 2.1 times higher stability than commercial E-TEK Pt/C catalyst. 0D mesoporous Nb-doped TiO$_2$ hollow spheres is a promising alternative catalyst support for PEMFC applications.

6.1 Introduction

Proton exchange membrane fuel cells (PEMFCs) have been attracting much attention as an alternative clean energy source because of their high efficiency, high power density and low pollution [1]. However, there are still challenges, such as low catalytic activity, low durability and high cost, which are hindering the commercialization of PEMFCs [2]. For automotive applications, PEMFCs must be durable enough for ~5,000 driving hours (i.e., 10 years) in vehicles.[2] The loss of platinum (Pt) electrochemical surface area (ECSA) over time due to carbon support corrosion and Pt dissolution/aggregation/Oswald ripening is considered one of the major contributors to the degradation of fuel cell performance [3]. Usually, carbon black (Vulcan XC-72) is used as Pt catalyst support in PEMFCs. However, carbon black is known to undergo electrochemical oxidation under a fuel cell operating environment, especially at potentials above 0.9 V (equation 1), leading to a loss of Pt and fuel cell performance degradation [4, 5].

$$C + 2H_2O \longrightarrow CO_2 + 4H^+ + 4e^- \qquad (6.1)$$

Therefore, it is necessary to explore non-carbon catalyst support materials with the current fuel cell operating strategy. Some metal oxides have been studied by different research groups as alternative catalyst support materials, such as sub-stoichiometric titanium oxide [6, 7], indium tin oxide [8], niobium-doped titania [9], tungsten oxide [10, 11], and tin oxide [12]. Among these, niobium-doped titania (Nb-TiO$_2$) [9, 13–15] is a particularly promising candidate. TiO$_2$ is notable for its photocatalytic and strong metal support interaction (SMSI) properties [16, 17]. TiO$_2$ is also readily available, cheap, and non-toxic [18]. The use of Nb doping has been found to significantly improve the electrical conductivity of TiO$_2$, which allows its use in electrocatalytic reactions [14]. In this study, we present a facile wet-chemical route to grow Pt nanoparticles (NPs) on mesoporous Nb-TiO$_2$ hollow spheres, with controlled Pt loadings, in environmentally-friendly aqueous solution. PtNPs/Nb-TiO$_2$ catalysts

exhibit higher catalytic activity for ORR and better stability than the benchmark E-TEK commercial Pt/C catalysts.

6.2. Experimental

6.2.1 Chemicals

Hexadecyltrimethylammoniumbromide (HATB), titanium (IV) isopropoxide (TTIP), niobium (V) ethoxide (8 mol %), ethanol, HNO_3, hexachloroplatinic acid ($H_2PtCl_6.6H_2O$, 99.95%), and formic acid (HCOOH, 98%) were purchased from Sigma–Aldrich. Aqueous latex (mean diameter 200 nm) suspension (10 wt %) was purchased from Duke Scientific. All chemicals were used as received without further purifications. All solutions were prepared with ultrapure water purified with the Millipore water system (18.2 MΩ.cm resistivity @25 ^{o}C).

6.2.2 Preparation of Mesostructured Nb-TiO$_2$ Support

The mesostructured Nb-TiO$_2$ support was prepared according to the method described in reference 15. Briefly, 0.015 g of HATB, 14.7 mL of aqueous latex suspension, and 105 mL of ethanol were added in a PTFE beaker, and then the solution was stirred vigorously for 30 min while HNO_3 was added to adjust the pH to 3. A second solution was prepared by adding the precursors, 6.9 mL of TTIP and 0.5 mL niobium (V) ethoxide to 100 mL of ethanol. The second solution was added to the stirred latex-surfactant mixture using a peristaltic pump at a rate of 1 mL/min. The resulting suspension was processed using a Buchi B-290 spray drier to produce a fine white powder, consisting of the Nb–TiO$_2$ and latex template, which was followed by heat treatment at 500 ◦C for 2 h under argon in order to remove the latex template. To obtain rutile phase [19], the as-synthesized Nb–TiO$_2$ powder were heated at 1050 ◦C under hydrogen.

6.2.3 Preparation of PtNPs/Mesostructured Nb-TiO$_2$ Composite

The Pt nanoparticles were synthesized by the formic acid method as described in the literature [20–22]. The as-prepared mesostructured Nb-TiO$_2$ was used as the supporting substrate for Pt deposition. For the deposition of 40 wt % Pt on Nb-TiO$_2$, 22 mg of H$_2$PtCl$_6$.6H$_2$O (7.5 mg Pt) and 1 mL of HCOOH are added to 20 mL of water. Nb-TiO$_2$ (11.25 mg) was then dispersed in the above solution by mild ultrasonication for 30 min. After this initial dispersion, the solution is heated to 80 $^{\circ}$C and kept at this temperature for 30 min. After the reaction is completed, the product was washed thoroughly with deionized water and then dried in a vacuum oven at 60 $^{\circ}$C.

6.2.4 Physical Characterization

The morphologies and microstructures of the as-prepared samples were examined by scanning electron microscope (SEM, Hitachi S-4800) operated at 5kV, and transmission electron microscopy (TEM, JEOL JEM-2100) operated at 200 kV. X-ray diffraction (XRD) patterns were recorded on a Bruker D8 Advance diffractometer equipped with a Cu Ka radiation source. X-ray photoelectron spectroscopic (XPS) analysis was carried out in a VG ESCALAB 220iXL, using monochromated Al Ka source (1486.6 eV), at a base pressure of 2×10^{-9} mbar. High resolution spectra were obtained at a perpendicular take-off angle, using a pass energy of 20 eV and steps of 0.05 eV. All the binding energies were calibrated by referring to the C1s line at 284.8 eV from adventitious carbon. After Shirley background removal, the component peaks were separated using the public domain XPSPeak program version 4.1[23].

6.2.5 Electrode Preparation

The electrochemical measurements were conducted at room temperature in a standard three-electrode cell using a glassy carbon (GC) rotating disk electrode (RDE) setup with a Voltalab model PGZ100 potentiostat (Radiometer Analytical), and rotation control (MSR, Pine Instruments). A Pt wire served as the counter electrode, with a saturated calomel electrode (SCE) as the reference which was separated from the working electrode compartment by a closed electrolyte bridge. All potentials in this

study, however, are referenced to the reversible hydrogen electrode (RHE). The working electrode was prepared with a procedure similar to the one reported previously [8]. Typically, 5 mg catalyst was sonically mixed with 5 mL H_2O/isopropanol/Nafion (5/1/0.0017 in volume ratio) for 12 min to make a suspension. GC disk electrodes (5 mm diameter, 0.196 cm^2, Pine Research Instrument) served as the substrate and were polished to a mirror finish. An aliquot of catalyst suspension was pipetted onto the carbon substrate, resulting in approximate Pt loadings of 13 µgPt cm^{-2} for all catalysts. The catalyst films were dried under flowing nitrogen (N_2) at room temperature.

6.2.6 Electrochemical Measurements

The working electrode, in an argon (Ar) purged 0.1M $HClO_4$ solution at room temperature, was first cycled 200 times between 0 and 1.1 V at a 1V/s scan rate in order to produce a clean electrode surface. The cyclic voltammetry (CV) measurements were conducted by cycling the potential between 0 and 1.1 V, with a scan rate of 20 mV/s. The electrochemical surface areas (ECSA) were calculated from the hydrogen adsorption peak of the CV. The oxygen reduction reaction (ORR) experiments were performed in oxygen-saturated H_2SO_4 solution (0.5 M) at room temperature. The RDE rotating rate was 1600 rpm and sweep rate was 5 mV/s. Current densities were normalized in reference to the geometric area of the GC RDE electrode (0.196 cm^2). The CV measurements for accelerated durability tests (ADT) were conducted by potential cycling between 0.60 and 1.40 V in a N_2 purged 0.1M $HClO_4$ solution at room temperature, with a scan rate of 50 mV/s. In each case, ADT testing consisted of 30,000 cycles.

6.3 Results and Discussion

Figure 6.1a is an SEM image of the as-synthesized Nb-TiO_2 nanostructures that clearly shows the hollow structures which have diameters of 100–150 nm. The typical Nb-TiO_2 spheres have diameters of 100–150 nm, which is the rutile phase confirmed by XRD analysis (JCPDS, No. 21-1276, Figure SI-6.1). The TEM image
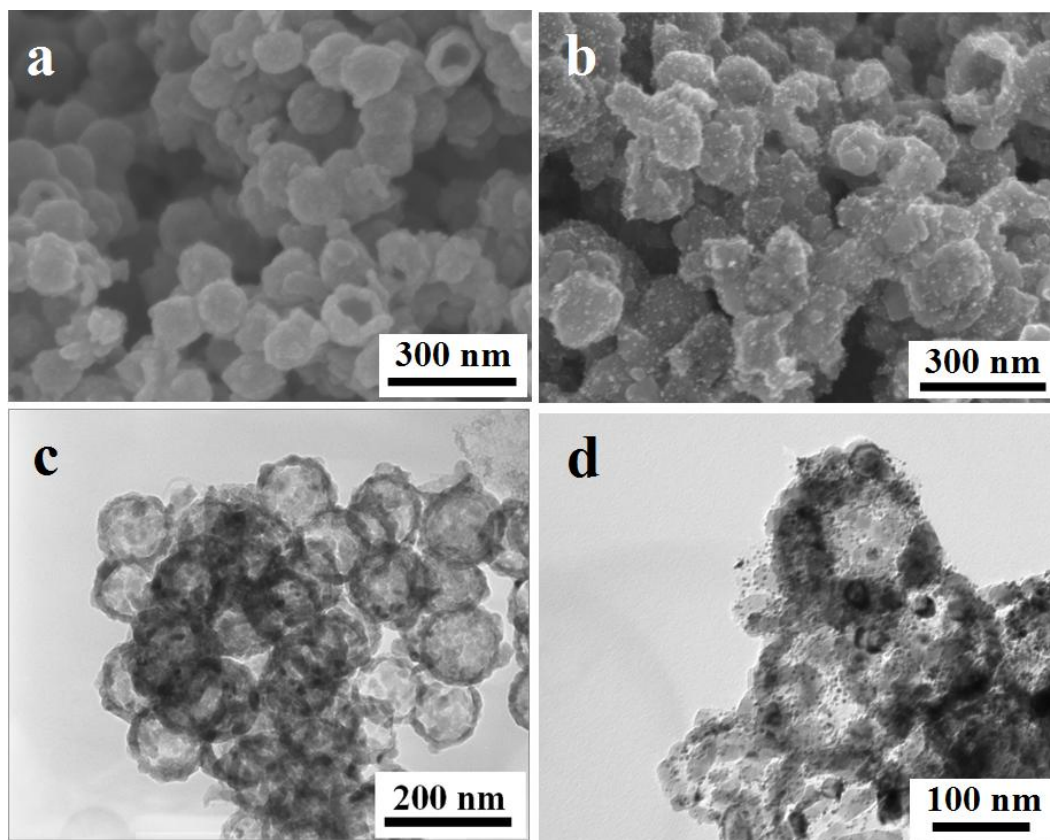
Figure 6.1. SEM (a) and TEM (c) images pristine hollow Nb-TiO$_2$ nanostructures. SEM (b) and TEM (d) images Pt nanoparticles deposited on hollow Nb-TiO$_2$ nanostructures.

in Figure 6.1c, further confirms that the shape of Nb-TiO$_2$ nanostructures with mesoporous shells are spherical and fairly uniform in size. Furthermore, each mesoporous shell is composed of small, 10-20 nm nanoparticles. Figures 6.1b and d show the SEM and TEM images respectively, of Pt NP/Nb-TiO$_2$ composite with 20 wt % Pt loading. These images clearly display the homogeneous Pt deposition throughout the Nb-TiO$_2$ support. The average sizes of Pt nanoparticles on Nb-TiO$_2$ were obtained by measuring 100 randomly chosen nanoparticles under higher
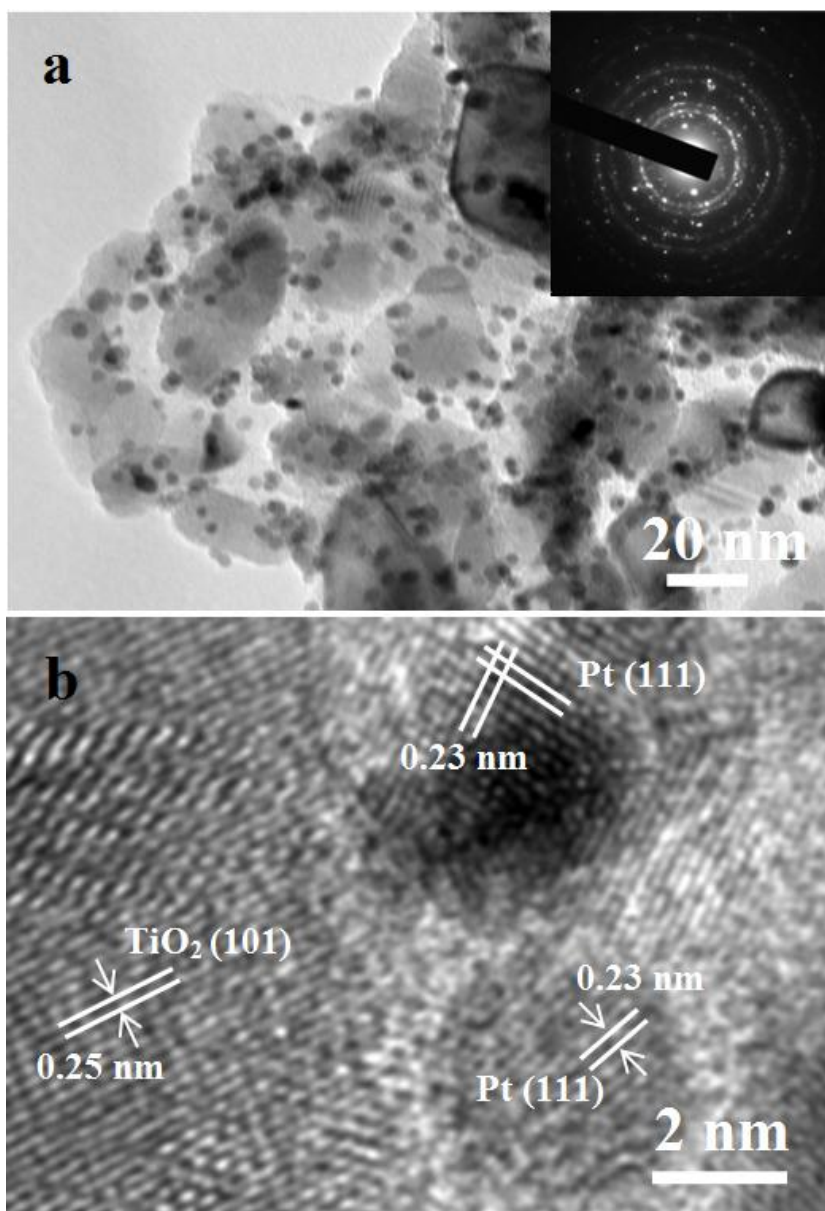
Figure 6.2. (a) TEM and (b) HRTEM images of Pt nanoparticles deposited on hollow Nb-TiO_2 nanosphere supports with 20wt% Pt loading. Pt NPs are single crystal, 4 nm in average size and uniformly dispersed on the surface of hollow Nb-TiO_2 nanosphere supports.

magnification TEM observation (Figure 6.2a). It is clearly seen that Pt nanoparticles with narrow size distribution have the mean size of 4 nm. The selected area electron diffraction (SAED) patterns reveal the single crystallinity of both Pt nanoparticles and the Nb-TiO$_2$ support. High-resolution TEM (HRTEM) analysis (Figure 6.2b) further confirms the highly crystalline features of the support as well as Pt nanoparticles. The fringes with lattice spacing of 0.23 nm can be indexed as the (111) plane of face-centered-cubic (fcc) Pt, and the angle between two (111) planes also matches well with the fcc Pt. The lattice spacing of 0.25 nm can be indexed to (101) plane of rutile TiO$_2$.
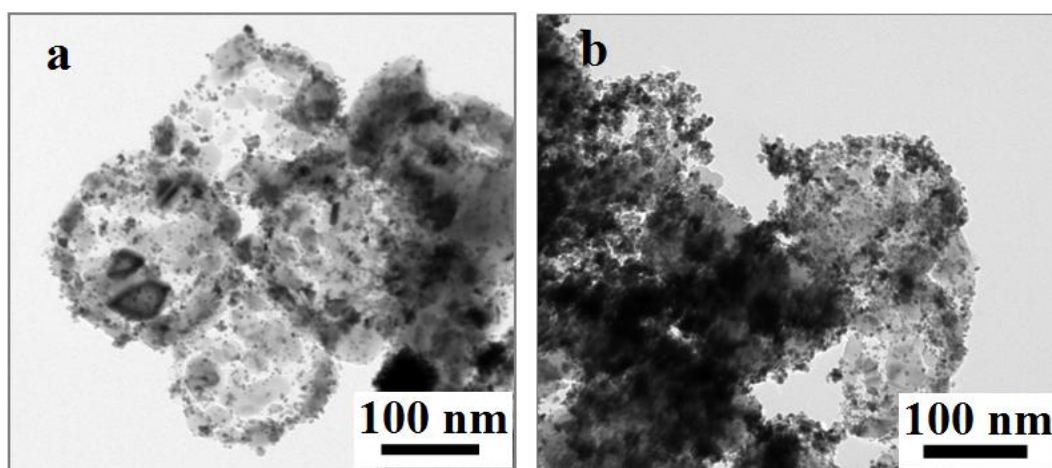
Figure 6.3. TEM images of Pt nanoparticles deposited on hollow Nb-TiO$_2$ nanosphere supports with different Pt loadings. (a) 10wt% and (b) 40wt%.

The Pt loading can be readily tuned by simply changing the mass ratio of the precursor and support, while keeping the ratio between Pt precursor and HCOOH constant. Figure 6.3a shows a TEM image of the product resulting from a mass ratio of H$_2$PtCl$_6$ precursor to substrate (Nb-TiO$_2$) of 1:9, corresponding to 10 wt% Pt. At a higher mass ratio of 2:3, corresponding to 40 wt% Pt, the density of the Pt

nanoparticles increases with some aggregation however their size remains consistent at approximately 4 nm.
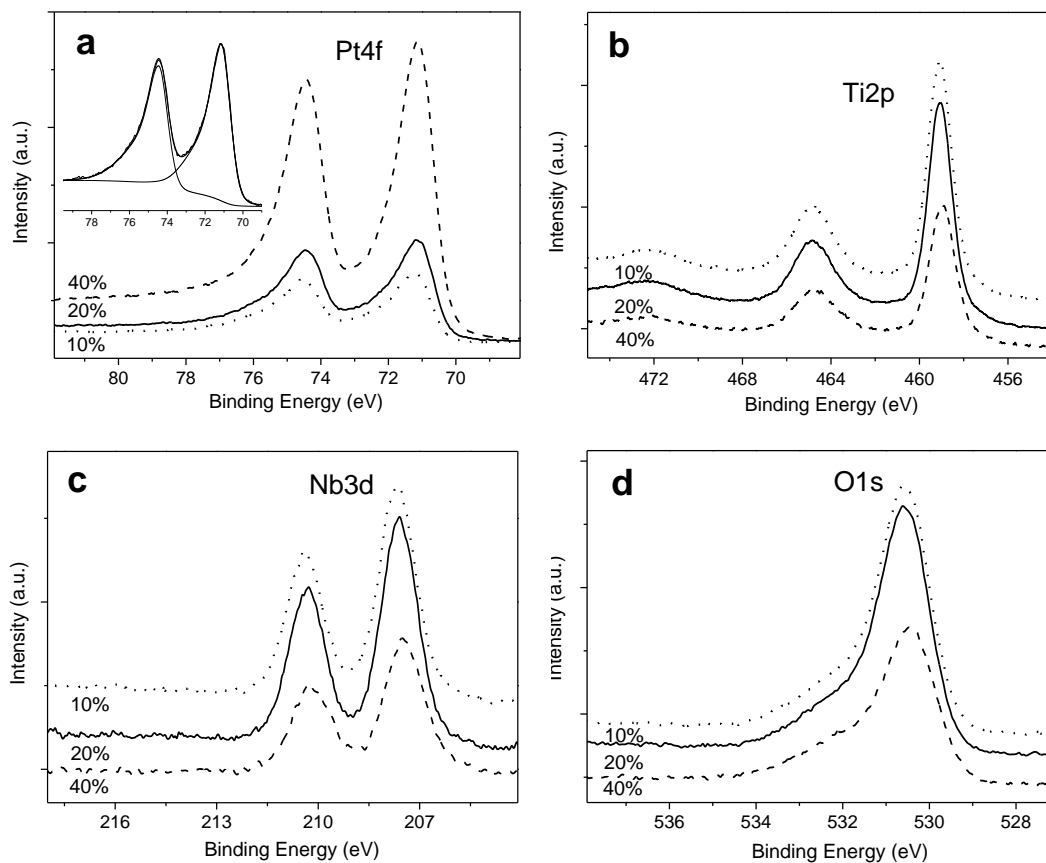
Figure 6.4. High resolution XPS spectra of (a) Pt 4f; (b) Ti2p; (c) Nb3d; (d) O1S. Inset in (a) shows the corresponding deconvolution of Pt 4f spectrum.

X-ray photoelectron spectroscopy (XPS) was employed to study the chemical composition and status of the product. Figure 6.4 shows the Pt 4f, Ti2p, Nb3d and O1s high-resolution XPS spectra taken from Pt/Nb-TiO$_2$ composites with different Pt loading levels (10, 20, and 40 wt% Pt), which were calibrated by placing the principal

C 1s peak at 284.8 eV. Obviously, continued weakening of the Ti2p signaled at 459.0 and 464.8 eV, Nb3d signaled at 207.6 and 210.3 eV, and O1s signaled at 532 eV, is accompanied by the continued strengthening of the Pt 4f signals at 71.1 and 74.4 eV with increasing Pt content [24]. These results suggest that the surface of the Nb-TiO$_2$ spheres becomes more covered with Pt nanoparticles that shield the Nb-TiO$_2$ surface from the XPS detection. The deconvolution of the Pt spectrum (inset in Figure 6.4a) shows only one doublet assigned as Pt 4f7/2 and Pt 4f5/2, which further confirms that the nanoparticles are pure metallic Pt. We obtained a relative atomic concentration ratio O:Ti of 2 for the products from the experimental XPS peak areas, which further confirms that the support is TiO$_2$ with 8 at% Nb doping.

To study the electrochemical properties of the Pt NP/Nb-TiO$_2$ composites, electrochemical measurements were conducted with a glassy carbon electrode (GCE) modified by Pt NPs/Nb-TiO$_2$ composites, with Pt loadings of 10, 20 and 40 wt%, respectively. For comparison, a GCE supporting a commercial Pt/C catalyst (E-TEK) with 30 wt% Pt loading was also tested. Figure 6.5a shows the cyclic voltammograms (CVs) of these fours catalysts recorded at room temperature in Ar-saturated 0.1 M HClO$_4$ solution at a scan rate of 20 mVs^{-1}. For all electrodes, the Pt loadings were kept at approximately 13.0 μgPt/cm^2. The CVs show strong peaks characteristic of hydrogen adsorption/desorption peaks below ~0.4 V and Pt oxidation/reduction peaks beyond ~0.6V, and no considerable change in the shape is seen among these catalysts. The electrochemical surface areas (ECSA) of Pt catalysts were determined by measuring the charge collected in the hydrogen (H) adsorption/desorption region after double-layer correction and assuming a value of 210 μC/cm^2 for the adsorption of a monolayer of hydrogen [20]. The obtained ECSA for the four catalysts are listed in Table 6.1. We can see that commercial Pt/C catalyst (E-TEK) shows the largest electrochemical surface area (ECSA) with 57 m^2/gPt. The 40 wt% Pt/Nb-TiO$_2$ has ECSA value of 47 m^2/gPt, followed by the 10 wt% and 20 wt% Pt/Nb-TiO$_2$ which have ECSA values of 40 m^2/gPt and 37 m^2/gPt respectively. Interestingly, while there is no observed trend in Pt ECSA with the increasing Pt loading on Nb-TiO$_2$, it can be

suggested that by this Pt deposition method, similar Pt particle size can be produced even at higher Pt loading on the metal oxide substrate.
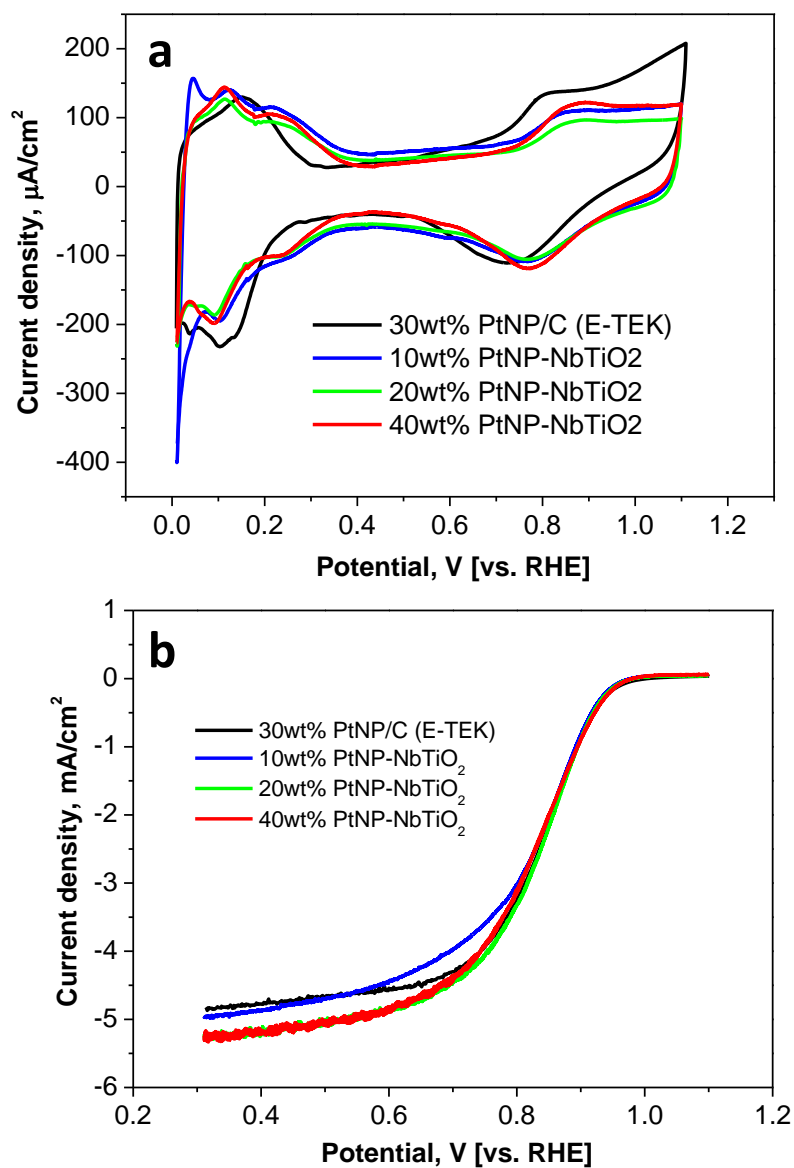
Figure 6.5. (a) CV curves and (b) Polarization curves for O_2 reduction on commercial ETEK Pt/C catalyst and Nb-doped TiO_2 with different Pt NP loadings in a 0.1M $HClO_4$ solution on a disk electrode.

Figure 6.5b shows the rotating disk measurements, at 1600 rpm, for the ORR on three Pt/Nb-TiO$_2$ catalysts, along with the commercial Pt/C catalyst (ETEK) for comparison. The corresponding electrochemical parameters are listed in Table 1. From the figure, the ORR on all catalysts is diffusion-controlled when the potential is less than 0.7 V and is under mixed diffusion-kinetic control in the potential region between 0.7 and 0.85 V. From Table 1, we can see that, as compared to the E-TEK Pt/C catalyst, 10 wt% PtNPs/NbTiO$_2$ composite shows the best performance with 15% and 63% higher mass and specific activities, respectively. Furthermore, overall comparison of the ORR activities indicates that all the homemade PtNPs/Nb-TiO$_2$ composites exhibit higher mass and specific activities than those of the commercial E-TEK Pt/C catalyst. This improvement in activity is significant considering 100 m^2/g BET surface area [15] which is 2/5 of that of Vulcan XC carbon support of commercial Pt/C catalyst. The enhancement in the ORR activity might be due to the homogeneous distribution of small Pt nanoparticles, and the mesoporous surface structure of the TiO$_2$ hollow spheres.

Table 6.1. Comparison of mass and specific activities for ORR and Pt electrochemical surface area of the different catalysts. All these three Pt NP/TiO$_2$ catalysts show better mass and specific activity than those of the state-of-the-art commercial Pt/C catalyst.

Catalyst	Current density @ 0.9V mA/cm^2	Mass activity @0.9V A/mgPt	Electrochemical specific surface area m^2/g	Specific activity @0.9V μA/cm^2 Pt
PtNP/C (E-TEK) 30wt% Pt	0.877	0.080	57	140
PtNP-NbTiO$_2$ 10wt% Pt	0.826	0.092	40	228
PtNP-NbTiO$_2$ 20wt% Pt	0.886	0.082	37	223
PtNP-NbTiO$_2$ 40wt% Pt	0.896	0.082	47	175
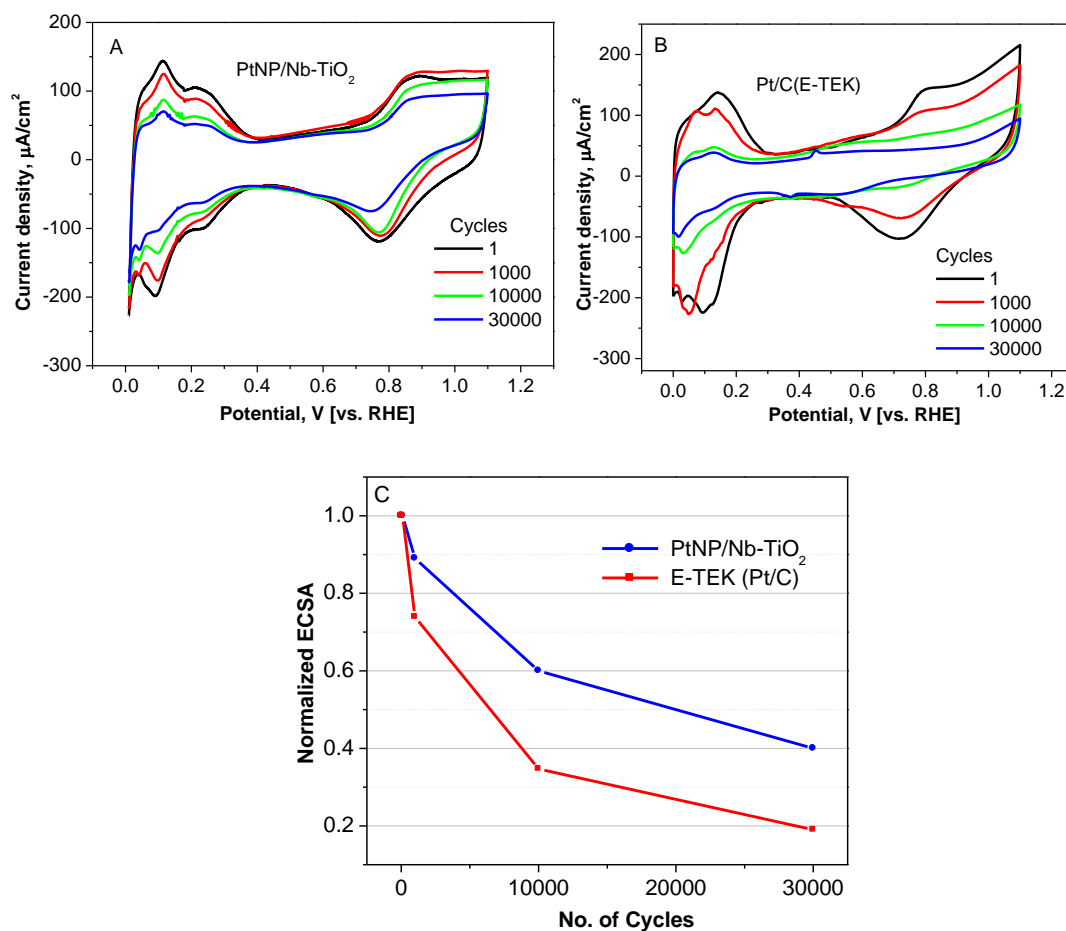
Figure 6.6. Cyclic voltammograms recorded on (a) PtNP/Nb-TiO$_2$ and (b) ETEK PtNP/C electrodes in 0.1 M HClO$_4$ solution at room temperature during ADT. (c) ECSA as a function of cycling numbers on PtNP/Nb-TiO$_2$ and ETEK PtNP/C electrodes.

The durability of the catalysts was determined in an accelerated durability test (ADT) by continuously applying linear potential sweeps from 0.60 to 1.4 V (vs RHE), causing surface oxidation/reduction of Pt and the oxidation of support. The surface reaction involves the formation of PtOH and PtO derived from the oxidation of water

that causes the dissolution of Pt via the Pt^{2+} oxidation state [25, 26]. The test was conducted by applying potential sweeps at scan rate of 50 mV/s in a N_2 saturated, 0.1M $HClO_4$ solution at room temperature. For comparison, commercial E-TEK Pt/C (30 wt% Pt) catalyst with a similar Pt loading as that in Pt/Nb-TiO_2 (40wt% Pt) was subjected to the same potential cycling conditions. It is generally believed that the performance degradation of the electrodes in PEMFC is mainly due to the ECSA decrease of the catalysts. After 30,000 cycles, changes in the Pt ECSA were determined. As shown in Figure 6.6a and b, cyclic voltammetry was used to determine the Pt surface area of Pt/Nb-TiO_2 and Pt/C electrodes by measuring the H adsorption before and after potential cycling. Figure 6.6c shows that, for Pt/Nb-TiO_2, ~40% of the original Pt surface area remained after 30,000 cycles potential cycling, which is 2.1 times higher than the ~19% remaining for the commercial E-TEK Pt/C catalyst. These results reveal that the Pt on Nb-TiO_2 support is more electrochemically stable. The enhanced stability might be attributed to: (a) the higher corrosion resistance of Nb-TiO_2 support compared to carbon in acidic environments, (b) a strong Pt–metal oxide support interaction inhibiting the sintering of the Pt [16, 17].

6.4 Conclusions

In summary, we have demonstrated a facile wet-chemical method to grow single-crystalline Pt nanoparticles on mesoporous Nb-doped TiO_2 hollow spheres in aqueous solution, without using any surfactant. The use of Nb-TiO_2 hollow spheres as substrate provides a new type of cost-effective support with high corrosion resistance for growing Pt nanoparticles. The growth density of Pt nanoparticles on Nb-TiO_2 support could be controlled by manipulating the mass ratios between the Pt precursor and the Nb-TiO_2 support. PtNP/Nb-TiO_2 catalysts show enhanced activity and stability compared with the commercial E-TEK Pt/C catalyst.

Acknowledgements

References

[1]   K. Kordesch, G. Simander. Fuel cells and their applications, VCH, Germany, 1996.

[2]   R. Borup, J. Meyers, B. Pivovar, Y. S. Kim, R. Mukundan, N. Garland, D. Myers, M. Wilson, F. Garzon, D. Wood, P. Zelenay, K. More, K. Stroh, T. Zawodzinski, J. Boncella, J. E. McGrath, M. Inaba, K. Miyatake, M. Hori, K. Ota, Z. Ogumi, S. Miyata, A. Nishikata, Z. Siroma, Y. Uchimoto, K. Yasuda, K. Kimijima, N. Iwashita, Scientific aspects of polymer electrolyte fuel cell durability and degradation. *Chem. Rev.,* **2007**, *107*, 3904–3951.

[3]   D. A. Stevens, J. R. Dahn. Thermal degradation of the support in carbon supported platinum electrocatalysts for PEM fuel cells. *Carbon* **2005**, *43*, 179–188.

[4]   Y. Y. Shao, G. P. Yin, Y. Z. Gao, Understanding and approaches for the durability issues of Pt-based catalysts for PEM fuel cell. *J. Power Sources* **2007**, *171*, 558–566.

[5]   M. S. Saha, R. Li, X. Sun, High loading and monodispersed Pt nanoparticles on multiwalled carbon nanotubes for high performance proton exchange membrane fuel cells. *J. Power Sources* **2008**, *177*, 314–322.

[6]   T. Ioroi, H. Senoh, S. Yamazaki, Z. Siroma, N. Fujiwara, K. Yasuda, Stability of corrosion-resistant magnéli-phase Ti_4O_7-supported PEMFC catalysts at high potentials. *J. Electrochem. Soc.* **2008**, *155*, B321–326.

[7]   T. Ioroi, N. Fujiwara, S. Yamazaki, K. Yasuda, Sub-stoichiometric titanium oxide-supported platinum electrocatalyst for polymer electrolyte fuel cells. *Electrochem. Commun.* **2005**, *7*, 183–188.

[8]   H. Chhina, S. Campbell, O. Kesler An oxidation-resistant indium tin oxide catalyst support for proton exchange membrane fuel cells. *J. Power Sources* **2006**, *161*, 893–900.

[9]   G. Chen, S. R. Bare, T. E. Mallouk, Development of supported bifunctional electrocatalysts for unitized regenerative fuel cells. *J. Electrochem. Soc.* **2002**, *149*, A1092–A1099.

[10] H. Chhina, S. Campbell, O. Kesler, Ex situ evaluation of tungsten oxide as a catalyst support for PEMFCs. *J. Electrochem. Soc.* **2007**, 154, B533–B539.

[11] M. S. Saha, M. N. Banis, Y. Zhang, R. Li, M. Cai, X. Sun, Tungsten oxide nanowires grown on carbon paper as Pt electrocatalyst support for high performance PEM fuel cells. *J. Powder Sources* **2009**, *192*, 330–335.

[12] M. S. Saha, R. Li, M. Cai, X. Sun, High Electrocatalytic Activities of Platinum Nanoparticles on SnO_2 Nanowire-based Electrodes. *Electrochem. Solid-State Lett.*, **2007**, *10*, B130–B133.

[13] M. Koninck, P. Manseau, B. Marsan, Preparation and characterization of Nb-doped TiO_2 nanoparticles used as a conductive support for bifunctional $CuCo_2O_4$ electrocatalyst. *J. Electroanal. Chem.* **2007**, *611*, 67–79.

[14] K. Park, K. Seol, Nb-TiO_2 supported Pt cathode catalyst for polymer electrolyte membrane fuel cells. *Electrochem. Commun.* **2007**, *9*, 2256–2260.

[15] M. Cai, Y. Lu, Z. Wu, L. Feng, M. Ruthkosky, J. Johnson, F. Wagner Making electrocatalyst supports for fuel cells. US patent, 2010, Application number: 12/716360.

[16] H. Chhina, D. Susac, S. Campbell, O. Kesler. Transmission electron microscope observation of Pt deposited on Nb-doped titania. Electrochem. Solid-State Lett. **2009**, *12*, B97–B100.

[17] S. Tauster, S. Fung, R. Garten, Strong metal-support interactions. Group 8 noble metals supported on titanium dioxide. *J. Am. Chem. Soc.* **1978**, *100*, 170–175.

[18] F. Leroux, P. Dewar, M. Intissar, G. Ourard, L. Nazar, Study of the formation of mesoporous titania via a template approach and of subsequent Li insertion. *J. Mater. Chem.* **2002**, *12*, 3245–3253.

[19] E. Traversa, M. L. Divona, S. Licoccia, M. Sacerdoti, M. C. Carotta, L. Crema, G. Martinelli. Sol-gel processed TiO_2-based nano-sized powders for use in thick-film gas sensors for atmospheric pollutant monitoring. *J. Sol–Gel Sci. Technol.* **2001**, *22*, 167–179.

[20] S. H. Sun, D. Q. Yang, D. Villers, G. X. Zhang, E. Sacher, J. P. Dodelet, Template-free, Surfactant-free Room Temperature Synthesis of Self-Assembled 3D Pt Nanoflowers from Single-Crystal Nanowires. *Adv. Mater.* **2008**, *20*, 571–574.

[21] D. Q. Yang, S. H. Sun, J. P. Dodelet, E. Sacher, A facile route for the self-organized high-density decoration of Pt nanoparticles on carbon nanotubes. *J. Phys. Chem. C* **2008**, *112*, 11717–11721.

[22] D. Q. Yang, S. H. Sun, H. Meng, J. P. Dodelet, E. Sacher, Formation of porous platinum nanoparticle froth for electrochemical applications, produced without templates, surfactants, or stabilizers. *Chem. Mater.* **2008**, *20*, 4677–4681.

[23] http://www.phy.cuhk.edu.hk/~surface/XPSPEAK/ (accessed March 2010).

[24] F. Moulder, W. F. Stickle, P. E. Sobol, K. D. Bomben. in Handbook of X-Ray Photoelectron Spectroscopy (Ed: J. Chastain), Perkin-Elmer, Eden Prairie, MN 1992.

[25] R. Woods in Electroanalytical Chemistry, (Ed: A. J. Bard), Marcel Dekker, New York, 1976.

[26] J. Zhang, K. Sasaki, R. R. Adzic, Stabilization of platinum oxygen-reduction electrocatalysts using gold clusters, *Science*, **2007**, *315*, 220–222.

Supporting Information
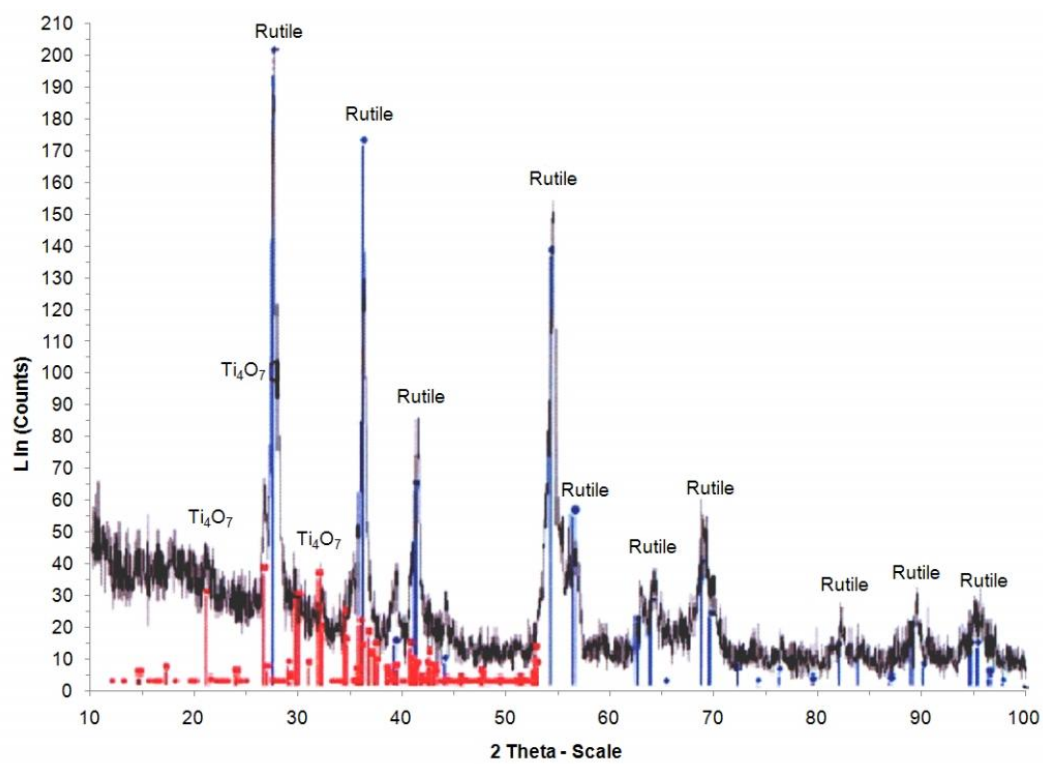
Figure SI-6.1. XRD patterns of Nb-TiO$_2$ sphere support.

Chapter 7. Pt/TiSi$_x$-NCNT Janus Nanostructures for Highly Stable and CO-Tolerant PEM Fuel Cell Electrocatalyst

Shuhui Sun[1], Mohammad Norouzi Banis[1], Gaixia Zhang[1], Mei Cai[2], Yong Zhang[1], Ruying Li[1], Xueliang Sun[1,*]

[1]Department of Mechanical and Materials Engineering, The University of Western Ontario, London, Ontario, N6A 5B9 (Canada)
[2]General Motors Research and Development Center, Warren, MI 48090-9055 (USA)
E-mail: xsun@eng.uwo.ca

A version of this chapter will be submitted for publishing.

In previous chapter, the authors introduced the work of using 0D mesoporous Nb-doped TiO$_2$ hollow spheres as alternative catalyst support. This new type of carbon-free Pt/Nb-TiO$_2$ electrocatalyst exhibited over 2 times higher stability than commercial E-TEK Pt/C catalyst.

Recently, transitional metal silicides, such as WSi$_x$, TiSi$_x$, TaSi$_x$, etc., have attracted much interest for using as alternative catalyst supports, to replace carbon in PEMFCs, due to their excellent thermal stability, corrosion resistance, and very high electrical conductivity. Previous studies from others and our group have indicated that Pt on transition metal silicides supports showed higher durability under fuel cell conditions, as well as higher electrocatalytic activity for methanol oxidation.

In this chapter, the authors propose another new type of alternative support, TiSi$_x$-NCNT 1D structure, for Pt deposition, forming Pt/TiSi$_x$-NCNT Janus nanostructure. This novel Janus nanostructured catalyst was prepared by sputtering TiSi$_x$ only on one side of N-doped carbon nanotubes, followed by wet-chemical deposition of Pt

nanoparticles on the other side. TEM investigations revealed that the Pt NPs formed dendritic and chain-like morphology between the gaps of TiSi$_x$ on NCNT surface, which is very important for enhancing the durability of Pt catalyst. Our results show that Pt/TiSi$_x$-NCNT Janus nanocatalyst exhibits ~3 times better stability and much improved CO tolerance compared to commercial Pt/C catalyst. The higher corrosion resistance of both NCNT and TiSi$_x$ than carbon black contributed greatly to the higher stability of the catalyst. Pt/TiSi$_x$-NCNT Janus nanostructure is a new type of promising electrocatalyst for PEMFC applications.

7.1 Introduction

Proton-exchange membrane fuel cells (PEMFCs) are promising power sources for many applications in the future because of their high efficiency, high power density and low pollution [1]. Despite considerable progress made in the past, their high production cost needs to be significantly reduced while improving the performance and durability before the fully commercialization of PEMFCs.

Platinum or platinum alloys are commonly used as the catalyst in PEMFCs [2-4], where it catalyzes oxygen reduction reaction (ORR) at the cathode and fuel (including hydrogen and methanol) oxidation reaction at the anode [5,6]. Various carbon materials, including carbon black (CB) [7,8], carbon nanofibers (CNFs) [9], and carbon nanotubes (CNTs) [10,11], are being widely used catalyst supports due to their high surface area for the dispersion of Pt nanoparticles, and good electrical conductivity required for electrochemical reactions. A range of key factors are known to contribute to the performance degradation of PEMFCs that occur during long term operation and/or start-up and shutdown [12]. These mainly include dissolution/aggregation/Oswald ripening and/or poisoning of Pt catalysts. The stability of carbon support material itself is also an important issue because carbon is known to undergo electrochemical oxidation ($C + 2H_2O \longrightarrow CO_2 + 4H^+ + 4e^-$) under a fuel cell operating environment, especially at potentials above 0.9 V (equation 1), leading to a loss of Pt active surface area and fuel cell performance degradation [13,14]. In literature, many methods have been reported to address these challenges, such as using carbide, nitride, or metal oxide as catalyst supports [15,16].

Recently, transitional metal silicides, such as $TiSi_x$, have attracted tremendous interest especially in semiconductor industry due to their excellent thermal stability, corrosion resistance, and very high electrical conductivity [17-19]. Meanwhile, these unique properties of metal silicide also make them as the potential catalyst supports, for replacing carbon, in PEMFCs. In fact, previous studies have indicated that using transition-metal silicides as electrocatalyst supports showed higher durability under

fuel cell conditions [20], as well as higher electrocatalytic activity for methanol oxidation [21]. However, most of these materials systems reported previously were based on thin films or powders, which is not be sufficient to meet the high surface area demand for using as catalyst supports. The combination of $TiSi_x$ and carbon materials as supports potentially allows the optimization of the dispersion and corrosion.

In this study, we described a new type of Janus nanostructure electrocatalyst ($Pt/TiSi_x$-NCNT) synthesized by $TiSi_x$ sputtering only on one side of NCNT, followed by wet-chemical deposition of Pt nanoparticles on the other side. Janus nanostructure, akin to the dual-face Roman god, Janus [22], has become a focus of attention in many fields since the first emphasis by Gennes in his Nobel Prize address [23]. Generally, Janus particles possess dual surface functionalities or consist of two different materials on opposite faces [24]. The integration of different nanomaterials with different properties permits versatile applications ranging from bio-sensing, drug delivery to catalysis. In addition, $Pt/TiSi_x$-NCNTs were directly grown on the carbon paper fuel cell backing, forming novel 3D fuel cell electrodes. Such 3D supports hold many additional advantages, including higher gas permeability, improved metal-support interactions, and enhanced mass transport. This approach allows us to combine the advantages of both $Pt/TiSi_x$-NCNT Janus catalyst and 3D supports for fuel cell applications.

7.2 Experimental

7.2.1 Synthesis of $TiSi_x$-NCNT support

$TiSi_x$-NCNT nanostructures were synthesized by a two-step approach through the combination of chemical vapour deposition (CVD) process and magnetron sputtering. In this process, nitrogen doped carbon nanotubes (NCNTs) were first synthesized on carbon paper, which was pre-sputtered with an aluminum buffer layer (30 nm) and an iron catalyst layer (1 nm), via a CVD process at 800 °C. In this method, melamine was use as source for both carbon and nitrogen [25]. Then the carbon paper grown

with N-CNTs was placed in a modified PECVD/sputtering system, 10 cm from the sputtering target. Before the sputtering process, the chamber pressure was lowered to 1.9×10^{-5} torr to purge the oxygen from the system. Pure Argon was introduced into the system to adjust the pressure to 1.5×10^{-3} torr. During the sputtering process, a flow of 15 sccm Ar was maintained. A 100 nm layer of $TiSi_x$ is deposited on the NCNTs from a $TiSi_2$ (2-inch) target using a RF magnetron (150W, 10 min).

7.2.2 Synthesis of Pt NPs on $TiSi_x$-NCNT support

The deposition of Pt NPs on $TiSi_x$/NCNT were conducted by the reduction of hexachloroplatinic acid ($H_2PtCl_6.6H_2O$) with formic acid (HCOOH) under 80 ^{o}C [26]. In a typical procedure, 0.032 g $H_2PtCl_6.6H_2O$ (Aldrich) and 1 mL HCOOH (Aldrich) were added simultaneously into 20 mL H_2O at room temperature to form a golden orange solution. The $TiSi_x$/NCNT/carbon paper was immersed into the reaction solution, acting as the growth substrates, and then the reactions was proceeded at 80 ^{o}C for 30 min. After the completion of the reaction, the sample was washed with deionized water and dried at 80 °C over night in a vacuum oven. The Pt loading was determined by inductively coupled plasma-optical emission spectroscopy (ICP-OES).

7.2.3 Physical Characterization

The morphologies and microstructures of the as-prepared samples were examined by scanning electron microscope (SEM, Hitachi S-4800) operated at 5kV, and transmission electron microscopy (TEM, JEOL JEM-2100) operated at 200 kV. X-ray diffraction (XRD) patterns were recorded on a Bruker D8 Advance diffractometer equipped with a Cu Ka radiation source.

7.2.4 Electrochemical Measurements

The electrochemical properties of Pt/$TiSi_x$-NCNT Janus nanostructure/carbon paper composites were evaluated by cyclic voltammetry (CV) in a standard three-electrode cell at room temperature. Pt wire and Ag/AgCl (3 M NaCl) were used as the counter

and reference electrodes, respectively. All potentials in this study, however, are referenced to the reversible hydrogen electrode (RHE). CV measurements were carried out on a CHI 600C electrochemical workstation (CH Instrument Company), using 0.5 M H_2SO_4 solution purged with N_2 at a sweep rate of 50 mV/s. The CV measurements for accelerated durability test (ADT) were conducted by potential cycling between 0.60 and 1.2 V in a O_2 purged 0.5 M H_2SO_4 solution at room temperature, with scan rate of 50 mV/s. Total 4,000 cycles of CV were performed for each case. The electrochemical surface areas (ECSA) were calculated from the hydrogen adsorption peak of the CV. For methanol oxidation reaction, the CVs were measured in an air-free aqueous solution containing 1 M MeOH and 0.5 M H_2SO_4. For CO stripping voltammetry, pure CO (99.5%) was purged into the solution at a position close to the working electrode for 1 h, with the electrode polarized at 0.05 V versus RHE in a fume hood. The electrode was then purged with pure Ar for 1 h under potential control followed by voltammetric stripping.

For comparison, $TiSi_x$-NCNT, and PtNP/NCNT and a conventional electrode made with commercial 30 wt% Pt/C catalyst from ETEK (USA) were also evaluated. To prepare the conventional electrode, typically, 10 mg catalyst was sonically mixed with 1 mL H_2O/isopropanol (1/1 in volume ratio) to make a suspension. GC disk electrodes (5 mm diameter, Pine Research Instrument) that serve as the support were polished to a mirror finish before using. 20 μl of catalyst suspension was pipetted onto the GC disk substrate, leading to a Pt loading of 0.3058 mg/cm^2, which is similar to that for PtNP/$TiSi_x$-NCNT composite electrode. The catalyst films were dried under flow N_2 at room temperature. Finally, 10 μl 0.05 wt% Nafion solution was pipetted onto the catalyst film, and then dried. The currents were normalized on the basis of Pt loading.

7.3 Results and Discussion

Figure 7.1 shows the representative SEM and TEM images of NCNTs before and after $TiSi_x$ sputtering. It can be seen that the pristine NCNTs have diameters ranging
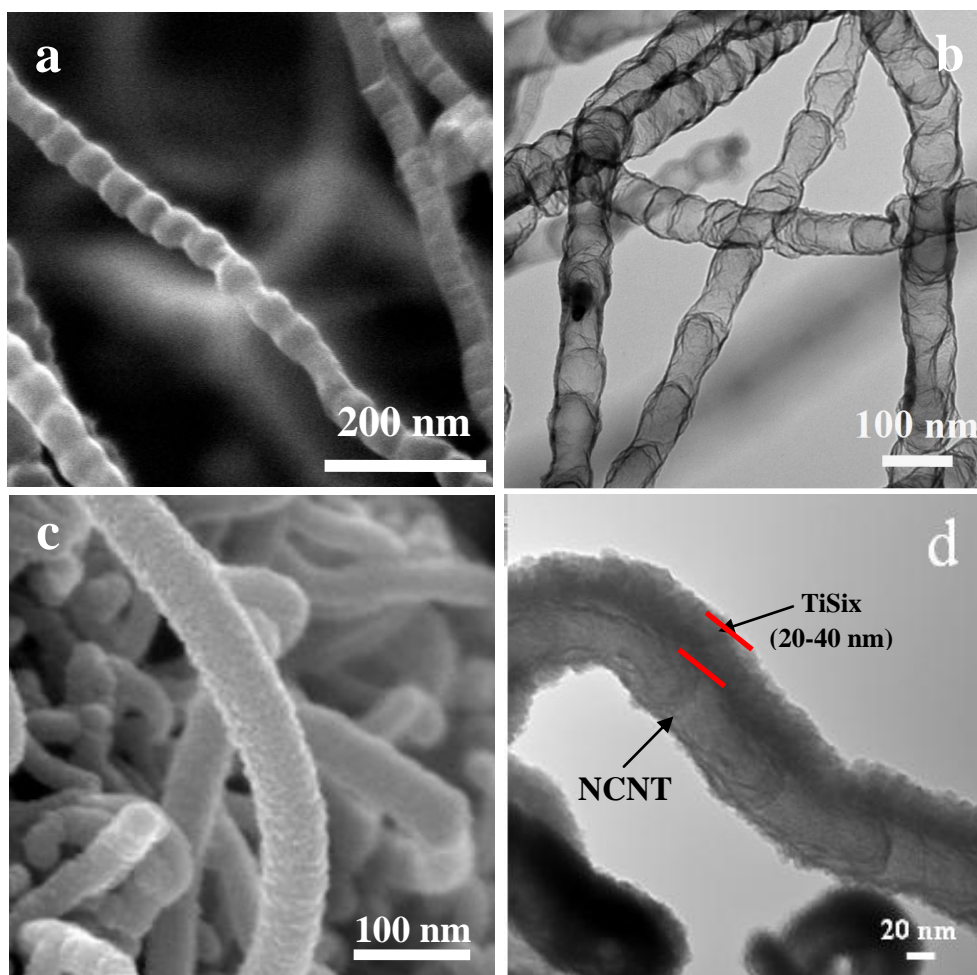
Figure 7.1. SEM and TEM images of NCNT before (a,b) and after (c,d) TiSi$_x$ deposition.

from 40 to 60 nm (Figure 7.1a,b), and the bamboo-like structure can be attributed to the integration of N into the graphitic structure. After the sputtering deposition of TiSi$_x$ film, the surface of NCNTs become very rough and the bamboo structure can not be obviously observed. Interestingly, the NCNTs still maintain their "free-standing" 3D structures (Figure 7.1c). From the TEM image (Figure 7.1d), we can see that for each single NCNT, only one side is covered with thick TiSi$_x$ film (20–40

nm), while other parts are either covered by very thin film or even totally without TiSi$_x$ film. This might be due to the shadow effect during sputtering process.
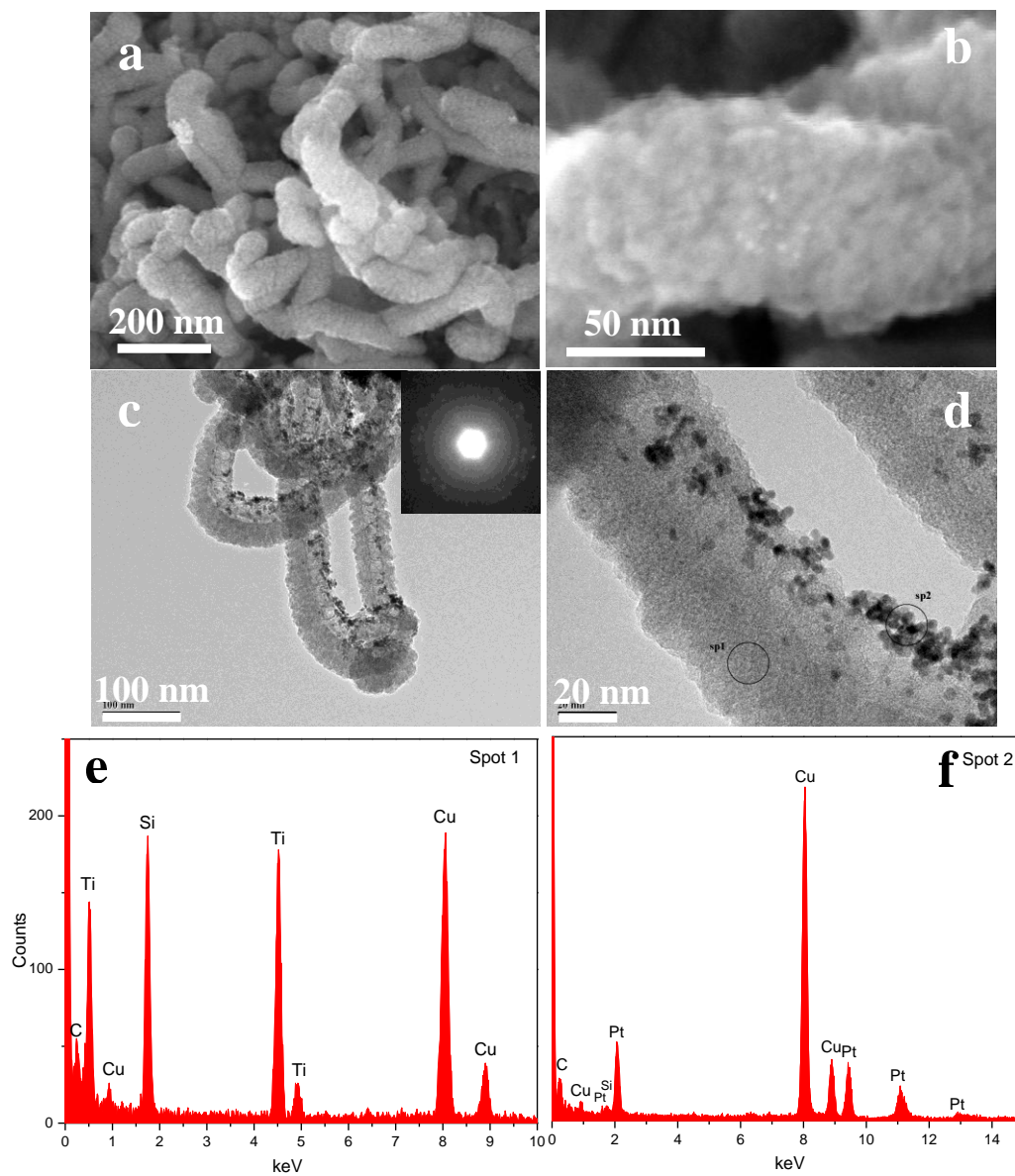
Figure 7.2. SEM (a,b) and TEM (c,d) images of PtNPs on TiSi-NCNT. (e,f) EDS spectrum taken from different area as shown in (d).
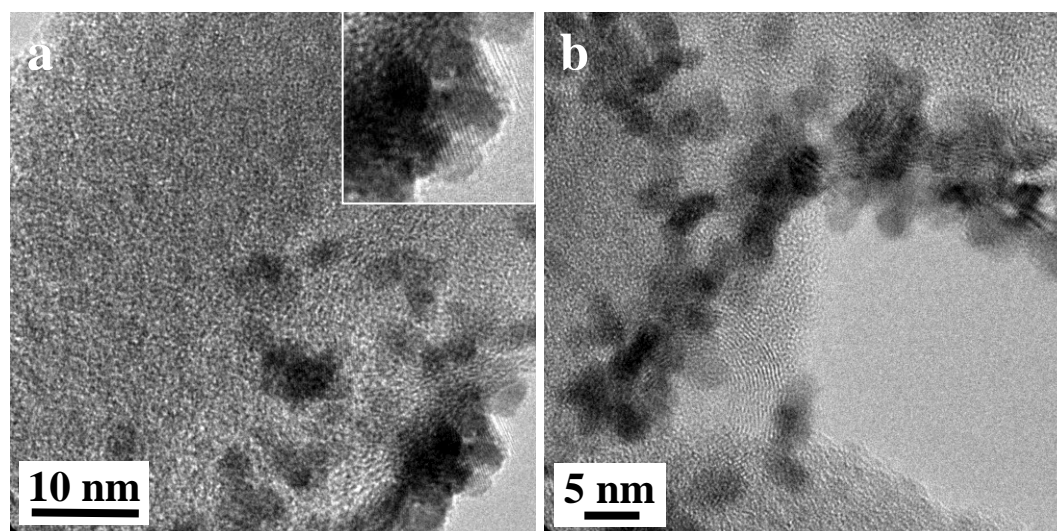
Figure 7.3. RTEM images of PtNP/TiSi$_x$-NCNT.

After Pt deposition process, we can see that Pt nanoparticles, with diameter of 3-4 nm, uniformly distribute on the whole surface of pristine NCNTs (Figure SI-7.1). Interestingly, Pt nanoparticles selectively deposit on the surface of NCNT where without TiSi$_x$ film covering, forming a Pt/TiSi$_x$-NCNT Janus nanostructure (Figure 7.2a-d). This might be due to the inert surface of TiSi$_x$ film. The selected area electron diffraction (SAED) patterns (inset of Figure 7.2c) reveal the crystallinity of Pt nanoparticles and the amorphous phase of TiSi$_x$ film. The EDX spectra record from two different areas, indicated by cycle 1 and 2 respectively, of Pt/TiSi$_x$-NCNT Janus nanostructure confirm the only existence of TiSi$_x$ on one side and Pt on the other side of the Janus nanostructure (Figure 7.2e,f). High-resolution TEM (HRTEM) analysis (Figure 7.3a,b) further confirms the highly crystalline feature of Pt nanoparticles and the amorphous feature of TiSi$_x$ film. The fringes with lattice spacing of 0.23 nm can be indexed as the (111) plane of face-centered-cubic (fcc) Pt. The lattice spacing of 0.34 nm can be indexed to (002) plane of CNT support.

Interestingly, Pt nanoparticles deposit selectively on the surface of NCNT where without TiSi$_x$ covering, i.e., Pt nanoparticles preferentially deposit between the gaps of TiSi$_x$ film/nanoparticles, elongating to form dendritic or chain-like nanostructures on NCNTs.
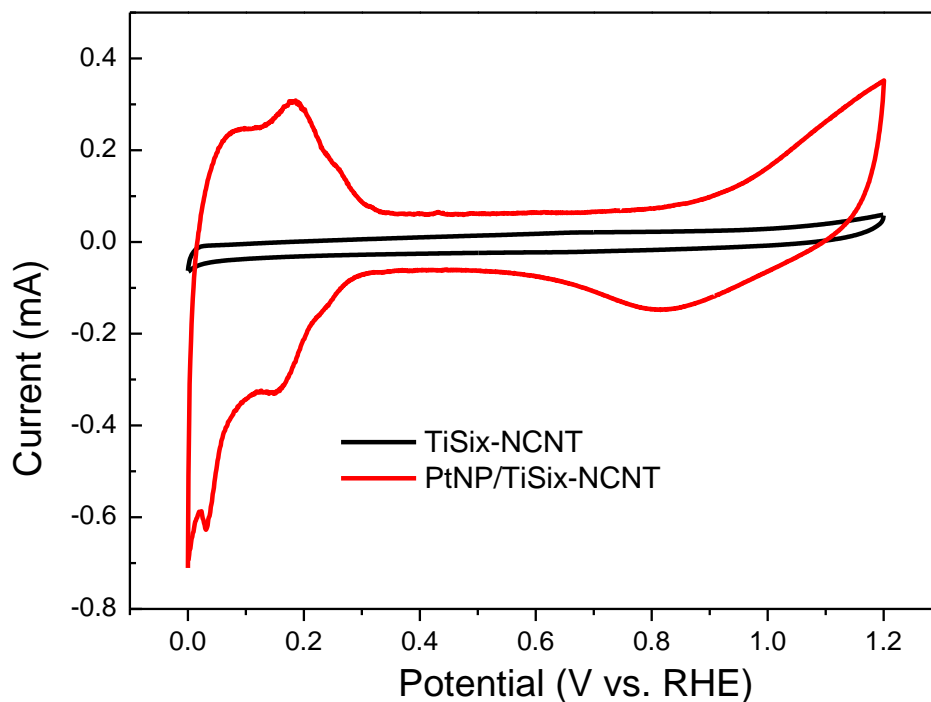
Figure 7.4. Cyclic voltammograms of pristine TiSi$_x$-NCNT support and PtNP/TiSi$_x$-NCNT. Measured at a scan rate of 50 mV/s, in degassed 0.5 M H$_2$SO$_4$.

We evaluated the electrochemical properties of the Pt/TiSi$_x$-NCNT composite and, for comparison, pristine TiSi$_x$-NCNT and commercial Pt/C (ETEK) catalysts, using cyclic voltammetry (CV). Figure 7.4 shows the CVs of TiSi$_x$-NCNT support and Pt/TiSi$_x$-NCNT recorded between 0 and 1.2 V vs RHE in a deaerated 0.5 M H$_2$SO$_4$ solution. Before Pt deposition, only background currents representing characteristic of CNT electrodes, are observed (black line). After the deposition of Pt nanoparticles,

clear and characteristic Pt surface electrochemistry is observed (red line), with hydrogen adsorption and desorption between 0 and 0.3 V, and Pt oxidation in the range of 0.75 to 1.2 V with reduction peak at 0.82 V. Multiple peaks for hydrogen adsorption and desorption, rather than a single broad peak, were observed, indicating that the reaction involved multiple exposed Pt crystallographic planes.[8]
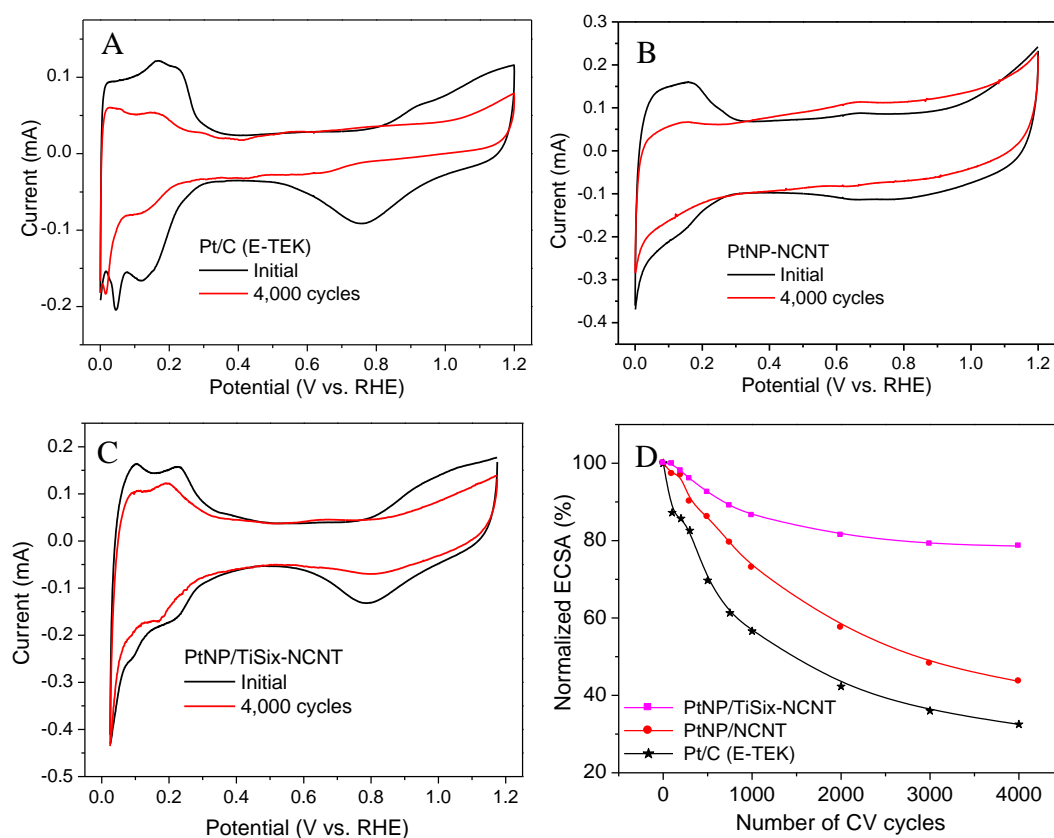
Figure 7.5. CV curves for A) Pt/C (E-TEK), B) PtNP/NCNT; C) PtNP/TiSi$_x$-NCNT catalysts before and after 4,000 cycles. D) Loss of electrochemical surface area (ECSA) of Pt/C (E-TEK), PtNP/NCNT, and PtNP/TiSi$_x$-NCNT catalysts as a function of cycling numbers in O$_2$-purged 0.5 M H$_2$SO$_4$ solution at room temperature (0.6-1.2 V vs RHE, sweep rate 50 mV/s).

The durability of the catalysts was determined in an accelerated durability test (ADT) by continuously applying linear potential sweeps from 0.6 to 1.2 V (vs RHE), which caused surface oxidation/reduction cycles of Pt and the oxidation of support. The surface reaction involves the formation of PtOH and PtO derived from the oxidation of water that causes the dissolution of Pt via the Pt^{2+} oxidation state [27]. The tests were conducted by applying potential sweeps at scan rate of 50 mV/s in O_2 saturated 0.5 M H_2SO_4 solution at room temperature. After 4,000 cycles, changes in the Pt ECSA were determined by measuring the H adsorption before and after potential cycling. The degradation of commercial Pt/C (E-TEK) catalyst was quite severe, with 67.5% loss of the initial Pt ECSA (Figure 5a and d), while as shown in Figure 7.5c,d, Pt/TiSi$_x$-NCNT Janus nanostructure catalyst lost only 20% of the original Pt surface area, which was 3.4 times more durable than that of Pt/C catalyst. To further study the effect of TiSi$_x$, Pt nanoparticles were deposited on NCNT and tested under same condition. 4,000 ADT results show that Pt/NCNT lost 56.5% of the original Pt surface area (Figure 5b and d). That means, on the same NCNT support, with the addition of TiSi$_x$, the durability of Pt increased by 2.8 times than that without TiSi$_x$.

Clearly, Pt/TiSi$_x$-NCNT Janus nanostructure shows the best durability among the three catalysts, followed by Pt/NCNT catalyst which shows enhanced stability than that of commercial Pt/C catalyst. This might be attributed to the following reasons: First, the higher corrosion resistance of NCNT than carbon, in acidic condition, increases the durability of Pt/NCNT catalyst [28], and with the addition of more corrosion resistant TiSi$_x$, the durability of Pt/TiSi$_x$-NCNT catalyst is further increased. Second, the TiSi$_x$ aside the Pt offers an energy barrier to prevent the migration of individual Pt atoms or nanoparticles [29]. Third, the unique one dendritic and chainlike morphology of Pt makes it less vulnerable to dissolution, Ostwald ripening, and aggregation during fuel cell operation than the platinum nanoparticles (0D nanostructure) [8]. Thus, the Pt/TiSi$_x$-NCNT catalyst exhibited higher stability under electrochemical oxidation conditions.
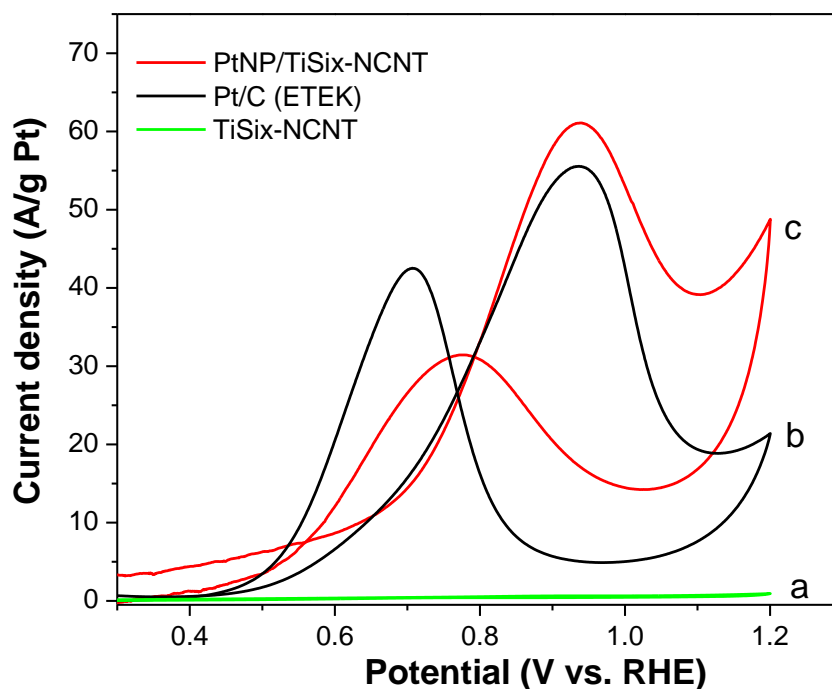
Figure 7.6. Cyclic voltammograms for methanol oxidation (1 M methanol in 0.5 M H_2SO_4). Trace a, $TiSi_x$-NCNT; trace b, Pt/C; trace c, PtNP/$TiSi_x$-NCNT.

The electrocatalytic activity of the Pt/$TiSi_x$-NCNT Janus nanostructure for methanol oxidation in the anodic half-cell reaction, was demonstrated by using a well-used electrochemical reaction in a solution containing 1 M MeOH and 0.5 M H_2SO_4. For comparison, the pristine $TiSi_x$-NCNT and the commercial Pt/C catalyst were also tested under the same experimental conditions. From the voltammograms shown in Figure 7.6, no obvious oxidation peaks could be observed from the CV curve of the pristine $TiSi_x$-NCNT electrode, indicating the support itself is catalytically inactive for methanol oxidation (curve a). Two typical oxidation peaks appear for the CV curves of the Pt/C catalysts (curve b) and Pt/$TiSi_x$-NCNT (curve c), which arise from the oxidations of methanol and their intermediates [30]. The methanol oxidation peak

current, normalized on the basis of Pt loading, for Pt/TiSi$_x$-NCNT is about 62.0 A/gPt, which is slightly higher than that (56 A/gPt) for ETEK Pt/C catalyst. Goodenough et al. suggested the anodic peak in the reverse scan might be attributed to the removal of the incomplete oxidized carbonaceous species, such as CO, HCOO$^-$ and HCO$^-$, accumulated on catalyst surface during the forward scan. Consequently, the ratio of current densities for these two anodic peaks, I_f/I_b, can be used to infer the CO tolerance of the catalyst [31]. The low I_f/I_b value usually indicates poor oxidation of methanol to CO_2 during the forward anodic scan and excessive accumulation of residual carbon species on catalyst surface. On the other hand, a higher I_f/I_b ratio is indicative of improved CO tolerance. In our study, the observation of a much higher I_f/I_b value on Pt/TiSi$_x$-NCNT Janus nanostructure (2.0 vs. 1.3 on Pt/C) suggests that methanol molecules can be more effectively oxidized on Pt/TiSi$_x$-NCNT during the forward scan, generating relatively less poisoning species as compared to commercial Pt/C catalyst, indicating the better CO tolerance.

To further explore the observed enhancement of CO tolerance, carbon monoxide stripping voltammograms were completed for Pt/TiSi$_x$-NCNT, Pt/NCNT and Pt/C catalysts. Carbon monoxide adsorption was conducted at a potential of 0.05 V versus RHE for 20 min. The applied potential ensured that all available carbon monoxide was not oxidized prior to stripping voltammetry. From Figure 7.7, we can see that, for three catalysts, a sharp peak appears during the first scan (red line) and disappears in the subsequent scan (black line), indicating that the adsorbed CO is completely oxidized during the first forward scan. The peak potentials for carbon monoxide oxidation for Pt/TiSi$_x$-NCNT, Pt/NCNT and Pt/C catalysts are 0.837 V, 0.862 V, and 0.867 V versus RHE, respectively. The lower potential value in Pt/TiSi$_x$-NCNT electrode indicates that less applied potential is required to reach the hydroxide adsorption region and oxidize carbon monoxide. All these results indicate that Pt/TiSi$_x$-NCNT is more tolerant to CO poisoning which can be attributed to the addition of TiSi$_x$. In previous studies of Pt nanoparticle catalysts, the CO tolerance enhancements were also observed on Pt/metal oxide nanostructures, which was
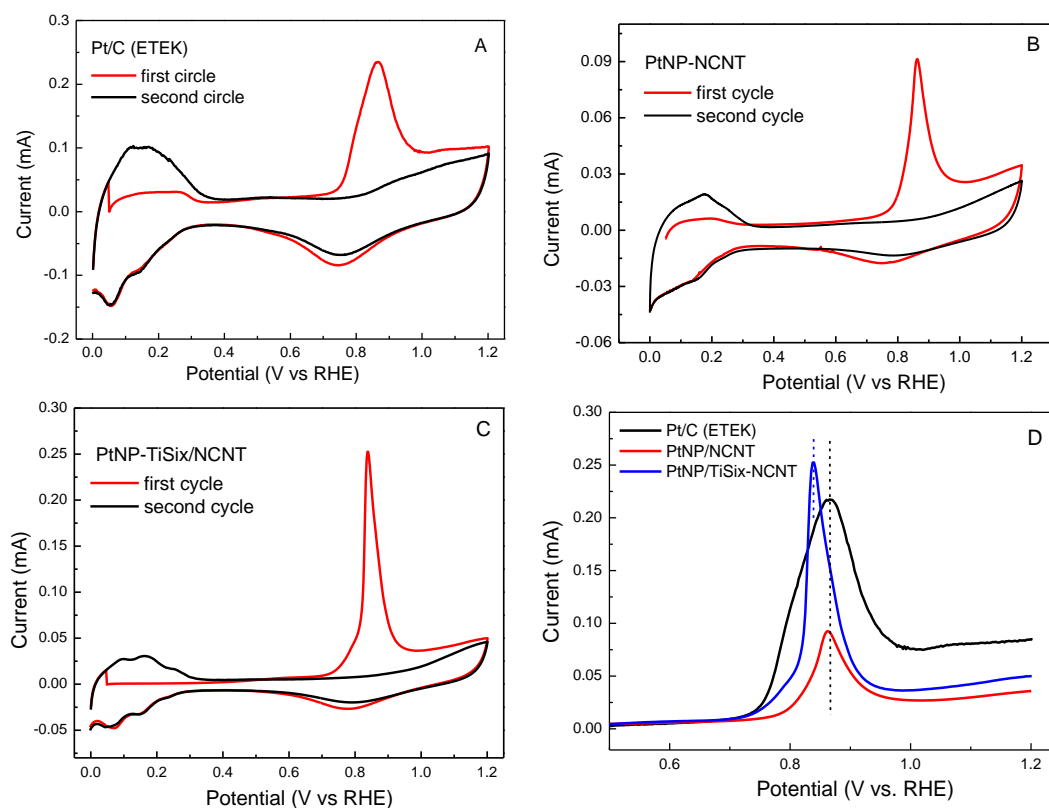
Figure 7.7. CVs of A) a commercial Pt/C ETEK electrode; B) PtNP/NCNT; C) PtNP/TiSi$_x$-NCNT in the presence of CO in 0.5 M H$_2$SO$_4$ aqueous solution at room temperature. Potential scan rate: 50 mV/s. For three catalysts, a sharp peak appears during the first scan (red line) and disappears in the subsequent scan (black line). D) The oxidative CO-stripping peak potential centers at 0.867 V for the commercial Pt/C catalyst, whereas on PtNP/TiSi$_x$-NCNT, it is located at 0.837 V. There is a 30 mV negative shift.

attributed to the fact that metal oxide could supply an oxygen containing (e.g. -OH groups) surface to remove strongly absorbed species like CO, according to a so-called bi-functional mechanism [31-33]. Therefore, the improved CO tolerance observed in

our study may originate from the addition of $TiSi_x$ which could supply an oxygen containing (e.g. -OH groups) surface.

7.4 Conclusions

In summary, Pt nanoparticles have been successfully synthesized on $TiSi_x$-NCNT supports, forming unique Janus nanostructures, by an environmentally friendly aqueous solution approach at 80 ^{o}C. Pt NPs formed dendritic and chain-like morphology between the gaps of $TiSi_x$ on NCNT surface. Electrochemical measurements demonstrated that the Pt/$TiSi_x$-NCNT Janus nanocatalyst exhibited enhanced stability and CO tolerance compared to commercial Pt/C catalyst.

Acknowledgements

References

[1]   K. Kordesch, G. Simander, *Fuel Cells and their Applications*, VCH, Germany, **1996** (p. 73)

[2]   E. Antolini, Formation of carbon-supported PtM alloys for low temperature fuel cells: a review. *Mater. Chem. Phys.* **2003**, *78*, 563–573.

[3]   D. R. Rolison, Catalytic Nanoarchitectures: The Importance of Nothing and the Unimportance of Periodicity. *Science* **2003**, *299*, 1698–1701.

[4]   H. A. Gasteiger, S. S. Kocha, B. Sompalli, F. T. Wagner, Activity Benchmarks and Requirements for Pt, Pt-Alloy, and Non-Pt Oxygen Reduction Catalysts for PEMFCs. *Appl. Catal. B* **2005**, *56*, 9–35.

[5]   N. P. Brandon, S. Skinner, B. C. H. Steele, Recent advances in materials for fuel cells. *Annu. Rev. Mater. Res.* **2003**, *33*, 183–213.

[6]   R. K. Rao, D. C. Trivedi, Chemical and electrochemical depositions of platinum group metals and their applications. *Coord. Chem. Rev.* **2005**, *249*, 613–631.

[7]   Z. Zhou, S. Wang, W. Zhou, G. Wang, L. Jiang, W. Li, S. Song, J. Liu, G. Sun, Q. Xin, Novel synthesis of highly active Pt/C cathode electrocatalyst for direct methanol fuel cell. *Chem. Commun.* **2003**, *3*, 394–395.

[8]   S. H. Sun, G. X. Zhang, D. S. Geng, Y. G. Chen, R. Y. Li, M. Cai, X. Sun, A New Highly Durable Pt Nanocatalyst for PEM Fuel Cells: the Multiarmed Star-like Nanowire Single Crystal. *Angew. Chem. Int. Ed*. **2011**, *50*, 422–426.

[9]   J. Zheng, M. Wang, X. Zhang, Y. Wu, P. Li, X. Zhou, W. Yuan, Platinum/carbon nanofiber nanocomposite synthesized by electrophoretic deposition as electrocatalyst for oxygen reduction. *J. Power Sources* **2008**, *175*, 211–216.

[10] S. Guo, S. Dong, E. Wang, Gold/Platinum Hybrid Nanoparticles Supported on Multiwalled Carbon Nanotube/Silica Coaxial Nanocables: Preparation and Application as Electrocatalysts for Oxygen Reduction. *J. Phys. Chem. C* **2008**, *112*, 2389–2393.

[11] S. H. Sun, D. Q. Yang, G. X. Zhang, E. Sacher, J. P. Dodelet. Synthesis and Characterization of Carbon Nanotube–Platinum Nanowire Heterostructures. *Chem. Mater.*, **2007**, *19*, 6376–6378.

[12] R. Borup, J. Meyers, B. Pivovar, Y. S. Kim, R. Mukundan, N. Garland, D. Myers, M. Wilson, F. Garzon, D. Wood, P. Zelenay, K. More, K. Stroh, T. Zawodzinski, J. Boncella, J. E. McGrath, M. Inaba, K. Miyatake, M. Hori, K. Ota, Z. Ogumi, S. Miyata, A. Nishikata, Z. Siroma, Y. Uchimoto, K. Yasuda, K. Kimijima, N. Iwashita, Scientific aspects of polymer electrolyte fuel cell durability and degradation. *Chem. Rev.,* **2007**, *107*, 3904–3951.

[13] Y. Y. Shao, G. P. Yin, Y. Z. Gao, Understanding and approaches for the durability issues of Pt-based catalysts for PEM fuel cell. *J. Power Sources* **2007**, *171*, 558–566.

[14] M. S. Saha, R. Li, X. Sun, High loading and monodispersed Pt nanoparticles on multiwalled carbon nanotubes for high performance proton exchange membrane fuel cells. *J. Power Sources* **2008**, *177*, 314–322.

[15] Y. Y. Shao, J. Liu, Y. Wang, Y. H. Lin, Novel Catalyst Support Materials for PEM Fuel Cells: Current Status and Future Prospects. *J. Mater. Chem*. **2008**, *19*, 46–59.

[16] H. A. Gasteiger, S. S. Kocha, B. Sompalli, F. T. Wagner, Activity Benchmarks and Requirements for Pt, Pt-Alloy, and Non-Pt Oxygen Reduction Catalysts for PEMFCs. *Appl. Catal. B* **2005**, *56*, 9–35.

[17] A. L. Schmitt, J. M. Higgins, J. R. Szczech, S. Jin, Synthesis and Applications of Metal Silicide Nanowires. *J. Mater. Chem.* **2010**, *20*, 223–235.

[18] S. Zhou, X. H. Liu, Y. J. Lin, D. W. Wang, Spontaneous growth of highly conductive two-dimensional TiSi2 nanonets. *Angew. Chem. Int. Ed.* **2008**, *47*, 7681–7684.

[19] S. Zhou, X. H. Liu, D. W. Wang, Si/TiSi2 Heteronanostructures as High-Capacity Anode Material for Li Ion Batteries. *Nano. Lett*. **2010**, *10*, 860–863.

[20] B. Merzougui, I. C. Halalay, J. T. Johnson, G. C. Garabedian, M. P. Balogh, S. Swathirajan, U.S. Patent Pub. No. US 2008/0118818 A1.

[21] T. Ukawa, H. Daimon, Japan Patent Pub. No. P2005-310418A.

[22] P. G. de Gennes, Soft Matter. *Science* **1992**, *256*, 495–497.

[23] P. G. de Gennes, Soft matter. *Rev. Mod. Phys*. **1992**, *64*, 645–648.

[24] C. J. Xu, B. D. Wang, S. H. Sun, Dumbbell-like Au-Fe$_3$O$_4$ nanoparticlesfor target-specific platin delivery. *J. Am. Chem. Soc*. **2009**, *131*, 4216–4217.

[25] Y. Zhong, M. Jaidann, Y. Zhang, G. Zhang, H. Liu, R. Li, X. Sun, H. Abou-Rachid, L. Lussier, Synthesis of High Nitrogen-Doping of Carbon Nanotubes and Modeling the Stabilization of Filled DAATO@CNTs (10, 10) for Nanoenergetic Materials. *J. Phys. Chem. Soli.* **2010**, *71*, 134–139.

[26] a) S. H. Sun, D. Q. Yang, D. Villers, G. X. Zhang, E. Sacher, J. P. Dodelet, Template-free, Surfactant-free Room Temperature Synthesis of Self-Assembled 3D Pt Nanoflowers from Single-Crystal Nanowires. *Adv. Mater.* **2008**, *20*, 571–574; b) D. Q. Yang, S. H. Sun, J. P. Dodelet, E. Sacher, A facile route for the self-organized high-density decoration of Pt nanoparticles on carbon nanotubes. *J. Phys. Chem. C* **2008**, *112*, 11717–11721; c) D. Q. Yang, S. H. Sun, H. Meng, J. P. Dodelet, E. Sacher, Formation of porous platinum

nanoparticle froth for electrochemical applications, produced without templates, surfactants, or stabilizers. *Chem. Mater.* **2008**, *20*, 4677–4681.

[27] J. Zhang, K. Sasaki, R. R. Adzic, Stabilization of platinum oxygen-reduction electrocatalysts using gold clusters, *Science*, **2007**, *315*, 220–222.

[28] Y. Chen, J. Wang, H. Liu, R. Li, X. Sun, S. Ye, S. Knights, Enhanced Stability of Pt Electrocatalysts by Nitrogen Doping in CNTs for PEM Fuel Cells. *Electrochem. Commun.* **2009**, *11*, 2071–2076.

[29] Y. Dai, B. Lim, Y. Yang, C. M. Cobley, W. Li, E. C. Cho, B. Grayson, P. T. Fanson, C. T. Campbell, Y. Sun, Y. Xia, A Sinter-Resistant Catalytic System Based on Platinum Nanoparticles Supported on TiO_2 Nanofibers and Covered by Porous Silica. *Angew. Chem. Int. Ed.* **2010**, *49*, 8165–8168.

[30] G. Che, B. B. Lakshmi, E. R. Fisher, R. Martin, Carbon Nanotubule Membranes for Electrochemical Energy Storage and Production. *Nature* **1998**, *393*, 346–349.

[31] R. Manohara, J. B. Goodenough, Methanol oxidation in acid on ordered NiTi. *J. Mater. Chem.* **1992**, *2*, 875–887.

[32] F. Colmati, E. Antolini, E. R. Gonzalez, Effect of temperature on the mechanism of ethanol oxidation on carbon supported Pt, PtRu and Pt_3Sn electrocatalysts. *J. Power Sources* **2006**, *157*, 98–103.

[33] P. Bommersbach, M. Mohamedi, D. Guay, Electro-oxidation of Ethanol at Sputter-Deposited Platinum–Tin Catalysts. *J. Electrochem. Soc.* **2007**, *154*, B876–B882.

Supporting Information
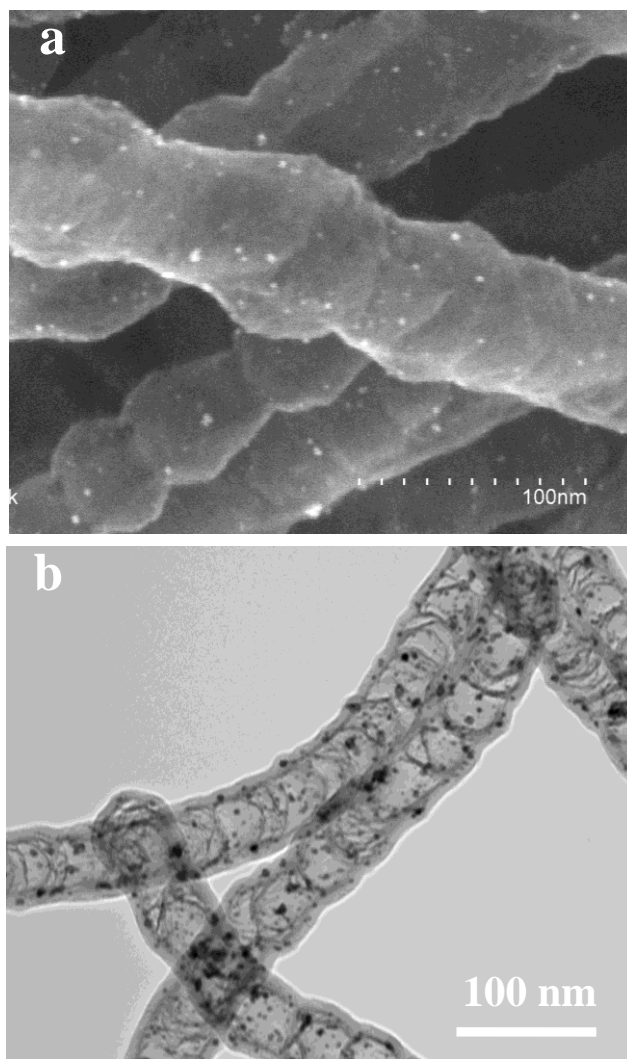
Figure SI-7.1. SEM and TEM images of Pt NPs on NCNT.

Chapter 8. Atomic layer deposition of subnanometer Pt clusters on graphene as highly active and CO-tolerant electrocatalyst for methanol oxidation

Shuhui Sun, Xiangbo Meng, Gaixia Zhang, Dongsheng Geng, Ruying Li, Xueliang Sun*

Department of Mechanical and Materials Engineering, University of Western Ontario, London, ON, N6A 5B9 Canada

Nicolas Gauquelin, Gianluigi Botton*

McMaster University, Hamilton, ON, Canada, L8S 4L8

Siyu Ye, Shanna Knights

Ballard Power Systems Inc., 9000 Glenlyon Parkway, Burnaby, BC, Canada V5J 5J8

* Email addresses: xsun@eng.uwo.ca (X. Sun); gbotton@mcmaster.ca (G. Botton);

A version of this chapter will be submitted for publishing.

In chapter 6 and 7, two novel alternative catalyst supports: 0D Nb-doped TiO$_2$ hollow nanospheres and 1D TiSi$_x$-NCNT nanostructures were demonstrated and used as Pt nanoparticle catalyst supports, showing much improved durability. Despite the progresses, Nb-doped TiO$_2$ only has 1/3 electrical conductivity that of carbon black; and both of the above supports have relative smaller or equal surface area than carbon black commercial catalyst supports. Therefore, it is highly desirable to find a material that possesses not only high corrosion resistance, but also higher surface area and higher conductivity.

Graphene, a recently emergent 2D carbon material with single (or a few) atomic layer, is a wonder material. Graphene is a flat monolayer of carbon atoms tightly packed into a two-dimensional (2D) honeycomb lattice, and is a basic building block for graphitic materials of all other dimensionalities. It can be wrapped up into 0D fullerenes, rolled into 1D nanotubes or stacked into 3D graphite. Since individual graphene sheets were produced by Andre Geim and Konstantin Novoselov in 2004, this perfect material has attracted great attention for both fundamental science and applied research. The Nobel Prize in Physics for 2010 was therefore awarded to these two scientists "for their groundbreaking experiments regarding the two-dimensional material graphene". The combination of ultrahigh surface area (theoretical value of 2630 m^2/g), high electrical conductivity (similar to Cu), high thermal conductivity (5 times that of Cu) and high corrosion resistance (due to its unique graphitized basal plane structure) and potential low manufacturing cost makes graphene a promising candidate for many applications, including the catalyst support in PEMFCs.

Atomic layer deposition (ALD) is a promising technique to prepare catalyst because it utilizes alternating, self-limiting exposures between a substrate surface and different reactive precursor vapours to deposit materials in an atomic layer-by-layer fashion. Previous studies have revealed that ALD allows one to control the morphology of the deposited metal, from discrete tiny nanoparticles to a continuous thin film, through the surface chemistry. In addition, due to the self-limiting nature of the process, ALD can be used to control the amount of catalyst deposited on the support material. Hence, ALD process is ideally suited to determine the lower limits of metal loading in a catalytic system.

In this chapter, the authors report the work by employing the novel ALD deposition technique to synthesize ultrafine platinum (Pt) nanoparticles on the surfaces of graphene nanosheet support. Graphene supported ALD-deposited Pt catalysts display 3.5 times higher activity and 2 folds higher durability for methanol oxidation than those of commercial Pt/C catalyst. This novel catalyst also exhibited much

higher CO tolerance and slower CO adsorption rate than commercial Pt/C catalyst. HAADF-STEM investigations indicate the existence of large amount of ultrafine sub-nanometer Pt clusters and single Pt atoms on the surface of graphene nanosheets. It is believed that the sub-nanometer Pt clusters and individual Pt atoms as well as the strong interaction between Pt and graphene substrate contribute to the enhanced performance of ALD Pt/graphene catalyst.

8.1 Introduction

Platinum-base catalysts are widely used in the chemical and automobile industries because of their high activity and/or selectivity for many important chemical processes [1-5]. Generally, in such systems, fine Pt nanoparticles are dispersed uniformly on a support with high surface area for the efficient use of catalytically active sites. However, the efficiency of Pt catalysts is still very low on a per Pt atom basis, because only the surface active atoms are used in the reactions. So downsizing Pt nanoparticles to clusters or even single atoms could significantly increase their catalytic activity and is highly desirable to maximize the efficiency [6]. However, reducing metal particles to stable clusters and single atoms remains a major challenge because clusters and single atoms are too mobile and easy to sinter under realistic reaction conditions [7-9].

Recently, it has been reported that subnanometer clusters and single atoms demonstrated better activity than nanometer-sized particles [6]. A more practical approach for the large scale synthesis remains challenging. Here, we used atomic layer deposition (ALD) to prepare subnanometer clusters and single atoms on graphene nanosheet. ALD is a promising technique to prepare catalyst because it utilizes alternating, self-limiting exposures between a substrate surface and different reactive precursor vapors to deposit materials in an atomic layer-by-layer fashion [10]. Previous studies have revealed that ALD allows one to control the morphology of the deposited metal, from discrete tiny nanoparticles to a continuous thin film, through the surface chemistry [11-13]. In addition, due to the self-limiting nature of the process, ALD can be used to control the amount of catalyst deposited on the support material. Hence, ALD process is ideally suited to determine the lower limits of metal loading in a catalytic system.

Graphene, a recently emergent two-dimensional (2D) carbon material with single (or a few) atomic layer, has attracted great attention for both fundamental science and applied research. The combination of the high surface area (theoretical value of 2630

m^2/g), high conductivity, unique graphitized basal plane structure and potential low manufacturing cost makes graphene a promising candidate for catalyst support in PEMFCs [14]. It is expected that graphene may offer a new carbon-metal nanocomposite as the catalyst material for next generation materials [15].

8.2 Experimental

8.2.1 Preparation of graphene.

Graphene nanosheets (GRNs) were synthesized via a modified Hummers method [16] which involves graphite oxidation, thermal exfoliation, and chemical reduction. In detail, natural graphite powder (1 g, 99.99%, Sigma-Aldrich) was first stirred in concentrated sulphuric acid (H$_2$SO$_4$, 23 mL) with a following addition of sodium nitrate (NaNO$_3$, 0.5 g) at room temperature. The stirring lasted for 16 h, and then the mixture was cooled down to 0 ℃. Potassium permanganate (K$_2$MnO$_4$, 3 g) was then added into the solution. After 2 h, the solution formed green slurry at around 35 ℃, which was stirred for another 3 h. Then, H$_2$O (46 mL) was slowly added at around 98 ℃. The suspension was kept at this temperature for 30 min before it was further diluted with another addition of water and hydrogen peroxide (H$_2$O$_2$, 140 mL). The suspension was subsequently filtered and washed until reaching a neutral pH, and dried in a vacuum oven at 60 ℃ to obtain graphite oxide (GO). To obtain graphene, the as-synthesized GO was heated at around 1050 ℃ in Ar atmosphere for 30 s in a tube furnace.

8.2.2 ALD of Pt on graphene

Platinum was deposited on graphene supports by ALD (Savannah 100, Cambridge Nanotechnology Inc., USA) using the (methylcyclopentadienyl)-trimethylplatinum (MeCpPtMe$_3$, Aldrich, purity 98 %) and oxygen (99.999 %) as precursors, and nitrogen (99.9995 %) as purge gas. The schematic illustration of the apparatus used for ALD is shown in Figure SI-8.1. It consists of a wall reactor with an outlet leading to a vacuum pump which can also prevent air from getting into the system. The inlet

is connected to a system of valves which can control the delivery of purge gas and precursors. To increase the heat transfer from the stage to the graphene, hot wall conditions were replicated by placing graphene powder inside a machined stainless steel container with a perforated Al lid. The container for graphene was then placed inside the reactor directly on the heated stage. The wall and stage temperatures of the reactor were kept at 150 $^{\circ}$C and 250 $^{\circ}$C, respectively. The container for MeCpPtMe$_3$ was kept at 65 $^{\circ}$C, providing a steady state flux of MeCpPtMe$_3$ to the reactor [17]. In each ALD cycle, 1 s of MeCpPtMe$_3$ pulse and 5 s of O$_2$ pulse were separated by 20 s of N$_2$ purge. As the focus of this work is on the ultralow loading regime, the GRNs were exposed to 100 ALD cycles.

8.2.3 Characterization.

The morphologies and microstructures of the as-prepared samples were examined by scanning electron microscopy (SEM, Hitachi S-4800) operated at 5kV. Subangstrom-resolution aberration-corrected scanning transmission electron microscopy (STEM, FEI Titan 80-300 Cubed TEM) was used to characterize the dispersion and configuration of Pt clusters on graphene. The instrument is fitted with a Super-Twin lens in order to achieve sub-angstrom resolution both for phase contrast imaging and STEM. The probe diameter is less than 0.1 nm. Energy Dispersive X-ray Spectrometry (EDXS) was performed using an INCA Detector with acquisition time of 120 s. The sample was tilted towards the detector in order to increase the integrated intensity. Individual heavy atoms in practical catalysts can be discerned with atomic resolution in high angle annular dark field (HAADF) images [6]. The Pt loadings were confirmed by inductively coupled plasma-optical emission spectroscopy (ICP-OES).

8.2.4 Electrode Preparation

The working electrode was prepared with a procedure similar to the one reported previously [18]. Typically, the catalyst dispersions were prepared by mixing 5 mg of catalyst in 5 mL aqueous solution containing 1 mL of isopropyl alcohol and 30 mL of

5 wt% Nafion solution (4:1:0.0017 v/v) followed by 12 min ultrasonication. Glassy carbon (GC) disk electrodes (5 mm diameter, 0.196 cm^2, Pine Research Instrument) served as the substrate for the support and were polished to a mirror finish. An aliquot of catalyst suspension was pipetted onto the carbon substrate to obtain the same Pt loading for all catalysts. The catalyst films were dried under flowing N$_2$ at room temperature.

8.2.5 Electrochemical Measurements.

Electrochemical properties of the catalysts were measured on an Autolab potentiostat/galvanostat (Model, PGSTAT-30, Eco-chemie, Brinkman Instruments) with rotation control (MSR, Pine Instruments) using a three-electrode system that consists of a GC rotating disk electrode (RDE), a Pt wire counter electrode, and a Ag/AgCl (3M NaCl) reference electrode separated from the working electrode compartment by a closed electrolyte bridge. For convenience, all potentials in this study are referenced to the reversible hydrogen electrode (RHE). The working electrode was first cycled between 0 and 1.2 V for 50 times in an Ar-purged H$_2$SO$_4$ solution (0.5 M) at room temperature, to produce a clean electrode surface. The scan rate used was 50 mVs^{-1}. Cyclic voltammetry (CV) measurements were conducted by cycling the potential between 0 and 1.2 V, with sweep rate of 50 mVs^{-1}. The electrochemical surface areas (ECSA) of Pt were calculated from the hydrogen adsorption peak of the CV. For methanol oxidation reaction (MOR), the CVs were measured in an air-free aqueous solution containing 1 M MeOH and 0.5 M H$_2$SO$_4$ at room temperature in an Ar atmosphere. For CO stripping voltammetry, 30%CO/N$_2$ gas was purged into the solution at a position close to the working electrode for 1 s to 20 min, with the electrode polarized at 0.05 V versus RHE in a fume hood. The excess CO was purged with Ar for 30 min under potential control followed by CO stripping at a scan rate of 50 mVs^{-1}.

8.3 Results and Discussion

ALD of Pt follows a similar pathway as CVD of Pt [19] during the oxidative decomposition of MeCpPtMe$_3$:

$$Pt(s) + O_2(g) \longrightarrow Pt\text{-}O_x \qquad (8.1)$$

$$CH_3C_5H_4Pt(CH_3)_3 + Pt\text{-}O_x \longrightarrow Pt(s) + CO_2(g) + H_2O(g) + \text{fragments} \qquad (8.2)$$
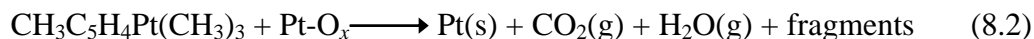
As shown in Figure 8.1, the oxygen exposure forms an adsorbed oxygen layer on the Pt surface (Eq. 1). During the subsequent MeCpPtMe$_3$ exposure, some of the precursor ligands react with the adsorbed oxygen, to form CO_2, H_2O, and hydrocarbon fragments shown in Eq. 2. The limited supply of surface oxygen prevents all of the ligands from oxidizing and provides the self-limiting growth necessary for ALD. Complete oxidation occurs during the following O_2 exposure and forms a new adsorbed oxygen layer on the Pt. This mechanism is supported by quadrupole mass spectrometry (QMS) measurements in which CO_2 and H_2O were observed during both the MeCpPtMe$_3$ and the oxygen exposures [20].
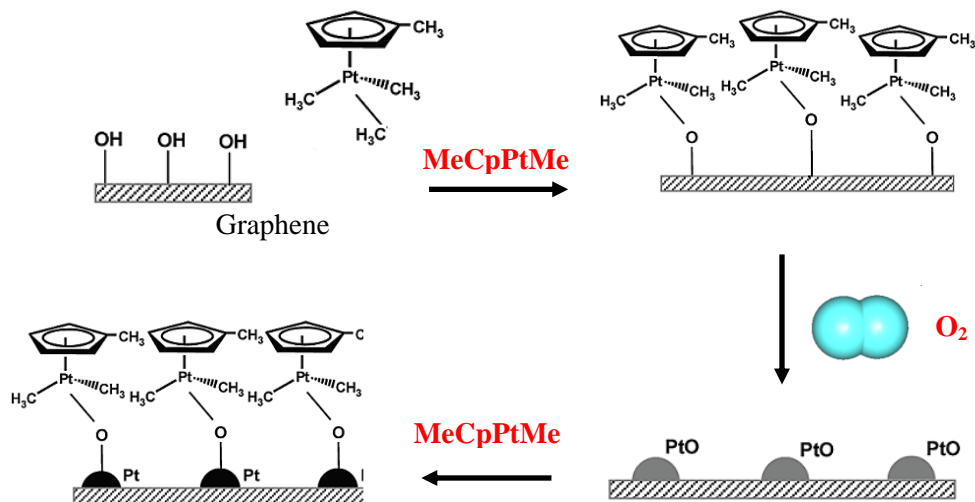
Figure 8.1. Proposed schematic illustrations of ALD process of Pt on Graphene.
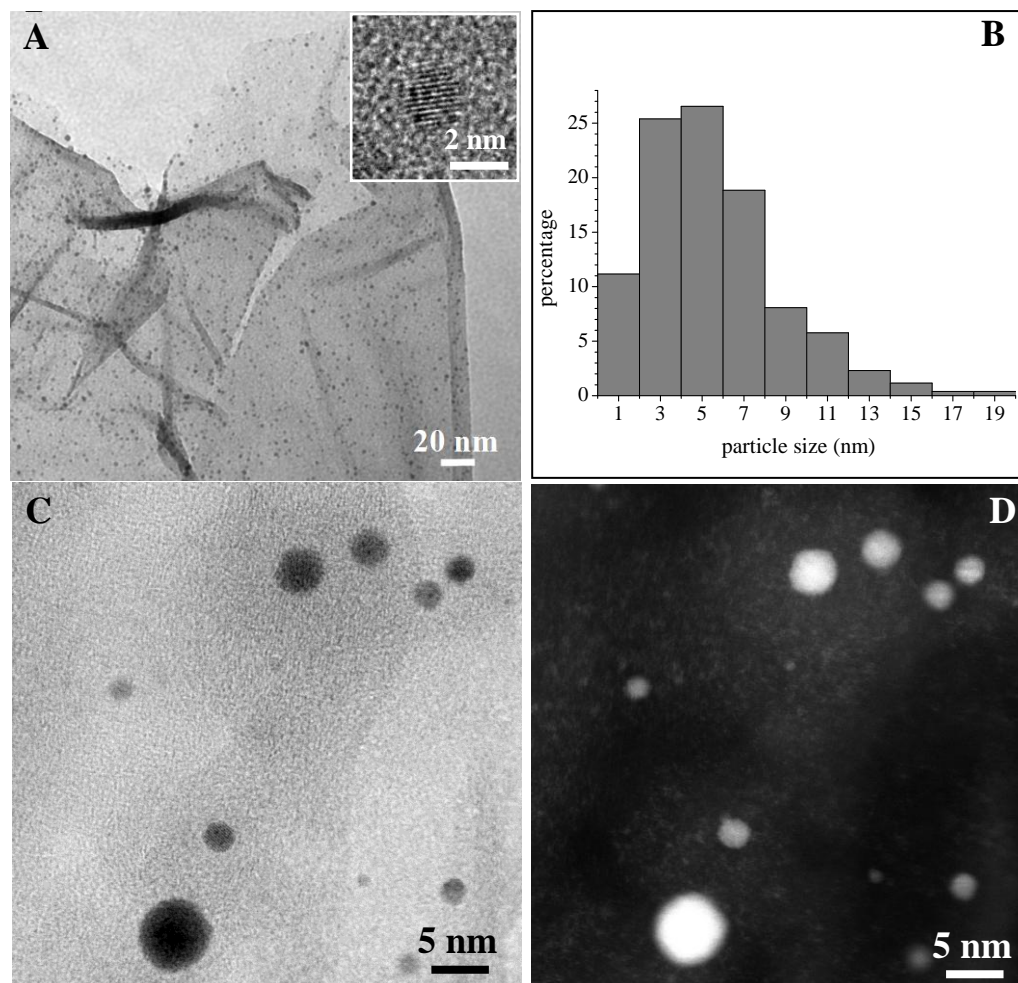
Figure 8.2. TEM (A) image and histogram (B) of Pt/GNS with100 ALD cycles. Bright field TEM (C) and (D) HAADF-STEM image of 100 ALD cycles. The scale bar in inset of A is 2 nm.

Figure SI-8.2 shows the SEM (A) and TEM (B) images of graphene. It can be seen that the material is transparent with the voile-like structure and consists of randomly crumpled sheets closely associated with each other and forming a disordered solid. The planar sheets are clearly observed, indicating the features of high surface/volume ratio and the two-dimensional structure of graphene. The morphological structure, the

particle size, and the metal dispersion of Pt electrocatalysts were examined by TEM. Figure 8.2A and B show the TEM image and repartition of Pt particle size of Pt/graphene with 100 ALD cycles, respectively. We can see that discrete, well dispersed Pt nanoparticles have been uniformly deposited on the surface of the graphene nanosheet. One hundred particles were randomly measured to obtain the particle size distribution. The Pt particles display an average size of 2 nm and are uniformly distributed on the graphene nanosheet support. From the HRTEM image shown in inset of Figure 8.2A, we can see that each Pt nanoparticles or clusters are single crystalline and arranged in the cubic close-packed structure with a spacing of 0.235 nm revealed by the FFT.

On the bright-field TEM image, only Pt nanoparticles of 1–4 nm in size are observed (Figure 8.2C). Interestingly, on the contrary, the sensitivity to atomic number (Z)-contrast of HAADF-STEM revealed (Figure 8.2D), in addition to these Pt nanoparticles, the presence of numerous individual Pt atoms, as well as very small Pt clusters of size $\leq$ 1 nm that consisting only of a few atoms. Figure 8.3A and B show respectively the EDXS spectra and the corresponding HAADF-STEM image of Pt/graphene. The EDXS spectra were collected from five different areas with Pt-clusters ranging from 1.2 to 6.7 nm on a graphene nanosheet as well as an area containing only a few atoms. Presence of Pt and C is confirmed by all measurements. The Cu peak is attributed to the Cu mesh on which the catalyst is dispersed for TEM measurement. This further indicates that the bright spots in the HAADF-STEM image are subnanometer Pt clusters and individual atoms attached on the surface of the graphene nanosheets. The peak intensities were normalized according to the Cu K_α intensity. We can see that all areas show obviously Pt signals, even areas where only a few Pt atoms are present, and a decrease of particle size results in a decrease of the Pt peaks intensity. It is inferred that these subnanometer-sized Pt clusters and individual atoms observed for the first time with appreciable amounts must be connected to the unprecedented MOR performance of Pt catalyst deposited using ALD [21].
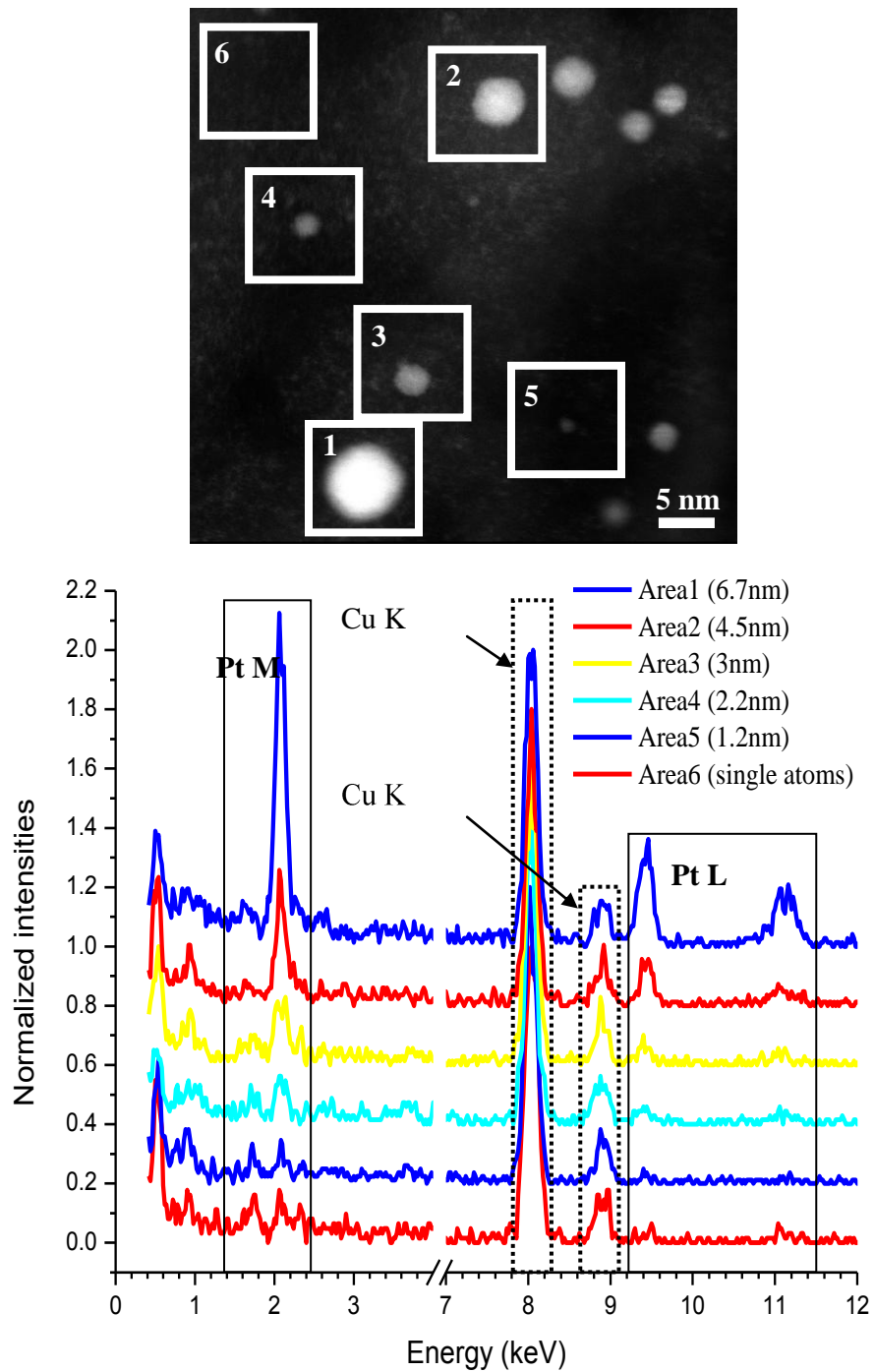
Figure 8.3. EDX spectrum of Pt/GNS taken from different areas.

The presence of these extremely small Pt clusters and individual atoms suggests a strong interaction between graphene and platinum atoms, which may induce some modulation in the electronic structure of the Pt clusters. Okamoto et al. have reported based on density-functional calculations that introducing a carbon vacancy into a graphene sheet enhanced the interaction between graphene and Pt13 clusters [22]. They concluded that the stability of the metal clusters on graphene with carbon vacancies was higher than that on a defect free graphene [22]. Graphene used in this study must involve many carbon vacancies and defects, because of the preparation method by chemical reduction of exfoliated graphite oxide sheets. It is thus indicated that carbon atoms with dangling bond or oxygen-containing functional groups exist at the defect sites of the graphene nanosheets used in this work. The Pt precursor used in this study reacts with these defects. The present study indicates that graphene is expected as a new carbon support material modifying catalytic properties of Pt as fuel cell catalysts.

Direct methanol fuel cell has several advantages such as high efficiency and low polluting emissions [23,24]. The study on the electrocatalytic activity for methanol oxidation is therefore important for future applications. Cyclic voltammetry (CV) was used to systematically study the catalytic activity and onset of methanol oxidation, and chronoamperometry (CA) was used to determine the stability and performance of the catalysts. Figure 8.4A shows the CVs for methanol oxidation on ALD Pt/graphene and Pt/C (ETEK) catalysts. Two typical oxidation peaks appear on the CV curves of the Pt/graphene (red curve) and Pt/C (ETEK) (black curve) catalysts, arising from oxidations of methanol and their intermediates [25]. The onset potential of methanol oxidation was 0.5 and 0.6 V (vs. RHE) for Pt/graphene and Pt/C, respectively. Obviously, the peak potential for methanol oxidation in the forward scan on Pt/graphene composite (0.82 V vs. RHE) is much lower than that (0.94 V vs. RHE) for Pt/C catalyst. The negative shifts of the onset and peak potentials indicate that the Pt supported on graphene is able to significantly reduce the overpotential for methanol oxidation. These improvements may be attributed to the presence of oxygen
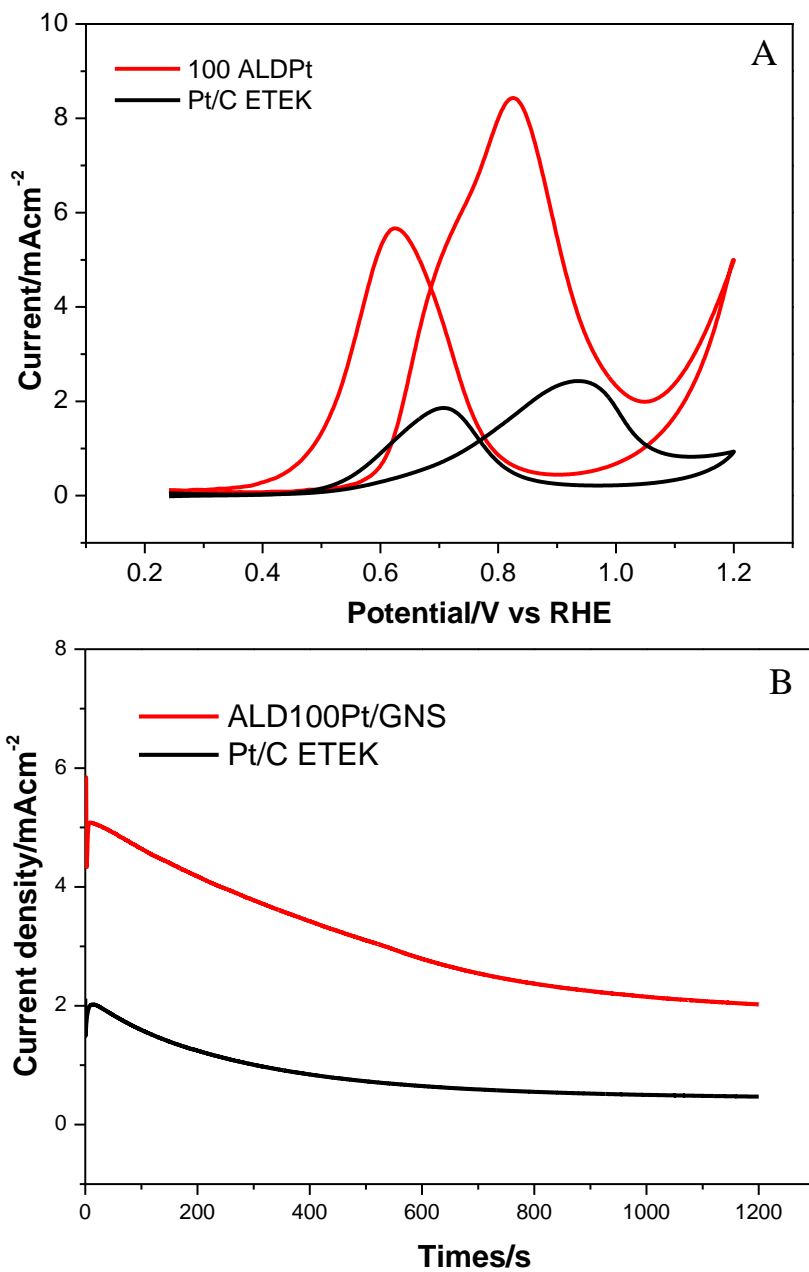
Figure 8.4. (A) CVs and (B) CAs of MeOH oxidation on (a) ETEK Pt/C, (b) ALD100Pt/GNS.

containing functional groups on graphene nanosheet as the graphene used in this study involves preparation-induced defects [2]. The methanol oxidation peak current density for Pt/graphene (8.48 mA cm^{-2}) is 3.5 times higher than for the ETEK Pt/C catalyst (2.41 mA cm^{-2}). Chronoamperometry data were recorded at 0.7 V (vs. RHE) for 1200 s as a measure of the catalyst deactivation (Figure 8.4B). We observed that the current density of both samples degrades with increasing time during the methanol oxidation reaction, but Pt/graphene exhibited a slower current decay over time than Pt/C. Keeping 40 and 23% of their initial values, for Pt/graphene and Pt/C respectively, indicates a higher tolerance of Pt/graphene to CO-like intermediates [26]. After 1200 s of continuous operation, Pt/graphene showed 4.6 times higher current density (2.1 mA cm^{-2}) than that of Pt/C (0.45 mA cm^{-2}). The enhancement may be attributed to the intrinsic nature of subnanometer Pt clusters and individual atoms [6,9], as well as the carbons substrate materials [2]. Goodenough et al [27] suggested the anodic peak in the reverse scan to be linked to the removal of the incomplete oxidized carbonaceous species, such as CO, HCOO^{-} and HCO^{-}, accumulated on the catalyst surface during the forward scan. CO, a critical intermediate of MOR, can poison Pt catalysts; consequently, the ratio of the forward peak current density (I_f) to the reverse anodic peak current density (I_b), I_f/I_b, can be used to indicate the CO tolerance of the catalyst [27]. A low I_f/I_b value usually indicates poor oxidation of methanol to CO_2 during the forward anodic scan and excessive accumulation of residual carbon species on the catalyst surface. On the other hand, a higher I_f/I_b ratio is indicative of improved CO tolerance. In our study, the observation of a relatively higher I_f/I_b value on Pt/graphene composite (1.5 vs. 1.3 on ETEK Pt/C) suggests that methanol molecules can be more efficiently oxidized on Pt/graphene during the forward scan than on conventional Pt/C catalyst. This generates relatively less poisoning species as compared to commercial Pt/C catalyst, indicating a better CO tolerance. To further investigate the observed enhancement of CO tolerance, a CO electrostripping experiment was carried out. From Figure 8.5, we notice, for both catalysts, a sharp peak appearing during the first scan (red line) and disappearing in the subsequent scan (black line), indicating that the adsorbed CO is completely

oxidized during the first forward scan. When comparing the peak potential for CO electro-oxidation, significant differences between the two catalysts can be observed. The peak potential of CO oxidation on Pt/graphene is at 0.77 V (vs. RHE), which is about 100 mV lower than that on commercial Pt/C catalyst (0.87 V vs. RHE). The significant negative shift for the peak potentials indicate that the adsorbed CO can be more easily removed from Pt/graphene catalyst than ETEK commercial Pt/C catalyst. All these results indicate that ALD deposited Pt/graphene is much more tolerant to CO poisoning than commercial Pt/C catalyst.
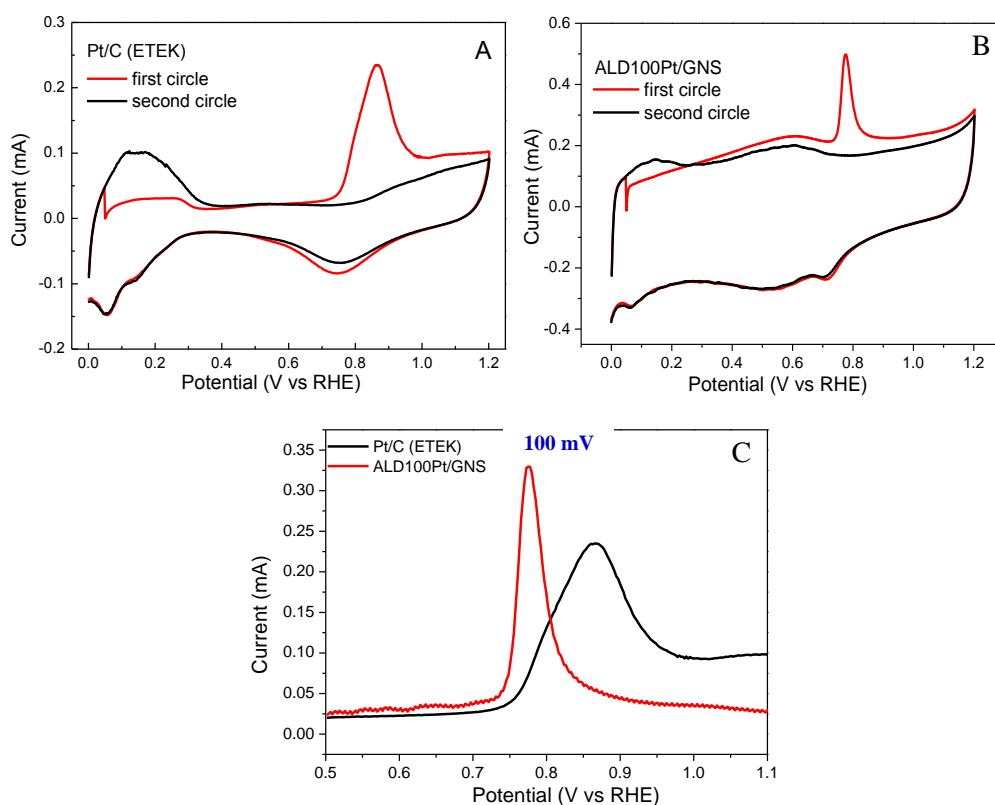
Figure 8.5. The CO stripping voltammogram as a function of CO poison time of (A) ETEK Pt/C; (B) ALD100Pt/GNS; (C) Peak potential comparison.
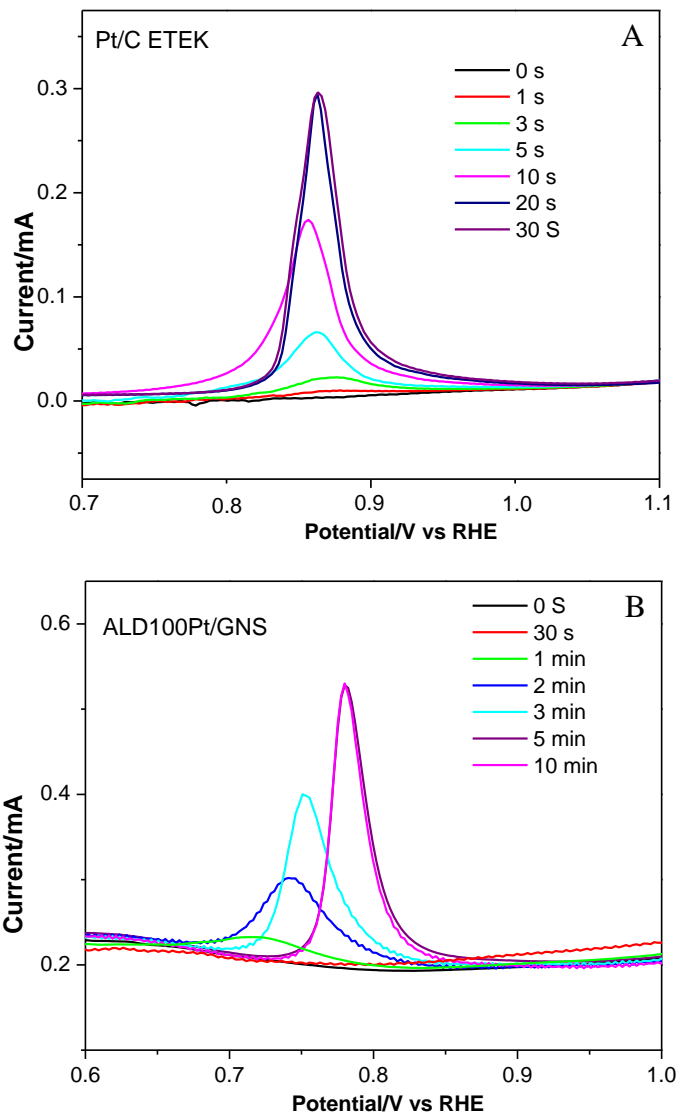
Figure 8.6. The CO stripping as a function of CO poison time. (A) ETEK Pt/C; (B) ALD100Pt/GNS.

To further investigate the reason of high MOR activity for Pt/graphene, the CO stripping voltammetry was conducted as a function of CO poisoning times in 0.5 M H_2SO_4 at room temperature. Figure 8.6 A and B show the CO stripping voltammograms for Pt/C and Pt/graphene, respectively. An obvious CO oxidation peak of Pt/C was observed at 0.87 V (vs. RHE) after passing 30% CO/Ar gas for 3 s (Figure 8.6A). However, the CO oxidation peak of Pt/graphene was not observed until an exposure time of 1 minute to 30% CO/Ar was reached (Figure 8.6B). Further, we found that the equilibrium CO coverage of Pt/graphene was reached after passing 30% CO/Ar for more than 5 min, while, for the Pt/C the equilibrium CO coverage was reached after passing 30% CO/Ar gas for 20 s. This indicates that the state of CO adsorption on Pt/graphene is different from traditional Pt catalysts supported on carbon black [2]. The CO adsorption rate on Pt/graphene was obviously much slower compared to that on Pt/carbon black, which might be due to the superior CO tolerance of ultrafine Pt catalysts [2]. Although the detailed mechanism of the CO poisoning tolerance is not clear for the Pt/ graphene catalyst, it is found that the CO tolerance and adsorption rates of Pt electrocatalysts are significantly different depending on the size of Pt and the carbon support.

8.4 Conclusions

In conclusion, ALD was used to uniformly deposit ultrafine platinum (Pt) nanoparticles on graphene nanosheets. HAADF-STEM investigations indicate large amount of ultrafine sub-nanometer Pt clusters and individual Pt atoms on the surface of graphene nanosheets. Graphene nanosheets give rise to an extraordinary modification to the properties of Pt nanocatalysts. Graphene supported ALD-deposited Pt catalysts display a higher electrocatalytic activity and durability in methanol oxidation, and enhanced CO tolerance that commercial Pt on carbon black catalyst.

Acknowledgments

References

[1] R. J. Davis, E. G. Derouane, A Non-porous Supported Platinum Catalyst for Aromatization of n-Hexane. *Nature* **1991**, *349*, 313–315.

[2] A. Kolmakov, D. O. Klenov, Y. Lilach, S. Stemmer, M. Moskovits, Enhanced Gas Sensing by Individual SnO_2 Nanowires and Nanobelts Functionalized with Pd Catalyst Particles. *Nano Lett.* **2005**, *5*, 667–673.

[3] A. Roucoux, J. Schulz, H. Patin, Reduced transition metal colloids: A novel family of reusable catalysts? *Chem. Rev.* **2002**, *102*, 3757–3778.

[4] D. R. Rolison, Catalytic Nanoarchitectures: The Importance of Nothing and the Unimportance of Periodicity. *Science* **2003**, *299*, 1698–1701.

[5] H. A. Gasteiger, S. S. Kocha, B. Sompalli, F. T. Wagner, Activity Benchmarks and Requirements for Pt, Pt-Alloy, and Non-Pt Oxygen Reduction Catalysts for PEMFCs. *Appl. Catal. B* **2005**, *56*, 9–35.

[6] B. Qiao, A. Wang, X. Yang, L. F. Allard, Z. Jiang, Y. Cui, J. Liu, J. Li, T. Zhang, Single-atom catalysis of CO oxidation using Pt_1/FeO_x. *Nature Chem.* **2011**, *3*, 634–641.

[7] A. Uzun, V. Ortalan, N. D. Browning, B. C. Gates, A Site-Isolated Mononuclear Iridium Complex Catalyst Supported on MgO: Characterization by Spectroscopy and Aberration-Corrected Scanning Transmission Electron Microscopy. *J. Catal.* **2010**, *269*, 318–328.

[8] A. Uzun, V. Ortalan, Y. Hao, N. D. Browning, B. C. Gates, Nanoclusters of Gold on a High-Area Support: Almost Uniform Nanoclusters Imaged by Scanning Transmission Electron Microscopy. *ACS Nano* **2009**, *3*, 3691–3695.

[9] C. Susut, G. B. Chapman, G. Samjeske, M. Osawa, Y. Tong, An unexpected enhancement in methanol electro-oxidation on an ensemble of Pt(111)

nanofacets: a case of nanoscale single crystal ensemble electrocatalysis. *Phys. Chem. Chem. Phys.*, **2008**, *10*, 3712–3721.

[10] S. Christensen, J. Elam, B. Lee, Z. Feng, M. Bedzyk, M. Hersam, Nanoscale structure and morphology of atomic layer deposition platinum on SrTiO3 (001). *Chem. Mater.* **2009**, *21*, 516–521.

[11] A. Johansson, J. Lu, J. O. Carlsson, M. Boman, Deposition of palladium nanoparticles on the pore walls of anodic alumina using sequential electroless deposition. *J. Appl. Phys.* **2004**, *96*, 5189–5194.

[12] J. S. King, A. Wittstock, J. Biener, S. O. Kucheyev, Y. M. Wang, T. F. Baumann, S. K. Giri, A. V. Hamza, M. Baeumer, S. F. Bent, Ultralow loading Pt nanocatalysts prepared by atomic layer deposition on carbon aerogels. *Nano Lett.* **2008**, *8*, 2405–2409.

[13] Y. Zhu, K. A. Dunn, A. E. Kaloyeros, Properties of Ultra-thin Platinum Deposited by Atomic Layer Deposition for Nanoscale Copper Metallization Schemes. *J. Mater. Res.* **2007**, *22*, 1292-1298.

[14] R. Kou, Y. Shao, D. Wang, M. H. Engelhard, Ja H. Kwak, J. Wang, V. V. Viswanathan, C. Wang, Y. Lin, Y. Wang, I. A. Aksay, J. Liu. Enhanced activity and stability of Pt catalysts on functionalized graphene sheets for electrocatalytic oxygen reduction. *Electrochem. Commun.* **2009**, 11, 954–957.

[15] E. Yoo, T. Okata, T.Akita, M Kohyama, J. Nakamura, I. Honma. Enhanced Electrocatalytic Activity of Pt Subnanoclusters on Graphene Nanosheet Surface. *Nano. Lett.* **2009**, *9*, 2255–2259.

[16] (a) W. S. Hummers, R. E. Offeman, Preparation of graphite oxide. *J. Am. Chem. Soc.* **1958**, *80*, 1339–1339; (b) D. Geng, S. Yang, Y. Zhang, J. Yang, J. Liu, R. Li, T. K. Sham, X. Sun, S. Ye, S. Knights. Nitrogen Doping Effects on the Structure of Graphene. *Applied Surface Science*, **2011**, *257*, 9193–9198.

[17] C. Liu, C. C. Wang, C. C. Kei, Y. C. Hsueh, T. P. Perng, Atomic Layer Deposition of Platinum Nanoparticles on Carbon Nanotubes for Application in Proton-Exchange Membrane Fuel Cells *Small* **2009**, *5*, 1535–1538.

[18] S. H. Sun, G. X. Zhang, D. S. Geng, Y. G. Chen, R. Y. Li, M. Cai, X. Sun, A New Highly Durable Pt Nanocatalyst for PEM Fuel Cells: the Multiarmed Star-like Nanowire Single Crystal. *Angew. Chem. Int. Ed*. **2011**, *50*, 422–426.

[19] Z. L. Xue, H. Thridandam, H. D. Kaesz, R. F. Hicks, Organometallic chemical vapor deposition of platinum. Reaction kinetics and vapor pressures of precursors. *Chem. Mater.* **1992**, *4*, 162–166.

[20] T. Aaltonen, A. Rahtu, M. Ritala, M. Leskela, Reaction Mechanism Studies on Atomic Layer Deposition of Ruthenium and Platinum. *Electrochem. Solid-State Lett.* **2003**, *6*, C130–C133.

[21] E. Yoo, T. Okata, T.Akita, M Kohyama, J. Nakamura, I. Honma. Enhanced Electrocatalytic Activity of Pt Subnanoclusters on Graphene Nanosheet Surface. *Nano. Lett.* **2009**, *9*, 2255–2259.

[22] Y. Okamoto, Density-functional calculations of icosahedral M_{13} (M = Pt and Au) clusters on graphene sheets and flakes. *Chem. Phys. Lett.* **2006**, *420*, 382–386.

[23] S. Wasmus, A. Kuver, Methanol oxidation and direct methanol fuel cells: a selective review. *Journal of Electroanalytical Chemistry* **1999**, *461*, 14–31.

[24] Y. Liu, S. L. Luo, W. Z. Wei, X. Y. Liu, X. D. Zeng, Methanol sensor based on the combined electrocatalytic oxidative effect of chitosan-immobilized nickel(II) and the antibiotic cefixime on the oxidation of methanol in alkaline medium. *Microchim Acta* **2009**,*164,* 351–355.

[25] G. Che, B. B. Lakshmi, E. R. Fisher, R. Martin, Carbon Nanotubule

Membranes for Electrochemical Energy Storage and Production. *Nature* **1998**, *393*, 346–349.

[26] E. P. Lee, Z. Peng, W. Chen, S. Chen, H. Yang, Y. Xia, Electrocatalytic Properties of Pt Nanowires Supported on Pt and W Gauzes. *ACS Nano*, **2008**, *2*, 2167–2173.

[27] R. Manohara, J. B. Goodenough, Methanol oxidation in acid on ordered NiTi. *J. Mater. Chem.* **1992**, *2*, 875–887.

Supporting Information
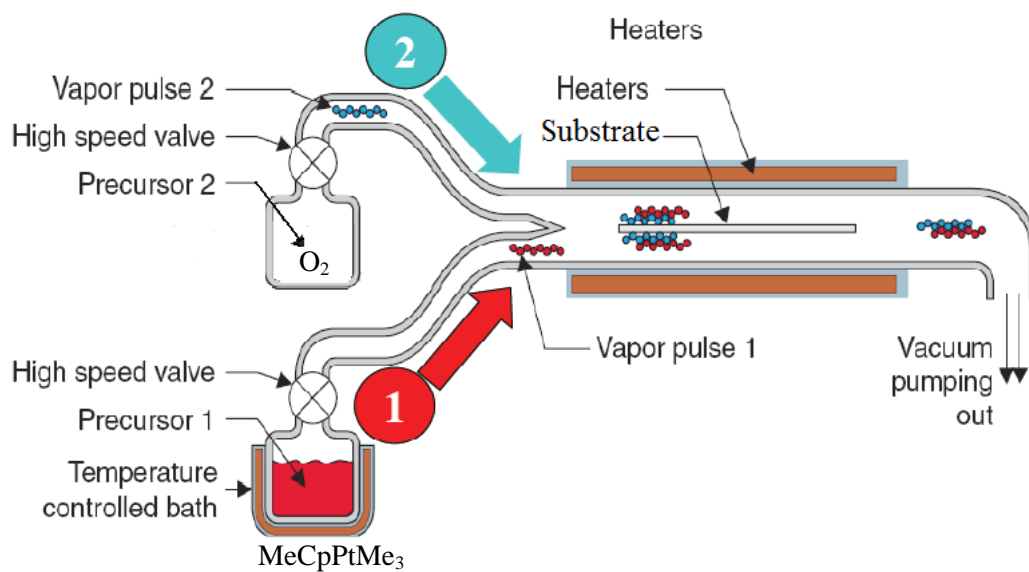
Figure SI-8.1. Schematic illustration of ALD Pt process.
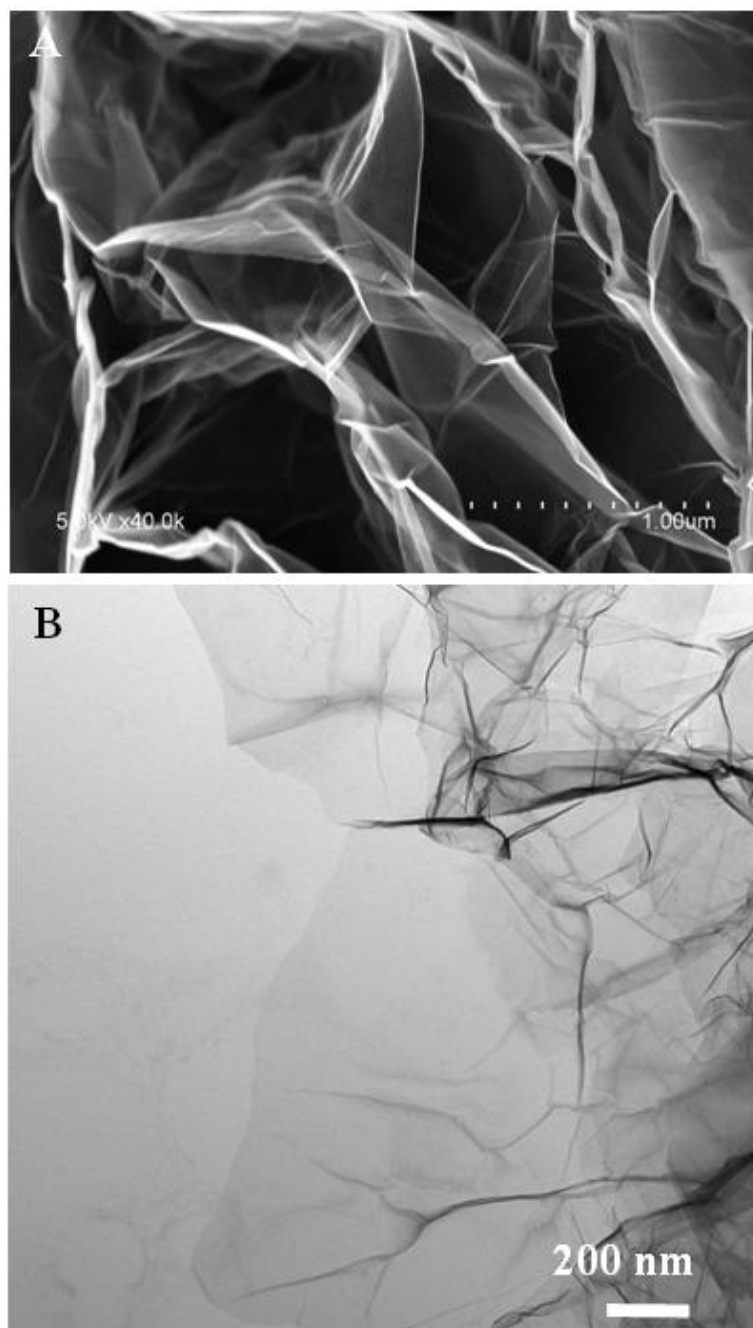
Figure SI-8.2. SEM (A) and TEM (B) images of graphene.

Chapter 9. Controlled Synthesis of Pt on Graphene Nanosheets by ALD and Their Electrochemical Properties

Shuhui Sun, Gaixia Zhang, Xiangbo Meng, Ruying Li, Xueliang Sun*

Department of Mechanical and Materials Engineering, University of Western Ontario, London, ON, N6A 5B9 Canada

Nicolas Gauquelin, Gianluigi Botton*

McMaster University, Hamilton, ON, Canada, L8S 4L8

Jigang Zhou, Ning Chen, Songlan Yang

Canadian light source, Saskatoon, SK, Canada S7N 0X4,

Tsun-Kong Sham*

Department of Chemistry, University of Western Ontario, London, Canada N6A 5B7.

Siyu Ye, Shanna Knights

Ballard Power Systems Inc., 9000 Glenlyon Parkway, Burnaby, BC, Canada V5J 5J8

* Email addresses: xsun@eng.uwo.ca (X. Sun); gbotton@mcmaster.ca (G. Botton); tsham@uwo.ca (T. Sham)

A version of this chapter will be submitted for publishing.

In chapter 8, the authors demonstrated that on graphene nanosheet support, numerous sub-nanometer Pt clusters and individual Pt atoms have been fabricated by

ALD technique. This Pt/graphene nanocomposite displayed several times higher activity and durability for methanol oxidation, as well as much higher CO tolerance and slower CO adsorption rate than those of commercial Pt/C catalyst. The sub-nanometer Pt clusters and individual Pt atoms as well as the strong interaction between Pt and graphene substrate were believed to contribute to the excellent performance of Pt/graphene. As we know, ALD is a very powerful technique which can precisely control the deposition in an atomic level. Through modulating the experimental parameters, such as the deposition cycles, temperatures, substrates, etc., one can control the size, morphology of the deposited metals, for example, from discrete tiny nanoparticles to a continuous thin film, through the surface chemistry.

In this chapter, based on previous work, the authors select to study the effect of the cycle numbers on the morphology and size of deposited Pt on graphene nanosheets, and to compare their electrochemical performance as well. It is found that the morphology, size, density and loading of Pt on graphene can be precisely controlled by simply adjusting ALD cycles from 50 to 100 and 150. HAADF-STEM investigations revealed that, in addition to the relative bigger nanoparticles, there are many sub-nanometer Pt clusters and Pt atoms on graphene surface for all three samples with different ALD cycles. The electrochemical properties of ALD Pt/graphene with different ALD cycles were systematically investigated and compared. ALD50Pt/graphene showed the best performance, with 3.8, and 2.7 times better activity than those of ALD150Pt/ graphene and ALD100Pt/ graphene, respectively.

9.1 Introduction

Due to the rising energy demands, depletion of fossil fuel reserves, and environmental pollution problems, there is great interest in developing different kinds of high-efficient and low-cost renewable energy technologies, for example fuel cells, as a replacement for combustion-based energy sources [1,2]. Among the multitude of fuel cell technologies available, direct methanol fuel cell (DMFC) has drawn much attention because of its eco-friendly system, higher efficiency, high powder density and short start-up transient-response time [3]. DMFC has thus been identified as a promising candidate to compete with the conventional batteries for powering portable electronic devices [4]. Methanol, as a liquid at room temperature, makes storage and transport much easier. The theoretical potential for the standard methanol fuel cell is 1.25 V, which is close to that for hydrogen fuel cell. Furthermore the theoretical energy density of methanol fuel cell can reach 6.1 kWh/kg [5], which is 10 times higher than that of lithium-ion battery [6] that is a critical factor in the transportation sector.

Despite considerable advances in recent years, the widespread application of DMFC is hindered by some technical and economical barriers. One of the most challenges is the poor electrocatalytic activity toward methanol oxidation reaction (MOR) and serious CO poising of Pt catalyst at the anode [7]. For standard DMFC, Pt-based nanoparticles (2-5 nm) supported on carbon black are most commonly employed as the anode catalyst because of their excellent performance in MOR. Although Pt is an efficient, it can be the most expensive component. Thus scientists have been trying to reducing the diameters of Pt nanoparticles to as small as 1 nm in order to increase the active surface area of the catalyst, and therefore increase the catalytic activity of Pt in fuel cells. Downsizing Pt nanoparticles to clusters or even single atoms could significantly increase their catalytic activity and is therefore highly desirable to maximize the efficiency [8]. However, the synthesis of practical and stable clusters and single atoms of catalysts remains a significant challenge because clusters and single atoms are too mobile and easy to sinter under realistic reaction conditions [9-

11]. Atomic layer deposition (ALD) is a promising technique for small-size catalyst fabrication [12].

In the ALD process, a substrate is alternately exposed to different reactive precursor vapours, which react in a self-limiting manner to deposit materials in an atomic layer-by-layer fashion. Previous studies have revealed that ALD allows one to control the morphology of the deposited metal, from discrete tiny nanoparticles to a continuous thin film, through the surface chemistry [13-16]. ALD relies on a series of gas-precursor and solid-substrate interactions, and the nucleation and growth of metallic particles on a substrate are dependent on the precursor adsorption onto the substrate. Therefore, the selection of a support for the Pt-based catalyst is of critical importance to both the catalytic activity and durability of catalyst.

In a conventional system, carbon black is commonly used as Pt nanoparticle catalyst support [17, 18]. This system is intrinsically limited in terms of life span, and the catalytic surface area of the electrode may decrease with time due to the corrosion of carbon black support. Recently, due to their unique electric and micro-structural characteristics, nanostructured carbon materials with graphene structures such as carbon nanotubes (CNTs) and carbon nanofibers (CNFs) have been studied extensively as alternative supports of electrocatalysts, showing much enhanced fuel cell performance [19-22]. Graphene, a unique structure of two-dimensional (2D) sheet composed of sp^2-bonded carbon atoms with one-atomic thickness, has inspired a flurry of interests for both fundamental science and applied research due to its extraordinary properties [23,24]. One hopes to employ such 2-D sheets as conductive supports to both anchor electrocatalysts and modulate the electrochemical reactions in a controlled fashion [25-30]. The combination of the high surface area (theoretical value of 2630 m^2/g), high conductivity, unique graphitized basal plane structure and potential low manufacturing cost makes graphene a promising candidate for catalyst support in fuel cells [31]. It is expected that graphene may offer a new carbon-metal nanocomposite as the catalyst material for next generation catalysts [26].

In this work, we employ the novel ALD technique to fabricate sub-nanometer clusters and single atoms of Pt on the surfaces of graphene nanosheet support. The morphology, size, density and loading of Pt on graphene can be precise controlled by simply adjusting the number of ALD cycles. Morphological and electrochemical characterizations were carried out to determine how the structure changes with increasing Pt deposition, and how it affects the MOR activity and CO adsorption.

9.2 Experimental

9.2.1 Preparation of graphene.

Graphene nanosheet (GRN) support was prepared using the procedure described previously [32-34] which involves graphite oxidation, thermal exfoliation, and chemical reduction. In detail, natural graphite powder (1 g, 99.99%, Sigma-Aldrich) was first stirred in concentrated sulphuric acid (H_2SO_4, 23 mL) with a following addition of sodium nitrate ($NaNO_3$, 0.5 g) at room temperature. The stirring lasted for 16 h, and then the mixture was cooled down to 0 °C. Potassium permanganate (K_2MnO_4, 3 g) was then added into the solution. After 2 h, the solution formed green slurry at around 35 °C, which was then stirred for another 3 h. Then, H_2O (46 mL) was slowly added into the solution at around 98 °C. The suspension was kept at this temperature for 30 min before it was further diluted with another addition of water and hydrogen peroxide (H_2O_2, 140 mL). The suspension was subsequently filtered and washed until reaching a neutral pH, and dried in a vacuum oven at 60 °C to obtain graphite oxide (GO). To obtain graphene, the as-synthesized GO was heated at around 1050 °C in Ar atmosphere for 30 s in a tube furnace. The GNS shows a rippled and crumpled structure with several layers stacking of the monatomic graphene sheets. The surface area of GNS was 455.6 m^2 g^{-1} as measured by the Brunauer−Emmett−Teller (BET) method [34].

9.2.2 ALD synthesis of Pt on graphene

For Pt ALD, the precursor was Trimethyl(methylcyclopentadienyl)platinum(IV) (MeCpPtMe$_3$, Aldrich, purity 98 %), which is widely used for Pt ALD [13-16]. Since the Pt ALD temperature window is relatively narrow, it was important to ensure that the graphene support was at the right temperature during deposition. To increase the heat transfer from the stage to the graphene powder, hot wall conditions were replicated by placing graphene powder inside a machined stainless steel container with a perforated Al lid. The container for graphene was then placed inside the reactor directly on the heated stage of ALD (Savannah 100, Cambridge Nanotechnology Inc., USA). The deposition temperature was 250 ^{o}C, while the container for the Pt precursor was kept at 65 ^{o}C to provide a steady state flux of MeCpPtMe$_3$ to the reactor (~800 mTorr at 65 ^{o}C) [16]. Gas lines were held at 100-150 ^{o}C to avoid precursor condensation. High purity of O$_2$ (99.999 %) was used as the counter reactant, and high-purity N$_2$ (99.9995 %) was used as both a purging gas and carrier gas. In each ALD cycle, 1 s of MeCpPtMe$_3$ pulse and 5 s of O$_2$ pulse were separated by 20 s of N$_2$ purge. The Pt loading on graphene was accurately controlled by the number of ALD cycles, and was further confirmed by inductively coupled plasma-optical emission spectroscopy (ICP-OES).

9.2.3 Physical Characterization.

The morphologies and microstructures of the as-prepared samples were examined by scanning electron microscopy (SEM, Hitachi S-4800) operated at 5kV. Subangstrom-resolution aberration-corrected scanning transmission electron microscopy (STEM, FEI Titan 80-300 Cubed TEM) was used to characterize the dispersion and configuration of Pt clusters and single atoms on graphene. The instrument is fitted with a Super-Twin lens in order to achieve sub-angstrom resolution both for phase contrast imaging and STEM. The probe diameter is less than 0.1 nm. The sample was tilted towards the detector in order to increase the counts. Individual heavy atoms in practical catalysts can be discerned with atomic resolution in high angle annular dark field (HAADF) images [10].

9.2.4 X-ray Absorption Spectroscopy

The Pt L$_3$-edge adsorption spectra Extended X-Ray Absorption Fine Structure (EXAFS) measurements were performed in transmission mode at the Hard X-ray Micro-Analysis (HXMA) beamline of the Canadian Light Source (CLS) operated at 2.9 GeV. A Si (111) monochromator crystal was used in conjunction with rhodium mirrors was used to reduce the harmonic component of the monochrome beam. For solid-state measurements the powder was cast onto Kapton tape.

9.2.5 Electrode Preparation

The working electrodes were prepared with a procedure similar to the one reported previously [35]. Typically, the catalyst dispersions were prepared by mixing 5 mg of catalyst in 5 mL aqueous solution containing 1 mL of isopropyl alcohol and 30 mL of 5 wt% Nafion solution followed by 12 min ultrasonication. Glassy carbon (GC) disk electrodes (5 mm diameter, 0.196 cm^2, Pine Research Instrument) served as the substrate and were polished to a mirror finish. An aliquot of catalyst suspension was pipetted onto the GC disk substrate to obtain the same Pt loadings for all catalysts. The catalyst films were dried under flowing N$_2$ at room temperature.

9.2.6 Electrochemical Measurements.

Electrochemical properties of the catalysts were test on an Autolab potentiostat/galvanostat (Model, PGSTAT-30, Eco-chemie, Brinkman Instruments) with rotation control (MSR, Pine Instruments) using a three-electrode system that consists of a GC rotating disk electrode (RDE), a Pt wire counter electrode, and a Ag/AgCl (3M NaCl) reference electrode separated from the working electrode compartment by a closed electrolyte bridge. For convenience, all potentials in this study are referenced to the reversible hydrogen electrode (RHE). The working electrode was first cycled between 0 and 1.2 V at a scan rate of 50 mVs^{-1} for 50 times in an Ar-purged H$_2$SO$_4$ solution (0.5 M) at room temperature until a clean electrode surface was obtained. Cyclic voltammetry (CV) measurements were conducted by

cycling the potential between 0 and 1.2 V, with sweep rate of 50 mVs^{-1}. For methanol oxidation reaction (MOR), the CVs were measured in an air-free aqueous solution containing 1 M MeOH and 0.5 M H$_2$SO$_4$ at room temperature in an Ar atmosphere. For CO stripping voltammetry, 30%CO/N$_2$ gas was purged into the solution at a position close to the working electrode for 1 s to 20 min, with the electrode polarized at 0.05 V versus RHE in a fume hood. The excess CO was purged with Ar for 30 min under potential control followed by CO stripping at a scan rate of 50 mVs^{-1}.

9.3 Results and Discussion

Structure characterization reveals that ALD is an efficient method to deposit highly dispersed Pt particles on the surface of graphene nanosheet. Figure 9A-C show the SEM images of Pt on graphene with 50, 100 and 150 ALD cycles, respectively. The corresponding TEM images are shown in Figure 9.1A'-C'. We can see that discrete, well dispersed Pt nanoparticles have been uniformly deposited on the surface of the graphene nanosheets. The Pt nucleation densities, as illustrated by the number of particles counted in a unit area of graphene nanosheets, increase with the cycle numbers. One hundred particles were randomly measured under TEM to obtain the particle size distributions. The Pt particles, displaying an average size of 0.5 nm, 1-2 nm and 2-4 nm, respectively, are uniformly distributed on graphene nanosheet supports with 50, 100 and 150 ALD cycles (50ALDPt/graphene, 100ALDPt/graphene and 150ALDPt/graphene). Consequently, the Pt loadings on graphene also increase from 1.52, to 2.67 and 10.5 wt%, which were confirmed by ICP-OES. From the HRTEM images shown in Figure 9.2A-C and their insets, we can see that each Pt nanoparticle or cluster is single crystalline and arranged in the cubic close-packed structure. Especially, as shown in Figure 9.2A and its inset, Pt clusters that consist of only less than ten atoms are assembled into closely packed crystal structure. This indicates the crystalline nature of Pt in the early stage of ALD growth.

To further investigate the details of ALD Pt on graphene, subangstrom-resolution, aberration-corrected scanning transmission electron microscopy (STEM) was used to
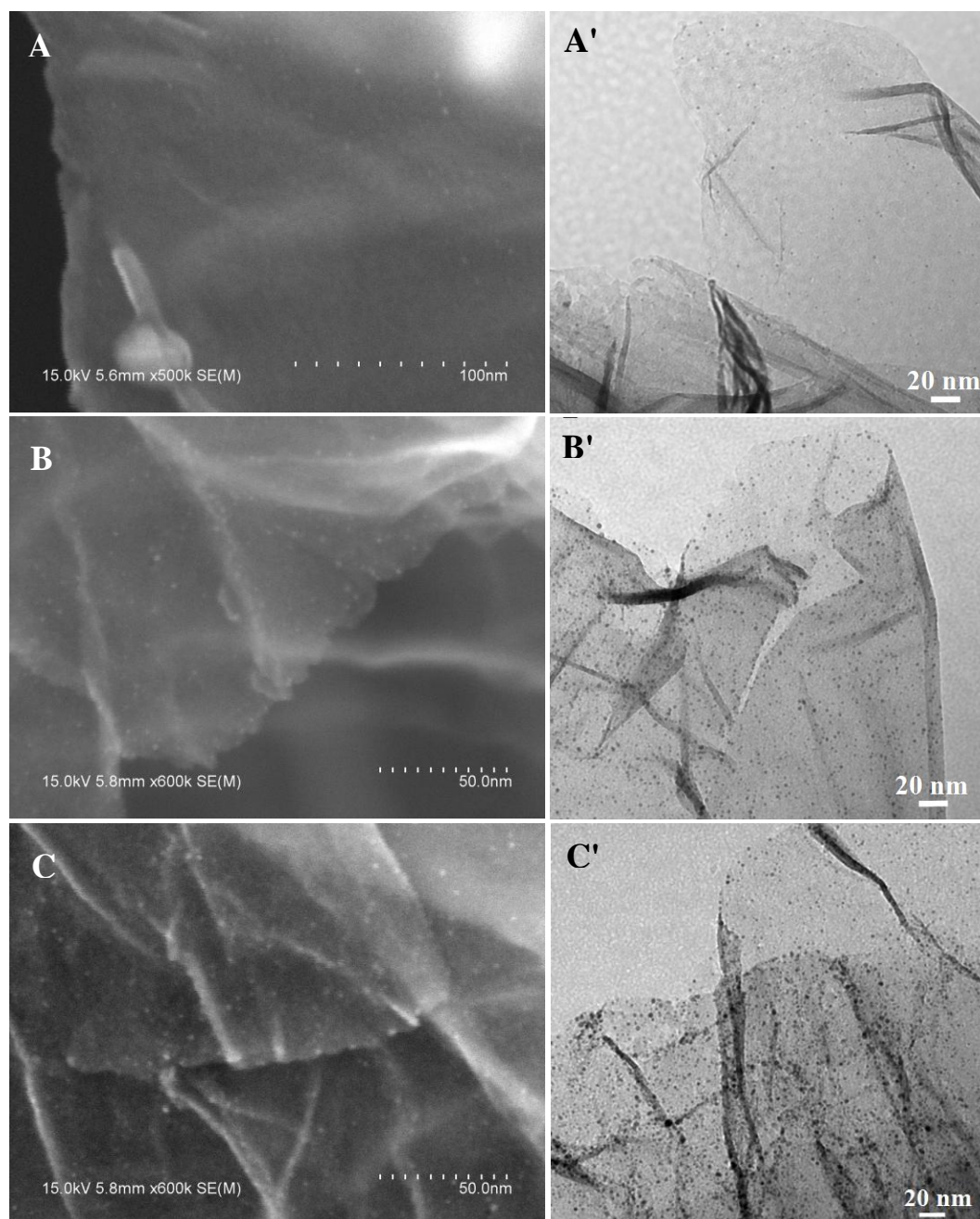
Figure 9.1. SEM (A, B, C) and TEM (A', B', C') images of Pt/GNS with 50, 100, and 150 ALD cycles, respectively.
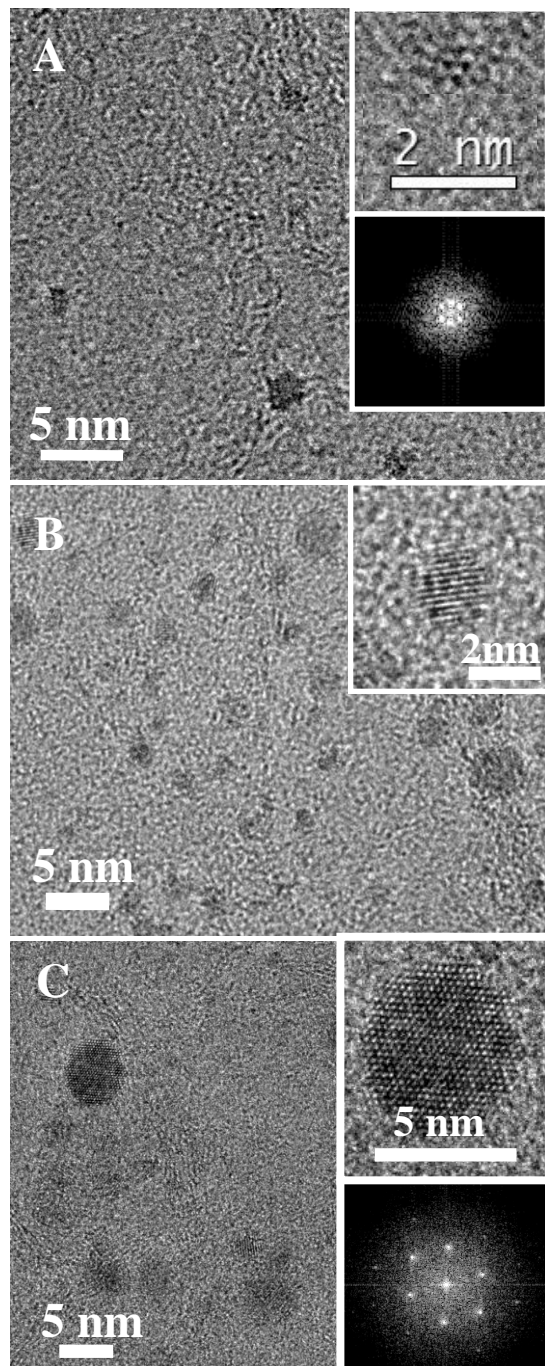
Figure 9.2. HRTEM (A, B, C) images of Pt/GNS with 50, 100, and 150 ALD cycles, respectively.

characterize the Pt clusters on graphene. Atomic resolution high-angle annular dark-field (HAADF) images were proved previously to be of efficient way to study individual heavy atoms in catalysts [8, 36-40]. For Pt/graphene sample after undergoing 50 ALD cycles, Figure 9.3A and A' clearly show many small Pt clusters and single atoms (white spots) uniformly distributed on the surface of graphene nanosheet. Occasionally, Pt nanoparticles with size of 1-2 nm can also be found. After 100 cycles (Figure 9.3B and B'), some clusters appear to be larger, forming nanoparticles with two groups of average size with 1nm and 2 nm, whereas the others remaining to be similar to the clusters and atoms seen on the 50 cycle sample in Figure 9.3A and A'. It is believed that the clusters existing from the 50 cycle sample have grown, creating the larger particles, whereas at the same time, newer clusters and atoms have formed showing smaller size in the HAADF images. Finally, after 150 cycles (Figure 9.3C and C'), in addition to the newly formed clusters and atoms, some existing clusters and particles from the 50 and 100 cycle samples appear to be even larger with three groups of sizes with 1, 2 and 4 nm. SEM, TEM and HAADF STEM images of the three Pt/graphene samples with different ALD cycles reveal that, at different magnifications, the deposited Pt form disperse particles, growing from small clusters and single atoms by agglomeration in a cubic closely pack manner, instead of layer-by-layer growth. Many single atoms can be seen on each of the sample in addition to these particles. Previous studies have observed that the thin-film growth rate increases after a Pt seed is formed [41]. This growth rate increase has been attributed to a higher affinity for MeCpPtMe$_3$ adsorption and decomposition on Pt sites [42,43]. The reactivity difference between C and Pt sites leads to a preference to grow particles rather than nucleate new particles, as observed in Figure 9.1-3.

These findings raise key issues for fabricating Pt nanoparticles or sub-nanometer clusters on graphene and other support materials by using ALD. One of the key issues is the chemical state of ALD Pt at the early stage. The conversion of Pt from the +4 oxidation state in MeCpPtMe$_3$ precursor to the zero-valent metallic chemical state on
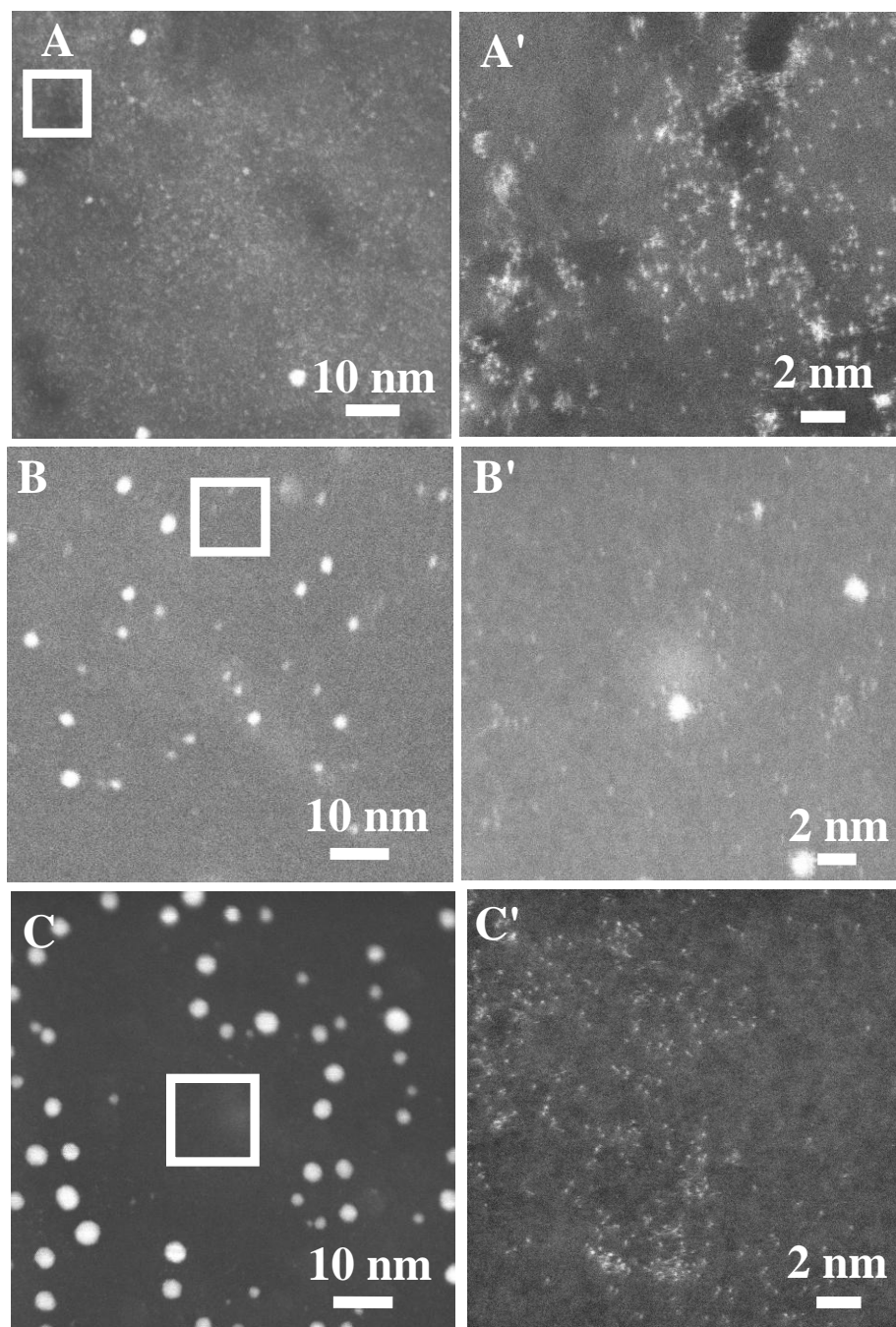
Figure 9.3. HAADF-STEM (A, B, C) images of Pt/GNS with 50, 100, and 150 ALD cycles, respectively. (A', B', C') show the corresponding magnified images.
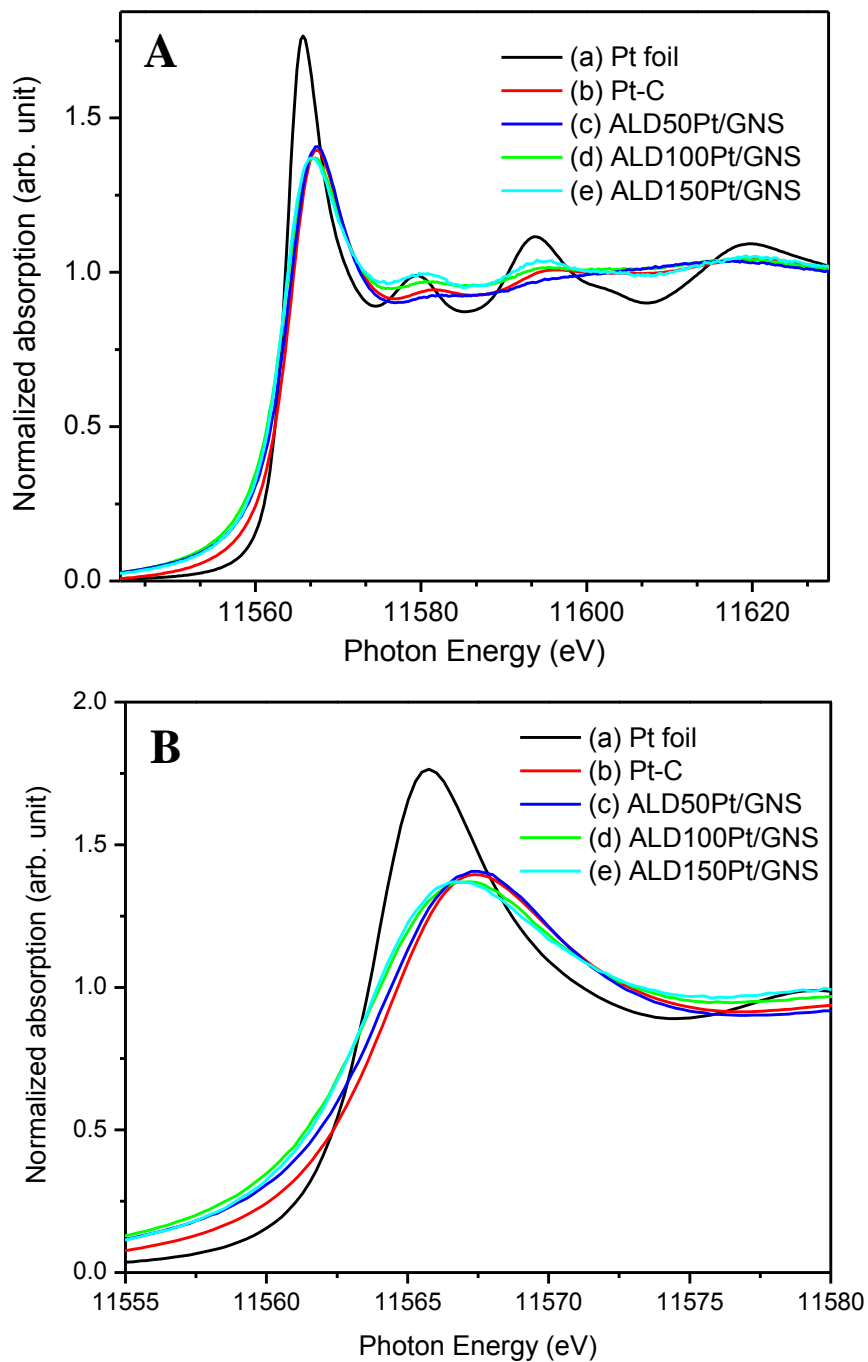
Figure 9.4. (A) The normalized XANES spectra and (B) the enlarged spectra at Pt L_3 edge of samples (a) Pt foil (black line); (b) Pt/C (red line); (c) ALD50Pt/GNS (blue line); (d) ALD100Pt/GNS (green line); (e) ALD150Pt/GNS Pt/GNS (cyan line).

graphene offers promising opportunities to employ ALD-grown metal nanostructures for catalysis and fuel cell applications.

X-ray Absorption Near Edge Structure (XANES) in the set of X-ray absorption spectra are shown in Figure 9.4, including three ALD cases, a platinum metal foil, and Pt/C commercial catalyst. We can see that the oscillation beyond whiteline increase as ALD cycles increase and then Pt-C and then Pt, which means crystalline order increase. The white-line intensity decreases as the number of ALD cycles increases, with an order ALD50>ALD100>ALD150>Pt-C, which follows same order of MOR and CO tolerance. The increase of whiteline in ALD samples than Pt-C indicate stronger interaction between GNS and Pt [30]. This is supported by the negative E_0 shift in ALD samples relative to that in Pt-C (Figure 9.4B). An increase in the white-line intensity indicates a decrease in the number of electrons in the d orbital. So, lower ALD cycle has relatively higher whiteline (more available unoccupied 5d states) means more single Pt atoms. A reduction of the d-electron density of states would be consistent with the oxidation of Pt. All factors, oxidation state (Pt_0 in Pt metal or oxidized Pt in Pt-O or Pt-OH), charge transfer (electron exchange between GNS and Pt), surface oxidation (expose Pt nanoparticles to moisture will make a OH- covered surface), have impact on the whiteline position and intensity. It should be noticed that even the surface covered O species affect the whiteline, but this cannot play a key role in real electrochemical operations because the applied potential will refresh the surface for instance the covered oxygen containing species will be deprived).

The Fourier transforms of the EXAFS region are plotted in Figure 9.5 for various cases. ALD150Pt/GNS has coordination number (CN=9.2) being most closed to Pt foil (CN=12). ALD50Pt/GNS doesn't show Pt-Pt bonding in Pt crystals which agrees with the observation in XANES (absence of oscillation beyond the whiteline). ALD50Pt/GNS and ALD100Pt/GNS have much lower CN (CN=0, 1.5, respectively) than Pt foil and ALD150 Pt/GNS, which can offer more available catalytic positions for electrochemical reaction.
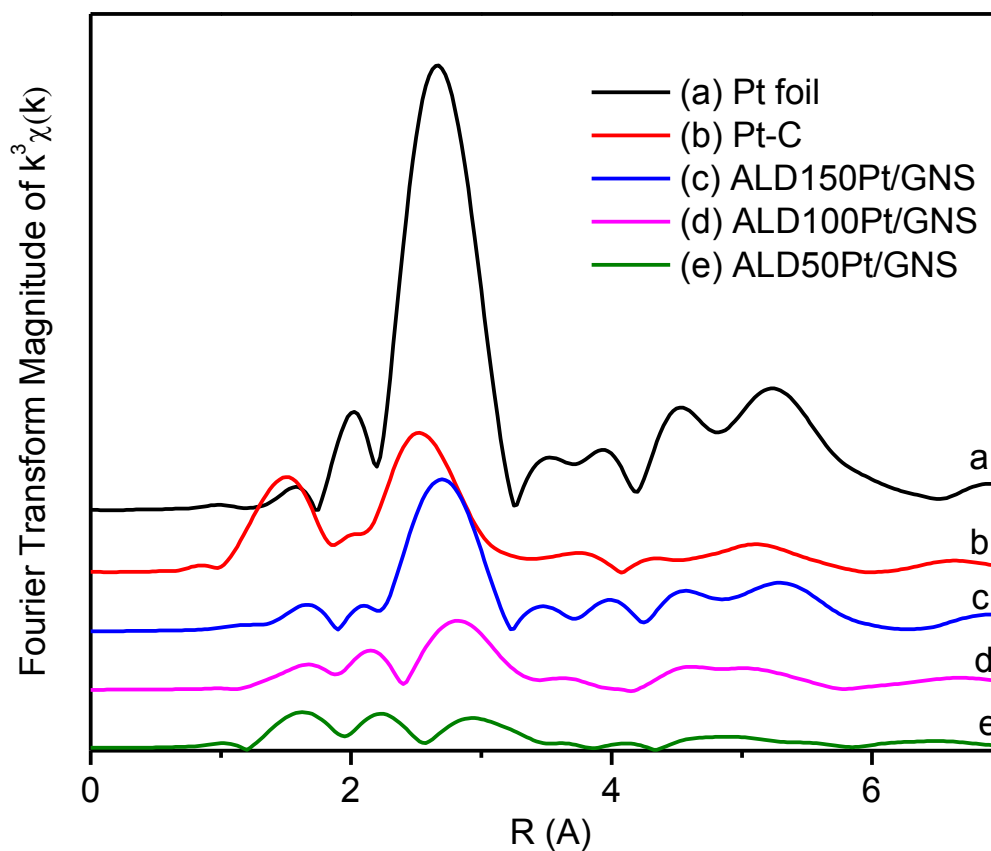
Figure 9.5. The K^3-weighted Fourier transform spectra from EXAFS of samples (a) Pt foil (black line); (b) Pt/C (red line); (c) ALD50Pt/GNS (blue line); (d) ALD100Pt/GNS (pink line); (e) ALD150Pt/GNS Pt/GNS (olive line).

The presence of these extremely small Pt clusters and single atoms suggests a strong interaction between graphene and platinum atoms, which may induce some modulation in the electronic structure of the Pt clusters. This has been proved by our XAS analysis discussed in previous part. Okamoto et al. have reported based on density-functional theory (DFT) calculations that introducing a carbon vacancy into a

graphene sheet enhances the interaction between graphene and Pt_{13} clusters [41]. They concluded that the stability of the metal clusters on graphene with carbon vacancies was higher than that on a defect free graphene [42]. The graphene used in this study must exhibit many carbon vacancies and defects, due to the preparation method by chemical reduction of exfoliated graphite oxide sheets. It is thus indicated that carbon atoms with dangling bond or oxygen-containing functional groups exist at the defect sites of the graphene nanosheets used in this work. The Pt precursor used in this study reacts with these defects. The present study indicates that graphene is expected as a new carbon support material modifying catalytic properties of Pt as fuel cell catalysts.
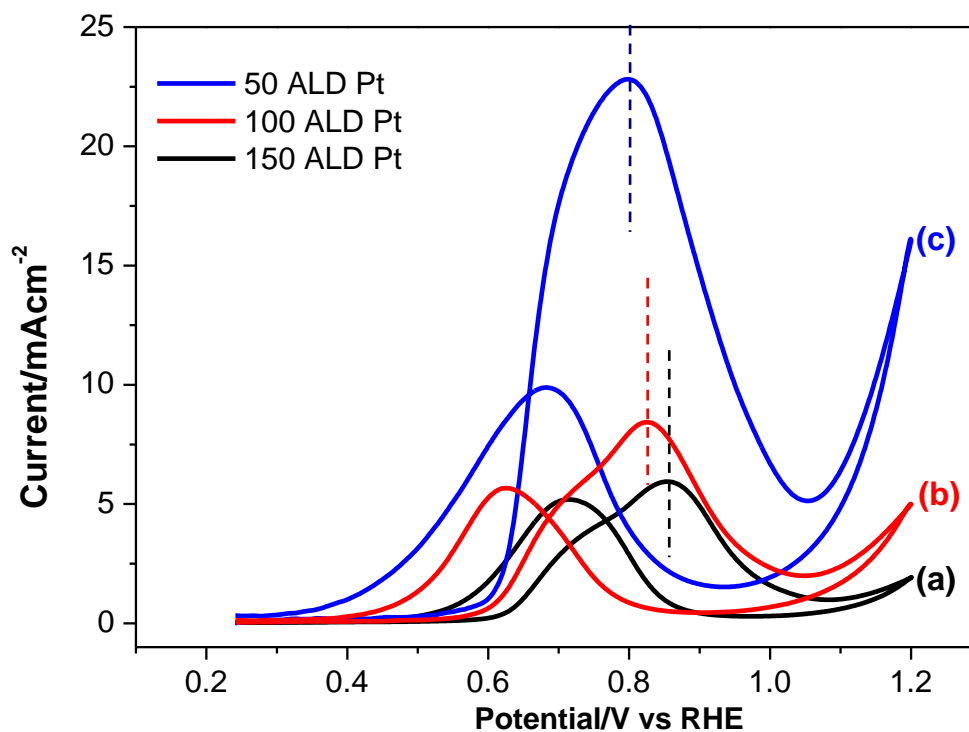
Figure 9.6. CVs of MeOH oxidation on (a) ALD150Pt/GNS, (b) ALD100Pt/GNS, (c) ALD50Pt/GNS.

We choose the methanol oxidation reaction (MOR) to investigate the catalytic performance of ALDPt/graphene, as such reaction is the heart in DMFC. Cyclic voltammetry (CV) was used to systematically study the catalytic activity and the onset potential of methanol oxidation of the catalysts. A better catalyst is characterized by a higher induced current density at a given applied potential or a lower onset potential. Figure 9.6 shows the CVs for methanol oxidation on Pt/graphene samples with different ALD cycles. Two typical oxidation peaks appear on the CV curves of the three ALD Pt/graphene samples, arising from the oxidations of methanol and their intermediates [45]. The onset potentials of methanol oxidation are 0.59, 0.60 and 0.62 V (vs. RHE) for ALD Pt/graphene with 50, 100 and 150 cycles, respectively. Obviously, the peak potentials for methanol oxidation in the forward scan of Pt/graphene composites are increasing with the number of ALD cycles with the order of 50 cycles (0.79V) < 100 cycles (0.82V) < 150 cycles (0.85V) (vs. RHE). The negative shifts of the onset and peak potentials indicate that the 50ALDPt/graphene catalyst is able to significantly reduce the overpotential for methanol oxidation. These improvements may be attributed to the presence of oxygen containing functional groups on graphene nanosheet as the graphene used in this study involves preparation-induced defects [46]. The methanol oxidation peak current density for 50ALDPt/graphene is 22.9 mAcm^{-2}, which is 4 and 2.7 times those of 100ALDPt/graphene (8.48 mA cm^{-2}) and 150ALDPt/graphene (5.73 mA cm^{-2}) catalysts. Interestingly, 50ALDPt/graphene shows 9.5 times higher current density than that of ETEK Pt/C catalyst (2.41 mA cm^{-2}). The enhancement may be attributed to the intrinsic nature of subnanometer Pt clusters and single atoms [11] as well as the carbons substrate materials [46]. Goodenough et al. [47] suggested the anodic peak in the reverse scan to be linked to the removal of the incomplete oxidized carbonaceous species, such as CO, HCOO$^-$ and HCO$^-$, accumulated on the catalyst surface during the forward anodic scan. CO, a critical intermediate of methanol oxidation, can poison Pt catalyst, causing a lower fuel cell potential and energy conversion efficiency. Consequently, the ratio of the forward anodic peak current density (I_f) to the backward anodic peak current density (I_b), I_f/I_b, can be used to indicate the CO

tolerance of the catalyst [47]. A low I_f/I_b value usually indicates poor oxidation of methanol to CO_2 during the forward anodic scan and excessive accumulation of residual carbon species on the catalyst surface. On the other hand, a higher I_f/I_b ratio is indicative of improved CO tolerance. In our study, Pt/graphene with 50 ALD cycles shows much higher I_f/I_b value (2.23) than that for 100 (I_f/I_b =1.51) and 150 (I_f/I_b =1.13) Pt cycles. This suggests that methanol molecules can be more efficiently oxidized on 50ALDPt/graphene during the forward scan, generating much less poisoning species as compared to 100ALDPt/graphene and 150ALDPt/graphene catalysts, indicating a much better CO tolerance. To further investigate the observed enhancement of CO tolerance, CO electrostripping experiments was carried out.

More input on the origin of the high MOR activity and enhanced CO tolerance for Pt/graphene catalysts was obtained from CO stripping voltammetry was conducted as a function of CO poisoning times in 0.5 M H_2SO_4 at room temperature. Figure 9.7 A-C show the CO stripping voltammograms for Pt/graphene with 50, 100 and 150 Pt cycles, respectively. An obvious CO oxidation peak of 150ALDPt/graphene is observed after passing 30% CO/Ar gas for 30 s (Figure 9.7C). However, the CO oxidation peaks for 100ALD Pt/graphene and 50ALD Pt/graphene are not observed until an exposure time of 1 minute and 2 min, respectively, was reached (Figure 9.7A, B). Moreover, the peak potentials for CO oxidation keep nearly constant at 0.77 V (vs. RHE) for 150ALDPt/graphene with difference CO exposure time, while for ALDPt/graphene samples with 50 and 100 Pt cycles, the peak potentials for CO oxidation are initially at 0.72 V(vs. RHE) and steadily move to 0.73, 0.74 and 0.77 V with time. Further, we found that the equilibrium CO coverage of all ALDPt/graphene samples was reached after passing 30% CO/Ar for more than 5 min, while, for the Pt/C the equilibrium CO coverage was reached after passing 30% CO/Ar gas for 20 s. This indicates that the state of CO adsorption on Pt/graphene is different from traditional Pt catalysts supported on carbon black [46]. The CO adsorption rate on Pt/graphene was obviously much slower compared to that on
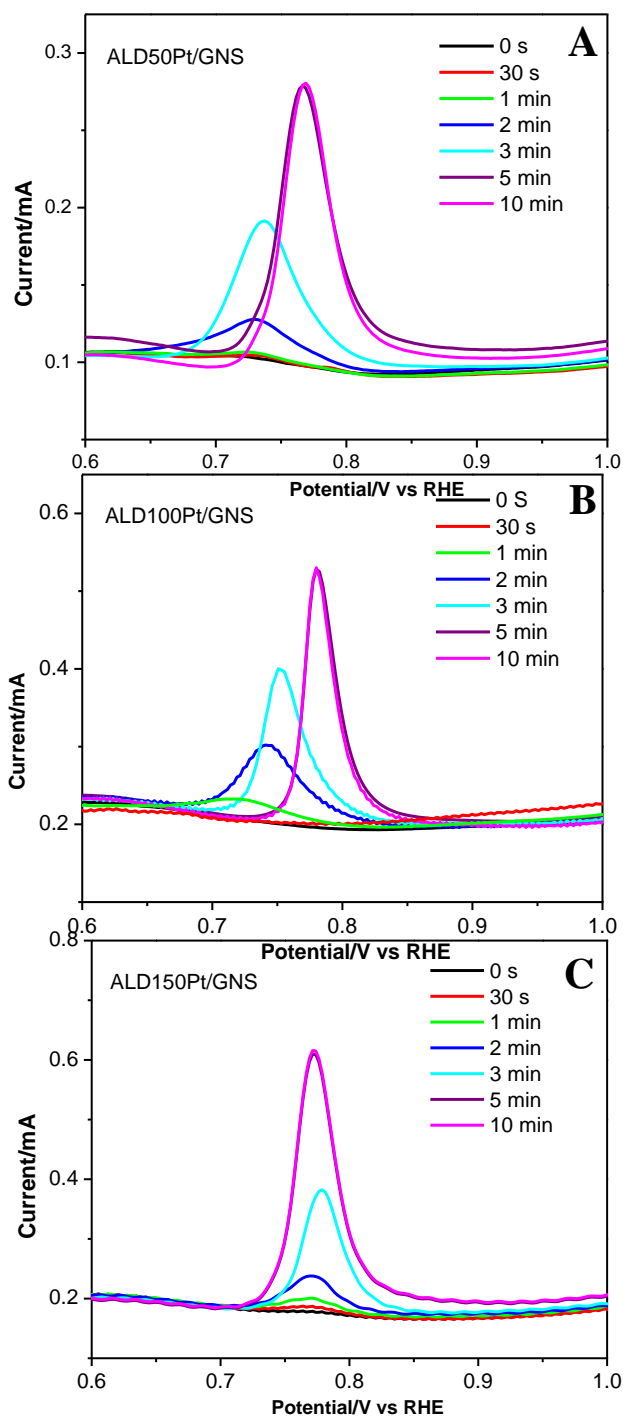
Figure 9.7. The CO stripping voltammogram as a function of CO poison time of (A) ALD50Pt/GNS; (B) ALD100Pt/GNS; (C) ALD150Pt/GNS, respectively.

Pt/carbon black, which might be due to the superior CO tolerance of ultrafine Pt catalysts [46]. Although the detailed mechanism of the CO poisoning tolerance is not clear for the Pt/graphene catalyst, it is found that the CO tolerance and adsorption rates of Pt electrocatalysts are significantly different depending on the size of Pt and the carbon support.

9.4 Conclusions

In conclusion, ALD was used to uniformly deposit platinum (Pt) on graphene nanosheets. The morphology, size, density and loading of Pt on graphene can be precisely controlled by simply adjusting ALD cycle numbers from 50 to 100 and 150. SEM and TEM investigations revealed that the size of Pt nanoparticles increase with the number of ALD cycles. HAADF-STEM images indicate that in addition to the relative bigger nanoparticles, there are many sub-nanometer Pt clusters and Pt atoms on the graphene surface for all three samples despite the different number of ALD cycles. For methanol oxidation, 50ALDPt/graphene showed 4 and 2.7 times better activity than that of 150ALDPt/ graphene and 100ALDPt/ graphene, respectively. In addition, 50ALDPt/graphene exhibits the highest CO tolerance among the three samples.

Acknowledgments

References

[1]   A. Chen, P. Holt-Hindle, Platinum-based nanostructured materials: synthesis, properties, and applications. *Chem. Rev.,* **2010**, *110*, 3767–3804.

[2]   C. Koenigsmann, S. S. Wong, One-dimensional noble metal electrocatalysts: a promising structural paradigm for direct methanol fuel cells. *Energy Environ. Sci.* **2011**, *4*, 1161–1176.

[3]   R. Borup, J. Meyers, B. Pivovar, Y. S. Kim, R. Mukundan, N. Garland, D. Myers, M. Wilson, F. Garzon, D. Wood, P. Zelenay, K. More, K. Stroh, T. Zawodzinski, J. Boncella, J. E. McGrath, M. Inaba, K. Miyatake, M. Hori, K. Ota, Z. Ogumi, S. Miyata, A. Nishikata, Z. Siroma, Y. Uchimoto, K. Yasuda, K. Kimijima, N. Iwashita, Scientific aspects of polymer electrolyte fuel cell durability and degradation. *Chem. Rev.,* **2007**, *107*, 3904–3951.

[4]   Y. Chen, J. Wang, X. Meng, Y. Zhong, R. Li, X. Sun, S. Ye, S. Knights. Atomic layer deposition assisted Pt-SnO$_2$ hybrid catalysts on nitrogen-doped CNTs with enhanced electrocatalytic activities for low temperature fuel cells. *International Journal of Hydrogen Energy* **2011**, *36*, 11085–11092.

[5]   K. M. McGrath, G. K. S. Prakash, G. A. Olah, Direct methanol fuel cells. *J. Ind. Eng. Chem.* **2004**, *10*, 1063–80.

[6]   H. Q. Li, Y. G. Wang, H. T. Na, H. M. Liu, H. S. Zhou, Rechargeable Ni–Li battery integrated aqueous/nonaqueous system. *J. Am. Chem. Soc.* **2009,** *131*, 15098–15099.

[7]   M. P. Hogarth, T. R. Ralph, Catalysis for low temperature fuel cells PART III: challenges for the direct methanol fuel cell. *Platinum Metals Rev.* **2002**, *46*, 146–164.

[8]   B. Qiao, A. Wang, X. Yang, L. F. Allard, Z. Jiang, Y. Cui, J. Liu, J. Li, T.

Zhang, Single-atom catalysis of CO oxidation using Pt_1/FeO_x. *Nature Chem.* **2011**, *3*, 634–641.

[9]   A. Uzun, V. Ortalan, N. D. Browning, B. C. Gates, A Site-Isolated Mononuclear Iridium Complex Catalyst Supported on MgO: Characterization by Spectroscopy and Aberration-Corrected Scanning Transmission Electron Microscopy. *J. Catal.* **2010**, *269*, 318–328.

[10]   A. Uzun, V. Ortalan, Y. Hao, N. D. Browning, B. C. Gates, Nanoclusters of Gold on a High-Area Support: Almost Uniform Nanoclusters Imaged by Scanning Transmission Electron Microscopy. *ACS Nano* **2009**, *3*, 3691–3695.

[11]   C. Susut, G. B. Chapman, G. Samjeske, M. Osawa, Y. Tong, An unexpected enhancement in methanol electro-oxidation on an ensemble of Pt(111) nanofacets: a case of nanoscale single crystal ensemble electrocatalysis. *Phys. Chem. Chem. Phys.*, **2008**, *10*, 3712–3721.

[12]   S. T. Christensen, J. W. Elam, F. A. Rabuffetti, Q. Ma, S. J. Weigand, B. Lee, S. Seifert, P. C. Stair, K. R. Poeppelmeier, M. C. Hersam, M. J. Bedzyk, Controlled Growth of Platinum Nanoparticles on Strontium Titanate Nanocubes by Atomic Layer Deposition. *Small* **2009**, *5*, 750–757.

[13]   J. W. Elam, A. Zinovev, C. Y. Han, H. H. Wang, U. Welp, J. N. Hryn, M. J. Pellin, *Thin Solid Films* Atomic Layer Deposition of Palladium Films on Al_2O_3 Surfaces. **2006**, *515*, 1664–1673.

[14]   J. S. King, A. Wittstock, J. Biener, S. O. Kucheyev, Y. M. Wang, T. F. Baumann, S. K. Giri, A. V. Hamza, M. Baeumer, S. F. Bent, Ultralow loading Pt nanocatalysts prepared by atomic layer deposition on carbon aerogels. *Nano Lett.* **2008**, *8*, 2405–2409.

[15]   I. J. Hsu, D. A. Hansgen, B. E. McCandless, B. G. Willis, J. G. Chen. Atomic Layer Deposition of Pt on Tungsten Monocarbide (WC) for the Oxygen

Reduction Reaction *J. Phys. Chem. C*, **2011**, *115*, 3709–3715.

[16] C. Liu, C. C. Wang, C. C. Kei, Y. C. Hsueh, T. P. Perng, Atomic Layer Deposition of Platinum Nanoparticles on Carbon Nanotubes for Application in Proton-Exchange Membrane Fuel Cells *Small* **2009**, *5*, 1535–1538.

[17] F. Su, J. Zeng, X. Bao, Y. Yu, J. Y. Lee, X. S. Zhao, Preparation and Characterization of Highly Ordered Graphitic Mesoporous Carbon as a Pt Catalyst Support for Direct Methanol Fuel Cells, *Chem. Mater.* **2005**, *17*, 3960–3967.

[18] X. W. Yu, S. Y. Ye, Recent Advances in Activity and Durability Enhancement of Pt/C Catalytic Cathode in PEMFC. *J. Power Sources* **2007**, *172*, 145–154.

[19] T. Matsumoto, T. Komatsu, K. Arai, T. Yamazaki, M. Kijima, H. Shimizu, Y. Takasawa, J. Nakamura, Reduction of Pt usage in fuel cell electrocatalysts with carbon nanotube electrodes, *Chem. Commun.* **2004**, *7*, 840– 841.

[20] E. J. Yoo, T. Okada, T. Kizuka, J. Nakamura, Effect of carbon substrate materials as a Pt-Ru catalyst support on the performance of direct methanol fuel cells. *J. Power Sources* **2008**, *180*, 221–226.

[21] J. Prabhuram, T. S. Zhao, Z. K. Tang, R. Chen, Z. X. Liang, Multiwalled Carbon Nanotube Supported PtRu for the Anode of Direct Methanol Fuel Cells. *J. Phys. Chem. B.* **2006**, *110*, 5245–5252.

[22] S. Liao, K.-A. Holmes, H. Tsaprailis, V. I. Briss, High Performance PtRuIr Catalysts Supported on Carbon Nanotubes for the Anodic Oxidation of Methanol. *J. Am. Chem. Soc.* **2006**, *128*, 3504–3505.

[23] A. K. Geim, K. S. Novoselov, The rise of graphene. The Rise of Graphene. *Nat. Mater.* 2007, *6*, 183–191.

[24] B. Seger, P. V. Kamat, Electrocatalytically Active Graphene-Platinum

Nanocomposites. Role of 2-D Carbon Support in PEM Fuel Cells. **2009**, *113,* 7990–7995.

[25] R. Kou, Y. Shao, D. Wang, M. H. Engelhard, J. H. Kwak, J. Wang,V. V. Viswanathan, C. Wang, Y. Lin, Y. Wang, I. A. Aksay, J. Liu. Enhanced activity and stability of Pt catalysts on functionalized graphene sheets for electrocatalytic oxygen reduction. *Electrochemistry Communications* **2009**, *11*, 954–957.

[26] E. Yoo, T. Okata, T.Akita, M Kohyama, J. Nakamura, I. Honma. Enhanced Electrocatalytic Activity of Pt Subnanoclusters on Graphene Nanosheet Surface. *Nano. Lett.* **2009**, *9*, 2255–2259.

[27] P. Ferreira-Aparicio, M.A. Folgado, L. Daza, High surface area graphite as alternative support for proton exchange membrane fuel cell catalysts. *Journal of Power Sources* **2009**, *192*, 57–62.

[28] Y. Shao, S. Zhang, C. Wang, Z. Nie, J. Liu, Y. Wang, Y. Lin, Highly durable graphene nanoplatelets supported Pt nanocatalysts for oxygen reduction. *Journal of Power Sources* **2010**, *195*, 4600–4605.

[29] Y. Li, L. Tang, J. Li, Preparation and electrochemical performance for methanol oxidation of Pt/graphene nanocomposites. *Electrochemistry Communications* **2009**, *11*, 846–849.

[30] J. G. Zhou, J. Wang, C. L. Sun, J. M. Maley, R. Sammynaiken, T. K. Sham and W. F. Pong. Nano-scale chemical imaging of a single sheet of reduced graphene oxide.*J. Mater. Chem.*, 2011, **21**, 14622–14630.

[31] L. Tang, Y. Wang, Y. Li, H. Feng, J. Lu, J. Li. Preparation, Structure, and Electrochemical Properties of Reduced Graphene Sheet Films. *Adv. Funct. Mater.* **2009**, *19*, 1–8.

[32] W. S. Hummers, R. E. Offeman, Preparation of graphite oxide. *J. Am. Chem. Soc.* **1958**, *80*, 1339–1339.

[33] S. Stankovich, D. A. Dikin, R. D. Piner, K. A. Kohlhaas, A. Kleinhammes, Y. Jia, Y. Wu, S. T. Nguyen, R. S. Ruoff, Synthesis of graphene-based nanosheet via chemical reduction of exfoliated graphite oxide. *Carbon* **2007**, *45*, 1558–1565.

[34] D. Geng, S. Yang, Y. Zhang, J. Yang, J. Liu, R. Li, T. K. Sham, X. Sun, S. Ye, S. Knights. Nitrogen Doping Effects on the Structure of Graphene. *Applied Surface Science*, **2011**, *257*, 9193–9198.

[35] S. H. Sun, G. X. Zhang, D. S. Geng, Y. G. Chen, R. Y. Li, M. Cai, X. Sun, A New Highly Durable Pt Nanocatalyst for PEM Fuel Cells: the Multiarmed Star-like Nanowire Single Crystal. *Angew. Chem. Int. Ed.* **2011**, *50*, 422–426.

[36] A. A. Herzing, C. J. Kiely, A. F. Carley, P. Landon, G. J. Hutchings, Identification of active gold nanoclusters on iron oxide supports for CO oxidation. *Science* **2008**, *321*, 1331–1335.

[37] P. D. Nellist, S. J. Pennycook, Direct imaging of the atomic configuration of ultradispersed catalysts. *Science* **1996**, *274*, 413–415.

[38] S. Wang, A. Y. Borisevich, S. N. Rashkeev, M. V. Glazoff, K. Sohlberg, S. J. Pennycook, S. T. Pantelides. Dopants adsorbed as single atoms prevent degradation of catalysts. *Nature Mater.* **2004**, *3*, 143–146.

[39] P. D. Nellist, M. F. Chisholm, N. Dellby, O. L. Krivanek, M. F. Murfitt, Z. S. Szilagyi, A. R. Lupini, A. Borisevich, W. H. Sides Jr., S. J. Pennycook. Direct sub-angstrom imaging of a crystal lattice. *Science* **2004**, *305*, 1741–1741.

[40] V. Ortalan, A. Uzun, B. C. Gates, N. D. Browning, Direct imaging of single metal atoms and clusters in the pores of dealuminated HY zeolite. *Nature*

Nanotech. **2010**, *5*, 506–510.

[41] H. C. M. Knoops, A. J. M. Mackus, M. E. Donders, M. C. M. van de Sanden, P. H. L. Notten, W. M. M. Kessels, Remote plasma ALD of platinum and platinum oxide film. *Electrochem. Solid State Lett.* **2009**, *12*, G34–G36.

[42] T. Ngo, L. Brandt, R. S. Williams, H. D. Kaesz, Scanning tunneling microscopy study of platinum deposited on graphite by metalorganic chemical vapor deposition. *Surf. Sci.* **1993**, *291*, 411–417.

[43] S. Takakusagi, K. Fukui, R. Tero, F. Nariyuki, Y. Iwasawa, Self-limiting growth of Pt nano-particles from $MeCpPtMe_3$ adsorbed on $TiO_2(110)$ studied by STM. *Phys. Rev. Lett.* **2003**, *91*, 066102 (4 pages).

[44] Y. Okamoto, Density-functional calculations of icosahedral M_{13} (M = Pt and Au) clusters on graphene sheets and flakes. *Chem. Phys. Lett.* **2006**, *420*, 382–386.

[45] G. Che, B. B. Lakshmi, E. R. Fisher, R. Martin, Carbon Nanotubule Membranes for Electrochemical Energy Storage and Production. *Nature* **1998**, *393*, 346–349.

[46] A. Kolmakov, D. O. Klenov, Y. Lilach, S. Stemmer, M. Moskovits, Enhanced Gas Sensing by Individual SnO_2 Nanowires and Nanobelts Functionalized with Pd Catalyst Particles. *Nano Lett.* **2005**, *5*, 667–673.

[47] R. Manohara, J. B. Goodenough, Methanol oxidation in acid on ordered NiTi. *J. Mater. Chem.* **1992**, *2*, 875–887.

Chapter 10. Conclusions and Future Perspectives

10.1 Conclusions

Fuel cells, in particular the proton exchange membrane fuel cells (PEMFCs), are one of the cleanest energy devices and also offer the highest energy conversion efficiencies, and therefore are regarded as one of the best choices for future energy sources, except for their high price and insufficient durability. The platinum-based catalyst and their associated catalyst layers amount to over 50% of the device cost, which keeps rising with the price of platinum. Therefore, catalyst design is one of the keys to overcome the above challenges. The advance of nanomaterials and nanotechnology has shed light on almost every field of science and technology, particularly in the development of renewable energies, including PEMFCs.

The main objective of this thesis project has been to develop various advanced nanomaterials for designing highly active and durable catalysts for PEMFCs, thereby enhancing PEM fuel cell performance.

A series of experiments were conducted in this study to synthesize a variety of novel nanostructured Pt-based electrocatalysts and alternative catalyst supports using various methods, including wet-chemical, chemical vapour deposition (CVD) and atomic layer deposition (ALD). The growth characteristics of these nanostructures and their underlying mechanisms were also investigated and explored. In addition, the electrochemical properties of the as-synthesized catalysts were systematically studied and compared, and the underlying mechanisms for their enhanced fuel cell performance were also explored. In summary, this study mainly worked on three areas: nanomaterials synthesis, growth characteristics and underlying mechanisms, and fuel cell performance.

First, star-like single-crystal platinum nanostructures were produced, each with several nanowire arms with diameters of ~4 nm on carbon black (star-like PtNW/C), in an environmentally friendly process, which does not require high temperatures,

organic solvents, surfactants or complicated electrochemical deposition apparatus, by reducing a Pt precursor (H_2PtCl_6) with formic acid (HCOOH) in aqueous solution at room temperature. The star-like PtNW/C showed greatly improved activity (3 times) and durability (2 times) compared to a state-of-the-art commercial Pt nanoparticles/C catalyst. More interestingly, the durability can be further improved up to 5 times by eliminating the carbon support, forming supporteless Pt nanowire catalyst. The key for this strategy relies on the combination of a multi-armed network structure and the one-dimensional shape of the arms. This helps the activity and durability. In addition, the few surface defects and the preferential exposure of certain crystal facets further improve the activity. The higher activity and durability means that the amount of Pt needed on an electrode can be reduced, which could significantly lower the cost of PEMFCs.

Further, Pt nanowires were grown on Sn@CNT nanocable supports which directly root on carbon paper fuel cell backing, forming a novel 3D opening fuel-cell electrode (PtNW/Sn@CNT). The Sn@CNT nanocable supports were first synthesized by CVD method using Sn powder and C_2H_2 as precursors at 850 $^{\circ}$C. Then Sn@CNT/carbon paper was immersed into the reaction solution of H_2PtCl_6 and HCOOH, acting as the growth substrates for Pt nanowires. The PtNW-Sn@CNT composite shows, for ORR, 1.2 times higher mass activity and 2.4-fold better specific activity, and for MOR, 1.35 times higher mass activity and 2.8-fold better specific activity, than those of the commercial catalyst made of Pt nanoparticles on carbon black. This novel structure combines the advantages of both a PtNW catalyst and a Sn@CNT 3D nanocable support, and has the potential to possess higher Pt utilization, higher activity, and higher durability for fuel cell applications.

Moreover, ultrathin (2.5 nm in diameter) Pt nanowires have been synthesized when using N-doped carbon nanotubes (N-CNTs) as the substrate. Time dependent growth process of ultrathin Pt nanowires on N-CNT support was systematically investigated by collecting products at different reaction time and investigated by TEM. Combining TEM, XPS and EELS mapping techniques, it is believed that the widely distributed

defects, associated with N incorporation, on the N-CNTs surface, confine the Pt atoms and play a key role in the formation of the tiny nuclei that further leads to the anisotropic growth of ultrathin nanowires. This synthetic strategy and the underlying mechanism provide new insight into the synthesis of other metal nanowires with dimensions similar to those reported here. These ultrathin nanowires and their composites with N-CNTs hold potential for catalysis, fuel cells and electrochemical sensors.

0D mesoporous Nb-doped TiO_2 hollow spheres were synthesized by the sol-gel method using polystyrene (PS) sphere templates. Pt nanoparticles (NPs) were then deposited onto the mesoporous Nb-TiO_2 hollow spheres via a wet-chemical route in aqueous solution at 80 ^{o}C. The Pt loadings on Nb-TiO_2 supports could be easily modulated from 10 to 40%, with similar Pt particle size, by simply adjusting the precursor and support ratios. Electrochemical studies show that Pt/Nb-TiO_2 composites exhibit up to 1.6 times higher activity and 2.1 times higher stability than commercial E-TEK Pt/C catalyst. 0D mesoporous Nb-doped TiO_2 hollow spheres is a promising alternative catalyst support for PEMFC applications.

1D $TiSi_x$-NCNT structures were prepared by sputtering $TiSi_x$ only on one side of N-doped carbon nanotubes. Pt nanoparticles (NPs) were then deposited onto another side of NCNT, forming Pt/$TiSi_x$-NCNT Janus nanostructure. TEM investigations revealed that the Pt NPs formed dendritic and chain-like morphology between the gaps of $TiSi_x$ on NCNT surface, which is very important for enhancing the durability of Pt catalyst. Electrochemical measurements demonstrated that the Pt/$TiSi_x$-NCNT Janus nanocatalyst exhibited ~3 times better stability and enhanced CO tolerance compared to commercial Pt/C catalyst. The higher corrosion resistance of NCNT and $TiSi_x$ than carbon black contribute greatly to the higher stability of the catalyst.

2D graphene nanosheets have been synthesized via a modified Hummers method which involves graphite oxidation, thermal exfoliation, and chemical reduction. By adopting a unique technique, atomic layer deposition (ALD), ultrafine platinum

nanoparticles were uniformly deposited on graphene nanosheets. In addition to nano-sized particles observed under bright-field TEM, HAADF-STEM investigations indicate the existence of numerous sub-nanometer Pt clusters and individual Pt atoms on the surface of graphene nanosheets. Graphene nanosheets give rise to an extraordinary modification to the properties of Pt nanocatalysts. ALD Pt/graphene showed 3.5 times higher activity and 2 times higher durability for methanol oxidation than commercial Pt/C catalyst. This novel catalyst also exhibited much higher CO tolerance and slower CO adsorption rate than commercial Pt/C catalyst. The enhancement may be attributed to the intrinsic nature of subnanometer Pt clusters and individual atoms, as well as the strong interaction between Pt and graphene substrate.

Combining 2D graphene nanosheets support and ALD technique, the morphology, size, density and loading of Pt on graphene can be precisely controlled by simply adjusting ALD cycle numbers from 50 to 100 and 150. HAADF-STEM investigations revealed that in addition to the relative bigger nanoparticles, there are many sub-nanometer Pt clusters and Pt atoms on graphene surface for all these three samples with different number of ALD cycles. The electrochemical properties of ALD Pt/graphene with different ALD cycles were systematically investigated and compared. ALD50Pt/graphene showed up to 10 times better activity than that of commercial Pt/C catalyst.

The major contributions of the study can be summarized as follows:

The author successfully developed several methods to synthesize various novel Pt nanostructures, including nanowires, ultrathin nanowires, nanostars, nanoparticles, sub-nanometer clusters and individual atoms, on various nanostructured supports, for using as highly efficient catalysts to address the high cost and insufficient durability challenges in PEMFCs. Most importantly, these novel Pt nanostructured catalysts exhibited up to 10 times better activity and 5 times better durability compared to the stat-of-the-art commercial Pt/C catalyst made of Pt nanoparticles. This is very

important to lower the cost and increase the lifetime of PEM fuel cells, and therefore to promote their commercialization.

10.2 Future perspectives

Despite the advances demonstrated in this thesis, a large number of unsolved challenges still remain. Future work could focus on the following aspects:

- This thesis exploited a new type of Pt nanowires-based catalyst which showed much improved activity and durability for ORR than the state-of-art Pt/C catalyst made from spherical Pt nanoparticles. Recently, increasing amount of research effort has been put on Pt alloy electrocatalysts. One thrust is on Pt_3M (M = Ni, Co, Fe, Ti, V) alloys which show substantial improvement in specific activity for ORR compared with platinum. Specifically, a recent study indicates that Pt_3Ni (1 1 1) surface is about 90 times more active than the state-of-art Pt/C catalysts for ORR. It is expected that Pt_3M with nanowire shape could be even more active.

- As established with Pt single crystals, the catalytic activity and selectivity for ORR is sensitive to the crystallographic planes. Through adjusting experimental parameters, it is possible to modulate the shapes of the seeds and reaction kinetics, and therefore to control the orientation of Pt nanowires to expose only a specific set of most active facets.

- Due their unique hollow structure and 1D anisotropic property, nanotubes possess higher surface area than nanowires with similar size. Pt and Pt alloy nanotubes have shown enhanced activities for ORR. However, the diameter of the nanotubes synthesized so far are relative bigger (>50 nm). The activities and durability could be further increased if thinner (<20 nm) Pt and Pt alloy nanotubes could be synthesized and used in fuel cells.

- This thesis revealed that ALD Pt on graphene exhibited extraordinary electrochemical properties. In the future, ALD PtM alloy on various new supports is a very promising direction to further increase the activity and durability of the catalyst. Moreover, using N-doped graphene as catalyst support and combining ALD for catalyst deposition could further enhance the performance.

Besides resolving the above-mentioned aspects, the focus for the coming decades are not just the synthesis of these different shapes, but also the fully understanding of how the sizes, shapes, surface structures and capping agents affect the electrocatalytic properties of Pt nanostructures. Once these relationships have been established, it will become possible to design the next-generation highly active and durable electrocatalysts for high performance and low cost PEM fuel cells, as well as a broad range of other technologically important applications.

APPENDICES

APPENDIX I: PERMISSION FROM JOHN WILEY AND SONS FOR PUBLISHED ARTICLE

Published article: A Highly Active and Durable Platinum Nanocatalyst for Proton Exchange Membrane Fuel Cells: Multiarmed Starlike Nanowire Single Crystal. *Angewandte Chemie International Edition*, 2011, 50, 422-426.

Link to the paper on Wiley website:

http://onlinelibrary.wiley.com/doi/10.1002/anie.201004631/abstract

Copyright Clearance Center — RightsLink®

Title:	A Highly Durable Platinum Nanocatalyst for Proton Exchange Membrane Fuel Cells: Multiarmed Starlike Nanowire Single Crystal
Author:	Shuhui Sun,Gaixia Zhang,Dongsheng Geng,Yougui Chen,Ruying Li,Mei Cai,Xueliang Sun
Publication:	Angewandte Chemie International Edition
Publisher:	John Wiley and Sons
Date:	Jan 10, 2011

Copyright © 2011 WILEY-VCH Verlag GmbH & Co. KGaA, Weinheim

Logged in as: Shuhui SUN

Order Completed

Thank you very much for your order.

This is a License Agreement between Shuhui SUN ("You") and John Wiley and Sons ("John Wiley and Sons"). The license consists of your order details, the terms and conditions provided by John Wiley and Sons, and the payment terms and conditions.

Get the printable license.

License Number	2772010147558
License date	Oct 18, 2011
Licensed content publisher	John Wiley and Sons
Licensed content publication	Angewandte Chemie International Edition
Licensed content title	A Highly Durable Platinum Nanocatalyst for Proton Exchange Membrane Fuel Cells: Multiarmed Starlike Nanowire Single Crystal
Licensed content author	Shuhui Sun,Gaixia Zhang,Dongsheng Geng,Yougui Chen,Ruying Li,Mei Cai,Xueliang Sun
Licensed content date	Jan 10, 2011
Start page	422
End page	426
Type of use	Dissertation/Thesis
Requestor type	Author of this Wiley article
Format	Print and electronic
Portion	Full article

APPENDIX II: PERMISSION FROM JOHN WILEY AND SONS FOR PUBLISHED ARTICLE

Published article: Direct Growth of Single-Crystal Pt Nanowires on Sn@CNT Nanocable: 3D Electrodes for Highly Active Electrocatalysts. *Chemistry – A European Journal*, 2010, 16, 825-839.

Link to the paper on Wiley website:
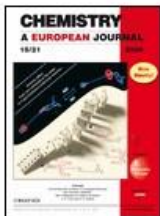
http://onlinelibrary.wiley.com/doi/10.1002/chem.200902320/full

Copyright Clearance Center — RightsLink®

Home | Account Info | Help

Title:	Direct Growth of Single-Crystal Pt Nanowires on Sn@CNT Nanocable: 3D Electrodes for Highly Active Electrocatalysts
Author:	Shuhui Sun,Gaixia Zhang,Dongsheng Geng,Yougui Chen,Mohammad Norouzi Banis,Ruying Li,Mei Cai,Xueliang Sun
Publication:	Chemistry - A European Journal
Publisher:	John Wiley and Sons
Date:	Jan 18, 2010

Copyright © 2010 WILEY-VCH Verlag GmbH & Co. KGaA, Weinheim

Logged in as:
Shuhui SUN

LOGOUT

Order Completed

Thank you very much for your order.

This is a License Agreement between Shuhui SUN ("You") and John Wiley and Sons ("John Wiley and Sons"). The license consists of your order details, the terms and conditions provided by John Wiley and Sons, and the payment terms and conditions.

Get the printable license.

License Number	2772011305902
License date	Oct 18, 2011
Licensed content publisher	John Wiley and Sons
Licensed content publication	Chemistry - A European Journal
Licensed content title	Direct Growth of Single-Crystal Pt Nanowires on Sn@CNT Nanocable: 3D Electrodes for Highly Active Electrocatalysts
Licensed content author	Shuhui Sun,Gaixia Zhang,Dongsheng Geng,Yougui Chen,Mohammad Norouzi Banis,Ruying Li,Mei Cai,Xueliang Sun
Licensed content date	Jan 18, 2010
Start page	829
End page	835
Type of use	Dissertation/Thesis
Requestor type	Author of this Wiley article
Format	Print and electronic
Portion	Full article

APPENDIX III: PERMISSION FROM ROYAL SOCIETY OF CHEMISTRY (RSC) FOR PUBLISHED ARTICLE

Published article: Ultrathin single crystal Pt nanowires grown on N-doped carbon nanotubes. *Chemical Communications*, 2009, 7048-7050.

Link to the paper on RCS website:

http://pubs.rsc.org/en/Content/ArticleLanding/2009/CC/b916080a

Dear Dr Sun

The Royal Society of Chemistry (RSC) hereby grants permission for the use of your paper(s) specified below in the printed and microfilm version of your thesis. You may also make available the PDF version of your paper(s) that the RSC sent to the corresponding author(s) of your paper(s) upon publication of the paper(s) in the following ways: in your thesis via any website that your university may have for the deposition of theses, via your university's Intranet or via your own personal website. We are however unable to grant you permission to include the PDF version of the paper(s) on its own in your institutional repository. The Royal Society of Chemistry is a signatory to the STM Guidelines on Permissions (available on request).

Please note that if the material specified below or any part of it appears with credit or acknowledgement to a third party then you must also secure permission from that third party before reproducing that material.

Please ensure that the thesis states the following:

Reproduced by permission of The Royal Society of Chemistry

and include a link to the paper on the Royal Society of Chemistry's website.

Please ensure that your co-authors are aware that you are including the paper in your thesis.

Regards

Gill Cockhead
Publishing Contracts & Copyright Executive

Gill Cockhead (Mrs), Publishing Contracts & Copyright Executive
Royal Society of Chemistry, Thomas Graham House
Science Park, Milton Road, Cambridge CB4 0WF, UK
Tel +44 (0) 1223 432134, Fax +44 (0) 1223 423623
http://www.rsc.org

To: Gill Cockhead
This Email was sent from the following RSC.ORG page:
/AboutUs/Copyright/RightsRetainedbyJournalsauthors.asp

Dear Editor,

I am writing to request the permission for a paper entitled ""Ultrathin single crystal Pt nanowires grown on N-doped carbon nanotubes" (S. Sun et al, Chem. Commun., 2009, 7048-7050). As the first author, I am planning to include this paper in my PhD thesis. Herein I am requesting the permission for my aforementioned use.

Thank you very much and look forward to hearing from you soon.

Best regards,

Shuhui SUN

Department of Mechanical and Materials Engineering
The University of Western Ontario
London, Canada, N6A 5B9

CURRICULUM VITAE

Name: **Shuhui Sun**

Education: Department of Mechanical & Materials Engineering
The University of Western Ontario, London, ON, Canada
2008-2011, Ph.D.

Institute of Solid State Physics
Chinese Academy of Sciences, China
1999-2004, M.S./Ph.D.

Department of Chemistry
Hebei University, China
1995-1999, B.S.

Work Experience: Teaching & Research Assistant (2008-2011)
The University of Western Ontario, ON, Canada

Exchange visitor (2008)
General Motors R&D center, Warren, Michigan, US

Post-doctoral Fellow (2004-2007)
INRS-Énergie Matériaux Télécommunications
Quebec, Canada

Research Assistant (1999-2004)
Institute of Solid State Physics
Chinese Academy of Sciences, China

Relevant Publications:

(A) Book Chapters

1. **S. H. Sun** and X. L. Sun "Shape-Controlled Synthesis of Platinum-Based Nanostructures as Electrocatalyst for PEM Fuel Cell Applications" in the book of "Controlled Size and Shape of Nanostructured Materials and Their Applications". Pan Stanford Publishing, Ru-Shi Liu Ed (2011), in press

(B) Patents

1. G. X. Zhang, **S. H. Sun**, M. Cai, R. Y. Li, X. L. Sun. "A General Strategy for the Mass Production of Various Morphology-Controlled Metal and Bimetallic-Composite Nanostructures". US patent (application number: 12/704786), pended, 2010.

2. G. X. Zhang, **S. H. Sun**, M. Cai, R. Y. Li, X. L. Sun. "Porous Dendritic Platinum Nanotubes as Electrocatalysts for Fuel Cell Applications". US patent, pending, 2011.

*(C) Peer-reviewed Journal Papers Based on This Thesis (**First Author**)*

1. **S. H. Sun**, G. X. Zhang, D. S. Geng, Y. G. Chen, R. Y. Li, M. Cai, X. Sun, "A New Highly Durable Pt Nanocatalyst for PEM Fuel Cells: the Multiarmed Star-like Nanowire Single Crystal". *Angew. Chem. Int. Ed.* 50 (2011) 422. **[VIP, highlighted on the Cover; also**

highlighted in Nature Nanotechnology, and Materials Today]

2. **S. H. Sun**, X. L. Sun. "A Nanostar is born: Energy". *Materials Today*. 14 (2011) 132.

3. **S. H. Sun**, G. X. Zhang, D. S. Geng, Y. G. Chen, R. Y. Li, M. Cai, M. N. Banis, X. L. Sun. "Direct Growth of Single Crystal Pt Nanowires on Sn@CNT Nanocable: 3D Supports for Highly Active Electrocatalysts". *Chemistry-A European Journal*. 16 (2010) 829–835. **[It was highlighted on the Inside Cover]**

4. **S. H. Sun**, G. X. Zhang, Y. Zhong, H. Liu, R. Y. Li, X. R. Zhou, X. L. Sun. "Ultrathin single crystal Pt nanowires grown on N-doped carbon nanotubes". *Chem. Commun*. 45 (2009) 7048–7050.

5. **S. H. Sun**, G. X. Zhang, X. L. Sun, M. Cai, M. Ruthkosky. "Highly Stable and Active Pt/Nb-TiO2 Carbon-free Electrocatalyst for Proton Exchange Membrane Fuel Cells". Submitted to *J. Power Sources.*

6. **S. H. Sun**, M. Banis, G. X. Zhang, M. Cai, Y. Zhang, R. Y. Li, X. L. Sun. "Pt/TiSi$_x$-NCNT Janus Nanostructures for Highly Stable and CO-Tolerant PEM Fuel Cell Electrocatalyst". To be submitted.

7. **S. H. Sun**, X. B. Meng, G. X. Zhang, D. S. Geng, R. Y. Li, X. L. Sun, N. Gauquelin, G. Botton, S. Ye, S. Knights. "Atomic layer deposition of subnanometer Pt

clusters on graphene as highly active and CO-tolerant electrocatalyst for methanol oxidation". To be submitted.

8. **S. H. Sun**, G. X. Zhang, X. B. Meng, R. Y. Li, X. L. Sun, N. Gauquelin, G. Botton, J. Zhou, N. Chen, S. Yang, T. K. Sham, S. Ye, S. Knights. "Controlled Synthesis of Pt on Graphene Nanosheets by ALD and their Electrochemical Properties". To be submitted.

9. **S. H. Sun**, G. X. Zhang, X. L. Sun "Platinum-Based 1D Nanostructures as Electrocatalyst for PEM Fuel Cell Applications". To be submitted.

*(D) Peer-reviewed Journal Papers Related with This Thesis (**Coauthor**)*

10. G. X. Zhang, **S. H. Sun**, M. N. Banis, R. Y. Li, M. Cai, X. L. Sun. "Morphology-Controlled Green Synthesis of Single Crystalline Silver Dendrites, Dendritic Flowers and Rods, and their Growth Mechanism". *Crystal Growth & Design*, 11 (2011) 2493–2499.

11. X. Meng, M. Ionescu, M. Banis, Y. Zhong, H. Liu, Y. Zhang, **S. Sun**, R. Li, X. Sun, "Heterostructural Coaxial Nanotubes of CNT@Fe_2O_3 via Atomic Layer Deposition: Effects of Surface Functionalization and Nitrogen-doping". *J. Nanopart. Res*. 13 (2011) 1207–1218.

12. X. B. Meng, Y. Zhang, **S. H. Sun**, R. Y. Li, X. L. Sun. "Highly Structure-tunable SnO_2 Nanotube Arrays by

Template-directed Atomic Layer Deposition". *J. Mater. Chem.*, 21 (2011) 12321–12330.

13. G. X. Zhang, **S. H. Sun**, R. Y. Li, X. L. Sun. "New Insight into Conventional Replacement Reaction for the Large-Scale Synthesis of Various Metal Nanostructures and their Formation Mechanism". *Chemistry-A European Journal*, 16 (2010) 10630–10634. **[VIP, it was also highlighted on the Cover].**

14. G. X. Zhang, **S. H. Sun**, Y. Zhang, R. Y. Li, X. L. Sun. "Room Temperature Large-Scale Aqueous Synthesis of Single-Crystalline Nanoscrolls: the Case of Nickel". *Chem. Mater.* 22 (2010) 4721–4727.

15. G. X. Zhang, **S. H. Sun**, M. I. Ionescu, H. Liu, Y. Zhong, R. Y. Li, X. L. Sun. "Controlled Growth/Patterning of Ni Nanohoneycombs on Various Desired Substrates". *Langmuir*, 26, (2010) 4346–4350.

16. M. Banis, **S. H. Sun**, X. B. Meng, Y. Zhang, R. Y. Li, M. Cai, X. L. Sun. "Development of Novel TiSi-NCNT Nanostructures as Catalyst Supports for PEM Fuel Cells". To be submitted.

17. H. Meng, F. Y. Xie, J. Chen, **S. H. Sun**, P. K. Shen. "Controllable Growth of Single Crystal Pt Nanowires on Carbon Particles and Its Application as Novel Electrocatalyst for Methanol Electro-oxidation". Submitted to *ACS Nano.*

(E) Previous Publications

18. **S. H. Sun**, F. Jaouen, J. P. Dodelet, "Controlled Growth of Pt Nanowires on Carbon Nanospheres and Their Enhanced Performance as Electrocatalysts in PEM Fuel Cells". *Adv. Mater.*, 20 (2008) 3900–3904. **[Also reported in Nanowerk Spotlight, http://www.nanowerk.com/spotlight/spotid=7993.php, with a title of "Nanotechnology is key to improving fuel cell performance"]**

19. **S. H. Sun**, D. Q. Yang, D. Villers, G. X. Zhang, E. Sacher, J. P. Dodelet. "Template-free, Surfactant-free Room Temperature Synthesis of Self-Assembled 3D Pt Nanoflowers from Single-Crystal Nanowires". *Adv. Mater.*, 20 (2008) 571–574.

20. G. X. Zhang, **S. H. Sun**, M. Bostetter, S. Poulin, E. Sacher, "Chemical and morphological characterizations of Ni/Co alloy nanoparticles by co-evaporation onto highly oriented pyrolytic graphite". *J. Colloid Interface Sci.*, 350 (2010) 16–21.

21. D. Q. Yang, **S. H. Sun**, H. Meng, J. P. Dodelet, E. Sacher. "Formation of a Porous Platinum Nanoparticle Froth for Electrochemical Applications, Produced without Templates, Surfactants, or Stabilizers". *Chem. Mater.*, 20 (2008) 4677–4681.

22. H. Meng, **S. H. Sun**, J. P. Dodelet. "Electro-synthesis of Pd single crystal nanothorns and their application in the

oxidation of formic acid". *Chem. Mater.*, 20, (2008) 6998–7002.

23. D. Q. Yang, **S. H. Sun**, J. P. Dodelet, E. Sacher. "A facile route for the self-organized high-density decoration of Pt nanoparticles on carbon nanotubes." *J. Phys. Chem. C.*, 112 (2008) 11717–11721.

24. G. X. Zhang, **S. H. Sun**, D. Q. Yang, E. Sacher, J. P. Dodelet. "The surface analytical characterization of carbon fibers functionalized by H_2SO_4/HNO_3 treatment". *Carbon*, 46 (2008) 196–205.

25. **S. H. Sun**, D. Q. Yang, G. X. Zhang, E. Sacher, J. P. Dodelet. "Synthesis and Characterization of Carbon Nanotube–Platinum Nanowire Heterostructures". *Chem. Mater.*, 19 (2007) 6376–6378.

26. **S. H. Sun**, G. W. Meng, G. X. Zhang, J. P. Masse, L. D. Zhang. "Controlled Growth of SnO_2 Hierarchical Nanostructures by Using a Multi-Step Thermal Vapor Deposition Process". *Chemistry ─A European Journal*, 13 (2007) 9087–9092.

27. **S. H. Sun**, G. W. Meng, G. X. Zhang, L. D. Zhang. "Controlled Growth and Optical Properties of One-Dimensional ZnO Nanostructures on SnO_2 Nanobelts". *Crystal Growth & Design*, 7 (2007) 1988–1991.

28. D. Villers, **S. H. Sun**, A. M. Serventi, J. P. Dodelet, S. Désilets. "Characterization of Pt Nanoparticles Deposited onto Carbon Nanotubes Grown on Carbon

Paper and Evaluation of This Electrode for the Reduction of Oxygen". *J. Phys. Chem. B* 110 (2006) 25916–25925.

29. **S. H. Sun**, D. Villers, A. M. Serventi, R. Li, J. P. Dodelet, S. Désilets. "Pt loading on multiwalled carbon nanotubes obtained by CVD on fuel cell backings". *Proceedings on Electrocatalysis*, Edited by R. Adzic, V. Birss, G. Brisard, A. Wieckowski. The Electrochemical Society, 2005, p113.

30. X. H. An, G. W. Meng, M. G. Zhang, Y. T. Tian, **S. H. Sun**, L. D. Zhang. "Synthesis and optical absorption property of ordered macroporous titania film doped with Ag nanoparticles". *Materials Letters* 60 (2006) 2586–2589.

31. **S. H. Sun**, G. W. Meng, M. G. Zhang, X. H. An, G. S. Wu, L. D. Zhang. "Synthesis of SnO_2 nanostructures by carbothermal reduction of SnO_2 powders". *J. Phys. D: Appl. Phys.* 37(2004) 409–412.

32. Y. T. Tian, G. W. Meng, S. K. Biswas, P. M. Ajayan, **S. H. Sun**, L. D. Zhang. "Y-branched Bi nanowires with metal-semiconductor junction behavior". *Appl. Phys. Lett*. 85 (2004) 967–969.

33. Y. T. Tian, G. W. Meng, T. Gao, **S. H. Sun**, T. Xie, X. S. Peng, C. H. Ye, L. D. Zhang. "Alumina nanowire arrays standing on a porous anodic alumina membrane." *Nanotechnology* 15 (2004) 189–191.

34. **S. H. Sun**, G. W. Meng, M. G. Zhang, Y. F. Hao, X. R. Zhang, L. D. Zhang. "Microscopy Study of the Growth Process and Structural Features of Closely Packed Silica Nanowires". *J. Phys. Chem. B*. 107 (2003) 13029–13032.

35. A. W. Zhao, G. W. Meng, L. D. Zhang, T. Gao, **S. H. Sun**, Y. T. Pang. "Electrochemical synthesis of ordered CdTe nanowire arrays". *Appl. Phys. A* 76 (2003) 537–539.

36. **S. H. Sun**, G.W. Meng, G.X. Zhang, T. Gao, B.Y. Geng, L.D. Zhang, J. Zuo. "Raman scattering study of rutile SnO_2 nanobelts synthesized by thermal evaporation of Sn powders". *Chem. Phys. Lett.* 376 (2003) 103–107.

37. **S. H. Sun**, G. W. Meng, Y.W. Wang, T. Gao, M.G. Zhang, Y.T. Tian, X.S. Peng, L. D. Zhang. "Large-scale synthesis of SnO_2 nanobelts". *Appl. Phys. A* 76 (2003) 287–289.

38. X. S. Peng, L. D. Zhang, G. W. Meng, Y. T. Tian, Y. Lin, B. Y. Geng, **S. H. Sun**. "Micro-Raman and infrared properties of SnO_2 nanobelts synthesized from Sn and SiO_2 powders". *J. Appl. Phys.* 93 (2003) 1760–1763.

39. **S. H. Sun**, G. W. Meng, T. Gao, M. G. Zhang, Y. T. Tian, X. S. Peng, Y. X. Jin, L. D. Zhang. "Micrometer-sized Si-Sn-O novel structures with SiOx nanowires on their surfaces". *Appl. Phys. A* 76 (2003) 999–1002.

40. B. Y. Geng, G. Z. Wang, Z. Jiang, T. Xie, **S. H. Sun**, G.

W. Meng, L. D. Zhang. "Synthesis and optical properties of S-doped ZnO nanowires". *Appl. Phys. Lett.* 82 (2003) 4791–4793.

41. **<u>S. H. Sun</u>**, G. W. Meng, M. G. Zhang, Y. T. Tian, T. Xie, L. D. Zhang. "Preparation and characterization of oriented silica nanowires". *Solid State Commun.* 128 (2003) 287–290.

43. T. Gao, G. W. Meng, Y. W. Wang, **<u>S. H. Sun</u>**, L. D. Zhang, "Electrochemical synthesis of copper nanowires". *J. Phys.: Condens. Matter* 14 (2002) 355–363.

44. T. Gao, G. W. Meng, J. Zhang, **<u>S. H. Sun</u>**, L. D. Zhang. "Template Synthesis of Y-Junction Metal Nanowires". *Appl. Phys. A* 74 (2002) 403–406.

45. X. S. Peng, X. F. Wang, J. Zhang, Y. W. Wang, **<u>S. H. Sun</u>**, G. W. Meng, L. D. Zhang. "Blue-light emission from amorphous SiO_x nanoropes". *Appl. Phys. A* 74 (2002) 831–833.

46. T. Gao, G. W. Meng, Y. T. Tian, **<u>S. H. Sun</u>**, X. Liu, L. D. Zhang, "Photoluminescence of ZnO nanoparticles loaded into porous anodic alumina hosts". *J. Phys.: Condens. Matter.* 14 (2002) 12651–12656.

47. Y. W. Wang, L. D. Zhang, G.W. Meng, C. H. Liang, G. Z. Wang, **<u>S. H. Sun</u>**, "Zn Nanobelts: A New Quasi One-dimensional Metal Nanostructure". *Chem. Comm.* 24 (2001) 2632–2633.

(F) Conference Presentations

1. **S. H. Sun**, N. Gauquelin, G. X. Zhang, X. B. Meng, D. S. Geng, R. Li, G. Botton, S. Y. Ye, S. Knights, X. L. Sun. "Atomic Layer Deposition of Pt Nanocatalyst on Graphene and N-doped Graphene for PEM Fuel Cells". *61st Canadian Chemical Engineering Conference*, 2011, London, Canada.

2. **S. H. Sun**, G. X. Zhang, X. B. Meng, D. S. Geng, R. Y. Li, A. X. Sun. "Atomic Layer Deposition of Pt Nanocatalyst on Graphene Nanosheet for PEM Fuel Cell Applications". *219th Meeting of the Electrochemical Society*. 2011, Montreal, Canada.

3. **S. H. Sun**, G. X. Zhang, R. Y. Li, A. X. Sun. "Platinum Nanowire-based Highly Active and Durable Electrocatalyst for PEM Fuel Cells". *219th Meeting of the Electrochemical Society*. 2011, Montreal, Canada.

4. **S. H. Sun**, G. X. Zhang, R. Y. Li, M. Cai, X. L. Sun. "A Star Catalyst: New Pt Nanostructure for Cheap and Stable PEM Fuel Cells". *International Conference on Frontier Topics in Nanostructures and Condensed Matter Theory (NCMT-2011)*, 2011, London, Canada.

5. N. Gauquelin, **S. H. Sun**, H. Zhang, A. Sun, J. Y.T. Wei, G.A. Botton, "Applications of aberration-corrected STEM in the study of physical and chemical phenomena". *Canadian Microscopy Society Annual Meeting*. 2011, Ottawa, Canada.

6. **S. H. Sun**, G. X. Zhang, R. Y. Li, X. L. Sun. "Ultrathin Single-Crystal Pt Nanowire-based 3D Electrodes for Fuel Cell Application". *The 61st Annual Meeting of the International Society of Electrochemistry*. 2010, Nice, France. **(Invited talk)**

7. **S. H. Sun**, G. X. Zhang, R. Y. Li, X. L. Sun. "Development of Ultrathin Pt Nanowire-based Electrocatalyst for High-Performance and Low-Cost Fuel Cell Applications". *Symposium of Nanomaterials and Nanotechnology for Environment.* 2010, Hefei, China. **(Invited talk)**

8. **S. H. Sun**, G. X. Zhang, R. Y. Li, D. S. Geng, Y. Zhong, X. L. Sun. "Single-Crystal Pt Nanowire-based 3D Electrodes for PEM Fuel Cell Applications". *The International Green Energy Conference (IGEC)*. 2010, Waterloo, Canada.

9. **S. H. Sun**, G. X. Zhang, R. Y. Li, D. S. Geng, Y. Zhong, X. L. Sun. **"**Synthesis of Ultrathin Pt Nanowire-based 3D Hierarchical Nanostructures and Their Enhanced Performance as Electrocatalysts in Fuel Cells". *Ontario Nanoscience and Nanotechnology Workshop*. 2010, London, Canada.

10. **S. H. Sun,** G. X. Zhang, R. Y. Li, X. L. Sun. "Development of Novel Nanomaterials for High-Performance and Low-Cost Fuel Cell Applications--Nanowire-Based Electrodes for Fuel Cells". *Particle Technology Research Center Conference*. 2009, London, Canada.

11. **S. H. Sun**, J. P. Dodelet, D. Q. Yang, G. X. Zhang, F. Jaouen, E. Sacher. "Platinum Nanowires: Growth on Various Carbon Supports and Electrocatalysts for PEMFCs". *212th Meeting of the Electrochemical Society*. 2007, Washington DC, US.

12. **S. H. Sun**, D. Villers, A. M. Serventi, J. P. Dodelet. "Various Loadings of Pt Nanoparticles on MWCNTs for Fuel Cell Applications". *NanoForum Canada*. 2006, Edmonton, Canada.

13. J. P. Dodelet, D. Villers, **S. H. Sun**, A. M. Serventi, Sylvain Désilets. "Pt 3D electrodes for fuel cells". *89th Canadian Chemistry Conference*, 2006, Halifax, Canada.

14. A. M. Serventi, D. Villers, **S. H. Sun**, J. P. Dodelet. "Deposition of Pt Nanoparticles onto Multiwalled Carbon Nanotubes Grown on Fuel Cell Backings for Fuel Cell Applications". *1st Canadian Workshop on NanoCarbon*. 2005, Montreal, Canada.

15. D. Villers, **S. H. Sun**, A. M. Serventi, J. P. Dodelet. "Loading Platinum nanoparticles on Multiwalled Carbon Nanotubes for Fuel Cell Applications". *NanoForum Canada*. 2005, Montreal, Canada.

16. J. P. Dodelet, X. Sun, R. Li, D. Villers, **S. H. Sun**, A. M. Serventi. "Innovative use of carbon nanotubes in PEM fuel cell electrocatalysis". *207th Meeting of the Electrochemical Society*. 2005, Quebec City, Canada.

17. **S. H. Sun**, G. W. Meng, L. D. Zhang. "Preparation and growth mechanism of silica novel nanostructures". *1st Academic Forum for Chinese Doctoral Candidates*, 2003, Beijing, China.

18. **S. H. Sun**, G. W. Meng, M. G. Zhang, L. D. Zhang. "Synthesis and Raman Property of Single-Crystalline SnO_2 Nanobelts", *C-MRS 2002 Fall Meeting*, 2002, Beijing, P. R. China.

Awards and Honors:

1. **Alexander Graham Bell Canada Graduate Scholarship** (**NSERC CGS D**) (CAD $35,000/year), Canada, 2009-2011.

2. **Graduate Research and Thesis Award** (CAD $1,500/year), Faculty of Enginieering, the University of Western Ontario, Canada, 2009-2011.

3. **Electrochimica Acta Travel Award for Young Electrochemists** (Euro 1,000) (**1 of the 5** holders worldwide), 2010.

4. **Invited speaker** at *61st Annual Meeting of the International Society of Electrochemistry*. 2010, Nice, France.

5. **Invited speaker** at *Symposium of Nanomaterials and Nanotechnology for Environment.* 2010, Hefei, China.

6. **Western Engineering Scholarship**, the University of Western Ontario, Canada, 2008-2011.

7. **Merit Scholarship Program for Foreign Students** (ranked **#1**), (CAD $35,000/year), Quebec, Canada, 2006-2007.